Structural Dynamics of the Hsp90 Chaperone from ^{19}F NMR Spectroscopy

by

Suad Rashid

A thesis submitted in partial fulfillment of the requirements for the degree of

Doctor of Philosophy

Department of Biochemistry
University of Alberta

Abstract

Living cells have evolved a complex machinery of molecular chaperones to protect proteins from misfolding/aggregation in the protein-rich intracellular environment. Heat shock protein 90 (Hsp90) is an ATP-dependent molecular chaperone ubiquitously expressed in eubacteria and eukaryotes. The chaperone has been implicated in activating and stabilizing a diverse range of protein substrates (clients), including protein kinases, transcription factors, and nuclear hormone receptors. The diverse clients of Hsp90 are involved in the regulation of vital cellular processes such as cell survival and proliferation, transcriptional regulation, apoptosis, gene expression, and signal transduction. This makes Hsp90 an essential protein for maintaining cellular protein homeostasis.

Hsp90 is a homodimer with each protomer consisting of an N-terminal domain (N), a middle domain (M), and a C-terminal domain (C), forming the dimerization interface of the homodimer. The chaperone activity of Hsp90 is accompanied by a series of conformational alterations, which transforms Hsp90 from an N-terminally open conformation to a catalytically active closed conformation, bearing interprotomer N-N domain and intraprotomer N-M domain associations. Importantly, the rate of acquisition of this catalytically active closed conformation is slow, thus the rate-limiting step of the Hsp90 chaperone cycle. The overall conformational change of Hsp90 from an open to a closed conformation is driven by local transitions that are mainly localized within the N-terminal domain of Hsp90. In this work, we used a combination of ^{19}F NMR-based techniques and molecular dynamics simulations to investigate the dynamics of local and global motions occurring within the Hsp90 chaperone.

To facilitate a quantitative understanding of exchange contributions to the ^{19}F NMR linewidth of Hsp90, we quantified the internal motion of the sidechain of a trifluoroacetone cysteine derivative (CYF) commonly employed in ^{19}F NMR studies as a reporter of dynamic processes occurring in proteins. Our results show that the high flexibility of the CYF sidechain contributes to the narrow ^{19}F NMR linewidths of CYF tagged proteins and demonstrate the suitability of the CYF probe for studying dynamics occurring in large molecular weight proteins. The quantification of CYF sidechain motion allowed us to explore ATP-lid dynamics as well as the kinetics of nucleotide binding to the N-terminal domain of Hsp90. Our findings reveal priming of the ATP-lid by the γ-phosphate of nucleotide (ATP/AMPPNP), which is a prerequisite for full ATP-lid closure and subsequent ATP hydrolysis by Hsp90. Also, we investigated the dynamics of full-length Hsp90 in the presence of different nucleotides and the ATPase stimulating co-chaperone Aha1 using ^{19}F NMR as a reporter of conformational transitions. We found that binding of AMPPNP to full-length Hsp90 induces equilibrium populations of open and closed conformations of Hsp90 and Aha1 accelerates the slow conformational changes that lead to the formation of the closed conformation. Taken together, the research presented here highlight the remarkable utility of ^{19}F NMR spectroscopy for investigating local dynamics occurring within the N-terminal domain of Hsp90 and provides the basis for studying both local and global dynamics of the full-length chaperone in the presence of nucleotides, co-chaperones, and clients.

Preface

This thesis is organized into six chapters. The introduction in Chapter 1 and the conclusion in Chapter 6 are my original work. Chapter 2 and Chapter 3 are published work. Chapter 4 is part of a published paper and Chapter 5 is my original work, which has not been published.

Chapter 2 has been published as "**Rashid, S**., Lee, B.L., Wajda, B. & Spyracopoulos, L. Sidechain dynamics of the trifluoroacetone cysteine derivative characterized by 19F NMR relaxation and molecular dynamics simulations*. The Journal of Physical Chemistry B* **123**, 3665-3671 (2019)". S.R. expressed and purified all proteins with the help of B.W; S.R. collected NMR data. S.R. and L.S. conducted the MD simulations. S.R., B.L.L., and L.S. analyzed NMR data. S.R. and L.S. wrote the manuscript.

Chapter 3 has been published as "**Rashid, S**., Lee, B.L., Wajda, B. & Spyracopoulos, L. Nucleotide Binding and Active Site Gate Dynamics for the Hsp90 Chaperone ATPase Domain from Benchtop and High Field 19F NMR Spectroscopy. *The Journal of Physical Chemistry B* **124**, 2984-2993 (2020)". S.R. expressed and purified all proteins with the help of B.W; S.R. collected NMR data. S.R. and L.S. conducted the MD simulations. S.R., B.L.L., and L.S. analyzed NMR data. S.R. and L.S. wrote the manuscript.

Chapter 4 forms part of the publication "Lee, B. L., **Rashid, S.**, Wajda, B., Wolmarans, A., LaPointe, P. & Spyracopoulos, L. The Hsp90 chaperone: 1H and 19F dynamic nuclear magnetic resonance spectroscopy reveals a perfect enzyme. *Biochemistry* **58**, 1869-1877 (2019)". The data presented here are my contribution to the publication. I expressed, purified, collected, and analyzed NMR data for all the N-terminal domain and full-length Hsp90 constructs presented in Figure 4.1.

Dedication

To my late father, Alhaji Rashid. Although you went back to Allah early on in our lives, we hope you are proud of the adults we are today.

Acknowledgements

First, I am extremely grateful to Allah, the Lord of the Universe for the many blessings in my life. Praise be to Allah for His guidance and the successful completion of my PhD studies as I believe all success comes from Allah, the one who makes all things possible.

I would like to thank my Supervisor Dr. Leo Spyracopoulos for his support, mentorship, and immense contribution towards my studies. I am most grateful for the training I received in NMR data collection and analyses, the use of Mathematica, and most especially the use of AMBER suite of biomolecular programs to conduct molecular dynamics simulations. I appreciate the time you dedicated in teaching me various aspects of biophysics as well as the enormous feedback I received on my writings and presentations, which have made me a better scientist.

I am grateful to my supervisory committee members Dr. Paul LaPointe and Dr. Andrew MacMillan for their significant contributions towards my research and the constructive feedback I received during my supervisory committee meetings. I would like to thank former members of the Spyracopoulos lab Dr. Brian Lee, Dr. Anamika Singh, and Dr. Manoj Rout from whom I received a lot of help and support when I joined the lab. I would like to express a special gratitude to Dr. Brian Lee for his mentorship and immense support during the time we worked together in the lab. Also, I am grateful for the support I received from Dr. LaPointe's lab especially from Dr. Annemarie Wolmarans and Dr. Rebecca Mercier for answering my questions on Hsp90 and the training I received on Hsp90 expression and purification. I would like to thank my undergraduate supervisor, Dr. Felix Charles Mills-Robertson of KNUST for all the references he wrote for me, which contributed significantly to most of the awards I received during my PhD studies. I am thankful to all members of Dr. Peter Hwang's lab Gaddafi Danmaliki, Zabed Mahmud, Mohammad Rafid Feisal, and Philip Lui for their friendship and support. I am grateful to Dr. Rashmi Panigrahi, a special friend I made in the Biochemistry department who is always available to listen and ever willing to give a helping hand.

I am extremely thankful to my family, whose unwavering support and care has been instrumental throughout my studies. Many thanks to my mother, Hajia Batu who welcomed my daughter with open arms so I can focus on my studies. Mma, I appreciate all the sacrifices you made to see me through my studies and your endless support and prayers for my success. All I can say is may Allah bless all that you do and grant you the best of this world and the hereafter. I am especially grateful to my uncle, Mr. Habib who has played the role of a father throughout my life. Thank you for your immense care, support, and guidance, which have all contributed significantly to who I am today. I am thankful to my sisters Salwat, Babani, and Umaima as well as my extended family for their prayers and support. Many thanks to a great friend who is like an elder sister to me, Bisi Adewale who made my stay in Edmonton lively and enjoyable. I appreciate your company, advice, and the enormous help you have offered me throughout this journey.

To my amazing and ever supportive husband, Eng. Sulaiman Musah whose constant sacrifices and support made the successful completion of this journey possible. Words cannot fully express the extent of my gratitude. Thank you for your excellent advice and motivation that kept me going when the journey got tough. Thank you for offering a listening ear and being my go-to friend when I needed to destress. Thank you for all the sacrifices you have made in order to see me through my studies. Above all, thank you for being a great husband and father to our daughter Naana Hafsah.

Finally, I would like to thank the Natural Sciences and Engineering Research Council of Canada (NSERC) for their financial support. Special gratitude to the National High Field Nuclear Magnetic Resonance Center (NANUC) and The Metabolomics Innovation Center (TMIC) for use of NMR instruments at these facilities.

Table of Contents

List of Tables

List of Figures

Abbreviations

^{1}H NMR	Proton nuclear magnetic resonance spectroscopy
^{19}F NMR	Fluorine (19) nuclear magnetic resonance spectroscopy
ADP	Adenosine diphosphate
Aha1	Activator of Hsp90 ATPase protein 1
AMPPNP	Adenylyl-imidodiphosphate
ATP	Adenosine triphosphate
ATPγS	Adenosine 5′-[γ-thio]triphosphate
BTFA	3-Bromo-1,1,1-trifluoroacetone
Cdc37	Cell division cycle 37
Cdk4	Cyclin-dependent kinase 4
CPMG	Carr-Purcell-Meiboom-Gill
CSA	Chemical shift anisotropy
CTD	C-terminal domain
CYF	Trifluoroacetone cysteine derivative
DBD	DNA binding domain
DSS	4,4-dimethyl-4-silapentane-1-sulfonic acid
DTT	Dithiothreitol
EM	Electron microscopy
ER	Endoplasmic reticulum
FID	Free Induction decay
GA	Geldanamycin
GHKL	Gyrase, Hsp90, Histidine Kinase, MutL
GR	Glucocorticoid receptor
GR-LBD	Ligand binding domain of the glucocorticoid receptor
Grp94	Glucose-regulated protein 94
Hch1	High-copy Hsp90 suppressor protein 1
Hop	Hsp70-Hsp90 organizing protein

HSP	Heat shock protein
Hsp90	Heat shock protein 90
HSQC	Heteronuclear single quantum coherence spectroscopy
HtpG	High temperature protein G
IPTG	Isopropyl β-D-thiogalactopyranoside
MD	Molecular dynamics
NMR	Nuclear magnetic resonance spectroscopy
NSR	Nuclear spin relaxation
NTD	N-terminal domain
Pi	Inorganic phosphate
PPIase	peptidyl-prolyl cis-trans isomerase
RA	Radicicol
RESP	Restrained electrostatic potential
Sba1	Sensitivity to benzoquinone ansamycin 1
SHR	Steroid hormone receptor
Sti1	Stress induced phosphoprotein 1
TCEP	Tris(2-carboxyethyl)phosphine
TFA	Trifluoroacetate
TPR	Tetratricopeptide repeat
TRAP1	Tumor necrosis factor type 1 receptor-associated protein
ts	Temperature sensitive

Chapter 1

Introduction

Molecular Chaperones

Proteins constitute one of the major classes of macromolecules in cells, involved in a diverse range of biological processes. Proteins must fold into a distinct three-dimensional structure after their synthesis on the ribosome to function properly. In 1973, *in vitro* experiments pioneered by Anfinsen showed that the three-dimensional structure of a protein is determined by its amino acid sequence by demonstrating the ability of denatured ribonuclease (RNase) to refold spontaneously into its native three-dimensional structure once denaturants are removed[1]. However, the cellular environment *in vivo* is much more sophisticated due to high protein concentrations increasing the likelihood of aggregate formation, and the existence of folding intermediates prone to aggregation[2]. Also, large molecular weight proteins (>100 amino acids), which make up majority of the cellular proteome as well as proteins with multiple domains cannot fold effectively on their own[3]. Thus, most proteins require the assistance of a group of helper proteins termed molecular chaperones to avoid misfolding and formation of harmful aggregates[4,5].

Molecular chaperones are generally involved in housekeeping functions such as the proper folding of newly synthesized polypeptides as they are extruded from the ribosome during protein synthesis and re-maturation of denatured/misfolded proteins[6]. In addition to this, molecular chaperones play critical roles in cellular processes, including the transport of proteins across membranes, signal transduction, and protein turnover[7], making the molecular chaperone machinery a crucial component in cells. The significance of a well-functioning chaperone system in cells is highlighted by pathologies associated with protein misfolding/aggregation such as cystic fibrosis and neurodegenerative disorders like Alzheimer's and Parkinson's disease[8]. Also, molecular chaperones have been implicated in the pathogenesis of cancer as some oncoproteins are dependent on chaperones for their stabilization and activation[9,10].

The molecular chaperone network consists of a diverse family of structurally unrelated proteins the majority of which are heat shock proteins (HSPs). Heat shock proteins are also known as stress proteins because they are upregulated in response to stress conditions in cells. The major chaperone families are usually categorized according to their molecular

weights, namely Hsp100, Hsp90, Hsp70, Hsp60, Hsp40, and the small Hsps with molecular weights less than 40 kDa[11]. These chaperone families mostly function together as complex machineries made up of other chaperones, co-chaperones, regulators, and various cofactors/accessory proteins[9]. For instance, even though the Hsp90 and Hsp70 systems can function independently, the two sometimes collaborate to form a multichaperone complex responsible for the proper folding and remodeling of a diverse range of protein substrates[12]. In this multichaperone complex, Hsp90 is suggested to act downstream of Hsp70, consistent with the finding that Hsp90 is involved in later stages of protein folding[13]. However, the mechanism by which Hsp90 accomplishes its chaperone activity is less well understood compared to Hsp70.

The Hsp90 Chaperone

Heat shock protein 90 (Hsp90) belongs to the ~90 kDa family of molecular chaperones ubiquitously expressed in eubacteria and all eukaryotes but absent in archaea. Interestingly, Hsp90 is one of the most abundant proteins in cells under normal conditions making up about 1-2% of total soluble cell protein[7]. The Hsp90 chaperone machinery utilizes energy derived from ATP hydrolysis in the stabilization, activation, and maturation of a diverse range of protein substrates (clients) through a series of conformational transitions in a cyclical manner. Unlike other molecular chaperones, Hsp90 exhibits strong specificity for the type of clients it chaperones[14], although what determines whether a protein is an Hsp90 client or not is still elusive. In recent years, the number of proteins identified as Hsp90 clients has increased owing to advancements in global proteomic and genomic studies in yeast. Consequently, about 20% of yeast proteins depend on Hsp90 directly or indirectly for their function, making it the most connected protein in the yeast proteome[15,16]. Notably, the chaperone activity of Hsp90 is tightly regulated by a network of adaptor proteins known as co-chaperones which will be discussed in later sections.

Mammalian cells express four isoforms of Hsp90 within three cellular compartments: the cytosol (Hsp90α and Hsp90β), endoplasmic reticulum (Grp94), and mitochondrion

(TRAP1). On the contrary, *S. cerevisiae* contains two isoforms of Hsp90 located in its cytosol (Hsp82 and Hsc82), whereas the bacterium *E. coli* possesses a single isoform of Hsp90 called HtpG[17,18].

Mammalian Cytosolic Hsp90

Hsp90α (induced by heat shock) and Hsp90β (constitutively expressed) are expressed in the cytosol of mammalian cells, with the two isoforms sharing ~85% sequence identity and ~93% sequence similarity[19-21]. Intriguingly, functional differences have been observed between the two cytosolic isoforms. For instance, Hsp90β knockout mice are not viable as their embryos die at implantation. In contrast, Hsp90α knockout mice are viable besides the fact that male mice are sterile because of inability to produce sperm[22]. Also, Hsp90α has specific roles in antigen processing[23], oocyte meiosis in mice[24], and inhibition of caspase-2 activation[25]. In addition to this, Hsp90α is secreted outside the plasma membrane, and performs essential extracellular functions such as tumor cell invasiveness, angiogenesis, metastasis by activation of matrix metalloproteinase 2 (MMP2)[26,27] as well as promotion of wound healing by enhancement of skin cell migration[28]. On the other hand, Hsp90β has been implicated in mouse placental development[29] and regulation of antiapoptotic activity of Bcl-2 in mast cells[30].

Endoplasmic Reticulum (ER) Specific Grp94

Grp94 (Gp96/endoplasmin) is an Hsp90 isoform located in the lumen of the ER and sarcoplasmic reticulum of muscle cells, where it mainly chaperones secretory and membrane proteins[31,32]. Grp94 has the longest sequence among the mammalian Hsp90 isoforms, bearing ~42% sequence identity and ~59% sequence similarity with Hsp90α, and ~43% sequence identity and ~60% sequence similarity with Hsp90β[21]. The chaperone is upregulated in response to glucose deprivation, ER stress, and plays a major role in ER quality control pathways[33]. Since calcium is stored in the lumen of the ER, Grp94 like other ER-resident

proteins functions as a calcium carrier and participates in calcium homeostasis[34]. Additionally, Grp94 modulates the secretion and activity of insulin-like growth factor (IGF)-II, which causes lethality in Grp94 knockout mice[35,36]. Also, Grp94 plays a distinct role in cellular immune responses and has been implicated in cancers, autoimmune diseases, and inflammatory diseases, making it an attractive target for therapeutic intervention in these diseases[37-39].

Mitochondrial TRAP1

TRAP1 was initially identified as a protein that bound the cytoplasmic domain of type 1 Tumor Necrosis Factor Receptor-1 (TNFR1), hence the name TNFR1 Associated Protein (TRAP1)[40]. Subsequent sequence analysis showed that a 75 kDa Hsp90 isoform (Hsp75) that associated with Retinoblastoma (Rb) protein was identical to TRAP1[41,42]. Using biochemical and microscopic analyses, Hsp75/TRAP1 was found to primarily accumulate in the mitochondrial matrix, mitochondrial intermembrane space to a lesser extent, and quite a few non-mitochondrial sites[42-44]. Accordingly, TRAP1 bears an N-terminal pre-sequence that targets it to the mitochondria, which is removed after organelle import.

In terms of sequence, TRAP1 has the shortest sequence among the mammalian Hsp90 isoforms with ~26% sequence identity and ~45% sequence similarity with cytosolic Hsp90, and ~28% sequence identity and ~47% sequence similarity with Grp94[21]. Although TRAP1 has long been the least well studied of the Hsp90 isoforms, recent studies have highlighted its crucial role in maintaining cellular balance and mitochondrial integrity including, mitochondrial protein folding, oxidative stress, and transcriptional responses to proteotoxic stress[45]. Moreover, TRAP1 has been associated with human tumorigenesis as it is overexpressed in tumor cells of the lung, colon, breast, and pancreas, making it a potential diagnostic biomarker and a target for cancer therapeutics[46]. Likewise, there is evidence that phosphorylation of TRAP1 by PTEN induced putative kinase 1 (PINK1) prevents oxidative-stress induced apoptosis. This kinase activity is impaired in Parkinson's disease (PD) linked PINK1 mutations, thus highlighting the role of TRAP1 in PD pathogenesis[43].

Yeast Cytosolic Hsp90

S. cerevisiae expresses two isoforms of Hsp90 in its cytosol. Hsc82 is constitutively expressed at high levels and upregulated by 1.5 to 2-fold at elevated temperatures. On the other hand, Hsp82 is expressed at very low levels but accumulates (~20-fold increase) to nearly the same level as Hsc82 upon heat shock[47]. The two isoforms have a high sequence identity of ~97%, and the expression of at least one isoform can support normal growth in yeast cells[47]. Interestingly, mammalian and *S. cerevisiae* cytosolic Hsp90 homologs share up to ~60% sequence identity, and there is evidence that mammalian Hsp90 effectively complements growth in *S. cerevisiae* mutants lacking both Hsc82 and Hsp82[48]. Despite the high sequence identity between Hsc82 and Hsp82, distinct differences between the two isoforms have been reported. For instance, Hsp82 is more thermally stable than Hsc82 with melting temperatures of 60.4 ± 0.5 °C and 57.1 ± 0.2 °C reported for Hsp82 and Hsc82, respectively in the absence of nucleotide. Also, Hsc82 has a higher ATPase activity than Hsp82[49].

Bacterial HtpG

The bacterium *E. coli* expresses a single isoform of Hsp90 called HtpG. The chaperone has the smallest molecular weight among the Hsp90 isoforms and shares ~42% sequence identity with mammalian cytosolic Hsp90. Unlike the eukaryotic Hsp90s, deletion of HtpG is not lethal to bacterial cells. However, mutants show decreased growth rates at elevated temperatures[50,51]. As a molecular chaperone, HtpG participates in de novo protein folding particularly under stressful conditions[52]. In addition, extraintestinal pathogenic *E. coli* requires the activity of HtpG in the synthesis of the virulence factors colibactin and yersiniabactin. As a result, mice infected with HtpG knockout *E. coli* strains exhibit reduced virulence compared to wildtype mice, demonstrating the potential of HtpG as a therapeutic target in microbial infections[53].

Hsp90 Structural Organization

Hsp90 functions as a homodimer and each protomer is made up of three structurally independent domains. The N-terminal domain contains the site for ATP binding, some co-chaperones, and some client proteins[54-56]. This is followed by the middle domain, which contains the binding site for some co-chaperones and is thought to be the primary binding site for most clients. Also, the middle domain contains a conserved arginine residue (R380 in yeast) required for ATP hydrolysis[57]. Finally, the C-terminal domain contains the dimerization interface[58] and terminates with a conserved pentapeptide MEEVD motif in cytosolic Hsp90 isoforms, which binds tetratricopeptide repeat (TPR) containing co-chaperones[59]. This domain organization is highly conserved from bacteria to humans (Figure 1.1) except for a longer unstructured charged linker region, linking the N-terminal domain to the middle domain in eukaryotes[55]. Importantly, binding sites for clients and co-chaperones have been identified in all three domains, which will be discussed in later sections.

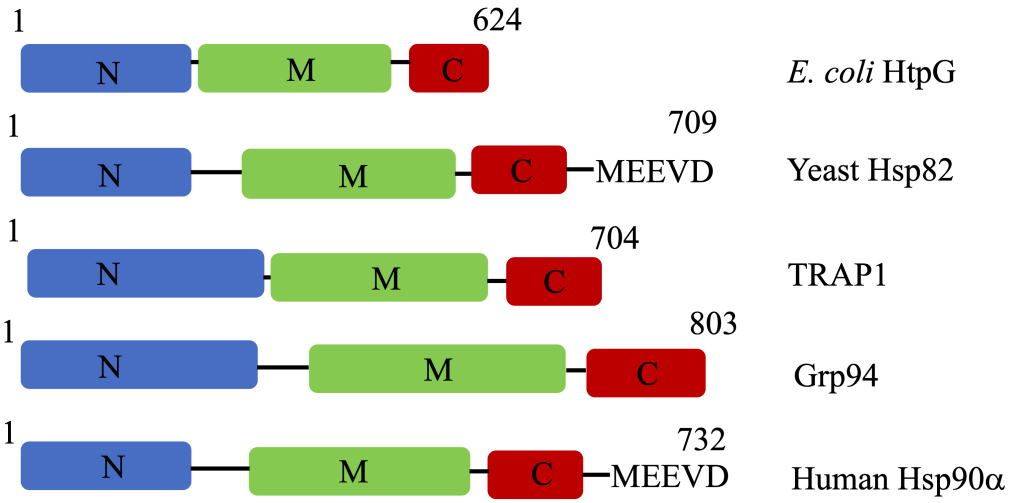

Figure 1.1: Schematic diagram showing the domain organization of *E. coli* HtpG, yeast Hsp82, TRAP1, Grp94, and human Hsp90α. N-terminal domain (blue), middle domain (green), and C-terminal domain (red).

The N-terminal Domain (NTD)

Although Hsp90 has a highly conserved domain organization, the N-terminal domain (NTD) is the most conserved and bears the highest sequence identity across all species[60]. Structurally, the NTD is made up of a combination of α-helices and antiparallel β-sheet (α/β sandwich) with a deep pocket (~15 Å deep) that serves as a nucleotide binding pocket[61,62]. This nucleotide binding fold is shared by all members of the gyrase, Hsp90, histidine kinase, MutL (GHKL) ATPase/kinase superfamily. In addition, members of the GHKL superfamily possess a two-hinged gate (ATP-lid) located over their nucleotide binding pockets. However, the composition and conformation of this ATP-lid is different in each class of protein[63].

Nucleotide binding to Hsp90 has been studied extensively. Crystal structures of ATP bound to the NTD of yeast and human Hsp90 show an unusual, kinked ATP conformation with the adenine base and ribose sugar of ATP inside the nucleotide binding pocket while the phosphates extend outwards[56,64] (Figure 1.2). The N6 amino group of adenine makes a direct hydrogen bond contact with D79 of the protein whereas bound water molecules mediate all other contacts between the pocket and ATP. Interestingly, this nucleotide binding pocket is also the binding site for naturally occurring compounds like geldanamycin (GA) and radicicol (RA), which have been shown to inhibit the activity of Hsp90. These inhibitors as well as their synthetic analogs bind the nucleotide binding pocket in a similar manner as ATP and serve as competitive inhibitors of Hsp90 ATPase activity[65,66].

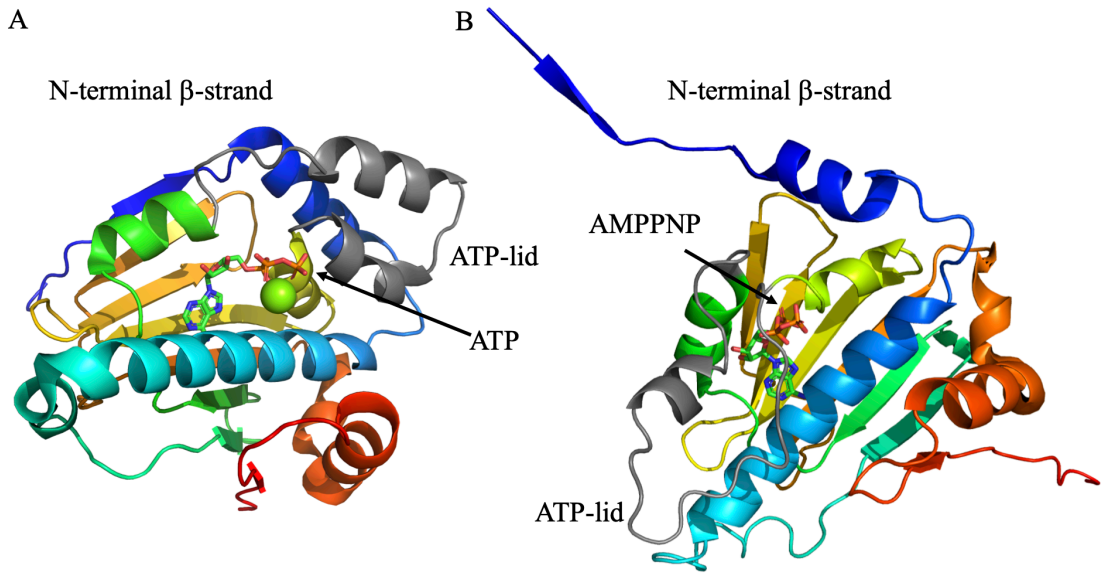

Figure 1.2: Nucleotide binding to the NTD of Hsp90. (A) Isolated NTD of human Hsp90 colored from N-terminus (blue) to C-terminus (red) bound to ATP shows the ATP-lid (grey) in an open conformation (PDB 3T0Z)[64]. (B) The NTD extracted from the structure of a catalytically active closed conformation of full-length yeast Hsp90 colored from N-terminus (blue) to C-terminus (red) bound to AMPPNP (a non-hydrolyzable ATP analog) shows the ATP-lid (grey) in a closed conformation (PDB 2CG9)[56]. ATP and AMPPNP are shown as sticks.

At the base of the nucleotide binding pocket is a lining of β-sheet, while a helix-loop-helix motif that forms an ATP-lid covers the top of the pocket. For the isolated NTD, the ATP-lid points away from the pocket, adopting an open lid conformation (Figure 1.2A) with ATP completely exposed[62,64]. Structures of the N-terminal domains of full-length yeast Hsp90 (Figure 1.2B) and human Hsp90 bound to nucleotide show a closed lid conformation that completely closes over the nucleotide binding site[56,67]. Lid closure leads to exposure of a hydrophobic patch, which forms a dimerization interface between the NTD in each protomer of the Hsp90 homodimer. In addition, the nucleotide bound full-length Hsp90 structures reveal a major conformational change involving the N-terminal β-strand of each protomer, which swaps and interacts with its opposing protomer[56,67]. These structural

changes within the NTD, together with interactions within the middle and C-terminal domains lead to the formation of a catalytically active closed conformation of Hsp90 where ATP is hydrolyzed. Given that these conformational changes are not observed in the isolated NTD, the domain on its own does not dimerize, and has negligible ATPase activity[54,58].

Insight into the link between nucleotide binding, N-terminal β-strand swapping, and ATP-lid dynamics came from mutational studies that involved deleting specific amino acid residues within the isolated NTD and full-length Hsp90 chaperone. Specifically, mutants lacking the ATP-lid residues were shown to have no ATPase activity, although this mutation did not significantly affect nucleotide binding[68]. Interestingly, deletion of the first twenty-four amino acid residues abolished the ATPase activity of Hsp90 and was shown to increase the flexibility of the ATP-lid[68,69]. In contrast, deletion of the first eight amino acid residues of the N-terminal β-strand led to an increase in dimer formation and a 1.5-fold increase in the ATPase activity of Hsp90[69]. Together, these studies demonstrate that nucleotide binding, N-terminal β-strand swapping, and ATP-lid dynamics of the Hsp90 chaperone are not independent but are coupled.

The Hsp90 Charged Linker

The Hsp90 NTD is connected to the middle domain by an unstructured charged linker that varies in length (~30-70 residues) among different homologs. Both bacterial HtpG and mitochondrial TRAP1 possess a considerably shorter linker compared to other homologs[42,51]. Deletion of a significant portion of the linker (residues 211-259) is dispensable in yeast[70]. On the other hand, deletion of the entire linker (residues 211-272) is lethal in yeast, and a minimal portion of the linker must be present for yeast cells to be viable. However, linker deletion does not affect the overall structure of Hsp90, even though mutants exhibit decreased ATPase activity and the ability to regulate ATPase stimulating and inhibiting co-chaperones is impaired[71]. Also, studies involving the replacement of human and yeast Hsp90 linkers with *Plasmodium falciparum* linker and artificial linkers showed that, the linker sequence is a critical regulator of client interaction with eukaryotic Hsp90 as well as chaperone activity *in*

vivo[72]. Taken together, these studies show that in addition to acting as a tether connecting the NTD and the middle domain, the linker modulates ATPase activity of Hsp90, co-chaperone binding, and client interactions with Hsp90.

The Middle Domain

The first high-resolution structure of the isolated middle domain of Hsp90 (yeast) was available in 2003[57]. Structurally, the middle domain can be divided into three parts: a large α-β-α sandwich (residues 273-409) followed by a right-handed α-helical coil (residues 411-420, 421-432, and 436-443) and finally, a small α-β-α sandwich (residues 435-525) with residues 526-560 being disordered[57] (Figure 1.3A). A common feature among the ATPases of the GHKL ATPase/kinase superfamily is a 'split ATPase' structural arrangement. In this scheme, the catalytically active conformation that can hydrolyze ATP is attained when ATP bound to the NTD contacts the middle domain. Accordingly, the middle domain of Hsp90 contains a catalytic loop (residues 370-390) made up of a highly conserved arginine residue (R380 in yeast Hsp90) (Figure 1.3A), which is remodeled in the catalytically active closed conformation (Figure 1.3B) to contact the γ-phosphate of ATP thus bringing the NTD and middle domain together to initiate hydrolysis [56,57,73]. It is no surprise that mutation of this arginine residue to alanine (Hsp90-R380A mutant) is lethal in yeast, decreases the ATPase activity of Hsp90, and inhibits the formation of the catalytically active closed conformation[57,73-75]. Importantly, this arginine residue is not directly involved in catalysis, but its main role is to stabilize NTD-middle domain (N-M) interaction[74].

A recent study has identified a conserved solvent exposed tryptophan residue located in the middle domain of Hsp90 (W300 in yeast Hsp90) (Figure 1.3A), as a molecular switch point that transfers client binding information from the middle domain to the NTD, thereby effecting critical conformational changes required for client activation[76]. Even though the Hsp90-W300A mutation does not affect the ATPase activity of Hsp90 *in vitro*, yeast cells bearing this mutation exhibit growth defects at 30 °C and are lethal at 37 °C[57]. In addition,

these mutants show impaired client activation, which further implicates W300 in client protein interactions[57,76].

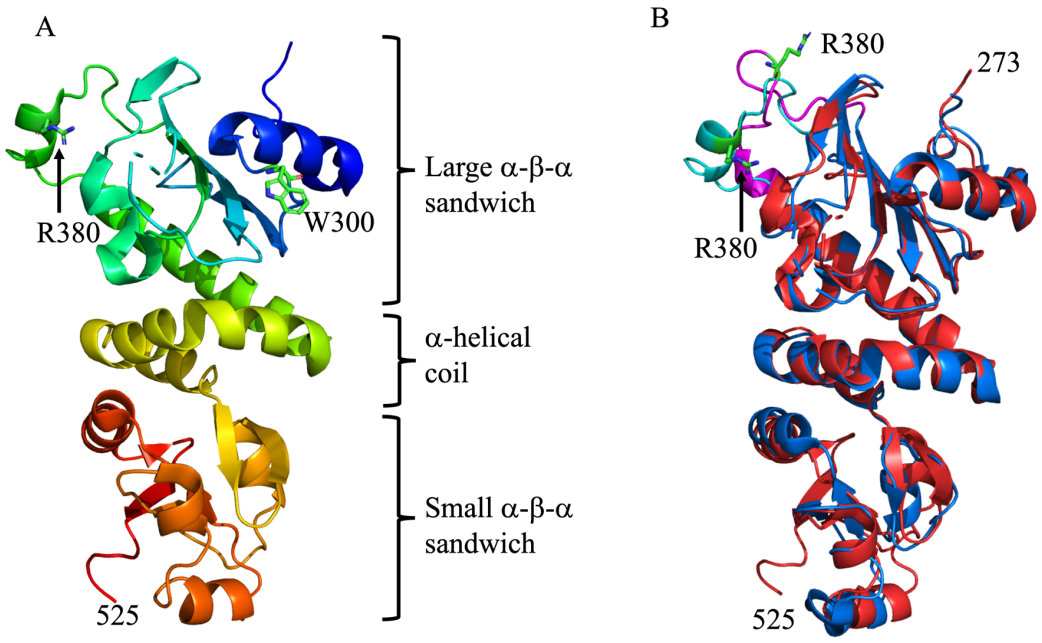

Figure 1.3: Structure of the middle domain of yeast Hsp90. (A) The isolated middle domain of Hsp90 colored from N-terminus (blue) to C-terminus (red) showing the three subdomains (PDB 1HK7)[57]. W300 and R380 are shown as sticks. (B) The isolated middle domain (red) showing the catalytic loop (cyan) (PDB 1HK7) superimposed with the middle domain extracted from a structure of the catalytically active closed conformation of full-length yeast Hsp90 (blue) showing a remodeled catalytic loop (magenta) (PDB 2CG9)[56]. R380 is shown as sticks.

The middle domain of Hsp90 has been identified as the main binding site for clients. The structure of the domain reveals a stretch of hydrophobic patches that spans its entire length and a solvent exposed amphipathic loop (327-APFDLFESKKKKNN-340), with one part being hydrophobic and the other part being positively charged[57]. The binding sites for three structurally distinct Hsp90 clients (Cdk4, Tau, and GR-LBD) have been mapped to the middle domain[13,67,77,78]. Whereas Cdk4 predominantly binds to the middle domain, the binding sites for GR-LBD and Tau are more extensive, spanning across all three domains.

Although the three clients are chemically and structurally diverse, their binding sites on Hsp90 share some common patterns with regards to their binding surface areas, hydrophobicity, and charges. Specifically, all three binding sites are stretched across the Hsp90 middle domain, are less hydrophobic compared to the binding sites for Hsp70 clients, and have either a net positive or negative charge[79]. In addition to clients, the binding sites for the ATPase stimulating co-chaperones Aha1 and Hch1 have been mapped to the middle domain[80], which further substantiates the crucial role of the middle domain in catalysis.

The C-terminal Domain (CTD)

The C-terminal domain (CTD) of Hsp90 is a homodimer with a binding affinity (K_D) of ~60 nM for yeast Hsp90[58], making Hsp90 an inherent dimer. A crystal structure of the isolated CTD of bacterial HtpG revealed that the domain begins with a short α-helix (H1) followed by a three-stranded antiparallel β-sheet (B1, B2, and B3) with a long loop between β-strands B2 and B3, which contains a short α-helix (H2) and finally terminates with three α-helices (H3, H4, and H5) (Figure 1.4)[81]. The dimerization interface is formed by the last two carboxy-terminal helices from the two protomers, which interact with each other to form a four-helix bundle (Figure 1.4). Also, this study identified the second α-helix (H2) of the CTD (Figure 1.4) as a potential binding site for Hsp90 clients owing to its intrinsic features. In particular, the location of the helix makes it easily accessible for interaction with other proteins. Additionally, the helix is conformationally flexible and amphipathic, bearing a conserved hydrophobic patch exposed to solvent[81]. Thus, the CTD bears characteristics that makes it a suitable binding site for the chemically and structurally diverse Hsp90 clients. Indeed, subsequent studies identified regions of the CTD that interact with Hsp90 clients GR-LBD and Tau[13,77,78]. The binding of clients to the CTD is undoubtedly not limited to GR-LBD and Tau. Perhaps additional client binding sites within the CTD will be identified as more structures of Hsp90 in complex with its clients are solved.

As noted above, the Hsp90 NTD on its own has negligible ATPase activity, implying that other domains are required for optimal ATPase activity[54,58]. CTD dimerization is critical

in this regard as Hsp90 mutants lacking the CTD exhibit decreased ATPase activities. Even though these mutants are intrinsically monomeric, they can dimerize in the presence of AMPPNP[54]. Thus, the inherent dimerization of the CTD is independent of nucleotide binding and NTD dimerization but required for maximal ATPase activity by serving as a pivot for the opening and closing of the NTD. Additionally, the CTD of Hsp90 has been implicated in trapping nucleotide bound to the NTD, an essential requirement to achieving maximal ATPase activity[82].

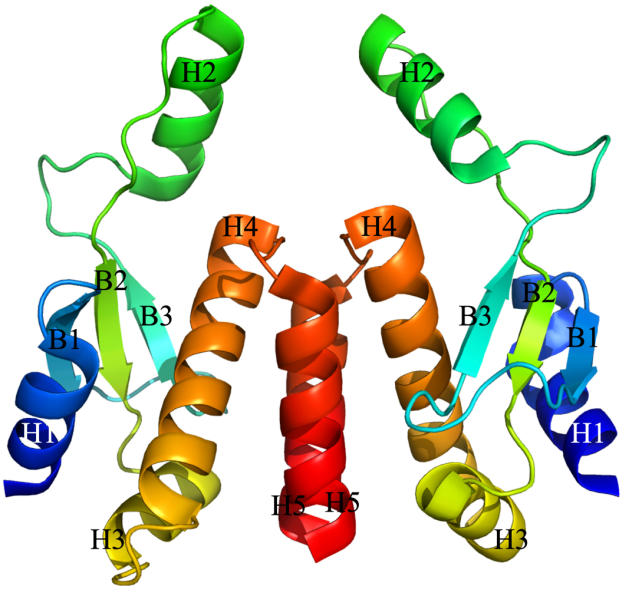

Figure 1.4: Structure of the C-terminal domain of *E. coli* HtpG colored from the N-terminus (blue) to C-terminus (red) showing the four-helix bundle that forms the dimerization interface (PDB 1SF8)[81]. α-helices are labeled (H1-H5) and β-sheets are labeled (B1-B3).

Interestingly, some studies have identified a cryptic nucleotide binding site within the CTD of Hsp90. Unlike the NTD, this binding site has less specificity, hence binds both purine and pyrimidine nucleotides[83-85]. Evidence of this second nucleotide binding site in the CTD made way for the exploration of small molecule inhibitors that bind the CTD. Consequently, the binding site for novobiocin, a known inhibitor of the chaperone activity of Hsp90, has been mapped to regions near the dimerization interface of the CTD[84].

The ATPase-Coupled Molecular Clamp Cycle

Elucidation of the structures of all three isolated domains of Hsp90 laid the foundation for understanding the mechanism of action of the Hsp90 chaperone. These structural studies together with biochemical studies led to the generally accepted model of the Hsp90 chaperone cycle –the ATPase-coupled molecular clamp model. In this model, the apoprotein of the Hsp90 homodimer is V-shaped, usually termed the open conformation, in which the NTDs are apart with the CTDs dimerized. ATP binding to the NTD induces a series of conformational alterations, which eventually leads to a catalytically active closed conformation (Figure 1.5). In this conformation, the NTDs are dimerized, the NTD and the middle domain of each protomer associate through an interaction involving the γ-phosphate of ATP bound to the NTD and a conserved arginine residue (R380 in yeast) in the middle domain, leading to the hydrolysis of ATP. Once ATP is hydrolyzed, ADP and inorganic phosphate (Pi) are released, and Hsp90 returns to its original open conformation[54,58,75,86,87]. Details of this mechanism are further confirmed by structures of the open and closed conformations of full-length Hsp90 homologs.

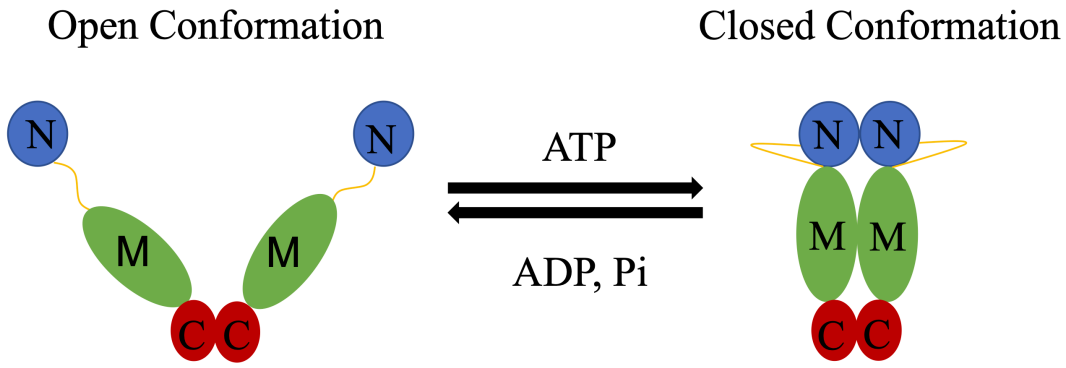

Figure 1.5: Schematic diagram of Hsp90 open conformation (left) and closed conformation (right). Binding of ATP leads to the formation of a catalytically active closed conformation. ATP hydrolysis to ADP and Pi returns the chaperone back to an open conformation. N-terminal domain (blue) charged linker (yellow), middle domain (green), and C-terminal domain (red).

Structural Details of the Closed and Open Conformations of the Hsp90 Chaperone

The Hsp90 Closed Conformation

Shortly after the structures of all three isolated domains of Hsp90 were solved, the first structure of a full-length construct was reported –the yeast Hsp90 in complex with AMPPNP (a non-hydrolyzable ATP analog) and the co-chaperone Sba1[56]. Importantly, Hsp90 in this complex had two major modifications. First, the study employed a mutant (Hsp90-A107N) that exhibits increased dimerization and ATPase activity[54]. Also, a significant proportion of the unstructured charged linker (residues 221-255) was removed.

Given that the co-chaperone Sba1 binds to and stabilizes the closed conformation of Hsp90 in the presence of ATP and its analogs[88,89], the structure of the complex showed Hsp90 trapped in a closed conformation and further uncovered details of conformational switches that make up this catalytically active conformation (Figure 1.6A). Noticeably, most conformational changes are centered within the NTD. In particular, the first α-helix (residues 13-22) is detached from the N-terminal β-strand (residues 1-9), which simultaneously swaps to hydrogen-bond with the main β-sheet of the opposing protomer. Also, the ATP-lid (residues 94-125) is flipped by an angle of ~180° over the nucleotide binding pocket compared to its conformation in the isolated NTD where bound nucleotide is fully exposed. Movement of the ATP-lid exposes a hydrophobic patch made up of residues N14, L15, L18 and T95, I96, A97, F120, which provides an interface for dimerization between the NTD of each protomer[56]. Additionally, compared to full-length Hsp90 of the Hsp90-AMPPNP-Sba1 complex, the middle domains of a middle domain-CTD construct (residues 273-709) move closer together by ~20 Å, whereas the CTDs remain unchanged[56].

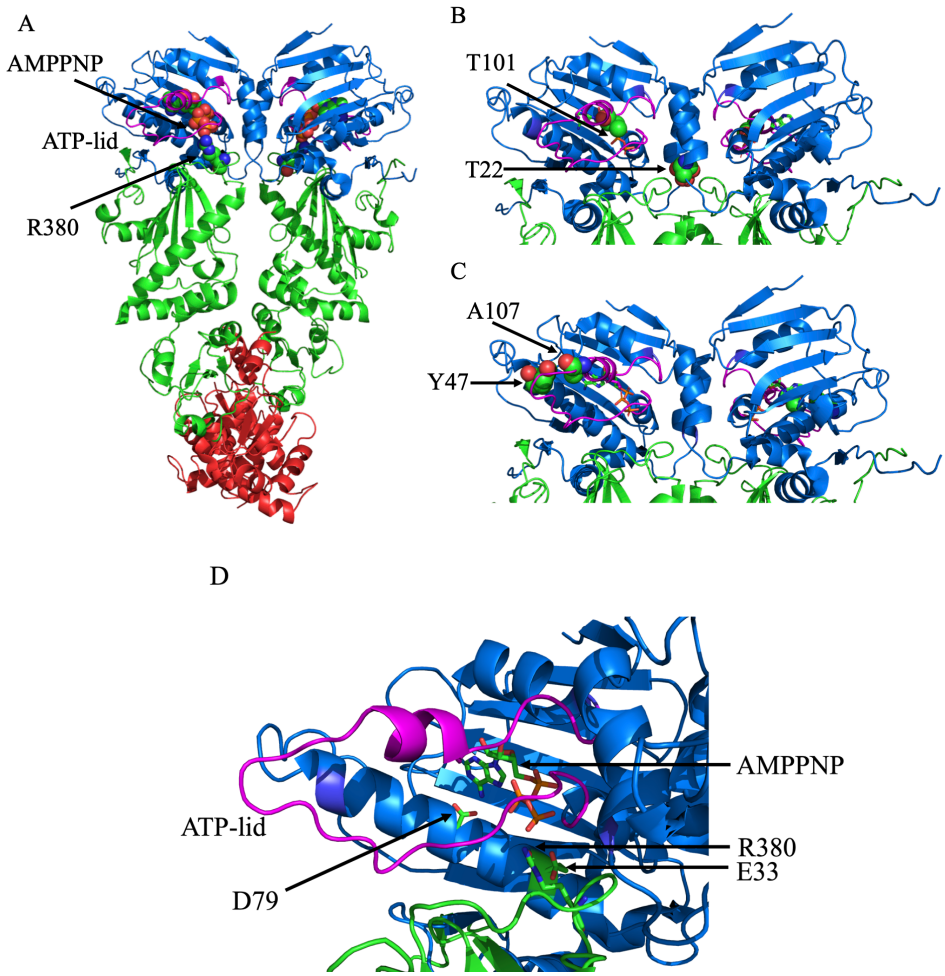

Figure 1.6: Structural features of the catalytically active closed conformation of yeast Hsp90 (PDB 2CG9)[56]. (A) Full-length yeast Hsp90 bound to AMPPNP showing the N-terminal domain (blue), middle domain (green), C-terminal domain (red), and ATP-lid (magenta). R380 (spheres) from the middle domain contacts the γ-phosphate of AMPPNP stabilizing NTD-middle domain association. (B) The NTD-NTD and NTD-middle domain interface showing the stabilizing effect of T22 and exposed location of T101 once the ATP-lid flips over the nucleotide binding site. T22 and T101 are shown as spheres, AMPPNP is shown as sticks. (C) NTD-NTD and NTD-middle domain interface showing the proximity of Y47 to A107. Both residues are shown as spheres and AMPPNP is shown as sticks. (D) The nucleotide binding pocket showing the positions of D79, E33, and AMPPNP. The structure shows the proximity of E33 to the γ-phosphate of AMPPNP and R380. All residues and AMPPNP are shown as sticks.

Also, the structure of the complex shows all atoms of bound AMPPNP at the same position they occupied in the nucleotide bound isolated NTD except the γ-phosphate of AMPPNP, which is positioned at the C-terminus of the ATP-lid. Consequently, the γ-phosphate of AMPPNP contacts the middle domain stabilizing NTD-middle domain association through a polar interaction involving R380 from the catalytic loop of the middle domain (Figure 1.6A). This intraprotomer interaction is further stabilized by both polar and hydrophobic interactions between T22, V23, Y24 from the NTD and L376, L378 from the middle domain, along with interactions involving residues 114-120 from the ATP-lid, which are in proximity with residues 372-379 of the catalytic loop in the middle domain[56].

The structure of the catalytically active closed conformation of Hsp90 exquisitely explained the structural basis underlying how previously identified mutations of Hsp90 affect ATPase activity and dimer formation. The increase and decrease in ATPase activity in the temperature-sensitive (*ts*) mutants T22I and T101I, respectively[54,90], can be explained by their respective locations in this closed conformation. First, T22 is located at the hydrophobic interface that stabilizes interprotomer NTD interaction (Figure 1.6B). Thus, a mutation of this residue to a more hydrophobic isoleucine stabilizes the catalytically active conformation, leading to an increase in ATPase activity. On the other hand, T101, which is buried in the open lid conformation, becomes fully exposed once the ATP-lid closes over the nucleotide binding pocket (Figure 1.6B). As a result, mutation of this threonine to the more hydrophobic isoleucine residue will favor the open lid conformation, consequently decreasing ATPase activity.

Also, the structure of the complex revealed why A107N mutation increases ATPase activity and dimerization[54]. Specifically, A107 is near Y47 (Figure 1.6C), and a mutation of this alanine to a more polar asparagine will favor a polar interaction with Y47, thus stabilizing the catalytically active conformation and increasing ATPase activity. A closer look at the nucleotide binding pocket of the complex explains why both E33A and D79N mutants have no ATPase activity, although the E33A mutant can bind nucleotide, whereas the D79N mutant cannot[91,92]. In the case of E33, both the γ-phosphate of the nucleotide and R380 are in proximity to E33, which activates a water molecule for γ-phosphate bond cleavage (Figure

1.6D). Consequently, mutation of this glutamate to alanine inhibits catalysis. D79 on the other hand is directly hydrogen-bonded to the adenine base of AMPPNP at the bottom of the nucleotide binding pocket (Figure 1.6D) and mutation to asparagine disrupts this hydrogen bond interaction and abolishes nucleotide binding and catalysis.

The Hsp90 Open Conformation

Following the elucidation of the structure of yeast Hsp90 in the closed conformation, structures of full-length *E. coli* HtpG in open and closed conformations were reported[93]. The structures revealed in this study further validated the ATPase-coupled molecular clamp mechanism of the Hsp90 chaperone cycle. Moreover, the structures confirmed the architectural conservation of the catalytically active closed conformation among Hsp90 homologs. In the absence of nucleotide, HtpG adopts a V-shaped conformation (open conformation) with the overall architecture of each of the three domains mostly equivalent to that observed in the isolated domains (Figure 1.7), except for major changes in the CTD and around the ATP-lid in the NTD[93]. Specifically, an exposed and ordered amphipathic helix in the isolated CTD is disordered in the full-length structure. Nevertheless, this helix was predicted to occupy the dimeric cleft with an exposed hydrophobic face making it suitable for client binding. One distinguishing feature of this open conformation of HtpG is the distribution of exposed hydrophobic patches in all three domains, which have been proposed to be potential binding sites for the diverse range of Hsp90 clients[93].

With regard to changes within the NTD, the ATP-lid of full-length apo HtpG adopts a distinct conformation, which sterically prohibits nucleotide binding. Thus, in the presence of nucleotide the NTD must undergo drastic conformational rearrangements to accommodate a nucleotide in its binding pocket. The structure of full-length HtpG in complex with ADP provides some insight into this rearrangement, where ADP binding induces an extended, almost linear dimer conformation[93]. In this conformation, the NTD points upwards away from the middle domain to unblock the nucleotide binding pocket. On the other hand, the unusual extended dimer conformation that was observed in the crystal structure of HtpG-ADP complex is very different from a highly compact conformation that was observed for

the same complex by electron microscopy (EM)[93], highlighting the possibility that the unusual conformation observed in the crystal structure could be a crystallization artifact.

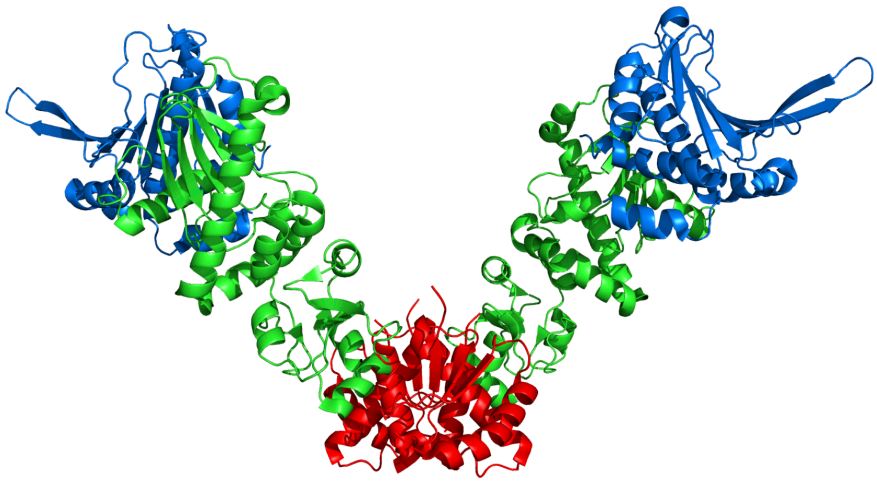

Figure 1.7: Structure of the open conformation of apo *E. coli* HtpG showing the N-terminal domain (blue), middle domain (green), and C-terminal domain (red) (PDB 2IOQ)[93].

High-resolution structures of full-length human cytosolic Hsp90β, mitochondrial TRAP1, and ER-specific Grp94 have also been reported[67,94-96]. These structural studies have provided important details into homolog-specific conformational states and overall dynamics of Hsp90. In all species, ATP binding induces a series of conformational changes leading to the catalytically active closed conformation where ATP is hydrolyzed. However, there is evidence that within this conserved conformational cycle, Hsp90 exists in a dynamic equilibrium between distinct conformational states, which is specific to each species[97]. It is possible this species-dependent conformational equilibrium is correlated with how each organism chaperones its clients as well as the nature of clients it chaperones.

Kinetics of Nucleotide Binding and Hydrolysis by Hsp90

Nucleotide binding to the NTD of Hsp90 has been studied extensively. The affinity for ATP binding is generally weak, with all values reported so far in the micromolar range. Hsp90 has

long been described as a slow ATPase because its catalytic turnover rate (k_{cat}) is very low compared to many known ATPases. Among different Hsp90 homologs, ATPase activities differ significantly; a k_{cat} of ~1 ATP min^{-1} has been reported for yeast Hsp90 and ~0.1 ATP min^{-1} for human Hsp90[91,98-100]. However, a recent kinetic analysis of the ATP hydrolysis step for the Hsp90 chaperone cycle showed that yeast Hsp90 has a lower limit for k_{cat} of ~1 s^{-1}, consistent with the typical rate of catalysis for many enzymes[75,101]. The study further revealed that although Hsp90 has an optimized k_{cat} for ATP hydrolysis, the structural changes that lead to the catalytically active closed conformation are slow; thus, the rate-limiting steps of the Hsp90 chaperone cycle[75]. This explained why previous studies had characterized Hsp90 as a slow ATPase even though its chemical step is optimized. Additionally, this direct kinetic analysis of the ATP hydrolysis step for the Hsp90 chaperone cycle has established the groundwork for research on how ATPase activity is coupled to client activation, which is mostly unknown.

In response to nucleotide binding, Hsp90 undergoes local conformational changes to adopt a catalytically active closed conformation, which hydrolyzes ATP. To gain an in-depth understanding of these conformational transitions, some studies have characterized the kinetics of these local structural changes and subsequently proposed kinetic models for the Hsp90 chaperone cycle[75,86,87,102]. Generally, all studies have reported slow kinetics for the accumulation of the catalytically active closed conformation with a net barrier height of ~20 kcal mol^{-1}. One of the models is a physicochemical kinetic model that was developed using ^{1}H and ^{19}F NMR spectroscopy[75]. This model has so far provided significant insights into the rates of opening, closing, and catalytic turnover of Hsp90 in the presence of diverse nucleotides. Specifically, in the presence of the non-hydrolyzable ATP analog AMPPNP, Hsp90 undergoes slow conformational changes from an open (k_{open} = 1.786 ± 0.004 h^{-1}) to a closed (k_{close} = 3.69 ± 0.02 h^{-1}) conformation until it reaches equilibrium populations of open and closed conformations of 0.4:0.6[75]. Interestingly, the catalytically active closed conformation of Hsp90 does not accumulate in the presence of ATP, highlighting the fact that the closed conformation is short-lived during active ATP hydrolysis[75]. Ultimately, this kinetic model substantiates previous findings on the slow conformational transitions of the

Hsp90 chaperone cycle. However, the model has the added potential to probe the influence of co-chaperones and clients on the Hsp90 chaperone cycle, which is limited in other models.

Chapter 3 of this work explores kinetics of the Hsp90 ATP-lid following ATP binding to the isolated NTD using a combination of ^{19}F NMR spectroscopy and molecular dynamics (MD) simulations[103]. Consistent with a previous NMR study[68], our results showed that some regions of the ATP-lid are intrinsically more flexible. However, upon nucleotide binding, the γ-phosphate of ATP perturbs the C-terminal end of the ATP-lid, making it even more flexible[103]. The structure of the catalytically active closed conformation of full-length yeast Hsp90 shows full closure of the ATP-lid over the nucleotide binding pocket (Figure 1.6A)[56]. This transition of the ATP-lid requires the N-terminal end of the lid to be released as well as interprotomer swapping of the N-terminal β-strand, which occurs in collaboration with NTD-NTD and NTD-middle domain interactions. Thus, ATP binding to the NTD serves as a first step for closure of the ATP-lid, which is required for optimal ATP hydrolysis by Hsp90.

Hsp90 Co-chaperones

Co-chaperones are accessory proteins that bind to specific conformational states of Hsp90 and act as regulators of the chaperone activity of Hsp90. Co-chaperones modulate the Hsp90 chaperone cycle through stimulation and inhibition of Hsp90 ATPase activity, recruitment of specific clients, and coordination of the Hsp90 chaperone system to other chaperone systems[15]. Interestingly, no co-chaperone has been identified in *E. coli* HtpG even though both yeast and human Hsp90 have a nearly conserved co-chaperone network, with 12 co-chaperones identified in yeast and more than 20 co-chaperones in humans[104]. In addition, except for the co-chaperones Cdc37, Cns1, and Sgt1, all other yeast co-chaperones are not required for viability[105]. Virtually all co-chaperones identified so far are specific for cytosolic Hsp90s except for one co-chaperone Canopy fibroblast growth factor signaling regulator 3 (CNPY3) that is required by Grp94 in the ER to promote folding of Toll-like receptors[106]. Binding sites for co-chaperones have been mapped to all three domains of Hsp90, with some co-chaperones capable of binding simultaneously, whereas others compete for binding to

Hsp90[107]. Currently, there is no single criterion for categorizing all the co-chaperones identified so far. However, some well-known co-chaperones affect the ATPase activity of Hsp90 and can be grouped into ATPase stimulating and ATPase inhibiting co-chaperones. Below are some examples of co-chaperones in this category.

Hch1 and Aha1

High-copy Hsp90 suppressor protein 1 (Hch1) was identified from a genetic screen of multicopy suppressors of the temperature-sensitive (*ts*) mutation E381K of yeast Hsp90. At the time of its identification, the function of Hch1 was unknown[108]. However, it shared ~37% sequence identity and ~55% sequence similarity with the N-terminal domain of an uncharacterized yeast ORF YDR214w, which was later identified as Activator of Hsp90 ATPase activity 1 (Aha1), a stimulator of Hsp90 ATPase activity[108,109]. Aha1 and its homolog Hch1 (found in yeast) are co-chaperones known to stimulate the ATPase activity of Hsp90, with stimulation by Hch1 ~30% of Aha1[109,110]. Structurally, Aha1 is made up of two domains (Figure 1.8A): an N-terminal domain (Aha1N) connected to a C-terminal domain (Aha1C) by an unstructured linker[80]. Aha1N alone can stimulate the ATPase activity of Hsp90 to the same extent as Hch1, while Aha1C alone has no ATPase stimulating activity[109,111]. Surprisingly, a homolog of Aha1C that can stimulate the ATPase activity of Hsp90 has been identified in the protozoa *Entamoeba histolytica*[112].

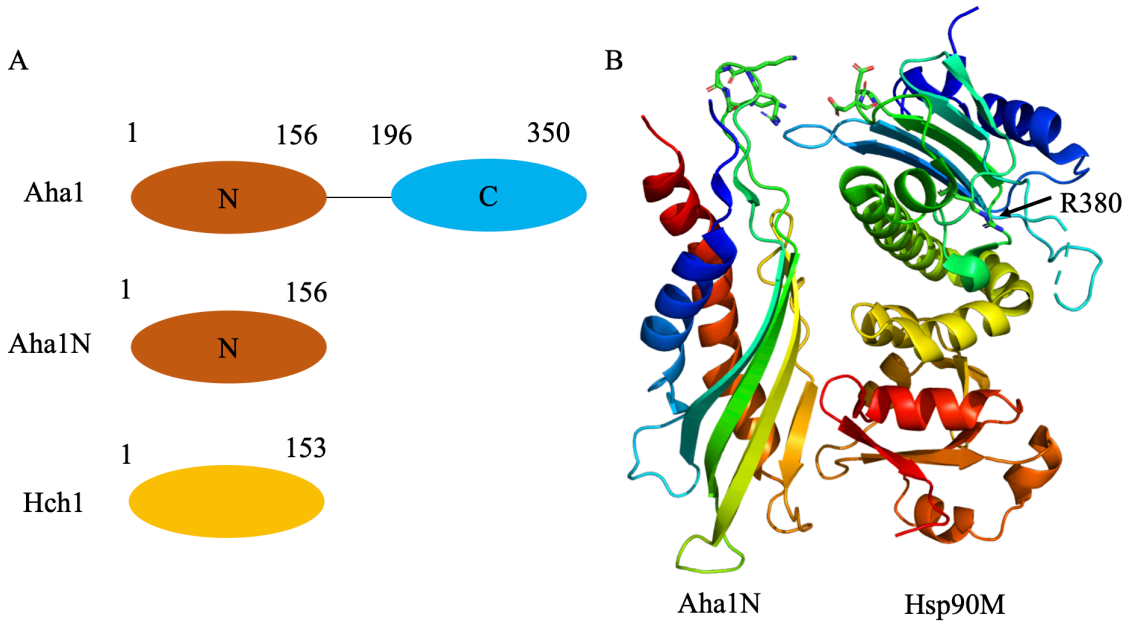

Figure 1.8: The ATPase stimulating co-chaperones Aha1 and Hch1. (A) Structural organization of Aha1 and its homolog Hch1. Aha1 N-terminal domain (orange), Aha1 C-terminal domain (blue), Hch1 (yellow). (B) Structure of Aha1N in complex with the middle domain of yeast Hsp90 (Hsp90M) colored from the N-terminus (blue) to C-terminus (red) (PDB 1USV)[80]. The conserved RKxK motif and its ion pair interaction residues (E372 and D373) are shown as sticks. R380 is shown as sticks.

Currently, a high-resolution structure of full-length Aha1 in complex with full-length Hsp90 is not available. However, a crystal structure of Aha1N (equivalent to full-length Hch1) bound to the middle domain of Hsp90 has been solved (Figure 1.8B). Also, Aha1C has been mapped to the NTD of Hsp90 based on NMR studies with isolated domains of both Aha1 and Hsp90[80,111]. Although Aha1N and Hch1 are structurally homologous and thought to bind similarly to the middle domain of Hsp90, some differences have been observed in their interactions with Hsp90. Specifically, NMR experiments with Hsp90 NTD-middle domain constructs revealed that in addition to changes observed in the Hsp90 middle domain and C-terminus of the NTD upon binding of either Aha1N or Hch1, significant changes in the NTD of Hsp90 are also observed for Hch1, which are absent for Aha1N[113]. This indicates a possible direct interaction between Hch1 and the NTD of Hsp90, bringing together the NTD

and middle domain. Moreover, differences in peak shifts and intensities have been observed between NMR spectra for an Hsp90 NTD-middle domain construct in complex with Aha1N and that for Hch1, which further highlights a difference in the mode of binding between the two homologs[113]. Accordingly, functional differences between Aha1 and Hch1 have been reported, including the resistance of yeast cells to the Hsp90 inhibitor NVP-AUY922 upon deletion of Hch1 but not Aha1. Also, Aha1 knockout yeast cells expressing the *ts* Hsp90 mutant E381K are viable, whereas Hch1 knockout cells are lethal. In addition, ATPase stimulation by Aha1 is reduced the Hsp90-E381K mutant although ATPase stimulation by Hch1 is unchanged[110,114].

The first insight into the mechanism of ATPase stimulation by Aha1 and Hch1 was obtained from the crystal structure of the Hsp90 middle domain in complex with Aha1N (Figure 1.8B). The structure showed a substantially large binding interface for the interaction between the two as well as a conformational change in the middle domain of Hsp90 that reorients the catalytic loop (residues 370-390) such that R380 adopts a conformation that can access the γ-phosphate of nucleotide bound to the NTD[80]. Also, mutations of some residues within the catalytic loop, including R380A, have been shown to impair ATPase stimulation by Aha1[57]. Interestingly, the Hsp90 middle domain-Aha1N complex reveals ion-pair interactions between a highly conserved basic RKxK (residues 59-62) motif found in all Aha1 homologs and two residues (E372 and D373) of the middle domain catalytic loop (Figure 1.8B)[80]. As a result, mutation of residues within the RKxK motif to alanine leads to impaired ATPase stimulation by Aha1 and Hch1[80,110]. Additionally, all homologs of Aha1 contain a highly conserved NxNNWHW motif (residues 5-11), which is unstructured in the Hsp90 middle domain-Aha1N complex. This motif was previously shown to have no significant effect on the *in vivo* functional activity of Aha1 and *in vitro* ATPase stimulation of Hsp90 by Aha1[80]. However, a recent study has revealed that deletion of the first eleven amino acids of both Aha1 and Hch1, which includes the NxNNWHW motif, impairs the *in vivo* functional activity and *in vitro* stimulation of Hsp90 ATPase activity by both co-chaperones[115]. The contrasting findings between these two studies has been attributed to the former research using Aha1 constructs bearing an N-terminal histidine tag.

Although the Hsp90 homodimer contains two binding sites for Aha1, binding of Aha1 to one monomer can stimulate ATPase activity in both NTDs of the dimer, consistent with an asymmetric mechanism of activation[111]. In the absence of a structure of Aha1C bound to Hsp90, NMR spectroscopy was used to identify the binding site for both Aha1N and Aha1C on Hsp90. ^{1}H-^{15}N HSQC experiments showed that Aha1N binds mainly to the Hsp90 middle domain, which substantiates the previously determined crystal structure of the Hsp90 middle domain-Aha1N complex[80,111]. Conversely, the binding site for Aha1C was localized to the interaction site between the two NTD of the Hsp90 dimer, thus stabilizing the closed dimer conformation[111]. This led to the proposal that binding of Aha1 to Hsp90 accelerates the slow conformational changes that lead to the catalytically active closed conformation, thereby stimulating the ATPase activity of Hsp90[86,87,111,116]. However, the structural mechanism that accompanies ATPase stimulation by Aha1 and Hch1 in the Hsp90 chaperone cycle remains unclear. Chapter 5 of this work explores the dynamics of Aha1 binding to Hsp90 using ^{19}F NMR, with the goal of determining the structural mechanism underlying Hsp90 ATPase stimulation by co-chaperones.

P23/Sba1

The co-chaperone p23 (in mammals) was first identified as part of a multiprotein complex made up of steroid hormone receptor, Hsp90, Hsp70, and immunophilins[117]. Sensitivity to benzoquinone ansamycin 1 (Sba1) is the yeast homolog of p23, sharing ~28% sequence identity and ~54% sequence similarity with the mammalian homolog[89,118,119]. P23/Sba1 is generally categorized as a late-acting co-chaperone due to its preference for binding to the N-terminally dimerized Hsp90 conformation[54,88,89,120]. Consistent with this, binding of p23/Sba1 to Hsp90 is dependent on the presence of ATP or ATP analogs that promote the formation of the closed dimer conformation of Hsp90[54,117,121,122]. Consequently, p23/Sba1 binding to Hsp90 is abolished in the presence of Hsp90 inhibitors such as GA, which bind the nucleotide binding pocket[118,119,121,123]. Therefore, it is not surprising that the isolated NTD of Hsp90, although capable of binding ATP and ATP analogs, cannot bind p23/Sba1 given

that the domain on its own cannot form a dimer[54]. Like most co-chaperones, Sba1 is not essential for yeast viability[118,119]. Although yeast cells lacking Sba1 exhibit mild growth defects, the loss of Sba1 does not significantly affect the chaperone activity of Hsp90 *in vivo*[118,119].

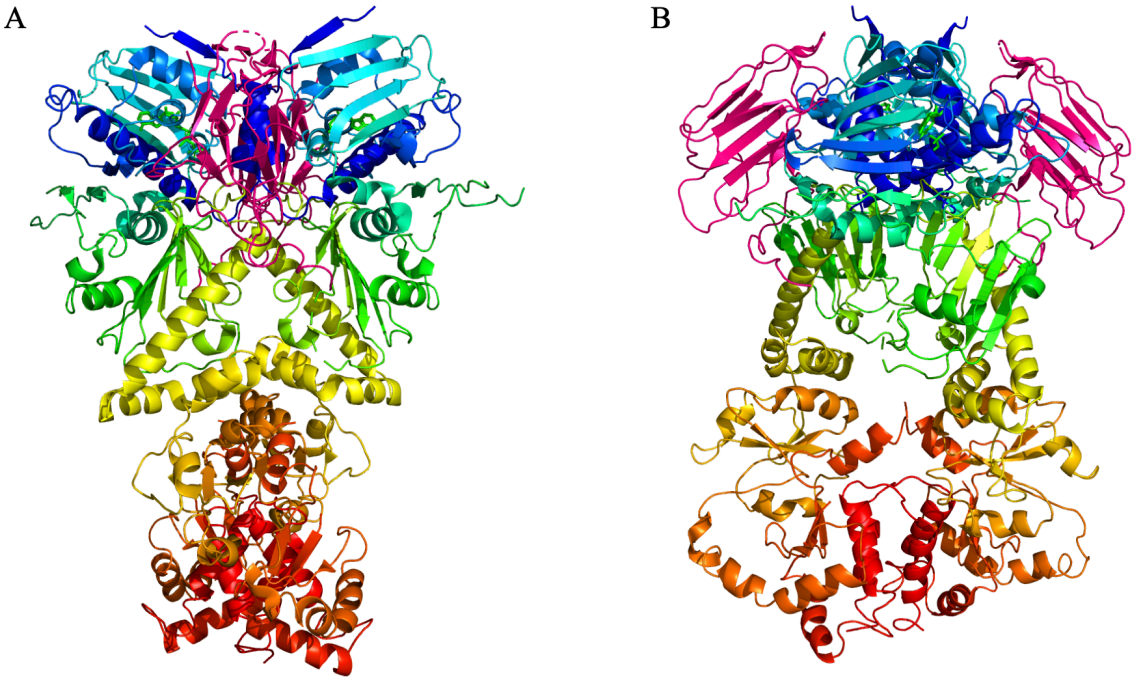

Figure 1.9: Structure of yeast Hsp90 in complex with AMPNP and the co-chaperone Sba1 (PDB 2CG9)[56]. (A) Hsp90 is colored from the N-terminus (blue) to C-terminus (red) and AMPPNP is shown as sticks. Two molecules of Sba1 (pink) each bound at the dimerization interface between the two N-terminal domains. (B) Structure A rotated to show both Sba1 molecules.

Structural detail into the binding of p23/Sba1 to Hsp90 was revealed by a crystal structure of full-length yeast Hsp90 in complex with AMPPNP and the co-chaperone Sba1[56]. The structure showed a 1:2 stoichiometry between Hsp90 and Sba1 (Hsp90 dimer: $Sba1_2$), with each Sba1 molecule bound mainly to the NTD of the closed conformation of Hsp90 (Figure 1.9). This ratio of binding is consistent with ITC and SPR experiments, which showed that two molecules of Sba1 bound the Hsp90 homodimer in the presence of

AMPPNP with a binding affinity (K_D) of 540 ± 80 nM[89]. Importantly, the Hsp90-AMPPNP-Sba1 complex provides a likely explanation for why p23/Sba1 binds Hsp90 in the presence of ATP or its analogs. Specifically, regions of the NTD and middle domain of Hsp90 that make up the binding interface between Hsp90 and Sba1 undergo local conformational changes, including NTD-NTD association, ATP-lid closure, N-terminal β-strand swapping, and NTD-middle domain association which are all induced by bound ATP. Consequently, Sba1 binds to Hsp90 once the catalytically active closed conformation is formed in order to stabilize this conformation. However, because optimal ATP hydrolysis by Hsp90 requires continuous opening and closing of the NTDs, stabilization of the closed conformation by Sba1 leads to a decrease in the ATPase activity of Hsp90, even though the ATPase activity is not completely abolished[88,89,109].

Intriguingly, a recent study has identified direct interactions between the DNA binding domain (DBD) of the tumor suppressor protein p53 and the C-terminal unstructured tail of the co-chaperone p23, which is independent of Hsp90. Given the overlapping binding sites for DNA and p23 on p53, DNA competes with p23 for binding to p53, highlighting a possible role of p23 in the modulation of DNA binding and, perhaps, transcription[124].

Hop/Sti1

The co-chaperones Hsp70-Hsp90 organizing protein (Hop) in humans and Stress inducible protein 1 (Sti1) in yeast are structural homologs that share ~42% sequence identity[125]. Hop/Sti1 is a member of the tetratricopeptide repeat (TPR) domain containing co-chaperones that constitute the largest category of Hsp90 co-chaperones. These co-chaperones contain a TPR domain made up of three or more TPR motifs (helix-turn-helix)[126], with Hop/Sti1 having nine TPR motifs that form three TPR domains; TPR1, TPR2A, and TPR2B[127]. In terms of function, Hop/Sti1 serves as a bridge that transfers substrates from the Hsp70 to Hsp90 chaperone system[128,129]. Although both Hsp70 and Hsp90 interact with Hop/Sti1 through its TPR domains, the interaction site for both chaperones on Hop/Sti1 is different, which allows simultaneous binding of the two chaperones to facilitate client transfer.

Specifically, the TPR1 and TPR2B domains of Hop interact with Hsp70 mainly through its C-terminal heptapeptide PTIEEVD motif[127,130]. On the other hand, Hsp90 mainly interacts with the TPR2A domain of Hop through its C-terminal MEEVD motif and a relatively weak interaction between TPR2B and the middle domain[127,130].

Molecular docking simulations of the Hsp90-TPR2A-TPR2B complex showed that TPR2B interacts with the middle domain of Hsp90 in an orientation that positions TPR2B between the two Hsp90 protomers hence impeding the formation of the catalytically active closed conformation[130]. This mode of interaction is consistent with a 15Å cryo-EM structure of Hsp90-Hop complex, which showed that Hop interacts with the open V-shaped conformation of Hsp90 in a manner that positions Hop between the two protomers of Hsp90[131]. However, this open conformation is more compact than the open conformation of apo *E. coli* HtpG[93,131]. Taken together, these findings provide a possible explanation for the inhibition of the ATPase activity of Hsp90 by Sti1 since Sti1 keeps Hsp90 in an open ATPase incompetent conformation. Interestingly, whereas Sti1 inhibits the ATPase activity of Hsp90, binding of Sti1 to Hsp70 stimulates ATPase activity[132,133]. In contrast, there is evidence that binding of the human homolog Hop to either Hsp90 or Hsp70 has no effect on ATPase activity in both chaperones[99,132,134]. Like most co-chaperones, Sti1is not essential for viability in yeast[135]. However, Sti1 knockout mutants exhibit growth defects at temperatures lower than 25 ºC and higher than 30 ºC. Also, these mutants display impaired activation of the Hsp90 clients GR and v-Src kinase, although the accumulation of these clients remains unchanged[135].

Post-translational Modifications of Hsp90

In addition to nucleotides and co-chaperones, the chaperone activity of Hsp90 is regulated by post-translational modifications including, phosphorylation, SUMOylation, ubiquitination, S-nitrosylation, methylation, and acetylation[136-139]. Residues involved in these modifications have been identified across all three domains of Hsp90 as well as some Hsp90 co-chaperones. Interestingly, some post-translational modification sites within Hsp90

overlap with co-chaperone and client binding sites, which adds another layer of complexity to the already intricate Hsp90 chaperone cycle. Therefore, it is no surprise that these modifications have been shown to regulate almost all aspects of the chaperone activity of Hsp90, including ATPase activity, binding and activation of clients, nucleotide binding, and interaction with co-chaperones[138]. Importantly, some post-translational modifications have been identified as allosteric switch points involved in interdomain communication across the Hsp90 chaperone[140,141].

Perhaps the most well-studied of the post-translational modifications reported so far is phosphorylation, with serine, tyrosine, and threonine identified as phosphorylation sites. Hsp90 is considered one of the most phosphorylated proteins in eukaryotic cells[142]. Several phosphorylation sites have been identified across all three domains of Hsp90, although some sites are species-dependent and isoform-specific[143]. Currently, protein kinases involved in phosphorylating most of these sites are unknown. Specific kinases that have been reported include double-stranded DNA protein kinase, Protein kinase A, B-Raf, Akt kinases, Casein kinase 2 (CK2) protein kinase, Swe1^{Wee1} kinase, and c-Src kinase, which are all Hsp90 clients[136]. Phosphorylation of T22 located within the NTD of yeast Hsp90 (T36 in human Hsp90) by CK2 reduces the ATPase activity of Hsp90 and impairs the interaction of Hsp90 with the co-chaperones Aha1 and Cdc37[144]. Likewise, phosphorylation of Y24 of yeast Hsp90 (Y38 in human Hsp90) by Swe1^{Wee1} kinase disrupts activation of some clients by Hsp90, and yeast cells lacking Swe1 exhibit increased sensitivity to the Hsp90 inhibitor GA[145]. With regards to dephosphorylation, the serine/threonine phosphatase 1 (Ppt1 in yeast), whose human homolog is protein phosphatase 5 (PP5) is a TPR-domain containing co-chaperone of Hsp90 that dephosphorylates Hsp90 and the co-chaperone Cdc37. Consequently, deletion of Ppt1 in yeast cells results in hyperphosphorylation of Hsp90 and impairs the maturation of clients by Hsp90[146]. Overall, dephosphorylation promotes the proper functioning of Hsp90 *in vivo*.

S-nitrosylation is the covalent modification of the thiol group of cysteine by nitric oxide (NO). Thus, this post-translational modification is associated with cysteine containing Hsp90 homologs, as some homologs like yeast Hsp90 have no cysteines. The human Hsp90α

homolog contains a highly conserved cysteine residue (C597) located within its CTD. Although the location of this residue is distant from the NTD ATPase hub of Hsp90, there is evidence that S-nitrosylation of C597 inhibits the ATPase activity of Hsp90 and impairs activation of Hsp90 clients[141,147]. This suggests a possible communication between the individual domains of Hsp90 and an allosteric mechanism of Hsp90 regulation. Post-translational modification of lysine by the small ubiquitin-like modifier (SUMO) protein is termed SUMOylation. K178 in yeast (K191 in humans) Hsp90 is a highly conserved residue located within the NTD. SUMOylation of this residue in one protomer of the Hsp90 dimer has been shown to facilitate the interaction of Hsp90 with the co-chaperone Aha1 and increases the sensitivity of yeast and human cells to Hsp90 inhibitors[148]. Ultimately, regulation of Hsp90 by post-translational modification is essential to the chaperone activity of Hsp90. Therefore, an in-depth understanding of these modifications will play a critical role in understanding the mechanism of client protein activation and recognition by Hsp90, which has remained enigmatic to date.

Client Proteins of Hsp90

To be considered an Hsp90 client, a protein must physically interact with Hsp90 or the inhibition of Hsp90 must impair the activity of the protein, possibly leading to its proteasomal degradation[15]. Presently, hundreds of proteins have been identified as potential Hsp90 clients. An extensive database of updated Hsp90 clients maintained by the Picard lab can be found at https://www.picard.ch/downloads/Hsp90interactors.pdf. Interestingly, the clients of Hsp90 are structurally and functionally diverse and do not possess a common sequence or structural motif. This extreme diversity among clients coupled to the highly dynamic nature of Hsp90 has made it challenging to elucidate the mechanism by which Hsp90 activates and stabilizes its clients. As a result, the role of clients in the Hsp90 chaperone cycle and the interactions of Hsp90 with its clients is currently an area of intense research in the Hsp90 field.

The diverse clientele of Hsp90 has been implicated in vital cellular processes such as cell survival and proliferation, transcriptional regulation, and signal transduction, making

Hsp90 an essential protein for maintaining proteostasis[15,147]. Protein kinases such as Akt/PKB, Cdk4, B-Raf, Plk1, Src, ERBB2, and Bcr-Abl make up the largest class of Hsp90 clients, with about 60% of all protein kinases in humans shown to interact with Hsp90[15,149]. Other classes of proteins that constitute Hsp90 clients are the Steroid hormone receptors (SHRs), including the estrogen, glucocorticoid, progesterone, mineralocorticoid, and androgen receptors as well as transcription factors such as the tumor suppressor protein p53[15]. The earliest insights into the chaperone activity of Hsp90 were obtained from extensive biochemical and mutational studies involving the steroid hormone receptor GR and the protein kinase v-Src kinase[150-152]. Hsp90 plays a critical role in the signal transduction pathway for GRs as well as other SHRs. *In vitro*, Hsp90 is a required component in the assembly of a fully functional GR-heterocomplex, and the *in vivo* activity of GR is strictly dependent on Hsp90[48,150]. There is evidence that binding of the ligand binding domain (LBD) of GR to Hsp90 stimulates the intrinsically low ATPase activity of human Hsp90 up to 200-fold[99]. Conversely, this extreme ATPase stimulation was not observed with the yeast Hsp90 homolog under similar conditions[99], highlighting the specificity of this GR-based ATPase stimulation.

The oncoprotein v-Src is one of the most stringent protein kinase clients of Hsp90[149,151-153]. Surprisingly, its cellular homolog c-Src, which shares ~98% sequence identity associates weakly with Hsp90 and is less dependent on Hsp90 for its activation and stabilization[149,151-153]. On the other hand, the mutation of c-Src residues, resulting in its modification to v-Src transforms c-Src into a stringent Hsp90 client[152,153]. This finding suggests that the intrinsic property of a protein can possibly determine if a protein can be chaperoned by Hsp90 or not. Indeed, subsequent studies identified inherent differences between c-Src and v-Src regarding their intrinsic stabilities and cooperativities in folding, which have been proposed to be determinants of Hsp90 kinase client specificity[149,152-154]. However, owing to the extreme diversity of Hsp90 clients, the possibility of extrinsic factors such as temperature, cellular interactions, and environmental conditions influencing client specificity cannot be dismissed entirely. Additionally, the specificity of Hsp90 for kinase clients has been linked to the ability of protein kinases to form stable complexes with the

kinase-specific co-chaperone Cdc37, which subsequently recruits protein kinase clients to the Hsp90 chaperone cycle[149,155].

Recent progress in biophysical techniques has provided some answers on how Hsp90 recognizes its clients. Currently, the interaction of Hsp90 with three clients (Cdk4, GR-LBD, and Tau) have been reported[13,67,77,78]. The picture emerging from these studies is that hydrophobic and amphipathic contact surfaces extend across the domains of Hsp90 over a large surface area, which serve as binding interfaces for clients. As a result, Hsp90 can recognize and accommodate those proteins whose surface features such as charge, hydrophobicity, and surface area match the properties of its binding interfaces[79,156]. Thus, the determinant of client interaction with Hsp90 is not a structural or sequence motif but rather the surface characteristics of clients. Even though some progress has been made regarding client interaction with Hsp90, the exact mechanism underlying client specificity and recognition remain largely unknown.

Model of the Hsp90 Chaperone Cycle

Models of the Hsp90 chaperone cycle have been proposed based on our current knowledge of the interactions of Hsp90 with nucleotides, co-chaperones, and clients. Importantly many more aspects of the Hsp90 chaperone cycle are yet to be uncovered. Currently, the best-characterized models are the chaperone cycles for the two most extensively studied classes of proteins that make up Hsp90 clients (SHRs and protein kinases).

A proposed model of the Hsp90 chaperone cycle for the steroid hormone receptor GR is shown in Figure 1.10. First, the Hsp70-Hsp40 complex interacts with a GR client to form a heterocomplex[157]. Next, the IEEVD motif of Hsp70 of the heterocomplex interacts with the co-chaperone Hop/Sti1[127], which is already bound to the open conformation of Hsp90 while the ligand binding domain (LBD) of GR interacts with Hsp90[158]. Hop/Sti1 interacts with the MEEVD motif and the middle domain of Hsp90 to stabilize the open conformation[130], such that Hsp90 is kept in a conformation ready to receive clients. This is followed by the binding of ATP and recruitment of a second TPR-domain containing co-chaperone belonging to the

peptidyl-prolyl cis-trans isomerase (PPIase) family of co-chaperones such as Cpr6[77]. ATP binds the nucleotide binding pocket located in the NTD of Hsp90, and the PPIase co-chaperone binds the other unoccupied MEEVD motif of the Hsp90 CTD. Once a client is transferred to Hsp90, Hsp70, Hsp40, and Hop/Sti1 leave the complex. This leads to the formation of the catalytically active closed conformation and subsequent recruitment of the co-chaperone p23/Sba1, which stabilizes the closed conformation[159]. In this conformation, the client gets activated and ATP is hydrolyzed to ADP and Pi. Finally, the activated client, co-chaperones, ADP, and Pi leave the complex and the chaperone returns to the open conformation ready for another cycle.

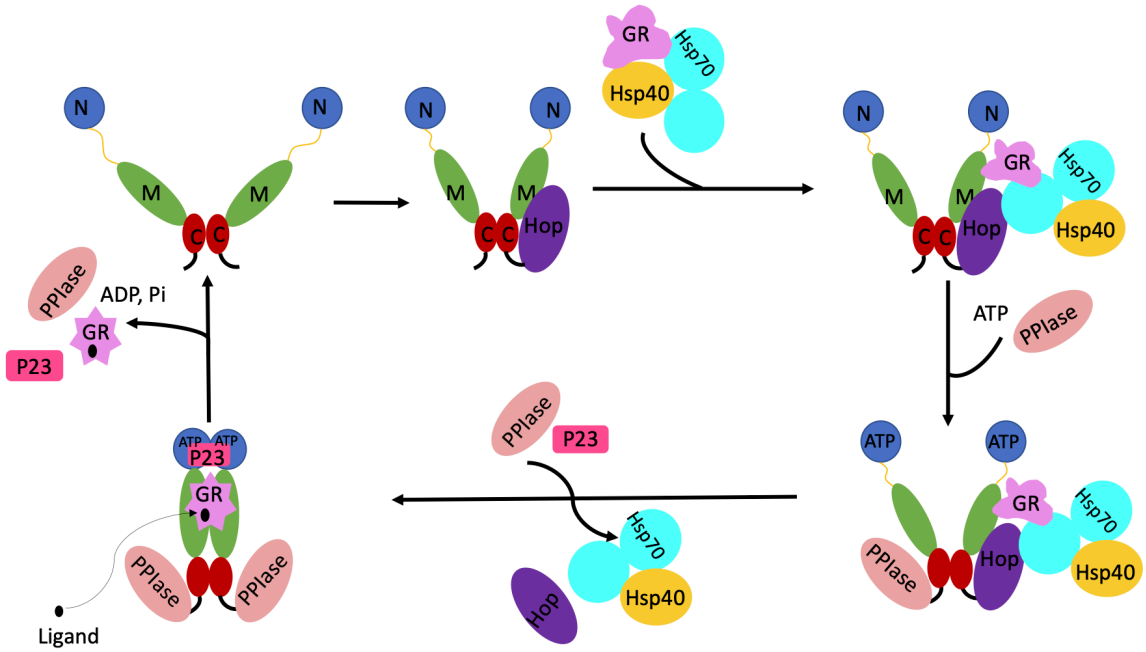

Figure 1.10: A proposed model of the Hsp90 chaperone cycle for GR. Hop/Sti1 keeps Hsp90 in an open conformation ready to receive clients from the Hsp70-Hsp40 heterocomplex. Binding of ATP and the recruitment of a PPIase releases the Hsp70-Hsp40 heterocomplex and Hop from the complex. Hsp90 adopts a catalytically active closed conformation stabilized by the co-chaperone p23/Sba1. GR is activated by the binding of a ligand, ATP is hydrolyzed, and all components leave the complex with the return of Hsp90 to an open conformation.

On the other hand, protein kinase clients are recruited to the Hsp90 complex by the kinase-specific co-chaperone Cdc37[149,155]. Also, the TPR containing co-chaperone PP5/Ppt1 is recruited, which dephosphorylates Cdc37 leading to the exit of Cdc37 from the Hsp90 complex[160], highlighting the importance of post-translational modifications in the Hsp90 chaperone cycle. Presently, what happens to clients as they navigate through the Hsp90 chaperone cycle remains unclear. Additionally, the last step in the Hsp90 chaperone cycle involving ATP hydrolysis and client exit from the cycle is poorly understood. Ultimately, the Hsp90 chaperone cycle for several clients remains elusive to date. Thus, a lot more research is needed to fully understand the chaperone activity of Hsp90.

Hsp90 in Disease

Hsp90 has been implicated in human diseases, including cancer, neurodegenerative disorders, cystic fibrosis, viral infections, and protozoan infections[104]. This is not surprising given the diverse range of cellular processes that are directly or indirectly regulated by Hsp90. In addition, some co-chaperones of Hsp90 such as Aha1, Hop/Sti1, and Cdc37 have been associated with disease pathogenesis, which further highlights the importance of targeting Hsp90 as well as its co-chaperones in the development of therapeutic interventions. For instance, the ATPase stimulating co-chaperone Aha1 has been implicated in the pathogenesis of cystic fibrosis through its effect on the stabilization of cystic fibrosis transmembrane conductance regulator (CFTR), which is an Hsp90 client. Particularly, a mutant version of CFTR ΔF508 with impaired folding has been implicated in the pathogenesis of cystic fibrosis, and downregulation of Aha1 has been shown to redeem this impairment[161]. Over the years, the role of Hsp90 in carcinogenesis has received a lot of attention because Hsp90 inhibitors have shown promising potential as therapeutic agents for cancer. Recently, there has been an increasing interest in the role of Hsp90 in neurodegeneration as numerous Hsp90 clients have been implicated in neurodegenerative disorders, including Alzheimer's and Parkinson's diseases.

Hsp90 in Cancer

The initial identification of unusually higher than normal levels of Hsp90 in tumor cells sparked an immense interest in research on the role of Hsp90 in the pathogenesis of cancer[10]. Indeed, subsequent studies confirmed that overexpression of Hsp90 is linked to poor prognosis in breast cancers[162,163], which highlighted the possible utilization of Hsp90 as a prognostic biomarker. Several Hsp90 clients have been identified as oncoproteins that are either upregulated or mutated in tumors, including RAF-1, ERBB2/HER2, androgen and estrogen receptors, PKB/Akt, mutant p53, and EGFR[164]. During tumorigenesis, there is increased expression of Hsp90 due to the cellular stress induced by the oncogenic process. As a result, oncoproteins become much more dependent on Hsp90 for survival, and inhibition of Hsp90 has been shown to facilitate the proteasomal degradation of oncoproteins[165]. Consequently, one of the major current activities in the Hsp90 field is the development of Hsp90 inhibitors as therapeutic agents for cancer.

Knowledge of the role of Hsp90 in carcinogenesis has come from studies of the tumor suppressor protein p53. Several mutations in p53 that lead to loss of tumor suppressor function have been implicated in ~50% of human cancers[166,167]. Following its mutation, p53 becomes dependent on Hsp90 for its stabilization and activation[168,169]. Also, mutant p53 is found in stable multichaperone complexes with Hsp90, Hsp70, Hsp40, and co-chaperones, which is thought to confer resistance to ubiquitination and impairs its proteasomal degradation[168]. Consequently, inhibition of the activity of Hsp90 by the Hsp90 inhibitor GA disrupts the multichaperone complexes formed by mutant p53 and leads to proteasomal degradation of the protein[168]. Although Hsp90 interacts with wildtype p53 and stabilizes its native conformation, this interaction is short-lived and independent of other molecular chaperones, leading to the susceptibility of wildtype p53 to proteolysis and degradation[168,170,171]. Thus, both wildtype and mutant p53 are Hsp90 clients, albeit interaction with Hsp90 in each case leads to a different outcome.

The structural architecture of p53 has been solved using a combination of X-ray crystallography, NMR, and other biophysical techniques. These studies have revealed that p53 is made up of folded domains (DBD and tetramerization domain) as well as unstructured

regions, which explains why the protein is inherently unstable[172,173]. Interestingly, binding of Hsp90 to p53 has been mapped to the DBD, which is a folded domain[171], and a great majority of p53 mutations that lead to the pathogenesis of cancer have also been linked to this region[172]. Additionally, these mutations abolish DNA binding to p53, since the DBD is the site for the interaction of p53 with DNA. Also, there is evidence that Hsp90 interacts with highly unfolded DBD[174] as well as a molten globule-like state of the DBD made up of a heterogenous ensemble of structures[175]. Taken together, although the DBD of p53 mediates its interaction with Hsp90, it remains unclear whether this interaction involves the folded or unfolded form of the DBD. Perhaps Hsp90 can bind all three states (folded, unfolded, and molten globule-like)[171,174,175] that have been reported given the highly dynamic nature of the Hsp90 chaperone. In addition to the stabilization of mutant p53 by Hsp90, Hsp90 bound mutant p53 can form heterocomplexes with wildtype p53, which further interferes with the function of the normal protein[9]. Thus, the proteasomal degradation of mutant p53 through the inhibition of Hsp90 activity is a critical therapeutic intervention for cancer.

Hsp90 in Neurodegeneration

The accumulation of misfolded proteins and protein aggregates in neurons has been linked to several neurodegenerative diseases[176], with age considered a major risk factor for most of these diseases. A possible explanation for this is that normal aging might lead to a decline in the expression and activity of molecular chaperones, resulting in the accumulation of misfolded proteins in neurons[177]. Given the role of Hsp90 in the stabilization and activation of diverse clients, it is not surprising that Hsp90 has been implicated in protein misfolding disorders such as Alzheimer's disease, Parkinson's disease, Huntington's disease, Creutzfeldt–Jakob disease, and Gaucher's disease.

In the case of Alzheimer's disease, the hyperphosphorylated tau protein and amyloid-β protein, which have been implicated in disease pathogenesis, are Hsp90 clients[178]. The inhibition of Hsp90 has been shown to eliminate tau aggregation in cellular and mouse models of tauopathies[179]. Also, the ATPase stimulating co-chaperone Aha1 in the presence

of Hsp90 increases tau aggregation, and overexpression of Aha1 in mice models lead to neuronal loss and cognitive impairment[180]. Consequently, the inhibition of Aha1 leads to a reduction in the accumulation of insoluble tau proteins[180], highlighting the potential of targeting Hsp90 and its co-chaperones in the treatment of tauopathies.

The accumulation of toxic aggregates of α-synuclein in Lewy bodies has been associated with the pathogenesis of Parkinson's disease (PD). Hsp90 is the most dominant molecular chaperone that associates with α-synuclein in Lewy bodies, and increased levels of Hsp90 have been found in the brains of PD patients[181,182]. Moreover, brain permeable Hsp90 inhibitors have shown promising potential as therapeutic agents for PD by hindering α-synuclein-induced toxicity and oligomerization[183]. Altogether, targeting Hsp90 in the development of therapeutic interventions for neurodegenerative diseases seems promising, considering how Hsp90 is directly involved in various aspects of neurodegeneration.

Hsp90 Inhibitors

Earlier studies on the mechanism of activation and transformation of the oncoprotein v-Src kinase led to the discovery of the first Hsp90-specific inhibitor[184]. The first group of inhibitors to be discovered were the naturally occurring molecules GA and RA[184,185]. Subsequent structural studies revealed that both GA and RA compete with ATP for binding to the nucleotide binding pocket located in the NTD of Hsp90[65,66]. Given that the binding affinities for both GA (K_D = 1.2 μM) and RA (K_D =19 nM) are higher than ATP[66], binding of ATP to Hsp90 is abolished in the presence of these inhibitors, which explains why the chaperone activity of Hsp90 gets compromised. Insights into the pharmacological application of Hsp90 inhibitors as therapeutic agents came from the observation that binding of GA and RA to Hsp90 led to proteasomal degradation of a diverse range of proteins including several oncoproteins. This inhibitor-based proteasomal degradation is mediated by the recruitment of the E3 ubiquitin ligase Carboxy-terminus of Hsp70-interacting protein (CHIP) to the chaperone complex[186].

Over the years, research into the development of Hsp90 inhibitors as therapeutic agents for cancer has received a lot of attention. Unfortunately, the two pioneering Hsp90 inhibitors GA and RA were not suitable candidates for clinical development because GA exhibited high toxicity[187], whereas the reactive structure of RA made it highly unstable *in vivo*. This led to the development of a new generation of GA and RA derivatives with improved pharmacological properties and lower toxicities. The GA derivative 17-AAG (17-Allylamino-17-demethoxygeldanamycin) exhibited comparable properties to GA but with lower toxicity, which led it into clinical trials[188,189]. This was followed by the development of more soluble analogs of 17-AAG such as 17-desmethoxy-17 N,N0-dimethylaminoethylamino geldanamycin (17-DMAG) and the hydroquinone salt IPI-504, which went into clinical trials as well[190,191]. Unfortunately, clinical trials for 17-AAG and 17-DMAG were discontinued in 2008 due to toxicity. Although the RA derivative radicicol oxime showed improved stability[192], it did not progress into clinical trials. However, based on the resorcinol moiety of RA, resorcinol containing molecules were explored through high throughput screening and fragment-based drug discovery, which led to the identification of STA-9090, NVP-AUY922 and other small molecule inhibitors[55].

Another generation of Hsp90 inhibitors that are being explored currently are synthetic small molecule inhibitors that mimic the structure of ATP. This includes the purine and purine-like Hsp90 inhibitors, some of which have progressed into clinical trials[193]. A lot more Hsp90 inhibitors that bind the NTD have been developed, which are at different stages of pre-clinical and clinical evaluation with promising potential. Although about eighteen Hsp90 inhibitors that bind the NTD have entered clinical trials[194], none of these inhibitors has been approved as a cancer drug due to challenges with efficacy and toxicity at the clinical level. Currently, research into Hsp90 inhibitors that bind the CTD such as novobiocin and its analogs is being explored. One major advantage of CTD inhibitors over NTD inhibitors is that the induction of Hsp70 and other molecular chaperones (heat shock response) associated with NTD inhibitors is not observed for CTD inhibitors[9]. Also, other inhibitors including derrubone, withaferin A, and celastrol, which disrupt the interaction between the co-

chaperone Cdc37 and Hsp90[147] have shown promising potential as therapeutic agents for cancer, although none of these have advanced into clinical trials.

The prospects for Hsp90 inhibitors as therapeutic agents for cancer look promising, albeit more work is needed to improve clinical outcomes. A combinatorial approach of targeting other molecular chaperones like Hsp70 will alleviate the negative effect of heat shock response associated with NTD inhibitors. Accordingly, in-depth exploration of inhibitors that do not elicit a heat shock response including CTD inhibitors is needed. Also, more research on other modes of Hsp90 inhibition such as targeting specific co-chaperones and post-translational modifications will identify novel therapeutics for cancer. Finally, toxicities associated with inhibitors can be reduced by targeting specific Hsp90 clients.

Biophysical Techniques for the Study of Hsp90 Dynamics

Hsp90 is a highly dynamic molecular chaperone, and its chaperone activity is modulated by local and global conformational changes that transition the chaperone from an open conformation to a catalytically active closed conformation. Accordingly, research into the structural dynamics of Hsp90 is required to better understand the molecular mechanism underlying its chaperone activity. In the work presented here, we used a variety of NMR techniques to study diverse dynamic processes occurring in the Hsp90 chaperone, including sidechain dynamics, nucleotide binding, ATP-lid dynamics, and conformational transitions.

NMR Methods for Studying Protein Dynamics

Proteins in solution are intrinsically dynamic molecules undergoing motions over a wide range of timescales from femtoseconds to hours. Motions detected over these timescales include bond vibrations, sidechain rotations, loop motions, molecular tumbling, and conformational transitions. The importance of these inherent motions is underscored by the diverse functions of proteins modulated by structural dynamics, including the rate and pathway of protein folding, enzymatic catalysis, and allosteric regulation[195].

Nuclear magnetic resonance (NMR) spectroscopy is one of the most potent tools employed in studying the structure and dynamics of proteins as it provides access to quantitative information at atomic resolution. The main limitation of conventional solution-state NMR has been protein size given that experiments with large molecular weight proteins are typically challenging. Consequently, strategies to overcome this size limitation are an area of intense research in the NMR field. Currently, high magnetic field strength spectrometers, new isotopic labeling techniques, and novel NMR pulse sequences have been developed, making it possible to study large proteins with molecular weights up to ~1 MDa[196]. Although the application of these modern strategies launched a new era of studying high molecular weight proteins by NMR, the cost and time involved in their use are very high compared to conventional NMR.

Several NMR techniques such as nuclear spin relaxation (NSR), Carr-Purcell Meiboom-Gill (CPMG) relaxation dispersion, dynamic NMR, lineshape analysis, and paramagnetic relaxation enhancement (PRE) have been developed to probe molecular motions over diverse timescales. These NMR techniques exploit the concept of chemical exchange, which arises from environmental changes of a dynamic molecule and simultaneous changes in NMR chemical shift. In the case of a two-state exchange process such as ligand binding and unbinding, the effect of chemical exchange observed in the NMR peaks for the two states depends on the relative population (p_a and p_b), frequency of precession (ω_a and ω_b), chemical shift difference ($\Delta\omega = |\omega_a - \omega_b|$), and the rate of exchange ($k_{ex} = k_a + k_b$). Consequently, the relationship between k_{ex} and $\Delta\omega$ is used to characterize the exchange regime of dynamic processes. For the slow exchange regime on the NMR timescale, $k_{ex} \ll |\Delta\omega|$ with distinct NMR peaks observed for each state. On the other hand, if $k_{ex} \gg |\Delta\omega|$ the exchange is fast on the NMR timescale and a single peak depicting the average of the two states is observed. In the intermediate exchange regime on the NMR timescale, $k_{ex} \approx |\Delta\omega|$ and a single peak with a broad linewidth contributed by the exchange process is observed.

The application of an NMR technique as a probe for a dynamic process depends on the exchange regime of the process. For instance, whereas CPMG relaxation dispersion is employed in the analysis of processes in the time window of molecular motion ranging from

microseconds (μs) to milliseconds (ms), NSR is more suited for processes in the picoseconds (ps) to nanoseconds (ns) timescales[195]. In this work, we employed various NMR methods to probe dynamic processes occurring in the Hsp90 chaperone (Figure 1.11)

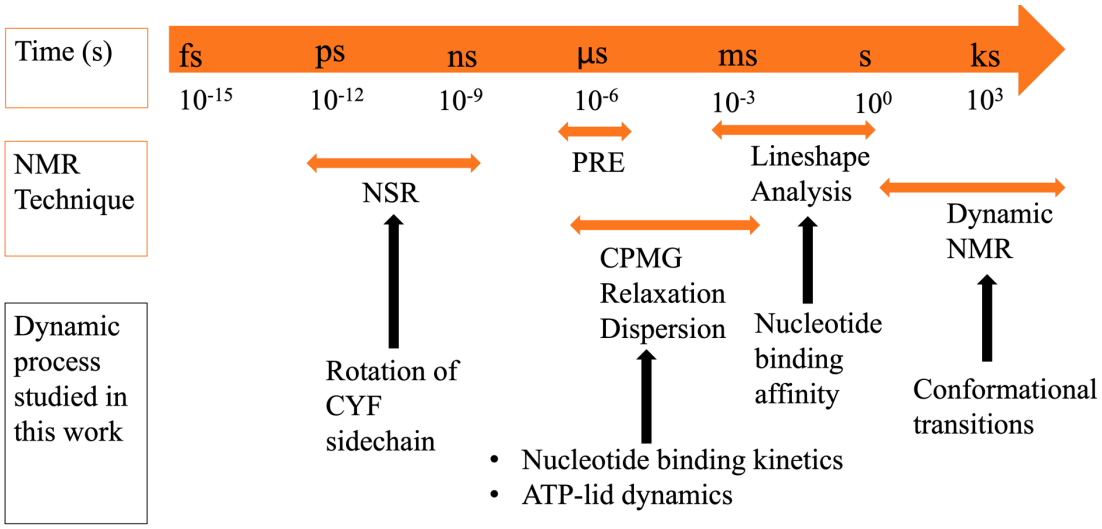

Figure 1.11: Schematic diagram of the timescales of protein motion showing suitable NMR techniques that can be used as a probe for each timescale and the corresponding dynamic process explored in this work. Image adapted from ref 195.

Nuclear Spin Relaxation (NSR)

NSR rate is the time it takes a nuclear spin to return to equilibrium after being perturbed by a radiofrequency (RF) pulse. NSR is typically employed in the analysis of molecular motion in the ps-ns timescale, which includes bond vibrations and liberation, sidechain rotations, and loop motions[195]. The NSR approach uses a combination of the longitudinal relaxation time (T_1), transverse relaxation time (T_2), and heteronuclear nuclear Overhauser effect (hnNOE) of a protein to quantify its overall rotation and internal dynamics[197]. The longitudinal relaxation time T_1 ($1/R_1$) is the time it takes for magnetization to return to the z-axis (that is aligned with the magnetic field). In an NMR experiment, T_1 determines the rate of acquisition of an NMR spectrum. A long T_1 means the recovery rate of magnetization is slow; thus, the time it takes to acquire a spectrum is long. Conversely, the transverse relaxation time T_2

($1/R_2$) is the time it takes for magnetization to dephase from the x-y plane, which determines the rate of decay of the free induction decay (FID). The more rapidly a signal decays, the shorter the T_2 relaxation time and the broader the NMR linewidth. The hnNOE on the other hand involves through-space transfer of magnetization from one nucleus to a different nucleus. The primary source of NSR is magnetic field fluctuations caused by the molecular motion of a protein placed in a magnetic field. This occurs via several mechanisms including dipole-dipole relaxation, chemical shift anisotropy (CSA), scalar coupling, quadrupolar relaxation, and spin rotation.

NSR experiments are frequently used to characterize mainchain and sidechain protein dynamics[197]. Model-free analysis and its extension of NSR rates allows the interpretation of mainchain and sidechain dynamics in terms of a generalized order parameter S^2 and an internal correlation time τ_i[198-200]. S^2 specifies the degree of freedom of a given bond vector. A value of 0 indicates no restriction in motion, whereas a value of 1 indicates total restriction in motion. τ_i is the rate of motion of a given bond vector typically on a fast NMR timescale of ps-ns. Also, it is possible to compute site-specific order parameters from MD simulations to complement NMR studies. A correlation function for a given bond vector, extracted from an MD simulation can subsequently be used to predict NMR relaxation parameters[201]. In chapter 2 of this work, we used a blend of NSR rates and MD simulations to interpret the internal dynamics of the sidechain of a trifluoroacetone cysteine derivative (CYF), which was incorporated into Hsp90 to serve as a probe for studying Hsp90 dynamics.

CPMG Relaxation Dispersion

CPMG relaxation dispersion experiments are employed in the analysis of molecular motions on the μs-ms timescale. Such motions include ligand binding and release, protein folding and unfolding, and loop motions[195,202]. As mentioned above, for exchange processes occurring in the intermediate regime ($k_{ex} \approx |\Delta\omega|$), increased broadening of the observed linewidth originates from an exchange contribution. Accordingly, this broadening contributes to the effective transverse relaxation rate ($R_{2,\,eff} = R_{2,\,0} + R_{2,\,ex}$), where $R_{2,\,0}$ is the transverse relaxation rate in the absence of exchange and $R_{2,\,ex}$ is the transverse relaxation rate

contributed by the exchange process. The CPMG relaxation dispersion experiment works by rephasing this exchange broadening through a series of 180° pulses (spin echo) applied along the x- or y-axis. In a CPMG relaxation dispersion experiment, NMR spectra are collected for a specific number of points at different frequencies ($\nu_{CPMG} = 1/4\tau_{CPMG}$) by varying the delay ($\tau_{CPMG}$) between the 180° pulse for each point at a fixed relaxation time, T. Subsequently, the signal intensity (I) for each point is extracted and used to calculate the effective transverse relaxation rate, $R_{2,\,eff} = (-1/T)\,\mathrm{Log}[I/I_o]$, where I_o is the signal intensity in the absence of a relaxation delay. Values for $R_{2,\,eff}$ are then used to generate a dispersion profile (a plot of $R_{2,\,eff}$ versus ν_{CPMG}). Based on the exchange regime (fast, intermediate, or slow) of the underlying process, the dispersion profile can be fit to an equation for two-site chemical exchange[203-205]. From the equations, kinetic parameters for the exchange process such as the rate of exchange (k_{ex}), chemical shift difference ($\Delta\omega$), and relative populations of each state (p_a, p_b) can be extracted. It is important to carry out CPMG relaxation dispersion experiments at two different magnetic field strengths for a more reliable characterization of kinetic parameters.

In chapter 3 of this work, we explored the kinetics of nucleotide binding and local dynamics of an ATP-lid structure located in the N-terminal domain of Hsp90 using a combination of CPMG relaxation dispersion, nuclear spin relaxation (NSR), and MD simulations. Consequently, we were able to characterize the rate of exchange (k_{ex}) for nucleotide binding to Hsp90 and revealed an underlying mechanism for ATP-lid closure, which is a prerequisite for ATP hydrolysis by Hsp90.

Dynamic NMR Spectroscopy

Dynamic NMR spectroscopy is perhaps the most direct technique of quantifying dynamic processes occurring in the seconds timescale, such as conformational changes, protein folding, and domain motions[195]. In practice, a dynamic process is initiated during a dead time by changing conditions of a protein already in an NMR tube. This can be in the form of changes in temperature, pH, the addition of a ligand or denaturation agent, and subsequent collection of a series of NMR spectra over a specific time. Direct spectral changes from one

state to the other in the form of either an increase or decrease in signal intensity or linewidth are monitored over time. Intensities for all peaks are then extracted, and the rate of change of each peak can be fit to an appropriate model to extract kinetic parameters such as the rate of exchange (k_{ex}), and the relative populations of each state (p_a, p_b). Importantly, the experimental set-up for dynamic NMR requires the interconverting states of a protein to have different chemical shifts in order to avoid signal overlap.

Hsp90 transitions from an open conformation to a catalytically active closed conformation to activate its clients. In chapters 4 and 5 of this work, we explored the dynamics of these conformational changes in the presence of nucleotides and the influence of ATPase stimulating co-chaperone Aha1 on the opening and closing of Hsp90 using dynamic NMR.

Fluorine-19 (^{19}F) NMR Spectroscopy of Proteins

Fluorine-19 (^{19}F) is an NMR active nucleus with spin ½ quantum number. ^{19}F NMR has been remarkably valuable for dynamic studies of high molecular weight proteins, which would otherwise be more challenging to study by conventional NMR. The popularity of ^{19}F NMR for the study of protein dynamics may be due to the several advantages of the ^{19}F nucleus over other NMR active nuclei. Particularly, the ^{19}F nucleus is 100% abundant, having only one isotope and does not occur naturally in proteins[206-208]. The advantage of this is an absence of background signals from other isotopes and endogenous nuclei. Thus, the only signals detected are those from the protein of interest, which reduces the complexity of ^{19}F NMR spectra of proteins. Also, the van der Waals radius of fluorine (0.14 nm) is only slightly higher than that of hydrogen (0.12 nm)[208], hence the replacement of a hydrogen with a fluorine is expected to have minimal structural perturbation in proteins. Indeed, several studies have substantiated this observation by showing that the incorporation of ^{19}F does not perturb the structure and function of proteins[209-213]. However, significant structural and functional perturbations have also been reported in a few cases[214,215]. Additionally, the ^{19}F nucleus is highly sensitive owing to its high gyromagnetic ratio, which is only slightly lower than ^{1}H among the spin ½ NMR active nuclei. Moreover, the ^{19}F spectrum spans a wide range

of chemical shifts (~400 ppm for ^{19}F compared to ~13 ppm for ^{1}H)[207], which makes the nucleus highly sensitive to subtle environmental changes. These advantages of the ^{19}F nucleus are exploited in ^{19}F NMR to study dynamic processes occurring in proteins.

Incorporation of ^{19}F into Proteins

The ^{19}F nucleus does not occur naturally in proteins. Hence proteins must be labeled with ^{19}F to enable protein ^{19}F NMR studies. Generally, ^{19}F is incorporated into proteins either by biosynthetic incorporation of fluorinated amino acid analogs during protein expression or chemical modification of amino acids with fluorinated reagents post expression. Each method of ^{19}F incorporation comes with a set of advantages and disadvantages, which should be considered when choosing a suitable ^{19}F label.

Biosynthetic Incorporation of Fluorinated Amino Acid Analogs into Proteins

In this labeling technique, fluorinated amino acid analogs are included in a bacterial growth medium during protein expression. Currently, several fluorinated amino acid analogs of both aliphatic and aromatic amino acids are commercially available. Notably, the successful incorporation of mono- and multiple (di-, tri-, tetra-, penta-, and to some extent hexa-) fluorinated aliphatic amino acid analogs of alanine, valine, leucine, isoleucine, methionine, and histidine into proteins have been reported by several studies[216]. Likewise, fluorinated analogs of all three aromatic amino acids (tryptophan, tyrosine, and phenylalanine) are commercially available, albeit the monofluorinated aromatic amino acid analogs are more commonly employed in ^{19}F NMR studies of proteins[216]. The biosynthetic incorporation of fluorinated amino acid analogs into proteins is achieved using a bacterial strain that is auxotrophic for that amino acid. Therefore, subsequent addition of the fluorinated amino acid of interest to the growth medium is required prior to induction of protein expression[206,216,217]. Another alternative in the case of fluorinated aromatic amino acid analogs is the addition of glyphosate to inhibit the synthesis of endogenous aromatic amino acids, and subsequent

addition of the fluorinated aromatic amino acid analog of interest and other non-fluorinated aromatic amino acids to the growth medium[216,218].

The method of biosynthetic ^{19}F labeling mentioned above allows for uniform incorporation of specific fluorinated amino acids in a protein during biosynthesis. However, it is possible to incorporate amino acids at specific sites in cases where uniform labeling of all sites might be undesirable. Site-specific biosynthetic incorporation of fluorinated amino acid analogs can be achieved using an orthogonal tRNA/aminoacyl-tRNA synthetase pair[219,220]; where an acylated suppressor tRNA can insert a specific fluorinated amino acid analog at a specific position in a protein in response to a stop codon. The technique has been used successfully to site-specifically incorporate some fluorinated amino acids such as 4-trifluoromethoxyphenylalanine (tfm-Phe) into proteins with increased expression yields[219]. Importantly, the prospects of site-specific ^{19}F labeling of proteins for ^{19}F NMR studies are enormous, especially for high molecular weight proteins owing to improvements in expression yield, prevention of heterogeneously labeled proteins, and avoidance of spectral crowding for large proteins, thus a simplification of the ^{19}F NMR spectrum.

The use of an auxotrophic bacterial expression system for biosynthetic incorporation of ^{19}F is the most widely used method of labeling proteins with ^{19}F. Consequently, this method is applicable to proteins that can be expressed successfully in bacterial systems. However, it should be noted that successful expression of a fluorinated amino acid analog in a yeast system has also been reported[221]. Although the site-specific method of biosynthetic labeling has addressed some drawbacks of the traditional auxotrophic method such as low expression yield, concurrent expression of unwanted unlabeled amino acids, and spectral crowding, chemical modification of a specific amino acid is an alternative method of ^{19}F incorporation into proteins. This method can be employed in situations where biosynthetic incorporation of ^{19}F is not feasible.

Chemical Modification of Amino Acids with Fluorinated Reagents

Chemical modification of amino acids with fluorinated reagents after protein expression is a much cheaper and direct alternative of labeling proteins with ^{19}F. In this method, a fluorinated

reagent reacts with the sidechain of a specific amino acid through a nucleophilic substitution reaction. Several fluorinated reagents that react with the highly nucleophilic sulfhydryl group of cysteine have been reported[222]. Generally, not many inherent cysteines are found in proteins; hence potential challenges with spectral crowding and resonance assignments are avoided with this labeling technique. Additionally, cysteine can be engineered at specific sites through site-directed mutagenesis, which allows for site-specific labeling with a fluorinated reagent. Cysteine reactive fluorinated reagents commonly used in labeling proteins include 3-bromo-1,1,1-trifluoroacetone (BTFA), 3-bromo-1,1,1-trifluoropropan-2-ol (BTFP), 2-bromo-N-(4-(trifluoromethyl)phenyl)acetamide (BTFMA), N-(4-bromo-3-(trifluoromethyl)phenyl)acetamide(3-BTFMA), 1-bromo-3,3,4,4,4-pentafluorobutan-2-one (BPFB), and 2,2,2-trifluoroethyl-1-thiol (TFET)[222]. Interestingly, the source of ^{19}F signal in all the reagents mentioned above is a trifluoromethyl ($-CF_3$) moiety. Some specific advantages of a trifluoromethyl probe for ^{19}F NMR studies include an increase in signal arising from three equivalent ^{19}F nuclei and limitation of CSA contribution to ^{19}F NMR linewidth (narrow linewidth) due to fast rotation about the methyl CF_3 axis. This is especially important for studies of large molecular weight proteins at higher magnetic field strengths because the contribution of CSA to ^{19}F relaxation, which leads to an increase in linewidth increases with the square of the magnetic field strength[223].

The most popular reagent for ^{19}F labeling is BTFA[216]. This is not surprising given the relatively small size of BTFA compared to the other reagents. Also, the lack of scalar coupled protons to the CF_3 moiety eliminates the need for proton decoupling and reduces the contribution of dipolar relaxation to the ^{19}F NMR linewidth. We have quantified the motional contribution of the sidechain of a cysteine modified with BTFA (CYF) to the ^{19}F NMR linewidth in terms of a principal order parameter S^2 and an internal correlation time (τ_i). Not surprisingly, the entire sidechain is very flexible with an S^2 of ~0.11 ± 0.02, which further explains the narrow ^{19}F NMR linewidths of proteins tagged with a BTFA[224]. Reasonably, one way of increasing the signal and sensitivity of ^{19}F probes will be to utilize highly fluorinated reagents. However, this can be disadvantageous in terms of structural perturbations because although the replacement of a single hydrogen with fluorine minimally perturbs the structure of a protein, the volume occupied by a CF_3 moiety is significantly larger than the volume

occupied by a CH_3 moiety[208]. Accordingly, this increase in volume increases with increasing fluorination. Thus, significant structural perturbations can be expected with the use of highly fluorinated probes.

Given that the incorporation of ^{19}F into proteins by chemical modification occurs post expression, issues with expression systems and yield are abrogated. This is particularly important for large molecular weight proteins where unconventional expression systems might be problematic, and yield might be minimal. Also, this method of labeling is a relatively more straightforward option for site-specific ^{19}F labeling of proteins. However, in cases where a cysteine(s) is introduced or eliminated from a protein through mutagenesis, potential structural and functional perturbations arising from such mutations must be examined. Moreover, this labeling method is not feasible when the cysteine of interest is buried thus, not available for chemical reaction.

It should be noted that the amino group and N-terminus of lysine, as well as the hydroxyl groups of serine, tyrosine, and threonine, are labile to chemical reaction with some fluorinated reagents, albeit to a much lesser degree[216]. Regardless of the method used for labeling proteins with ^{19}F, the structure and function of proteins before and after labeling must be examined to confirm wildtype properties, although deviation from wildtype properties after ^{19}F incorporation is generally rare. A possible reason for deviation from wildtype properties might be due to the significant differences in electronegativities between proton and fluorine as well as differences in bond lengths between the C-H bond (1.0 Å) and C-F bond (1.4 Å)[225]. Ultimately, the choice of a suitable method of ^{19}F incorporation into proteins will depend on several factors, including cost, intrinsic properties of a protein, the type ^{19}F NMR experiment, magnetic field strength, and availability of suitable labeling materials.

Applications of ^{19}F NMR in the Study of Protein Dynamics

^{19}F NMR has evolved into a powerful tool for studying a wide range of dynamic processes occurring in proteins. This is especially beneficial for studying large proteins and protein complexes whose molecular weights limit them for conventional solution-state NMR studies.

Perhaps the advancements in ^{19}F NMR of proteins emanate from progress in ^{19}F NMR-based techniques, more efficient site-specific ^{19}F labeling methods, and improved ^{19}F probes coupled to the exceptional sensitivity of the ^{19}F nucleus to its environment.

Protein Folding and Misfolding

To function properly, most proteins must fold into their native three-dimensional structures. Accordingly, studies into the mechanism of protein folding are an area of intense research. Contrary to methods such as absorbance, fluorescence, and circular dichroism (CD) spectroscopy used to probe for global changes during protein folding, ^{19}F NMR has enabled detailed exploration of site-specific changes along the protein folding pathway. For instance, using a 6-fluorotryptophan probe, dynamic ^{19}F NMR experiments were employed to monitor changes within specific regions of *E. coli* dihydrofolate reductase (DHFR) during urea-induced unfolding. Direct observation of spectral changes with time showed that DHFR unfolds by two pathways; the first pathway is rapid involving 20% of the protein, whereas the second pathway involving 80% of the protein is much slower[226].

^{19}F NMR has been successful in identifying intermediates of the protein folding pathway, which has been one of the most difficult areas of protein folding studies. In this regard, ^{19}F NMR was used to investigate the behavior of all eight phenylalanine (4-fluorophenylalanine probe) of a slow folding mutant (G121V) of rat intestinal fatty acid binding protein (IFABP) during the process of folding. Dynamic ^{19}F NMR experiments allowed for direct observation of distinct phases of folding, including a transient intermediate forming phase as well as specific residues involved in each phase[227]. Also, using a 3-fluorophenylalanine probe, the dynamics of an intermediate along the folding pathway of the calcium-binding protein calmodulin (CaM) after temperature-induced denaturation was investigated with ^{19}F CPMG relaxation dispersion experiments coupled to near-UV CD[228].

A detailed understanding of the mechanism of protein misfolding and aggregation is essential given the increasing number of protein-misfolding diseases. Many of these diseases are characterized by the accumulation of amyloid fibrils, whose process of formation is believed to be complex. Specifically, the accumulation of amyloid fibrils in islet amyloid

polypeptide (IAPP) has been implicated in type II diabetes, whereas amyloid-beta (Aβ) peptide aggregation, which leads to the formation of amyloid plaques, is associated with Alzheimer's disease[229,230]. To elucidate the mechanism of amyloid formation in IAPP, dynamic ^{19}F NMR experiments were used to follow amyloid formation using a 4-trifluoromethylphenylalanine probe. In this study, amyloid fiber formation in IAPP was shown to proceed without the accumulation of nonfibrillar intermediates[229]. In contrast, dynamic ^{19}F NMR experiments using a trifluoromethionine probe identified six distinct oligomers along the pathway of Aβ aggregation[230].

Protein Interaction and Binding Kinetics

Proteins in cells do not function as independent molecules but are in constant association and dissociation with other proteins and small molecules (ligands). ^{19}F NMR has been exploited to investigate the mechanism of these interactions in some proteins. For example, metafluorotyrosine was used as a probe to explore the interaction between the SH3 domain of Fyn tyrosine kinase and a proline-rich peptide. In this study, a global fit of all chemical shift titration curves and ^{19}F relaxation rates from multiple sites in the peptide binding pocket was used to extract kinetic parameters for the protein-peptide interaction, including binding affinity (K_D) and rate of exchange (k_{ex})[231]. In another study, ^{19}F NMR (4-fluorophenylalanine probe) was used to monitor the binding of aspartate to the ligand binding domain of the chemotaxis aspartate receptor and subsequent determination of kinetic parameters (k_{on} and k_{off}) for the interaction[209]. Additionally, ^{19}F NMR has been a valuable tool in the study of protein-membrane interactions. In this regard, ^{19}F NMR (5-fluorotryptophan) was used as a probe to characterize membrane binding by the actinoporin equinatoxin II (EqTII). Here, the structural basis for the interaction of EqTII with membranes was elucidated by following ^{19}F spectral changes in the presence of lipid micelles or bicelles[232].

Conformational and Structural Changes

The exceptional sensitivity of the ^{19}F nucleus to its environment has made it a valuable tool for investigating subtle conformational and structural changes occurring in proteins. An earlier ^{19}F NMR study identified specific residues involved in the polymerization of G-actin through direct observation of ^{19}F line broadening of cysteine residues labeled with BTFA[213]. Also, ^{19}F NMR has been applied in the study of conformational changes induced in various receptors upon ligand binding. For instance, the conformational changes induced by sugar binding to the D-galactose and D-glucose receptor as well as aspartate binding to the aspartate transducer have all been probed using ^{19}F NMR[233].

To better understand the signaling pathway for G-protein coupled receptors (GPCRs), ^{19}F NMR has been used as a probe to characterize the conformational changes induced by ligand binding to β_2 adrenergic receptor (β_2AR). In this study, three specific cysteine residues in the cytoplasmic region of β_2AR were chemically modified with the fluorinated reagent TFET. ^{19}F spectral changes (peak volume and chemical shifts) in the presence of different ligands, including agonists, inverse agonists, and antagonists were used to elucidate the mechanism underlying ligand induced conformational changes in terms of shifts in conformational equilibria between an active and an inactive state[234]. Subsequently, the thermodynamic and kinetic parameters associated with this ligand (agonist) induced conformational equilibria in β_2AR was quantified in a further study using ^{19}F NMR[235].

Recently, we have investigated the global dynamics of the molecular chaperone Hsp90 using ^{19}F NMR as a reporter of conformational changes. Accordingly, an aspartate (D61) residue located on a rigid loop within the N-terminal domain of Hsp90 was mutated to cysteine and then chemically modified with BTFA to serve as a ^{19}F probe. In this study, the conformational changes of Hsp90 from an open conformation to a catalytically active closed conformation were monitored using dynamic ^{19}F NMR experiments. This allowed us to characterize the rates of opening (k_{open}) and closing (k_{close}) of Hsp90 in the presence of the non-hydrolyzable ATP analog AMPPNP as well as the slowly hydrolyzable ATP analog ATPγS[75].

Summary

Hsp90 has gained a lot of attention owing to its role in the stabilization and activation of diverse protein substrates (clients) and consequent implications in several human diseases. However, the vast majority of work in the Hsp90 field has focused on the mechanism of Hsp90-dependent carcinogenesis due to the promising potential of Hsp90 inhibitors as therapeutic agents for cancer. Although there are no approved Hsp90-specific cancer drugs owing to challenges with toxicity at the clinical level, Hsp90 inhibitors are among the most actively pursued cancer drug targets by pharmaceutical industries[193]. Consequently, a better understanding of the mechanism of oncoprotein (client) stabilization by Hsp90 is required to improve these clinical outcomes.

The chaperone activity of Hsp90 is accompanied by large structural changes of the Hsp90 homodimer from an open conformation to a catalytically active closed conformation. To better understand the mechanism underlying these conformational changes, we used a combination of ^{19}F NMR-based techniques and MD simulations to explore local dynamics within the N-terminal domain (NTD) of Hsp90, which provides a basis for studying dynamics in the full-length chaperone. Chapter 2 of this work quantifies the internal dynamics of the sidechain of a trifluoroacetone cysteine derivative commonly employed as a reporter of dynamic processes in ^{19}F NMR studies of proteins. This allows for accurate interpretation of ^{19}F NMR linewidths as well as the separation of fast internal sidechain dynamics from slower dynamic processes occurring in proteins. In chapter 3, the methodology developed in chapter 2 was applied to investigate the kinetics of nucleotide binding to the N-terminal domain of Hsp90. Chapters 4 and 5 are a brief exploration of the dynamics of full-length Hsp90 in the presence of diverse nucleotides and the ATPase stimulating co-chaperone Aha1, respectively. Finally, chapter 6 is a general conclusion of all the work presented here and some future directions that will expand our understanding of the chaperone activity of Hsp90.

References

1. Anfinsen, C.B. Principles that govern the folding of protein chains. *Science* **181**, 223-230 (1973).

2. Ellis, R.J. & Minton, A.P. Protein aggregation in crowded environments. *Biol. Chem.* **387**, 485-497 (2006).

3. Balchin, D., Hayer-Hartl, M. & Hartl, F.U. In vivo aspects of protein folding and quality control. *Science* **353**, aac4354 (2016).

4. Ellis, J. Proteins as molecular chaperones. *Nature* **328**, 378-379 (1987).

5. Hendrick, J.P. & Hartl, F. Molecular chaperone functions of heat-shock proteins. *Annu. Rev. Biochem.* **62**, 349-384 (1993).

6. Young, J.C., Agashe, V.R., Siegers, K. & Hartl, F.U. Pathways of chaperone-mediated protein folding in the cytosol. *Nat. Rev. Mol. Cell Biol.* **5**, 781-791 (2004).

7. Wegele, H., Müller, L. & Buchner, J. Hsp70 and Hsp90—a relay team for protein folding. *Rev. Physiol. Biochem. Pharmacol.* **151**, 1-44 (2004).

8. Barral, J.M., Broadley, S.A., Schaffar, G. & Hartl, F.U. Roles of molecular chaperones in protein misfolding diseases. *Semin. Cell Dev. Biol.* **15**, 17-29 (2004).

9. Whitesell, L. & Lindquist, S.L. HSP90 and the chaperoning of cancer. *Nat. Rev. Cancer* **5**, 761-772 (2005).

10. Ferrarini, M., Heltai, S., Zocchi, M.R. & Rugarli, C. Unusual expression and localization of heat-shock proteins in human tumor cells. *Int. J. Cancer* **51**, 613-619 (1992).

11. Hartl, F.U., Bracher, A. & Hayer-Hartl, M. Molecular chaperones in protein folding and proteostasis. *Nature* **475**, 324-332 (2011).

12. Genest, O., Wickner, S. & Doyle, S.M. Hsp90 and Hsp70 chaperones: collaborators in protein remodeling. *J. Biol. Chem.* **294**, 2109-2120 (2019).

13. Karagöz, G.E. et al. Hsp90-Tau complex reveals molecular basis for specificity in chaperone action. *Cell* **156**, 963-974 (2014).

14. Pearl, L.H. & Prodromou, C. Structure and mechanism of the Hsp90 molecular chaperone machinery. *Annu. Rev. Biochem.* **75**, 271-294 (2006).

15. Taipale, M., Jarosz, D.F. & Lindquist, S. HSP90 at the hub of protein homeostasis: emerging mechanistic insights. *Nat. Rev. Mol. Cell Biol.* **11**, 515-528 (2010).

16. Zhao, R. et al. Navigating the chaperone network: an integrative map of physical and genetic interactions mediated by the hsp90 chaperone. *Cell* **120**, 715-727 (2005).

17. Sreedhar, A.S., Kalmár, É, Csermely, P. & Shen, Y. Hsp90 isoforms: functions, expression and clinical importance. *FEBS Lett.* **562**, 11-15 (2004).

18. Johnson, J.L. Evolution and function of diverse Hsp90 homologs and cochaperone proteins. *Biochim. Biophys. Acta Mol. Cell Res.* **1823**, 607-613 (2012).

19. Shen, Y. et al. Essential role of the first intron in the transcription of hsp90β gene. *FEBS Lett.* **413**, 92-98 (1997).

20. Zhang, S. et al. Regulation of human hsp90α gene expression. *FEBS Lett.* **444**, 130-135 (1999).

21. Chen, B., Piel, W.H., Gui, L., Bruford, E. & Monteiro, A. The HSP90 family of genes in the human genome: insights into their divergence and evolution. *Genomics* **86**, 627-637 (2005).

22. Grad, I. et al. The molecular chaperone Hsp90α is required for meiotic progression of spermatocytes beyond pachytene in the mouse. *PLoS One* **5**, e15770 (2010).

23. Kunisawa, J. & Shastri, N. Hsp90α chaperones large C-terminally extended proteolytic intermediates in the MHC class I antigen processing pathway. *Immunity* **24**, 523-534 (2006).

24. Metchat, A. et al. Mammalian heat shock factor 1 is essential for oocyte meiosis and directly regulates Hsp90α expression. *J. Biol. Chem.* **284**, 9521-9528 (2009).

25. Bouchier-Hayes, L. et al. Characterization of cytoplasmic caspase-2 activation by induced proximity. *Mol. Cell* **35**, 830-840 (2009).

26. Eustace, B.K. et al. Functional proteomic screens reveal an essential extracellular role for hsp90α in cancer cell invasiveness. *Nat. Cell Biol.* **6**, 507-514 (2004).

27. Song, X. et al. The regulatory mechanism of extracellular Hsp90α on matrix metalloproteinase-2 processing and tumor angiogenesis. *J. Biol. Chem.* **285**, 40039-40049 (2010).

28. Li, W. et al. Extracellular heat shock protein-90α: linking hypoxia to skin cell motility and wound healing. *EMBO J.* **26**, 1221-1233 (2007).

29. Voss, A.K., Thomas, T. & Gruss, P. Mice lacking HSP90beta fail to develop a placental labyrinth. *Development* **127**, 1-11 (2000).

30. Cohen-Saidon, C., Carmi, I., Keren, A. & Razin, E. Antiapoptotic function of Bcl-2 in mast cells is dependent on its association with heat shock protein 90β. *Blood* **107**, 1413-1420 (2006).

31. Sorger, P.K. & Pelham, H.R. The glucose-regulated protein grp94 is related to heat shock protein hsp90. *J. Mol. Biol.* **194**, 341-344 (1987).

32. Cala, S.E. & Jones, L.R. GRP94 resides within cardiac sarcoplasmic reticulum vesicles and is phosphorylated by casein kinase II. *J. Biol. Chem.* **269**, 5926-5931 (1994).

33. Eletto, D., Dersh, D. & Argon, Y. GRP94 in ER quality control and stress responses. *Semin. Cell Dev. Biol.* **21**, 479-485 (2010).

34. Koch, G., Smith, M., Macer, D., Webster, P. & Mortara, R. Endoplasmic reticulum contains a common, abundant calcium-binding glycoprotein, endoplasmin. *J. Cell. Sci.* **86**, 217-232 (1986).

35. Wanderling, S. et al. GRP94 is essential for mesoderm induction and muscle development because it regulates insulin-like growth factor secretion. *Mol. Biol. Cell* **18**, 3764-3775 (2007).

36. Ostrovsky, O., Makarewich, C.A., Snapp, E.L. & Argon, Y. An essential role for ATP binding and hydrolysis in the chaperone activity of GRP94 in cells. *Proc. Natl. Acad. Sci. U.S.A.* **106**, 11600-11605 (2009).

37. Pagetta, A. et al. Structural insights into complexes of glucose-regulated Protein94 (Grp94) with human immunoglobulin G. relevance for Grp94-IgG complexes that form in vivo in pathological conditions. *PLoS One* **9**, e86198 (2014).

38. Wu, B.X., Hong, F., Zhang, Y., Ansa-Addo, E. & Li, Z. GRP94/gp96 in cancer: biology, structure, immunology, and drug development. *Adv. Cancer Res.* **129**, 165-190 (2016).

39. Marzec, M., Eletto, D. & Argon, Y. GRP94: An HSP90-like protein specialized for protein folding and quality control in the endoplasmic reticulum. *Biochim. Biophys. Acta Mol. Cell Res.* **1823**, 774-787 (2012).

40. Song, H.Y., Dunbar, J.D., Zhang, Y.X., Guo, D. & Donner, D.B. Identification of a protein with homology to hsp90 that binds the type 1 tumor necrosis factor receptor. *J. Biol. Chem.* **270**, 3574-3581 (1995).

41. Chen, C. et al. A new member of the hsp90 family of molecular chaperones interacts with the retinoblastoma protein during mitosis and after heat shock. *Mol. Cell. Biol.* **16**, 4691-4699 (1996).

42. Felts, S.J. et al. The hsp90-related protein TRAP1 is a mitochondrial protein with distinct functional properties. *J. Biol. Chem.* **275**, 3305-3312 (2000).

43. Pridgeon, J.W., Olzmann, J.A., Chin, L. & Li, L. PINK1 protects against oxidative stress by phosphorylating mitochondrial chaperone TRAP1. *PLoS Biol.* **5**, e172 (2007).

44. Cechetto, J.D. & Gupta, R.S. Immunoelectron microscopy provides evidence that tumor necrosis factor receptor-associated protein 1 (TRAP-1) is a mitochondrial protein which also localizes at specific extramitochondrial sites. *Exp. Cell Res.* **260**, 30-39 (2000).

45. Altieri, D.C., Stein, G.S., Lian, J.B. & Languino, L.R. TRAP-1, the mitochondrial Hsp90. *Biochim. Biophys. Acta Mol. Cell Res.* **1823**, 767-773 (2012).

46. Kang, B.H. et al. Regulation of tumor cell mitochondrial homeostasis by an organelle-specific Hsp90 chaperone network. *Cell* **131**, 257-270 (2007).

47. Borkovich, K.A., Farrelly, F.W., Finkelstein, D.B., Taulien, J. & Lindquist, S. hsp82 is an essential protein that is required in higher concentrations for growth of cells at higher temperatures. *Mol. Cell. Biol.* **9**, 3919-3930 (1989).

48. Picard, D. et al. Reduced levels of hsp90 compromise steroid receptor action in vivo. *Nature* **348**, 166-168 (1990).

49. Girstmair, H. et al. The Hsp90 isoforms from S. cerevisiae differ in structure, function and client range. *Nat. Commun.* **10**, 1-15 (2019).

50. Thomas, J.G. & Baneyx, F. Roles of the Escherichia coli small heat shock proteins IbpA and IbpB in thermal stress management: comparison with ClpA, ClpB, and HtpG in vivo. *J. Bacteriol.* **180**, 5165-5172 (1998).

51. Bardwell, J.C. & Craig, E.A. Ancient heat shock gene is dispensable. *J. Bacteriol.* **170**, 2977-2983 (1988).

52. Thomas, J.G. & Baneyx, F. ClpB and HtpG facilitate de novo protein folding in stressed Escherichia coli cells. *Mol. Microbiol.* **36**, 1360-1370 (2000).

53. Garcie, C. et al. The bacterial stress-responsive Hsp90 chaperone (HtpG) is required for the production of the genotoxin colibactin and the siderophore yersiniabactin in Escherichia coli. *J. Infect. Dis.* **214**, 916-924 (2016).

54. Prodromou, C. et al. The ATPase cycle of Hsp90 drives a molecular 'clamp'via transient dimerization of the N-terminal domains. *EMBO J.* **19**, 4383-4392 (2000).

55. Jackson, S.E. Hsp90: structure and function. *Top Curr. Chem.* **328**, 155-240 (2013).

56. Ali, M.M. et al. Crystal structure of an Hsp90–nucleotide–p23/Sba1 closed chaperone complex. *Nature* **440**, 1013-1017 (2006).

57. Meyer, P. et al. Structural and functional analysis of the middle segment of hsp90: implications for ATP hydrolysis and client protein and cochaperone interactions. *Mol. Cell* **11**, 647-658 (2003).

58. Richter, K., Muschler, P., Hainzl, O. & Buchner, J. Coordinated ATP hydrolysis by the Hsp90 dimer. *J. Biol. Chem.* **276**, 33689-33696 (2001).

59. Allan, R.K. & Ratajczak, T. Versatile TPR domains accommodate different modes of target protein recognition and function. *Cell Stress Chaperones* **16**, 353-367 (2011).

60. Chen, B., Zhong, D. & Monteiro, A. Comparative genomics and evolution of the HSP90 family of genes across all kingdoms of organisms. *BMC Genomics* **7**, 1-19 (2006).

61. Prodromou, C., Roe, S.M., Piper, P.W. & Pearl, L.H. A molecular clamp in the crystal structure of the N-terminal domain of the yeast Hsp90 chaperone. *Nat. Struct. Biol.* **4**, 477-482 (1997).

62. Prodromou, C. et al. Identification and structural characterization of the ATP/ADP-binding site in the Hsp90 molecular chaperone. *Cell* **90**, 65-75 (1997).

63. Dutta, R. & Inouye, M. GHKL, an emergent ATPase/kinase superfamily. *Trends Biochem. Sci.* **25**, 24-28 (2000).

64. Li, J. et al. Structure insights into mechanisms of ATP hydrolysis and the activation of human heat-shock protein 90. *Acta Biochim. Biophys. Sin.* **44**, 300-306 (2012).

65. Stebbins, C.E. et al. Crystal structure of an Hsp90–geldanamycin complex: targeting of a protein chaperone by an antitumor agent. *Cell* **89**, 239-250 (1997).

66. Roe, S.M. et al. Structural basis for inhibition of the Hsp90 molecular chaperone by the antitumor antibiotics radicicol and geldanamycin. *J. Med. Chem.* **42**, 260-266 (1999).

67. Verba, K.A. et al. Atomic structure of Hsp90-Cdc37-Cdk4 reveals that Hsp90 traps and stabilizes an unfolded kinase. *Science* **352**, 1542-1547 (2016).

68. Richter, K. et al. Intrinsic inhibition of the Hsp90 ATPase activity. *J. Biol. Chem.* **281**, 11301-11311 (2006).

69. Richter, K., Reinstein, J. & Buchner, J. N-terminal residues regulate the catalytic efficiency of the Hsp90 ATPase cycle. *J. Biol. Chem.* **277**, 44905-44910 (2002).

70. Louvion, J., Warth, R. & Picard, D. Two eukaryote-specific regions of Hsp82 are dispensable for its viability and signal transduction functions in yeast. *Proc. Natl. Acad. Sci. U.S.A.* **93**, 13937-13942 (1996).

71. Hainzl, O., Lapina, M.C., Buchner, J. & Richter, K. The charged linker region is an important regulator of Hsp90 function. *J. Biol. Chem.* **284**, 22559-22567 (2009).

72. Tsutsumi, S. et al. Charged linker sequence modulates eukaryotic heat shock protein 90 (Hsp90) chaperone activity. *Proc. Natl. Acad. Sci. U.S.A.* **109**, 2937-2942 (2012).

73. Morra, G., Verkhivker, G. & Colombo, G. Modeling signal propagation mechanisms and ligand-based conformational dynamics of the Hsp90 molecular chaperone full-length dimer. *PLoS Comput. Biol.* **5**, e1000323 (2009).

74. Cunningham, C.N., Southworth, D.R., Krukenberg, K.A. & Agard, D.A. The conserved arginine 380 of Hsp90 is not a catalytic residue, but stabilizes the closed conformation required for ATP hydrolysis. *Protein Sci.* **21**, 1162-1171 (2012).

75. Lee, B.L. et al. The Hsp90 chaperone: 1H and 19F dynamic nuclear magnetic resonance spectroscopy reveals a perfect enzyme. *Biochemistry* **58**, 1869-1877 (2019).

76. Rutz, D.A. et al. A switch point in the molecular chaperone Hsp90 responding to client interaction. *Nat. Commun.* **9**, 1-14 (2018).

77. Lorenz, O.R. et al. Modulation of the Hsp90 chaperone cycle by a stringent client protein. *Mol. Cell* **53**, 941-953 (2014).

78. Oroz, J. et al. Structure and pro-toxic mechanism of the human Hsp90/PPIase/Tau complex. *Nat. Commun.* **9**, 1-13 (2018).

79. Radli, M. & Rüdiger, S.G. Dancing with the diva: Hsp90–client interactions. *J. Mol. Biol.* **430**, 3029-3040 (2018).

80. Meyer, P. et al. Structural basis for recruitment of the ATPase activator Aha1 to the Hsp90 chaperone machinery. *EMBO J.* **23**, 511-519 (2004).

81. Harris, S.F., Shiau, A.K. & Agard, D.A. The crystal structure of the carboxy-terminal dimerization domain of htpG, the Escherichia coli Hsp90, reveals a potential substrate binding site. *Structure* **12**, 1087-1097 (2004).

82. Weikl, T. et al. C-terminal regions of Hsp90 are important for trapping the nucleotide during the ATPase cycle. *J. Mol. Biol.* **303**, 583-592 (2000).

83. So″ ti, C., Vermes, A., Haystead, T.A. & Csermely, P. Comparative analysis of the ATP-binding sites of Hsp90 by nucleotide affinity cleavage: a distinct nucleotide specificity of the C-terminal ATP-binding site. *Euro. J. Biochem.* **270**, 2421-2428 (2003).

84. Marcu, M.G., Chadli, A., Bouhouche, I., Catelli, M. & Neckers, L.M. The heat shock protein 90 antagonist novobiocin interacts with a previously unrecognized ATP-binding domain in the carboxyl terminus of the chaperone. *J. Biol. Chem.* **275**, 37181-37186 (2000).

85. Garnier, C. et al. Binding of ATP to heat shock protein 90: evidence for an ATP-binding site in the C-terminal domain. *J. Biol. Chem.* **277**, 12208-12214 (2002).

86. Hessling, M., Richter, K. & Buchner, J. Dissection of the ATP-induced conformational cycle of the molecular chaperone Hsp90. *Nat. Struct. Mol. Biol.* **16**, 287-293 (2009).

87. Schulze, A. et al. Cooperation of local motions in the Hsp90 molecular chaperone ATPase mechanism. *Nat. Chem. Biol.* **12**, 628-635 (2016).

88. Siligardi, G. et al. Co-chaperone regulation of conformational switching in the Hsp90 ATPase cycle. *J. Biol. Chem.* **279**, 51989-51998 (2004).

89. Richter, K., Walter, S. & Buchner, J. The Co-chaperone Sba1 connects the ATPase reaction of Hsp90 to the progression of the chaperone cycle. *J. Mol. Biol.* **342**, 1403-1413 (2004).

90. Nathan, D.F. & Lindquist, S. Mutational analysis of Hsp90 function: interactions with a steroid receptor and a protein kinase. *Mol. Cell. Biol.* **15**, 3917-3925 (1995).

91. Panaretou, B. et al. ATP binding and hydrolysis are essential to the function of the Hsp90 molecular chaperone in vivo. *EMBO J.* **17**, 4829-4836 (1998).

92. Obermann, W.M., Sondermann, H., Russo, A.A., Pavletich, N.P. & Hartl, F.U. In vivo function of Hsp90 is dependent on ATP binding and ATP hydrolysis. *J. Cell Biol.* **143**, 901-910 (1998).

93. Shiau, A.K., Harris, S.F., Southworth, D.R. & Agard, D.A. Structural analysis of E. coli hsp90 reveals dramatic nucleotide-dependent conformational rearrangements. *Cell* **127**, 329-340 (2006).

94. Dollins, D.E., Warren, J.J., Immormino, R.M. & Gewirth, D.T. Structures of GRP94-nucleotide complexes reveal mechanistic differences between the hsp90 chaperones. *Mol. Cell* **28**, 41-56 (2007).

95. Huck, J.D., Que, N.L., Hong, F., Li, Z. & Gewirth, D.T. Structural and functional analysis of GRP94 in the closed state reveals an essential role for the pre-N domain and a potential client-binding site. *Cell Rep.* **20**, 2800-2809 (2017).

96. Lavery, L.A. et al. Structural asymmetry in the closed state of mitochondrial Hsp90 (TRAP1) supports a two-step ATP hydrolysis mechanism. *Mol. Cell* **53**, 330-343 (2014).

97. Southworth, D.R. & Agard, D.A. Species-dependent ensembles of conserved conformational states define the Hsp90 chaperone ATPase cycle. *Mol. Cell* **32**, 631-640 (2008).

98. Scheibel, T. et al. ATP-binding properties of human Hsp90. *J. Biol. Chem.* **272**, 18608-18613 (1997).

99. McLaughlin, S.H., Smith, H.W. & Jackson, S.E. Stimulation of the weak ATPase activity of human hsp90 by a client protein. *J. Mol. Biol.* **315**, 787-798 (2002).

100. Wegele, H., Muschler, P., Bunck, M., Reinstein, J. & Buchner, J. Dissection of the contribution of individual domains to the ATPase mechanism of Hsp90. *J. Biol. Chem.* **278**, 39303-39310 (2003).

101. Wolfenden, R. & Snider, M.J. The depth of chemical time and the power of enzymes as catalysts. *Acc. Chem. Res.* **34**, 938-945 (2001).

102. Schmid, S., Götz, M. & Hugel, T. Single-molecule analysis beyond dwell times: demonstration and assessment in and out of equilibrium. *Biophys. J.* **111**, 1375-1384 (2016).

103. Rashid, S., Lee, B.L., Wajda, B. & Spyracopoulos, L. Nucleotide Binding and Active Site Gate Dynamics for the Hsp90 Chaperone ATPase Domain from Benchtop and High Field 19F NMR Spectroscopy. *J. Phys. Chem. B* **124**, 2984-2993 (2020).

104. Biebl, M.M. & Buchner, J. Structure, function, and regulation of the Hsp90 machinery. *Cold Spring Harb. Perspect. Biol.* **11**, a034017 (2019).

105. Sahasrabudhe, P., Rohrberg, J., Biebl, M.M., Rutz, D.A. & Buchner, J. The plasticity of the Hsp90 co-chaperone system. *Mol. Cell* **67**, 947-961. e5 (2017).

106. Liu, B. et al. Folding of Toll-like receptors by the HSP90 paralogue gp96 requires a substrate-specific cochaperone. *Nat. Commun.* **1**, 1-11 (2010).

107. Harst, A., Lin, H. & Obermann, W.M. Aha1 competes with Hop, p50 and p23 for binding to the molecular chaperone Hsp90 and contributes to kinase and hormone receptor activation. *Biochem. J.* **387**, 789-796 (2005).

108. Nathan, D.F., Vos, M.H. & Lindquist, S. Identification of SSF1, CNS1, and HCH1 as multicopy suppressors of a Saccharomyces cerevisiae Hsp90 loss-of-function mutation. *Proc. Natl. Acad. Sci. U.S.A.* **96**, 1409-1414 (1999).

109. Panaretou, B. et al. Activation of the ATPase activity of hsp90 by the stress-regulated cochaperone aha1. *Mol. Cell* **10**, 1307-1318 (2002).

110. Horvat, N.K. et al. A mutation in the catalytic loop of hsp90 specifically impairs ATPase stimulation by aha1p, but not hch1p. *J. Mol. Biol.* **426**, 2379-2392 (2014).

111. Retzlaff, M. et al. Asymmetric activation of the hsp90 dimer by its cochaperone Aha1. *Mol. Cell* **37**, 344-354 (2010).

112. Singh, M., Shah, V. & Tatu, U. A novel C-terminal homologue of Aha1 co-chaperone binds to heat shock protein 90 and stimulates its ATPase activity in Entamoeba histolytica. *J. Mol. Biol.* **426**, 1786-1798 (2014).

113. Wolmarans, A., Lee, B., Spyracopoulos, L. & LaPointe, P. The mechanism of Hsp90 ATPase stimulation by Aha1. *Sci. Rep.* **6**, 1-15 (2016).

114. Armstrong, H., Wolmarans, A., Mercier, R., Mai, B. & LaPointe, P. The co-chaperone Hch1 regulates Hsp90 function differently than its homologue Aha1 and confers sensitivity to yeast to the Hsp90 inhibitor NVP-AUY922. *PLoS One* **7**, e49322 (2012).

115. Mercier, R. et al. The conserved NxNNWHW motif in Aha-type co-chaperones modulates the kinetics of Hsp90 ATPase stimulation. *Nat. Commun.* **10**, 1-12 (2019).

116. Li, J., Richter, K., Reinstein, J. & Buchner, J. Integration of the accelerator Aha1 in the Hsp90 co-chaperone cycle. *Nat. Struct. Mol. Biol.* **20**, 326 (2013).

117. Johnson, J.L. & Toft, D.O. A novel chaperone complex for steroid receptors involving heat shock proteins, immunophilins, and p23. *J. Biol. Chem.* **269**, 24989-24993 (1994).

118. Fang, Y., Fliss, A.E., Rao, J. & Caplan, A.J. SBA1 encodes a yeast hsp90 cochaperone that is homologous to vertebrate p23 proteins. *Mol. Cell. Biol.* **18**, 3727-3734 (1998).

119. Bohen, S.P. Genetic and biochemical analysis of p23 and ansamycin antibiotics in the function of Hsp90-dependent signaling proteins. *Mol. Cell. Biol.* **18**, 3330-3339 (1998).

120. Chadli, A. et al. Dimerization and N-terminal domain proximity underlie the function of the molecular chaperone heat shock protein 90. *Proc. Natl. Acad. Sci. U.S.A.* **97**, 12524-12529 (2000).

121. Johnson, J.L. & Toft, D.O. Binding of p23 and hsp90 during assembly with the progesterone receptor. *Mol. Endocrinol.* **9**, 670-678 (1995).

122. Sullivan, W. et al. Nucleotides and two functional states of hsp90. *J. Biol. Chem.* **272**, 8007-8012 (1997).

123. Grenert, J.P. et al. The amino-terminal domain of heat shock protein 90 (hsp90) that binds geldanamycin is an ATP/ADP switch domain that regulates hsp90 conformation. *J. Biol. Chem.* **272**, 23843-23850 (1997).

124. Wu, H., Hyun, J., Martinez-Yamout, M.A., Park, S.J. & Dyson, H.J. Characterization of an Hsp90-independent interaction between co-chaperone p23 and transcription factor p53. *Biochemistry* **57**, 935-944 (2018).

125. Honore, B. et al. Molecular cloning and expression of a transformation-sensitive human protein containing the TPR motif and sharing identity to the stress-inducible yeast protein STI1. *J. Biol. Chem.* **267**, 8485-8491 (1992).

126. Das, A.K., Cohen, P.T. & Barford, D. The structure of the tetratricopeptide repeats of protein phosphatase 5: implications for TPR-mediated protein–protein interactions. *EMBO J.* **17**, 1192-1199 (1998).

127. Scheufler, C. et al. Structure of TPR domain–peptide complexes: critical elements in the assembly of the Hsp70–Hsp90 multichaperone machine. *Cell* **101**, 199-210 (2000).

128. Smith, D.F. et al. Identification of a 60-kilodalton stress-related protein, p60, which interacts with hsp90 and hsp70. *Mol. Cell. Biol.* **13**, 869-876 (1993).

129. Wegele, H., Wandinger, S.K., Schmid, A.B., Reinstein, J. & Buchner, J. Substrate transfer from the chaperone Hsp70 to Hsp90. *J. Mol. Biol.* **356**, 802-811 (2006).

130. Schmid, A.B. et al. The architecture of functional modules in the Hsp90 co-chaperone Sti1/Hop. *EMBO J.* **31**, 1506-1517 (2012).

131. Southworth, D.R. & Agard, D.A. Client-loading conformation of the Hsp90 molecular chaperone revealed in the cryo-EM structure of the human Hsp90: Hop complex. *Mol. Cell* **42**, 771-781 (2011).

132. Wegele, H., Haslbeck, M., Reinstein, J. & Buchner, J. Sti1 is a novel activator of the Ssa proteins. *J. Biol. Chem.* **278**, 25970-25976 (2003).

133. Prodromou, C. et al. Regulation of Hsp90 ATPase activity by tetratricopeptide repeat (TPR)-domain co-chaperones. *EMBO J.* **18**, 754-762 (1999).

134. Johnson, B.D., Schumacher, R.J., Ross, E.D. & Toft, D.O. Hop modulates Hsp70/Hsp90 interactions in protein folding. *J. Biol. Chem.* **273**, 3679-3686 (1998).

135. Chang, H.C., Nathan, D.F. & Lindquist, S. In vivo analysis of the Hsp90 cochaperone Sti1 (p60). *Mol. Cell. Biol.* **17**, 318-325 (1997).

136. Mollapour, M. & Neckers, L. Post-translational modifications of Hsp90 and their contributions to chaperone regulation *Biochim. Biophys. Acta Mol. Cell Res.* **1823**, 648-655 (2012).

137. Scroggins, B.T. & Neckers, L. Post-translational modification of heat-shock protein 90: impact on chaperone function. *Expert Opin. Drug Discov.* **2**, 1403-1414 (2007).

138. Prodromou, C. Mechanisms of Hsp90 regulation. *Biochem. J.* **473**, 2439-2452 (2016).

139. Mayer, M.P. & Le Breton, L. Hsp90: breaking the symmetry. *Mol. Cell* **58**, 8-20 (2015).

140. Soroka, J. et al. Conformational switching of the molecular chaperone Hsp90 via regulated phosphorylation. *Mol. Cell* **45**, 517-528 (2012).

141. Retzlaff, M. et al. Hsp90 is regulated by a switch point in the C-terminal domain. *EMBO Rep.* **10**, 1147-1153 (2009).

142. Lees-Miller, S.P. & Anderson, C.W. The human double-stranded DNA-activated protein kinase phosphorylates the 90-kDa heat-shock protein, hsp90α at two NH2-terminal threonine residues. *J. Biol. Chem.* **264**, 17275-17280 (1989).

143. Mollapour, M., Tsutsumi, S., Kim, Y.S., Trepel, J. & Neckers, L. Casein kinase 2 phosphorylation of Hsp90 threonine 22 modulates chaperone function and drug sensitivity. *Oncotarget* **2**, 407 (2011).

144. Mollapour, M. et al. Threonine 22 phosphorylation attenuates Hsp90 interaction with cochaperones and affects its chaperone activity. *Mol. Cell* **41**, 672-681 (2011).

145. Mollapour, M. et al. Swe1Wee1-dependent tyrosine phosphorylation of Hsp90 regulates distinct facets of chaperone function. *Mol. Cell* **37**, 333-343 (2010).

146. Wandinger, S.K., Suhre, M.H., Wegele, H. & Buchner, J. The phosphatase Ppt1 is a dedicated regulator of the molecular chaperone Hsp90. *EMBO J.* **25**, 367-376 (2006).

147. Schopf, F.H., Biebl, M.M. & Buchner, J. The HSP90 chaperone machinery. *Nat. Rev. Mol. Cell Biol.* **18**, 345 (2017).

148. Mollapour, M. et al. Asymmetric Hsp90 N domain SUMOylation recruits Aha1 and ATP-competitive inhibitors. *Mol. Cell* **53**, 317-329 (2014).

149. Taipale, M. et al. Quantitative analysis of HSP90-client interactions reveals principles of substrate recognition. *Cell* **150**, 987-1001 (2012).

150. Dittmar, K.D. & Pratt, W.B. Folding of the glucocorticoid receptor by the reconstituted Hsp90-based chaperone machinery: The initial hsp90· p60· hsp70-dependent step is sufficient for creating the steroid binding conformation. *J. Biol. Chem.* **272**, 13047-13054 (1997).

151. Xu, Y. & Lindquist, S. Heat-shock protein hsp90 governs the activity of pp60v-src kinase. *Proc. Natl. Acad. Sci. U.S.A.* **90**, 7074-7078 (1993).

152. Xu, Y., Singer, M.A. & Lindquist, S. Maturation of the tyrosine kinase c-src as a kinase and as a substrate depends on the molecular chaperone Hsp90. *Proc. Natl. Acad. Sci. U.S.A.* **96**, 109-114 (1999).

153. Boczek, E.E. et al. Conformational processing of oncogenic v-Src kinase by the molecular chaperone Hsp90. *Proc. Natl. Acad. Sci. U.S.A.* **112**, E3189-E3198 (2015).

154. Falsone, S.F., Leptihn, S., Osterauer, A., Haslbeck, M. & Buchner, J. Oncogenic mutations reduce the stability of SRC kinase. *J. Mol. Biol.* **344**, 281-291 (2004).

155. Keramisanou, D. et al. Molecular mechanism of protein kinase recognition and sorting by the Hsp90 kinome-specific cochaperone Cdc37. *Mol. Cell* **62**, 260-271 (2016).

156. Karagöz, G.E. & Rüdiger, S.G. Hsp90 interaction with clients. *Trends Biochem. Sci.* **40**, 117-125 (2015).

157. Pratt, W.B. & Toft, D.O. Steroid receptor interactions with heat shock protein and immunophilin chaperones. *Endocr. Rev.* **18**, 306-360 (1997).

158. Pratt, W.B. & Dittmar, K.D. Studies with purified chaperones advance the understanding of the mechanism of glucocorticoid receptor–hsp90 heterocomplex assembly. *Trends Endocrinol. Metab.* **9**, 244-252 (1998).

159. Li, J., Richter, K. & Buchner, J. Mixed Hsp90–cochaperone complexes are important for the progression of the reaction cycle. *Nat. Struct. Mol. Biol.* **18**, 61 (2011).

160. Vaughan, C.K. et al. Hsp90-dependent activation of protein kinases is regulated by chaperone-targeted dephosphorylation of Cdc37. *Mol. Cell* **31**, 886-895 (2008).

161. Wang, X. et al. Hsp90 cochaperone Aha1 downregulation rescues misfolding of CFTR in cystic fibrosis. *Cell* **127**, 803-815 (2006).

162. Jameel, A. et al. Clinical and biological significance of HSP89 alpha in human breast cancer. *Int. J. Cancer* **50**, 409-415 (1992).

163. Pick, E. et al. High HSP90 expression is associated with decreased survival in breast cancer. *Cancer Res.* **67**, 2932-2937 (2007).

164. Pearl, L.H., Prodromou, C. & Workman, P. The Hsp90 molecular chaperone: an open and shut case for treatment. *Biochem. J.* **410**, 439-453 (2008).

165. Workman, P. Combinatorial attack on multistep oncogenesis by inhibiting the Hsp90 molecular chaperone. *Cancer Lett.* **206**, 149-157 (2004).

166. Soussi, T., Legros, Y., Lubin, R., Ory, K. & Schlichtholz, B. Multifactorial analysis of p53 alteration in human cancer: a review. *Int. J. Cancer* **57**, 1-9 (1994).

167. Vogelstein, B., Lane, D. & Levine, A.J. Surfing the p53 network. *Nature* **408**, 307-310 (2000).

168. Whitesell, L., Sutphin, P.D., Pulcini, E.J., Martinez, J.D. & Cook, P.H. The physical association of multiple molecular chaperone proteins with mutant p53 is altered by geldanamycin, an hsp90-binding agent. *Mol. Cell. Biol.* **18**, 1517-1524 (1998).

169. Blagosklonny, M.V., Toretsky, J., Bohen, S. & Neckers, L. Mutant conformation of p53 translated in vitro or in vivo requires functional HSP90. *Proc. Natl. Acad. Sci. U.S.A.* **93**, 8379-8383 (1996).

170. King, F.W., Wawrzynow, A., Höhfeld, J. & Zylicz, M. Co-chaperones Bag-1, Hop and Hsp40 regulate Hsc70 and Hsp90 interactions with wild-type or mutant p53. *EMBO J.* **20**, 6297-6305 (2001).

171. Müller, L., Schaupp, A., Walerych, D., Wegele, H. & Buchner, J. Hsp90 regulates the activity of wild type p53 under physiological and elevated temperatures. *J. Biol. Chem.* **279**, 48846-48854 (2004).

172. Cho, Y., Gorina, S., Jeffrey, P.D. & Pavletich, N.P. Crystal structure of a p53 tumor suppressor-DNA complex: understanding tumorigenic mutations. *Science* **265**, 346-355 (1994).

173. Cañadillas, J.M.P. et al. Solution structure of p53 core domain: structural basis for its instability. *Proc. Natl. Acad. Sci. U.S.A.* **103**, 2109-2114 (2006).

174. Rüdiger, S., Freund, S.M., Veprintsev, D.B. & Fersht, A.R. CRINEPT-TROSY NMR reveals p53 core domain bound in an unfolded form to the chaperone Hsp90. *Proc. Natl. Acad. Sci. U.S.A.* **99**, 11085-11090 (2002).

175. Park, S.J., Borin, B.N., Martinez-Yamout, M.A. & Dyson, H.J. The client protein p53 adopts a molten globule–like state in the presence of Hsp90. *Nat. Struct. Mol. Biol.* **18**, 537-542 (2011).

176. Muchowski, P.J. & Wacker, J.L. Modulation of neurodegeneration by molecular chaperones. *Nat. Rev. Neurosci.* **6**, 11-22 (2005).

177. Klaips, C.L., Jayaraj, G.G. & Hartl, F.U. Pathways of cellular proteostasis in aging and disease. *J. Cell Biol.* **217**, 51-63 (2018).

178. Bohush, A., Bieganowski, P. & Filipek, A. Hsp90 and its co-chaperones in neurodegenerative diseases. *Int. J. Mol. Sci.* **20**, 4976 (2019).

179. Luo, W. et al. Roles of heat-shock protein 90 in maintaining and facilitating the neurodegenerative phenotype in tauopathies. *Proc. Natl. Acad. Sci. U.S.A.* **104**, 9511-9516 (2007).

180. Shelton, L.B. et al. Hsp90 activator Aha1 drives production of pathological tau aggregates. *Proc. Natl. Acad. Sci. U.S.A.* **114**, 9707-9712 (2017).

181. Uryu, K. et al. Convergence of heat shock protein 90 with ubiquitin in filamentous α-synuclein inclusions of α-synucleinopathies. *Am. J. Pathol.* **168**, 947-961 (2006).

182. Falsone, S.F., Kungl, A.J., Rek, A., Cappai, R. & Zangger, K. The molecular chaperone Hsp90 modulates intermediate steps of amyloid assembly of the Parkinson-related protein α-synuclein. *J. Biol. Chem.* **284**, 31190-31199 (2009).

183. Putcha, P. et al. Brain-permeable small-molecule inhibitors of Hsp90 prevent α-synuclein oligomer formation and rescue α-synuclein-induced toxicity. *J. Pharmacol. Exp. Ther.* **332**, 849-857 (2010).

184. Whitesell, L., Mimnaugh, E.G., De Costa, B., Myers, C.E. & Neckers, L.M. Inhibition of heat shock protein HSP90-pp60v-src heteroprotein complex formation by benzoquinone ansamycins: essential role for stress proteins in oncogenic transformation. *Proc. Natl. Acad. Sci. U.S.A.* **91**, 8324-8328 (1994).

185. Schulte, T.W. et al. Antibiotic radicicol binds to the N-terminal domain of Hsp90 and shares important biologic activities with geldanamycin. *Cell Stress Chaperones* **3**, 100 (1998).

186. Xu, W. et al. Chaperone-dependent E3 ubiquitin ligase CHIP mediates a degradative pathway for c-ErbB2/Neu. *Proc. Natl. Acad. Sci. U.S.A.* **99**, 12847-12852 (2002).

187. Supko, J.G., Hickman, R.L., Grever, M.R. & Malspeis, L. Preclinical pharmacologic evaluation of geldanamycin as an antitumor agent. *Cancer Chemother. Pharmacol.* **36**, 305-315 (1995).

188. Schulte, T.W. & Neckers, L.M. The benzoquinone ansamycin 17-allylamino-17-demethoxygeldanamycin binds to HSP90 and shares important biologic activities with geldanamycin. *Cancer Chemother. Pharmacol.* **42**, 273-279 (1998).

189. Burger, A.M., Fiebig, H., Stinson, S.F. & Sausville, E.A. 17-(Allylamino)-17-demethoxygeldanamycin activity in human melanoma models. *Anticancer Drugs* **15**, 377-387 (2004).

190. Smith, V., Sausville, E.A., Camalier, R.F., Fiebig, H. & Burger, A.M. Comparison of 17-dimethylaminoethylamino-17-demethoxy-geldanamycin (17DMAG) and 17-allylamino-17-demethoxygeldanamycin (17AAG) in vitro: effects on Hsp90 and client proteins in melanoma models. *Cancer Chemother. Pharmacol.* **56**, 126-137 (2005).

191. Sydor, J.R. et al. Development of 17-allylamino-17-demethoxygeldanamycin hydroquinone hydrochloride (IPI-504), an anti-cancer agent directed against Hsp90. *Proc. Natl. Acad. Sci. U.S.A.* **103**, 17408-17413 (2006).

192. Soga, S. et al. KF25706, a novel oxime derivative of radicicol, exhibits in vivo antitumor activity via selective depletion of Hsp90 binding signaling molecules. *Cancer Res.* **59**, 2931-2938 (1999).

193. Neckers, L. & Workman, P. Hsp90 molecular chaperone inhibitors: are we there yet?. *Clin. Cancer Res.* **18**, 64-76 (2012).

194. Jaeger, A.M. & Whitesell, L. HSP90: enabler of cancer adaptation. *Annu. Rev. Cancer Biol.* **3**, 275-297 (2019).

195. Kleckner, I.R. & Foster, M.P. An introduction to NMR-based approaches for measuring protein dynamics. *Biochim. Biophys. Acta Proteins Proteom.* **1814**, 942-968 (2011).

196. Ruschak, A.M. & Kay, L.E. Methyl groups as probes of supra-molecular structure, dynamics and function. *J. Biomol. NMR* **46**, 75 (2010).

197. Palmer III, A.G. Probing molecular motion by NMR. *Curr. Opin. Struct. Biol.* **7**, 732-737 (1997).

198. Lipari, G. & Szabo, A. Model-free approach to the interpretation of nuclear magnetic resonance relaxation in macromolecules. 1. Theory and range of validity. *J. Am. Chem. Soc.* **104**, 4546-4559 (1982).

199. Lipari, G. & Szabo, A. Model-free approach to the interpretation of nuclear magnetic resonance relaxation in macromolecules. 2. Analysis of experimental results. *J. Am. Chem. Soc.* **104**, 4559-4570 (1982).

200. Clore, G.M. et al. Deviations from the simple two-parameter model-free approach to the interpretation of nitrogen-15 nuclear magnetic relaxation of proteins. *J. Am. Chem. Soc.* **112**, 4989-4991 (1990).

201. Levy, R.M., Karplus, M. & Wolynes, P.G. NMR relaxation parameters in molecules with internal motion: exact Langevin trajectory results compared with simplified relaxation models. *J. Am. Chem. Soc.* **103**, 5998-6011 (1981).

202. Mittermaier, A.K. & Kay, L.E. Observing biological dynamics at atomic resolution using NMR. *Trends Biochem. Sci.* **34**, 601-611 (2009).

203. Carver, J.P. & Richards, R.E. A general two-site solution for the chemical exchange produced dependence of T2 upon the Carr-Purcell pulse separation. *J. Magn. Reson.* **6**, 89-105 (1972).

204. Luz, Z. & Meiboom, S. Nuclear magnetic resonance study of the protolysis of trimethylammonium ion in aqueous solution—order of the reaction with respect to solvent. *J. Chem. Phys.* **39**, 366-370 (1963).

205. Tollinger, M., Skrynnikov, N.R., Mulder, F.A., Forman-Kay, J.D. & Kay, L.E. Slow dynamics in folded and unfolded states of an SH3 domain. *J. Am. Chem. Soc.* **123**, 11341-11352 (2001).

206. Sykes, B.D. & Hull, W.E. Fluorine nuclear magnetic resonance studies of proteins. *Meth. Enzymol.* **49**, 270-295 (1978).

207. Gerig, J.T. Fluorine NMR. *Biophysics Textbook Online*, 1-35 (2001).

208. Gerig, J.T. Fluorine NMR of proteins. *Prog. Nucl. Magn. Reson. Spectrosc.* **26**, 293-370 (1994).

209. Danielson, M.A., Biemann, H., Koshland Jr, D.E. & Falke, J.J. Attractant-and disulfide-induced conformational changes in the ligand binding domain of the chemotaxis aspartate receptor: a 19F NMR study. *Biochemistry* **33**, 6100-6109 (1994).

210. Drake, S.K., Bourret, R.B., Luck, L.A., Simon, M.I. & Falke, J.J. Activation of the phosphosignaling protein CheY. I. Analysis of the phosphorylated conformation by 19F NMR and protein engineering. *J. Biol. Chem.* **268**, 13081-13088 (1993).

211. Hull, W.E. & Sykes, B.D. Fluorine-19 nuclear magnetic resonance study of fluorotyrosine alkaline phosphatase: the influence of zinc on protein structure and a conformational change induced by phosphate binding. *Biochemistry* **15**, 1535-1546 (1976).

212. Arseniev, A.S. et al. 19F NMR study of 5-fluorotryptophan-labeled bacteriorhodopsin. *FEBS Lett.* **213**, 283-288 (1987).

213. Brauer, M. & Sykes, B.D. Fluorine-19 nuclear magnetic resonance studies of selectively fluorinated derivatives of G-and F-actins. *Biochemistry* **25**, 2187-2191 (1986).

214. Labroo, V.M. et al. Direct electrophilic fluorination of tyrosine in dermorphin analogues and its effect on biological activity, receptor affinity and selectivity. *Int. J. Pept. Protein Res.* **37**, 430-439 (1991).

215. Xiao, G., Parsons, J.F., Tesh, K., Armstrong, R.N. & Gilliland, G.L. Conformational changes in the crystal structure of rat glutathione transferase M1-1 with global substitution of 3-fluorotyrosine for tyrosine. *J. Mol. Biol.* **281**, 323-339 (1998).

216. Kitevski-LeBlanc, J.L. & Prosser, R.S. Current applications of 19F NMR to studies of protein structure and dynamics. *Prog. Nucl. Magn. Reson. Spectrosc.* **62**, 1-33 (2011).

217. Lu, P., Jarema, M., Mosser, K. & Daniel, W.E. lac repressor: 3-fluorotyrosine substitution for nuclear magnetic resonance studies. *Proc. Natl. Acad. Sci. U.S.A.* **73**, 3471-3475 (1976).

218. Kim, H., Perez, J.A., Ferguson, S.J. & Campbell, I.D. The specific incorporation of labelled aromatic amino acids into proteins through growth of bacteria in the presence of glyphosate: Application to fluorotryptophan labelling to the H -ATPase of Escherichia coli and NMR studies. *FEBS Lett.* **272**, 34-36 (1990).

219. Jackson, J.C., Hammill, J.T. & Mehl, R.A. Site-specific incorporation of a 19F-amino acid into proteins as an NMR probe for characterizing protein structure and reactivity. *J. Am. Chem. Soc.* **129**, 1160-1166 (2007).

220. Wang, L., Brock, A., Herberich, B. & Schultz, P.G. Expanding the genetic code of Escherichia coli. *Science* **292**, 498-500 (2001).

221. Williams, S.P., Fulton, A.M. & Brindle, K.M. Estimation of the intracellular free ADP concentration by fluorine-19 NMR studies of fluorine-labeled yeast phosphoglycerate kinase in vivo. *Biochemistry* **32**, 4895-4902 (1993).

222. Ye, L., Larda, S.T., Li, Y.F.F., Manglik, A. & Prosser, R.S. A comparison of chemical shift sensitivity of trifluoromethyl tags: optimizing resolution in 19 F NMR studies of proteins. *J. Biomol. NMR* **62**, 97-103 (2015).

223. Hull, W.E. & Sykes, B.D. Fluorotyrosine alkaline phosphatase: internal mobility of individual tyrosines and the role of chemical shift anisotropy as a 19F nuclear spin relaxation mechanism in proteins. *J. Mol. Biol.* **98**, 121-153 (1975).

224. Rashid, S., Lee, B.L., Wajda, B. & Spyracopoulos, L. Side-chain dynamics of the trifluoroacetone cysteine derivative characterized by 19F NMR relaxation and molecular dynamics simulations. *J. Phys. Chem. B* **123**, 3665-3671 (2019).

225. Marsh, E.N.G. & Suzuki, Y. Using 19F NMR to probe biological interactions of proteins and peptides. *ACS Chem. Biol.* **9**, 1242-1250 (2014).

226. Hoeltzli, S.D. & Frieden, C. Stopped-flow NMR spectroscopy: real-time unfolding studies of 6-19F-tryptophan-labeled Escherichia coli dihydrofolate reductase. *Proc. Natl. Acad. Sci. U.S.A.* **92**, 9318-9322 (1995).

227. Li, H. & Frieden, C. Observation of sequential steps in the folding of intestinal fatty acid binding protein using a slow folding mutant and 19F NMR. *Proc. Natl. Acad. Sci. U.S.A.* **104**, 11993-11998 (2007).

228. Kitevski-LeBlanc, J.L., Hoang, J., Thach, W., Larda, S.T. & Prosser, R.S. 19F NMR studies of a desolvated near-native protein folding intermediate. *Biochemistry* **52**, 5780-5789 (2013).

229. Suzuki, Y., Brender, J.R., Hartman, K., Ramamoorthy, A. & Marsh, E.N.G. Alternative pathways of human islet amyloid polypeptide aggregation distinguished by 19F nuclear magnetic resonance-detected kinetics of monomer consumption. *Biochemistry* **51**, 8154-8162 (2012).

230. Suzuki, Y. et al. Resolution of oligomeric species during the aggregation of Aβ1–40 using 19F NMR. *Biochemistry* **52**, 1903-1912 (2013).

231. Evanics, F., Kitevski, J.L., Bezsonova, I., Forman-Kay, J. & Prosser, R.S. 19F NMR studies of solvent exposure and peptide binding to an SH3 domain. *Biochim. Biophys. Acta Gen. Subj.* **1770**, 221-230 (2007).

232. Anderluh, G. et al. Interaction of the eukaryotic pore-forming cytolysin equinatoxin II with model membranes: 19F NMR studies. *J. Mol. Biol.* **347**, 27-39 (2005).

233. Falke, J.J., Luck, L.A. & Scherrer, J. 19F nuclear magnetic resonance studies of aqueous and transmembrane receptors. Examples from the Escherichia coli chemosensory pathway. *Biophys. J.* **62**, 82 (1992).

234. Liu, J.J., Horst, R., Katritch, V., Stevens, R.C. & Wüthrich, K. Biased signaling pathways in β2-adrenergic receptor characterized by 19F-NMR. *Science* **335**, 1106-1110 (2012).

235. Horst, R., Liu, J.J., Stevens, R.C. & Wüthrich, K. β2-Adrenergic Receptor Activation by Agonists Studied with 19F NMR Spectroscopy. *Angew. Chem. Int. Ed.* **52**, 10762-10765 (2013).

Chapter 2

Sidechain Dynamics of the Trifluoroacetone Cysteine Derivative Characterized by ^{19}F NMR Relaxation and Molecular Dynamics Simulations

This chapter has been published as "**Rashid, S.**, Lee, B.L., Wajda, B. & Spyracopoulos, L. Sidechain dynamics of the trifluoroacetone cysteine derivative characterized by 19F NMR relaxation and molecular dynamics simulations. *The Journal of Physical Chemistry B* **123**, 3665-3671 (2019)". S.R. expressed and purified all proteins with the help of B.W; S.R. collected NMR data. S.R. and L.S. conducted the MD simulations. S.R., B.L.L., and L.S. analyzed NMR data. S.R. and L.S. wrote the manuscript.

Introduction

Dynamic processes in proteins have been studied extensively using NMR relaxation techniques, allowing for characterization of mainchain and sidechain fluctuations as well as molecular tumbling, on the picosecond to millisecond timescale range[1,2]. ^{19}F NMR spectroscopy has proven to be a powerful tool for structural and dynamic analyses of proteins, especially high molecular weight proteins[3]. The advantages of ^{19}F NMR for protein studies include the fact that ^{19}F is not found in proteins, it is a 100% abundant, highly NMR sensitive nucleus, possesses a large chemical shift anisotropy, and can be incorporated into proteins through media supplementation, engineered tRNA synthetase/tRNA pairs[4], as well as chemical modification of cysteine residues[5,6]. With respect to the last point, one of the more common modifying reagents is 3-bromo-1,1,1-trifluoroacetone (BTFA)[7]. This compound allows for facile derivatization of cysteine residues to attach a terminal fluoromethyl group that functions as a valuable reporter on structural and dynamic processes in proteins[8,9]. However, interpretation of the sidechain dynamic properties of proteins bearing the non-standard cysteine-TFA derivative, or CYF residue, using ^{19}F NMR spectroscopy is hindered due to lack of a fully developed theoretical foundation.

^{19}F NMR relaxation for the non-standard CYF residue in proteins is sensitive to fast internal rotation about the methyl CF_3 symmetry axis of its sidechain[9], as well as the internal motion of the methyl symmetry axis. To develop a quantitative understanding of the combined contributions of methyl rotation and side chain dynamics to ^{19}F-T_2 NMR relaxation time (or rate constant, $R_2 = 1/T_2$), we extended the relaxation expressions for overall molecular tumbling with fast methyl rotation to include sidechain motions using the model free approach[10,11]. Using MD simulations, we developed an atomic view of sidechain motions on the pico- to nanosecond timescale[12]. We applied this methodology to the D61C mutant of the N-terminal domain of yeast Hsp90 (Hsp90N^{CYF61}), which resides on a rigid, solvent exposed loop. Our results indicate that as expected, rapid methyl rotation narrows the ^{19}F NMR linewidth. However, the flexibility of the CYF sidechain also has a substantial contribution to the linewidth, depending on the amplitude and rate of the internal motion.

Our findings highlight the utility of the CYF reporter as a sensitive indicator of sidechain environment and dynamics.

Materials and Methods

Cloning, Protein Expression, and Purification

DNA sequences for the N-terminal domain from yeast Hsp90 (Hsp90N, residues 1-210, UniProtKB entry P02829) and the D61C mutant (Hsp90N^{D61C}) were synthesized and inserted into the pHis-parallel1 vector[13] by Genscript. The constructs were amplified in *E. coli* DH5-α cells and expressed in *E. coli* strain BL21 (DE3) RIPL cells. [*U*-^{15}N]-Hsp90N and [*U*-^{15}N]-Hsp90N^{D61C} were produced according to previous methods[14]. Cells were grown to an OD_{600} of ~0.6-0.8 after which the cells were pelleted, suspended in 500 ml of MOPS/tricine wash buffer (40 mM MOPS, 4 mM tricine, 150 mM NaCl, pH 7.4), pelleted and resuspended in 500 ml of MOPS/tricine minimal media[15] containing 0.5 g of $(^{15}NH_4)_2SO_4$ as the sole source of nitrogen. Cells were then incubated at 37 °C for ~1 hour, after which the temperature was reduced to 16 °C and protein expression was induced with 0.4 mM Isopropyl β-D-thiogalactopyranoside (IPTG) after an additional 30 minutes, incubated overnight at 16 °C with shaking (260 rpm) and finally harvested by centrifugation.

For [*U*-^{15}N]-Hsp90N and [*U*-^{15}N]-Hsp90N^{D61C} purification, His-tagged proteins were first purified using a HisPrep FF 16/10 affinity column. The histidine tag was cleaved through addition of 150 µl of 210 µM TEV protease to ~20 mL of protein solution, and the tag was separated from protein using a second pass through the affinity column, and subsequently purified using size exclusion chromatography with a HiLoad 26/60 Superdex 75 column in 50 mM Tris pH 7.3, 150 mM NaCl, 1 mM DTT. To produce TFA labeled protein, [*U*-^{15}N]-Hsp90N^{CYF61}, purified [*U*-^{15}N]-Hsp90N^{D61C} was concentrated to ~250 µM, treated with 2 mM TCEP and incubated at room temperature for 30 minutes to reduce cysteine. Excess BTFA (PCR Inc.) was added to reduced protein in a 1.3:1 ratio and reacted at room temperature for 1 hour. Excess label was then removed using size exclusion chromatography as described above. We determined that the protein was fully labeled by referencing the ^{19}F

peak area for TFA-labeled protein to the peak area of the methyl group from trifluoroacetic acid with 1D ^{19}F NMR spectroscopy, using a long interscan delay of 10 s for peak area accuracy.

NMR Spectroscopy

Samples for NMR spectroscopy contained ~250 μM protein, 25 mM HEPES, pH 7.3, 150 mM NaCl, 10% D_2O, 0.2 mM 4,4-dimethyl-4-silapentane-1-sulfonic acid (DSS) as a chemical shift reference for ^{1}H, and 0.3 mM trifluoroacetic acid as a chemical shift reference for ^{19}F. Protein concentrations were determined using the Bio-Rad assay. NMR experiments were acquired at 25 °C on Bruker spectrometers operating at ^{1}H Larmor frequencies of 700 and 800 MHz, or 16.4 and 18.8 T, respectively, equipped with TCI Helium H&F/-C/N cryogenic probes. The 2D ^{1}H-^{15}N-HSQC spectrum for [*U*-^{15}N]-Hsp90N was acquired on a Varian Unity INOVA 600 MHz spectrometer at 25 °C. Mainchain amide ^{15}N-T_1 and ^{15}N-T_2 relaxation times were measured for [*U*-^{15}N]-Hsp90N^{CYF61} at 18.8 T. For the ^{15}N-T_1 experiment, relaxation delays were set to 20, 60, 100, 200, 400, 600, 800, 1200 ms. For ^{15}N-T_2 experiments, relaxation delays were set to n □ 17.96, with n = 1, 2, ... ,7, 8 ms. ^{19}F-T_2 values were measured using the CPMG experiment[16,17] with eight spacings (τ_{CPMG}) between 180° pulses of 0.6, 0.8, 1.0, 1.20, 1.41, 1.6, 2.0, and 2.4 ms at a ^{19}F Larmor frequency of 753 MHz (18.8 T), and two τ_{CPMG} spacings of 0.6 and 2.4 ms at 657 MHz (16.4 T). For these pulse repetition rates, T_2 decays were determined using five or six relaxation delays spread out over ~40 or 48 ms, at 16.4 and 18.8 T, respectively. NMR spectra were processed with NMRPipe[18] and analyzed with NMRViewJ[19]. Relaxation times were determined by fitting peak areas to a two-parameter exponential decay using non-linear regression in Mathematica.

The 2D ^{1}H-^{15}N HSQC NMR spectrum for Hsp90N was assigned using chemical shifts deposited in the Biological Magnetic Resonance Data Bank (accession number 5355).

Model-Free Analysis for the ^{19}F NMR Relaxation Rate of the Cysteine-TFA Derivative

For ^{19}F-labeled residues, the spin-spin, or R_2 relaxation rate is dominated by the chemical shift anisotropy (CSA) of the fluorine nucleus, and expressions for the combined effects of overall protein tumbling and fast methyl rotation have been derived[9]. We extended these expressions to include the internal motion of the CYF sidechain:

$$R_2^{CSA} = \frac{1}{40}\left[\gamma_F^2 B_0^2 \delta_z^2\right]\begin{bmatrix} c_0(\alpha,\beta)\{3J_0(\omega_F)+4J_0(0)\}+ \\ c_1(\alpha,\beta)\{3J_1(\omega_F)+4J_1(0)\}+ \\ c_2(\alpha,\beta)\{3J_2(\omega_F)+4J_2(0)\} \end{bmatrix} \quad [1]$$

with:

$$c_0(\alpha,\beta) = \frac{1}{4}\begin{bmatrix} \left(3\mathrm{Cos}(\alpha)^2-1\right)+ \\ \eta\,\mathrm{Sin}(\alpha)^2\,\mathrm{Cos}(2\beta) \end{bmatrix}^2 \quad [2]$$

$$c_1(\alpha,\beta) = \frac{1}{3}\mathrm{Sin}(\alpha)^2\begin{bmatrix} \mathrm{Cos}(\alpha)^2\left(3-\eta\,\mathrm{Cos}(2\beta)\right)^2+ \\ \eta^2\,\mathrm{Sin}(2\beta)^2 \end{bmatrix} \quad [3]$$

$$c_2(\alpha,\beta) = \left(\sqrt{\frac{3}{4}}\,\mathrm{Sin}(\alpha)^2 + \frac{\eta\left(1+\mathrm{Cos}(\alpha)^2\right)\mathrm{Cos}(2\beta)}{2\sqrt{3}}\right)^2 + \frac{1}{3}\eta^2\,\mathrm{Sin}(2\beta)^2\,\mathrm{Cos}(\alpha)^2 \quad [4]$$

where γ_F is the magnetogyric ratio for ^{19}F, 25.176×10^7 rad s^{-1} T^{-1}, B_0 is the applied magnetic field in T, $\omega_F = \gamma_F B_0$ for the methyl fluorines, δ_z is the anisotropy of the chemical shift (72 ppm)[9,20], α and β are the Euler angles for rotation of the diffusion principal axes into the chemical shift axes, 70° and 0°, respectively (Figure 2.1), and the asymmetry of the chemical shift tensor is given by η = –0.972. The components for the traceless part of the chemical shift tensor δ, are 72, –70, and –1 ppm for δ_z, δ_y, and δ_x, respectively[9,20].

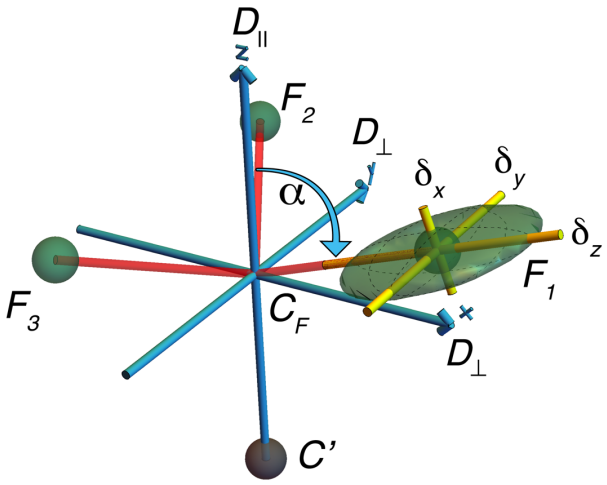

Figure 2.1: Orientation of the ^{19}F chemical shift tensor for a trifluoromethyl group. The tensor in the principal axis system was rendered by plotting the absolute values of δ normalized to $|\delta_z|$ with the magnitude of δ_x increased by a factor of ten to facilitate rendering. The parallel and perpendicular components of an axially symmetric diffusion tensor are shown. The D_y ($D_\perp$) and δ_y components are collinear with $\beta = 0°$.

The spectral densities in eq. 1 are given by[10,11]:

$$J_n(\omega) = 2\left[\frac{S^2\tau_n}{1+(\omega\tau_n)^2} + \frac{(1-S^2)\tau_n'}{1+(\omega\tau_n')^2}\right] \qquad [5]$$

where S^2 is the generalized order parameter, n = 0, 1, and 2, and the correlation times are given by

$$\tau_0 = \tau_c \qquad \tau_0' = \frac{\tau_c\tau_i}{\tau_c+\tau_i}$$

$$\tau_1 = \frac{\tau_c\tau_e}{\tau_c+\tau_e} \qquad \tau_1' = \frac{\tau_1\tau_i}{\tau_1+\tau_i}$$

$$\tau_2 = \frac{\tau_c\tau_e}{4\tau_c+\tau_e} \qquad \tau_2' = \frac{\tau_2\tau_i}{\tau_2+\tau_i} \qquad [6]$$

with the overall correlation time for protein tumbling given by τ_c, and the internal correlation time for the CYF sidechain given by τ_i, with $\tau_i << \tau_c$. Under the assumptions of isotropic overall tumbling and fast methyl rotation with $\tau_e \sim 0$, the coefficients c_n and correlation times τ_n reduce to zero for $n = 1, 2$. S^2 and τ_i model free parameters were obtained through global optimization of the squared difference between the experimental R_2 and that calculated using eqs. 1-6 , using the NMinimize command in Mathematica, with parameter errors obtained through Monte Carlo analyses, as previously described[21].

Calculation of Atomic Charges for the Non-Standard CYF residue

To conduct MD simulations for Hsp90N^{CYF61}, we developed a force field library for the non-standard derivative residue or CYF. Atom types and parameters for Lennard-Jones interactions, bonds, angles, and torsion angles were taken from the generalized AMBER force field[22]. Atomic charges for the CYF residue were generated using multiconformation[23], two-stage restrained electrostatic potential (RESP) calculations in the AMBER biomolecular suite of programs[24-26]. Extended and α-helical conformations for CYS-CH_2COCF_3 capped with N-methyl and acetyl groups (NME-CYF-ACE) were built for RESP calculations. Dihedral angles for the α-helical conformation were set at $\phi = -57°$, $\psi = -47°$, $\chi^1 = -60°$, for the extended conformation, $\phi = -135°$, $\psi = +135°$, $\chi^1 = -60°$. For each NME-CYF-ACE conformation, the Gaussian program[27] was used for geometry optimization, and the electrostatic potential was calculated in implicit solvent using the polarizable continuum model, at the HF/6-31G* level of theory. Atomic charges were subsequently calculated from the electrostatic potentials using multi-conformation, two-stage RESP, and used within the CYF force field library file for conducting MD simulations.

MD Simulations for Hsp90N^{CYF61}

Starting from the pdb file for the structure of Hsp90N (1ah6)[28] we added an N-terminal methionine and substituted aspartate 61 with a CYF residue to generate Hsp90N^{CYF61} using

the AMBER biomolecular suite of programs. MD simulations were carried out with the *ff*14SB[29] force field and the TIP3P water model. Hsp90N^{CYF61} was solvated in a truncated octahedron box of water with a minimum of 12 Å to the edges of the box and the system was neutralized using Na^+ ions. To begin MD simulations, energy minimization was applied for two rounds of 200 cycles, followed by heating from 0 to 300 K with 2 kcal/mol restraints on solute atoms over 50 ps, and subsequent density equilibration over 200 ps. Covalent bonds involving hydrogen were constrained using the SHAKE algorithm[30], and an 8 Å cut-off was used as the maximum distance for pairwise nonbonded and electrostatic interactions. Langevin dynamics with a collision frequency of 2 ps^{-1} were used to regulate temperature.

Production dynamics were conducted for ~160 ns with particle mesh Ewald molecular dynamics (PMEMD)[31]. Time steps were 2 fs, energy information was printed out every 5000 steps, and MD trajectories were written out every 1000 steps. MD trajectories from the simulation were processed with CPPTRAJ[32].

Time correlation functions for the C–F vector for methyl rotation and the methyl symmetry axis were calculated using the expression:

$$C(t) = \langle P_2[\bar{\mu}(0) \cdot \bar{\mu}(t)] \rangle \qquad [7]$$

with the second order Legendre polynomial given by $P_2(x) = \left(3x^2 - 1\right)/2$, $\bar{\mu}(t)$being the unit vector for the C–F bond or C–C_{methyl} bond, and the brackets indicating the average over the time steps of the simulation. Correlation functions for methyl rotation of the C–F vector were averaged over four 100 ps windows. The correlation function for the CF_3 methyl axis motion was calculated from the average of 128 1 ns windows from the last 128 ns of the simulation. The averaged correlation function was subsequently fit using the two-parameter Lipari-Szabo mono-exponential function to extract S^2 and τ_i[10,11]:

$$C(t) = S^2 + \left(1 - S^2\right) e^{-t/\tau_i} \qquad [8]$$

Results and Discussion

^{15}N and ^{19}F NMR Relaxation

Yeast Hsp90 does not contain cysteine; thus, to conduct ^{19}F NMR studies, we modified the ATPase domain of the yeast Hsp90^{D61C} mutant (residues 1-210, Hsp90N^{D61C}) with BTFA, a widely used cysteine modifying agent bearing a trifluoromethyl group. To determine the sidechain motional properties of the non-standard CYF residue, we used [*U*-^{15}N]-Hsp90N^{CYF61}. This approach allowed us to jointly determine the overall rotational correlation time for molecular tumbling using ^{15}N NMR relaxation, and the sidechain methyl dynamics using ^{19}F NMR relaxation from a single sample with a Bruker TCI Helium H&F/-C/N cryogenic probe. We chose aspartate 61 for mutation to cysteine as it is solvent exposed, and this region of the mainchain is rigid, as determined through previous model-free analysis[33]. The ^{19}F NMR spectrum at a Larmor frequency of 753 MHz (18.8 T) for Hsp90N^{CYF61} shows a single, narrow, and intense resonance (Figure 2.2A). Furthermore, the 2D ^{1}H-^{15}N-HSQC spectrum at a ^{1}H Larmor frequency of 600 MHz for Hsp90N, superimposed with that from Hsp90N^{CYF61} at 800 MHz shows that inclusion of CYF at position 61 does not cause significant structural perturbations, with small chemical shift changes localized to residues adjacent to position 61 (Figure 2.2B).

From the decay of the one-dimensional amide ^{1}H envelope from ^{1}H-^{15}N HSQC relaxation experiments, ^{15}N-T_1 and -T_2 relaxation times were determined to be 1200 ± 90 and 62 ± 2 ms, respectively, at a field strength of 18.8 T. The T_1/T_2 ratio was fit as previously described[34], to calculate a τ_c value for Hsp90N^{CYF61} of 10.6 ns, which is in excellent agreement with the value of 10.7 ns determined in a previous model-free analysis[33]. Importantly, this previous model-free study also determined that Hsp90N tumbles isotropically in solution, with a small anisotropy of $D_{\parallel}/D_{\perp}$ = 1.12 ± 0.01. However, the rotational diffusion anisotropy for many proteins exceeds 1.17[35]. For these cases, the spectral density functions for mainchain amide ^{15}N relaxation can be generalized to account for anisotropic diffusion[36]. Furthermore, MD simulations can facilitate a detailed molecular interpretation of dynamics for proteins with anisotropic shapes[37,38].

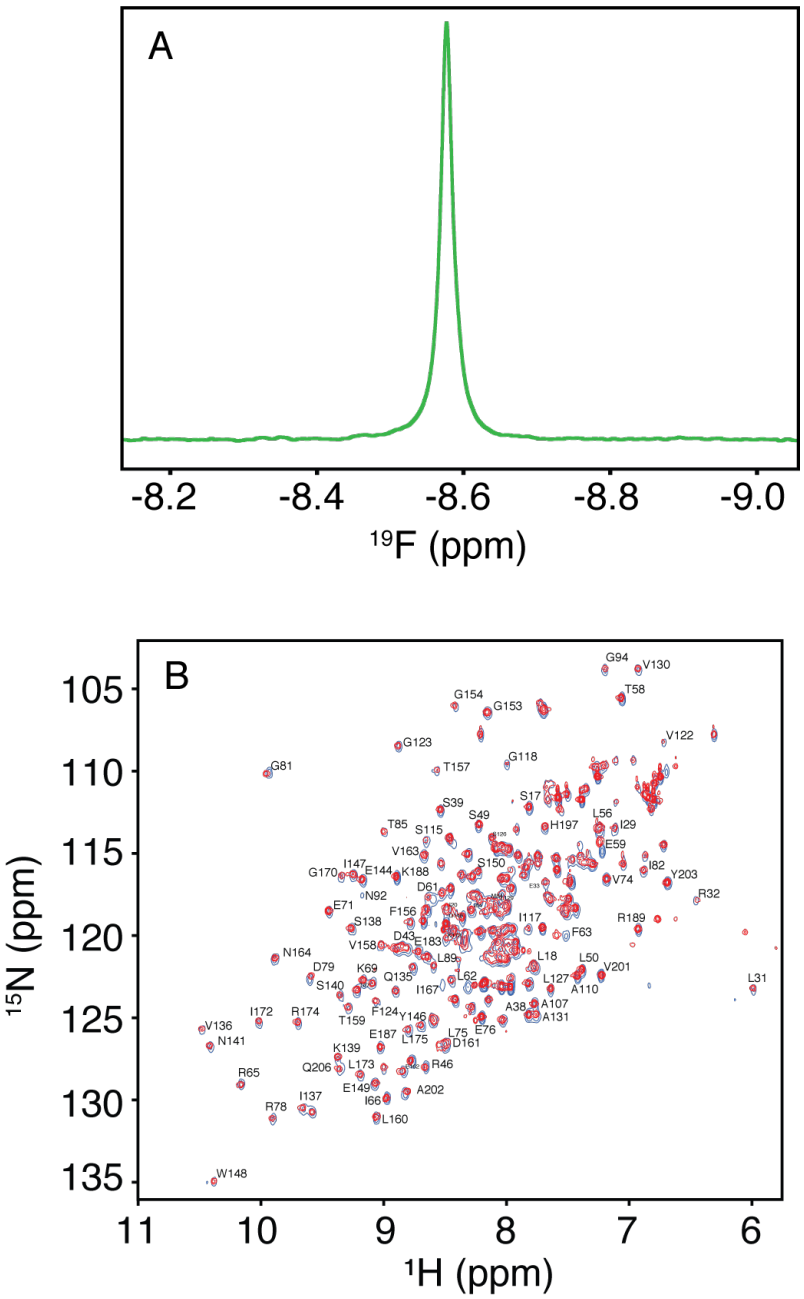

Figure 2.2: (A) ^{19}F NMR spectrum for Hsp90N^{CYF61}. The FID was multiplied with a 5 Hz exponential function prior to Fourier transformation. (B) ^{1}H-^{15}N HSQC NMR spectra for Hsp90N (blue) and Hsp90N^{CYF61} (red).

For the Hsp90N^{CYF61} fluoromethyl, we measured an average ^{19}F-T_2 relaxation time of 39.3 ± 0.5 ms, for multiple CPMG 180° pulse repetition times (τ_{CPMG}) at 18.8 T. ^{19}F-T_2 relaxation times at 16.4 T are 50.1 ± 0.3 and 51.3 ± 0.5 ms, at τ_{CPMG} values of 0.6 and 2.4 ms, respectively. The T_2 values at 16.4 and 18.8 T are dominated by ^{19}F chemical shift anisotropy (CSA). Furthermore, the measured ^{19}F-T_2 values do not show a dependence on the 180° pulse repetition rate during CPMG experiments, indicating that there are no contributions from micro- to millisecond timescale motions. Importantly, in cases where such contributions are present, they can be readily quantified using CPMG relaxation dispersion methods[1,39]. Thus, extension of the model free approach to the fast pico- to nanosecond timescale fluctuations of the CYF sidechain allows for separation and quantification of these motions from those arising as a result of slower motions that would be evident as dispersion profiles in CPMG relaxation experiments.

As in previous studies[8], we note that the ^{19}F-T_1 value we measured (~350 ms) cannot be interpreted quantitatively, as the expected contributions from both the ^{19}F CSA and ^{19}F-^{19}F dipolar interactions are extremely small (Supporting Methods and Figure 2.S1). This indicates that there are other contributions to the measured T_1 likely from dipolar interactions with solvent protons, as well as paramagnetic contaminants such as dissolved molecular oxygen and metal ions[8].

Model-Free Analyses of ^{19}F NMR Relaxation

Nuclear spin relaxation rates for proteins are widely interpreted using the model-free approach[2]. The relaxation of a given nucleus in a protein is governed by overall rotational tumbling and internal motions. The model free approach allows for relatively straightforward analyses of mainchain and sidechain dynamics in terms of a generalized order parameter S^2 and an associated internal correlation time τ_i[10,11]. S^2 specifies the degree of freedom of a given bond vector, where a value of 0 indicates no restriction in motion and 1 indicates complete restriction. The associated internal time τ_i specifies the timescale of motion for a given bond

vector and is generally fast on the ps-ns timescale. The combination of S^2 and τ_i parameters can adequately provide a physical interpretation of motion for protein dynamics[10,11].

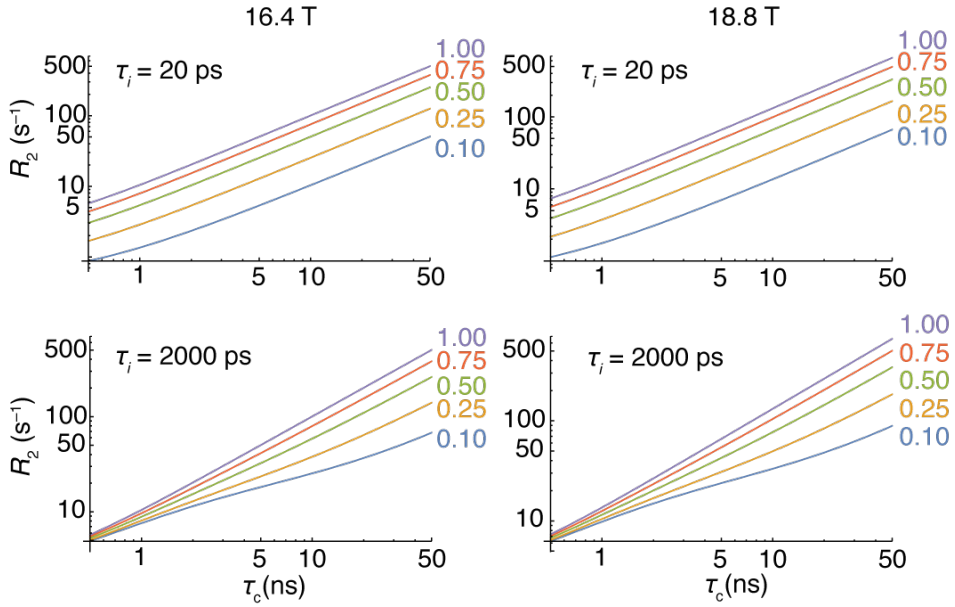

Figure 2.3: ^{19}F-R_2 ($1/T_2$) values for the CYF residue predicted from the model free approach for fast (top) and slow picosecond (bottom) sidechain internal motions at ^{19}F Larmor frequencies of 657 (left) and 753 MHz (right), with corresponding S^2 values.

To interpret the ^{19}F-T_2 value for the CYF residue, we modified previous expressions for ^{19}F-T_2 relaxation[9] that account for overall protein tumbling and fast rotation of the methyl group about the methyl axis, to include the internal motion of the CYF sidechain, according to the model-free approach (eqs. 1-6). We assume that methyl rotation is fast on the picosecond timescale, such that the lifetime for the internal motion, τ_e, is ~0. Under this condition, the modified expressions for the ^{19}F-T_2 of the CYF sidechain indicate that if the sidechain is flexible (S^2 ~0.1) when attached to a rigid protein backbone, the ^{19}F NMR linewidth at half height ($1/\pi T_2$, or R_2/π,), is reasonably narrow over a wide range of protein sizes (Figure 2.3). In this regard, the rotational correlation times (ns) for spherical proteins are proportional to half their molecular mass (kDa), or τ_c ~ kDa/2 (Figure 2.3). Under the condition of fast methyl rotation, and with a τ_c of 10.6 ns, we simultaneously fit the ^{19}F-T_2

values at 16.4T and 18.8 T to give $S^2 = 0.11 \pm 0.02$ and $\tau_i = 900 \pm 300$ ps (eq. 8). These values indicate that the CYF sidechain is highly flexible at the D61 position of the Hsp90 ATPase domain.

Model-Free Parameters for the CYF Residue from MD Simulations

Site-specific S^2 values can be derived from MD simulations to complement NMR studies, and provide atomistic information on the timescale and amplitude of molecular motion on the ps-ns range, through the analysis of correlation functions for given bond vectors[12,40]. To interpret the ^{19}F-T_2 relaxation parameters for the CYF residue, we conducted MD simulations with the AMBER suite of biomolecular simulation programs[26]. Partial atomic charges for the non-standard CYF residue were generated using multiple conformation two-stage RESP fits for the molecule NME-CYF-ACE and used in the *ff*14SB force field (Figure 2.4A).

The α-helical and extended conformations of NME-CYF-ACE were used for the multiple conformation fit as they represent the two most probable conformations CYF can adopt in proteins. The two-stage RESP method[25] for charge fitting ensures that chemically equivalent nuclei retain identical charges, which is appropriate for conformational analyses. Furthermore, atomic charges generated from a multiple conformation two-stage RESP fits offer the advantage of applicability to a broader range of systems[25,41]. Representative structures taken over an 8 ns window demonstrate the large amplitude movements of the CYF sidechain (Figure 2.4B). For fast methyl rotation, we calculated the correlation function for the C-F vector of the fluoromethyl group, and fit the decay to eq. 8 to determine values of S^2 and τ_i of 0.135 ± 0.001 and 2.77 ± 0.04 ps, respectively, in reasonable agreement with the expected S^2 value of 0.111 for a C–H methyl bond vector[11] (Figure 2.5A). Recently, for the methyl-bearing amino acids, greater accuracy between NMR-derived methyl group dynamics and MD simulations has been achieved through forcefield re-parameterization[42]. This result suggests that re-parameterization of the barriers for fluoromethyl rotation could also lead to better agreement between the NMR and MD results.

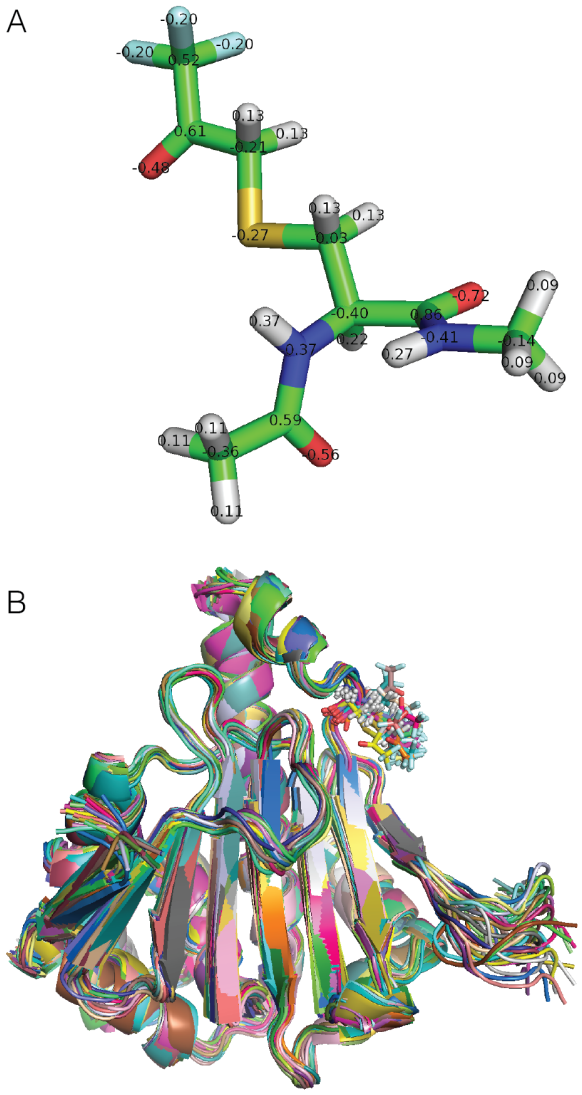

Figure 2.4: (A) Atomic charges for the CYF residue from multi-conformation, two-stage RESP calculations. (B) Snapshots taken from the MD simulation for Hsp90N^{CYF61}. The mainchain is shown in the cartoon representation, and the CYF sidechain is shown in the stick representation.

From our MD simulation, we also determined the correlation function for the vector representing the methyl axis (Figure 2.5B). This function decays rapidly on the picosecond timescale, and a fit to the model-free function (eq. 8) yields S^2 and τ_i of 0.129 ± 0.001 and 17.2 ± 0.3 ps, respectively, for the CYF sidechain. These values are in good agreement with the experimentally determined values of S^2 = 0.11 ± 0.02 and τ_i = 900 ± 300 ps, at 18.8 and

16.4 T. The slow tail in the correlation function up to ~250 ps (Figure 2.5B), represents slower subnano- to nanosecond timescale fluctuations around the CYF χ^1 and χ^2 dihedral angles that are evident in the MD simulation. A similar richness in dynamics has been observed for the methyl bearing amino acids in proteins through combined MD simulations and NMR relaxation measurements[35]. As demonstrated in that study, the two parameter Lipari-Szabo correlation function (eq. 8) does not adequately fit the total correlation function for more complex sidechain dynamics. However, a reasonable estimate for the methyl axis S^2 can be obtained, at the expense of overestimating the internal correlation time.

Finally, anisotropic overall tumbling, and potentially coupling of slower sidechain motions to overall tumbling, can lead to inaccuracies in the methyl axis order parameter[35]. For the methyl bearing amino acids, the RMSD between MD simulations and NMR relaxation measurements is ~0.1[35], indicative of the accuracy limit for the methyl axis S^2 derived from MD simulations.

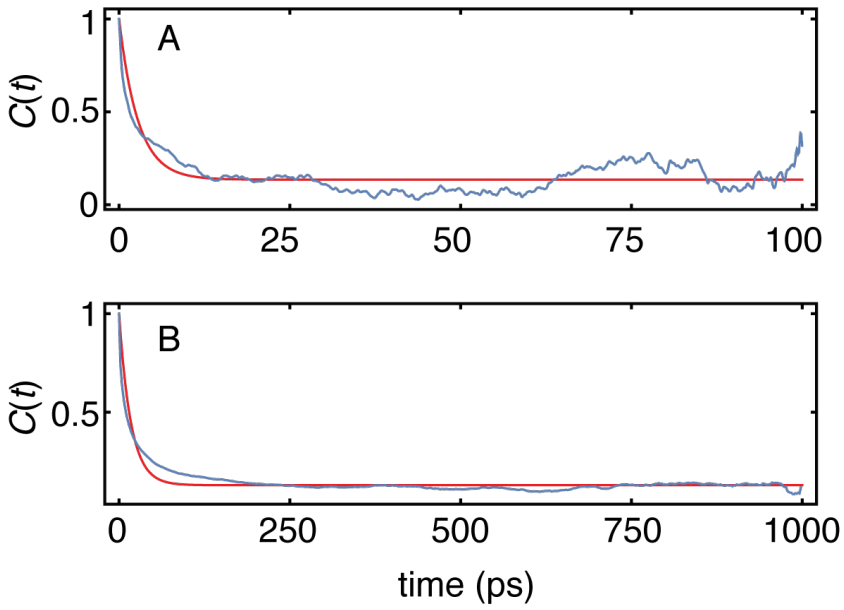

Figure 2.5: (A) Correlation functions for fast internal rotation of the CYF methyl group (blue) with the associated fit to a model free correlation function (red). (B) Correlation function for the CYF sidechain methyl axis, with the associated fit to the model-free correlation function (red).

These results demonstrate the utility of MD simulations to provide an atomic view of motions to understand sidechain dynamics of the non-standard CYF residue determined using the two-parameter model free approach for the methyl axis S^2. The approach can be applied to the methyl axis for various cysteine modifying reagents that bear trifluoromethyl groups, assuming that the components of the ^{19}F chemical shift tensor for the methyl group are similar. This would facilitate an understanding of pico- to nanosecond timescale sidechain dynamics for the derivatives in the context of protein structure[5]. In this regard, the bulk and polarity of the CYF probe would limit its usefulness for probing the interior of proteins. This challenge could potentially be overcome through use of trifluoromethyl variants of proteogenic amino acids such as alanine and threonine. However, methods for synthesis and incorporation of these labeled amino acids are not well developed.

Conclusion

The trifluoroacetone cysteine derivative, or CYF residue, has long been recognized as a useful probe for studying protein dynamics, structure, and interactions. The utility of the probe arises from the high sensitivity of the fluorine chemical shift to environment. Additionally, rapid methyl rotation and sidechain flexibility result in narrow NMR resonances, and this facilitates studies of large molecular weight proteins. However, both fast (pico- to nanosecond) and slow (micro- to millisecond) timescale motions contribute to the ^{19}F NMR linewidth, and separation of these contributions is difficult. We developed a model free approach to characterize the contributions of pico- to nanosecond timescale internal motions of the CYF sidechain to the ^{19}F-T_2 value. The methodology allows for separation of the contributions of fast dynamics from slower micro- to millisecond dynamics, and ultimately, can facilitate a quantitative understanding of changes in fast timescale fluctuations for dynamic processes occurring in proteins. Furthermore, the methodology can be applied to a variety of cysteine-specific trifluoromethyl probes.

References

1. Palmer, A. G. Probing molecular motion by NMR. *Curr. Opin. Struct. Biol.* **7**, 732-737 (1997).

2. Jarymowycz, V. A. & Stone, M. J. Fast time scale dynamics of protein backbones: NMR relaxation methods, applications, and functional consequences. *Chem. Rev.* **106**, 1624-1671 (2006).

3. Gerig, J. T. Fluorine NMR of proteins. *Prog. Nucl. Magn. Reson. Spectrosc.* **26**, 293-370 (1994).

4. Jackson, J. C., Duffy, S. P., Hess, K. R. & Mehl, R. A. Improving nature's enzyme active site with genetically encoded unnatural amino acids *J. Am. Chem. Soc.* **128**, 11124-11127 (2006).

5. Ye, L., Larda, S. T., Frank Li, Y. F., Manglik, A. & Prosser, R. S., A comparison of chemical shift sensitivity of trifluoromethyl tags: optimizing resolution in ^{19}F NMR studies of proteins. *J. Biomol. NMR* **62**, 97-103 (2015).

6. Danielson, M. A. & Falke, J. J. Use of ^{19}F NMR to probe protein structure and conformational changes. *Annu. Rev. Biophys. Biomol. Struct.* **25**, 163-195 (1996).

7. Brown, W. E. & Seamon, K. B. Quantitation and characterization of the trifluoroacetonyl derivative of cysteine: A useful NMR probe. *Anal. Biochem.* **87**, 211-222 (1978).

8. Brauer, M. & Sykes, B. D. ^{19}F nuclear magnetic resonance studies of selectively fluorinated derivatives of G-Actin and F-Actin. *Biochemistry* **25**, 2187-2191 (1986).

9. Hull, W. E. & Sykes, B. D. Fluorotyrosine alkaline phosphatase: Internal mobility of individual tyrosines and the role of chemical shift anisotropy as a ^{19}F nuclear spin relaxation mechanism in proteins. *J. Mol. Biol.* **98**, 121-153 (1975).

10. Lipari, G. & Szabo, A. Model-free approach to the interpretation of nuclear magnetic resonance relaxation in macromolecules. 1. Theory and range of validity. *J. Am. Chem. Soc.* **104**, 4546-4559 (1982).

11. Lipari, G. & Szabo, A. Model-free approach to the interpretation of nuclear magnetic resonance relaxation in macromolecules. 2. Analysis of experimental results. *J. Am. Chem. Soc.* **104**, 4559-4570 (1982).

12. Case, D. A. Molecular dynamics and NMR spin relaxation in proteins. *Acc. Chem. Res.* **35**, 325-331 (2002).

13. Sheffield, P., Garrard, S. & Derewenda, Z. Overcoming expression and purification problems of RhoGDI using a family of "parallel" expression vectors. *Protein Expr. Purif.* **15**, 34-39 (1999).

14. Marley, J., Lu, M. & Bracken, C. A method for efficient isotopic labeling of recombinant proteins. *J. Biomol. NMR* **20**, 71-75 (2001).

15. Neidhardt, F. C., Bloch, P. L. & Smith, D. F. Culture medium for enterobacteria. *J. Bacteriol.* **119**, 736-747 (1974).

16. Carr, H. Y. & Purcell, E. M., Effects of diffusion on free precession in nuclear magnetic resonance experiments. *Phys. Rev.* **94**, 630-638 (1954).

17. Meiboom, S. & Gill, D., Modified spin-echo method for measuring nuclear relaxation times. *Rev. Sci. Instrum.* **29**, 688-691 (1958).

18. Delaglio, F. et al. NMRPipe: A multidimensional spectral processing system based on UNIX pipes. *J. Biomol. NMR* **6**, 277-293 (1995).

19. Johnson, B. A. & Blevins, R. A. NmrView: A computer program for the visualization and analysis of NMR data. *J. Biomol. NMR* **4**, 603-614 (1994).

20. Griffin, R. G., Ellett, J. D., Mehring, M., Bullitt, J. G. & Waugh, J. S. Single crystal study of ^{19}F shielding tensors of a trifluoromethyl group. *J. Chem. Phys.* **57**, 2147-2155 (1972).

21. Spyracopoulos, L. A suite of *Mathematica* notebooks for the analysis of protein main chain 15N NMR relaxation data. *J. Biomol. NMR* **36**, 215-224 (2006).

22. Wang, J. M., Wolf, R. M., Caldwell, J. W., Kollman, P. A. & Case, D. A. Development and testing of a general amber force field. *J. Comput. Chem.* **25**, 1157-1174 (2004).

23. Reynolds, C. A., Essex, J. W. & Richards, W. G. Atomic charges for variable molecular conformations. *J. Am. Chem. Soc.* **114**, 9075-9079 (1992).

24. Bayly, C. I., Cieplak, P., Cornell, W. D. & Kollman, P. A. A well behaved electrostatic potential based method using charge restraints for deriving atomic charges: The RESP model. *J. Phys. Chem.* **97**, 10269-10280 (1993).

25. Cornell, W. D., Cieplak, P., Bayly, C. I. & Kollman, P. A. Application of RESP charges to calculate conformational energies, hydrogen-bond energies, and free energies of solvation. *J. Am. Chem. Soc.* **115**, 9620-9631 (1993).

26. Cornell, W. D. et al. A second generation force field for the simulation of proteins, nucleic acids, and organic molecules. *J. Am. Chem. Soc.* **117**, 5179-5197 (1995).

27. Frisch, M. J. et al. *Gaussian 16 Rev. B.01*, Wallingford, CT, (2016).

28. Prodromou, C., Roe, S. M., Piper, P. W. & Pearl, L. H. A molecular clamp in the crystal structure of the N-terminal domain of the yeast Hsp90 chaperone. *Nat. Struct. Biol.* **4**, 477-482 (1997).

29. Maier, J. A. et al. ff14SB: Improving the accuracy of protein side chain and backbone parameters from ff99SB. *J. Chem. Theory Comput.* **11**, 3696-3713 (2015).

30. Ryckaert, J. P., Ciccotti, G. & Berendsen, H. J. C. Numerical integration of cartesian equations of motion of a system with constraints: Molecular dynamics of N-alkanes. *J. Comput. Phys.* **23**, 327-341 (1977).

31. Salomon-Ferrer, R., Gotz, A. W., Poole, D., Le Grand, S. & Walker, R. C. Routine microsecond molecular dynamics simulations with AMBER on GPUs. 2. Explicit solvent particle mesh Ewald. *J. Chem. Theory Comput.* **9**, 3878-3888 (2013).

32. Roe, D. R. & Cheatham, T. E. PTRAJ and CPPTRAJ: Software for processing and analysis of molecular dynamics trajectory data. *J. Chem. Theory Comput.* **9**, 3084-3095 (2013).

33. Richter, K. et al. Intrinsic inhibition of the Hsp90 ATPase activity. *J. Biol. Chem.* **281**, 11301-11311 (2006).

34. Kay, L. E., Torchia, D. A. & Bax, A. Backbone dynamics of proteins as studied by ^{15}N inverse detected heteronuclear NMR spectroscopy: Application to staphylococcal nuclease. *Biochemistry* **28**, 8972-8979 (1989).

35. Hoffmann, F., Xue, M. J., Schafer, L. V. & Mulder, F. A. A. Narrowing the gap between experimental and computational determination of methyl group dynamics in proteins. *Phys. Chem. Chem. Phys.* **20**, 24577-24590 (2018).

36. Tjandra, N., Feller, S. E., Pastor, R. W. & Bax, A. Rotational diffusion anisotropy of human ubiquitin from ^{15}N NMR relaxation. *J. Am. Chem. Soc.* **117**, 12562-12566 (1995).

37. Ollila, O. H. S., Heikkinen, H. A. & Iwai, H. Rotational dynamics of proteins from spin relaxation times and molecular dynamics simulations. *J. Phys. Chem. B* **122**, 6559-6569 (2018).

38. Anderson, J. S., Hernandez, G. & LeMaster, D. M. Prediction of bond vector autocorrelation functions from Larmor frequency-selective order parameter analysis of NMR relaxation data. *J. Chem. Theory Comput.* **13**, 3276-3289 (2017).

39. Akke, M. NMR methods for characterizing microsecond to millisecond dynamics in recognition and catalysis. *Curr. Opin. Struct. Biol.* **12**, 642-647 (2002).

40. Showalter, S. A. & Brüschweiler, R. Validation of molecular dynamics simulations of biomolecules using NMR spin relaxation as benchmarks: Application to the AMBER99SB force field. *J. Chem. Theory Comput*. **3**, 961-975 (2007).

41. Cieplak, P., Cornell, W. D., Bayly, C. & Kollman, P. A. Application of the multimolecule and multiconformational RESP methodology to biopolymers: Charge derivation for DNA, RNA, and proteins. *J. Comput. Chem.* **16**, 1357-1377 (1995).

42. Hoffmann, F., Mulder, F. A. A. & Schafer, L. V. Accurate methyl group dynamics in protein simulations with AMBER force fields. *J. Phys. Chem. B* **122**, 5038-5048 (2018).

Supporting Methods

Model Free Expressions for the Contributions of ^{19}F-^{19}F Dipolar and CSA Relaxation Mechanisms to ^{19}F R_1 NMR Relaxation of the CYF Residue

The dipolar interactions between hydrogen nuclei in a methyl group[1], modified herein for ^{19}F, and to include the internal motion of the CYF methyl axis, according to the model free approach[2,3], are given by:

$$R_1^{DD} = D_{FF}\left[\begin{array}{l} 4\left(\frac{c_2(\beta)}{2}\right)^2 J_0(\omega_F) + 16\left(\frac{c_2(\beta)}{2}\right)^2 J_0(2\,\omega_F) + 12\left(c_1(\beta)\right)^2 J_1(\omega_F) + \\ 48\left(c_1(\beta)\right)^2 J_1(2\,\omega_F) + 3\left(c_0(\beta)\right)^2 J_2(\omega_F) + 12\left(c_0(\beta)\right)^2 J_2(2\,\omega_F) \end{array}\right] \quad [1]$$

where:

$$D_{FF} = \frac{\left(\frac{\mu_0}{4\pi}\right)^2 \left(3\gamma_F^2 \hbar\right)^2}{20\, r_{FF}^6} \qquad [2]$$

and

$$c_0(\beta) = \mathrm{Sin}(\beta)^2 \qquad [3]$$

$$c_1(\beta) = \mathrm{Sin}(\beta)\mathrm{Cos}(\beta) \qquad [4]$$

$$c_2(\beta) = 3\mathrm{Cos}(\beta)^2 - 1 \qquad [5]$$

and where μ_0 is the permeability constant of free space ($4\pi \times 10^{-7}$ kg m s^{-2} A^{-2}), γ_F is the magnetogyric ratio of ^{19}F (25.176×10^7 rad s^{-1} T^{-1}), $\hbar$ is Planck's constant divided by 2π (1.05×10^{-34} J s), and r_{FF} is the internuclear separation between ^{19}F atoms (220×10^{-12} m), and the spectral density functions[2,3] are given by:

$$J_n(\omega) = \left[\frac{S^2 \tau_n}{1 + (\omega \tau_n)^2} + \frac{(1 - S^2)\tau_n'}{1 + (\omega \tau_n')^2} \right] \qquad [6]$$

With n = 0, 1, 2, and

$$\begin{aligned} \tau_0 &= \tau_c & \tau_0' &= \frac{\tau_c \tau_i}{\tau_c + \tau_i} \\ \tau_1 &= \frac{\tau_c \tau_e}{\tau_c + \tau_e} & \tau_1' &= \frac{\tau_1 \tau_i}{\tau_1 + \tau_i} \\ \tau_2 &= \frac{\tau_c \tau_e}{4\tau_c + \tau_e} & \tau_2' &= \frac{\tau_2 \tau_i}{\tau_2 + \tau_i} \end{aligned} \qquad [7]$$

For the CSA contribution[4] to the ^{19}F methyl T_1, we have:

$$R_1^{CSA} = \frac{1}{40}\left(\gamma_F^2 B_0^2 \delta_z^2\right)\left[c_0(\alpha,\beta)\left(J_0(\omega_F)\right) + c_1(\alpha,\beta)\left(J_1(\omega_F)\right) + c_2(\alpha,\beta)\left(J_2(\omega_F)\right)\right] \qquad [8]$$

where the spectral densities and physical constants are as defined in the main text. Plots of R_1^{DD} and R_1^{CSA} as a function of the overall correlation time τ_c, two values for the internal correlation time τ_i (20 and 2000 ps), and various S^2 values, are shown below in Figure 2.S1.

Supporting Figures

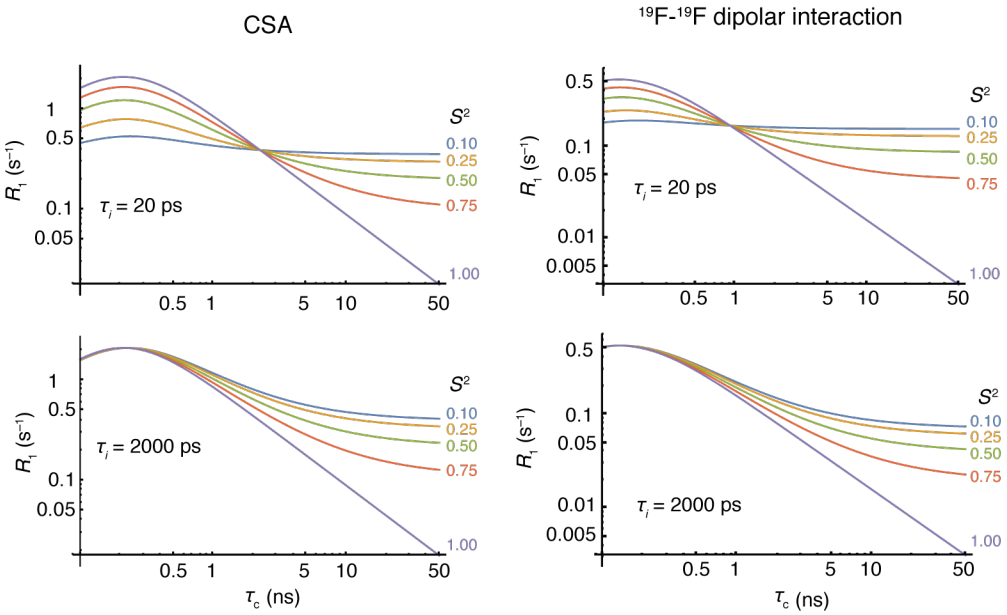

Figure 2.S1: ^{19}F R_1 relaxation rates as a function of CSA (left) and ^{19}F-^{19}F dipolar (right) relaxation mechanisms, at two internal correlation times and a range for S^2 from 0.1 – 1.0. Calculations were conducted using a magnetic field strength of 18.8 T, or a ^{19}F Larmor frequency of 753 MHz.

Supporting References

1. Werbelow, L. G. & Marshall, A. G., Internal rotation and methyl proton magnetic relaxation for macromolecules. *J. Am. Chem. Soc.* **95**, 5132-5134 (1973).

2. Lipari, G. & Szabo, A. Model-free approach to the interpretation of nuclear magnetic resonance relaxation in macromolecules. 1. Theory and range of validity. *J. Am. Chem. Soc.* **104**, 4546-4559 (1982).

3. Lipari, G. & Szabo, A. Model-free approach to the interpretation of nuclear magnetic resonance relaxation in macromolecules. 2. Analysis of experimental results. *J. Am. Chem. Soc.*, **104**, 4559-4570 (1982).

4. Hull, W. E. & Sykes, B. D. Fluorotyrosine alkaline phosphatase: Internal mobility of individual tyrosines and the role of chemical shift anisotropy as a ^{19}F nuclear spin relaxation mechanism in proteins. *J. Mol. Biol.* **98**, 121-153 (1975).

Chapter 3

Nucleotide Binding and Active Site Gate Dynamics for the Hsp90 Chaperone ATPase Domain from Benchtop and High Field ^{19}F NMR Spectroscopy

This chapter has been published as "**Rashid, S.**, Lee, B.L., Wajda, B. & Spyracopoulos, L. Nucleotide Binding and Active Site Gate Dynamics for the Hsp90 Chaperone ATPase Domain from Benchtop and High Field 19F NMR Spectroscopy. *The Journal of Physical Chemistry B* **124**, 2984-2993 (2020)". S.R. expressed and purified all proteins with the help of B.W; S.R. collected NMR data. S.R. and L.S. conducted the MD simulations. S.R., B.L.L., and L.S. analyzed NMR data. S.R. and L.S. wrote the manuscript.

Introduction

The Hsp90 chaperone is a central hub in the regulation of cellular protein turnover[1-4]. The function of this chaperone is critical for the folding of hundreds of client proteins under normal physiological conditions; this includes steroid hormone receptors, kinases, E3 ubiquitin ligases, transcription factors, and proteins involved in innate immunity, DNA repair, and RNA interference[2]. In addition to assisting normal cellular functions, expression of Hsp90 is upregulated under stress to combat the ensuing toxic effects on client protein stability[1].

To maintain functionality in cells, Hsp90 is an obligate homodimer[5]; each protomer consists of an N-terminal ATPase domain (N domain) that is part of the GHKL superfamily of ATP binding domains[6]. The N domain possesses a deep nucleotide binding pocket that is buttressed at one end with an active site gate composed of two short α-helices joined by a short linker[7]. The ATPase domain is connected by a ~70 residue acidic linker to a middle, or M domain, that binds substrate proteins, and which is essential for interacting with the N domain to facilitate ATP hydrolysis[8]. Homodimerization of Hsp90 is mediated by a C-terminal domain (C domain)[9] that possesses a short MEEVD sequence that interacts with tetratricopeptide repeats (TPR) on Hsp90 co-chaperone proteins[10].

The Hsp90 chaperone undergoes a slow conformational cycle[4,11-13] in which ATP binding to the N domain initiates a process that drives the dimeric chaperone from an open state where the N domains do not interact, to a closed, catalytically competent state where the N domains are dimerized, and in close contact with their respective M domains[14,15]. The closed state is maintained by a key electrostatic interaction between the sidechain of ARG380 of the M domain, and the γ-phosphate of ATP[16]. Upon closing, the chemical step for ATP hydrolysis is rapid, with a concomitant loss of the ARG380–γ-phosphate interaction, followed by rapid reversion to the open state[17]. The conformational cycle has been well characterized, possessing large, nearly isoenergetic barriers of ~20 kcal mol^{-1} for opening and closing[12,13,17]. In contrast, the initial changes induced in the ATPase domain upon ATP binding, and the impact on the active site gate dynamics are less well understood, though removal of the N-terminal strand of the N domain using mutagenesis has been shown to

destabilize one of the two gate helices, and results in liberation of the gate from the domain with an increase in its mainchain flexibility[18].

In this study, we set out to explore the nature of nucleotide binding to the ATPase domain of Hsp90 using a blend of benchtop and high field ^{19}F NMR spectroscopic methods, coupled with molecular dynamics (MD) simulations in explicit solvent for the apo and nucleotide bound states. ^{19}F NMR spectroscopy of biological systems has advantages of high sensitivity, the chemical shift is an exquisite reporter of subtle changes in chemical environment, and dynamic processes ranging from picoseconds to seconds can be characterized[19]. Furthermore, given its near total absence in biological molecules, incorporation of ^{19}F into large biomolecules and complexes facilitates versatile and affordable biophysical studies of such challenging systems[17,20,21].

We chemically modified the Hsp90 ATPase domain with bromo-1,1,1-trifluoroacetone to generate two cysteine-TFA derivative residues (CYF residues) bearing terminal trifluoromethyl groups. One residue was engineered at position 61 which resides on a rigid, solvent exposed loop, and another at position 110, which resides at the end of the first helix of the active site gate, near its apex. To facilitate an accurate interpretation of the CYF residue pico- to nanosecond timescale dynamics at these positions using our previously developed model free approach, we measured ^{19}F NMR linewidths at benchtop magnetic field strengths (1.41 T) and coupled these to measurements of R_2 relaxation rate constants at high field (16.4 T). This approach facilitates separation of the contributions of pico- to nanosecond timescale motions to the linewidths of the CYF61 and CYF110 residues from those due to micro- to millisecond timescale processes, ultimately allowing quantification of the kinetics of nucleotide binding using CPMG ^{19}F-R_2 relaxation dispersion experiments, as well as an assessment of nucleotide induced changes in gate dynamics.

Methods

Cloning, Protein Expression, and Purification

In this study, Hsp90 is synonymous with yeast Hsp82, and the accession code for the protein sequence is UniProKB entry P02829. DNA sequences for Hsp90N-D61C and Hsp90N-A110C mutants were cloned into the pHis-parallel1 vector by Genscript. The plasmids were amplified in *E. coli* DH5-α cells and expressed in *E. coli* BL21 DE3 RIPL cells. [U-^{15}N]-Hsp90N, [U-^{15}N]-Hsp90N-D61C, and [U-^{15}N]-Hsp90N-A110C were produced as follows: bacterial cells were grown to OD_{600} of ~0.7, subsequently pelleted with centrifugation, and suspended in 500 mL of MOPS/tricine wash buffer (40 mM MOPS, 4 mM tricine, 150 mM NaCl, pH 7.4). Cells were re-pelleted and resuspended in MOPS/tricine minimal medium (500 mL) that contained 0.5 g of $(^{15}NH_4)_2SO_4$ as the sole nitrogen source. Cell growth was initiated through incubation at 37 °C for approximately one hour, after which the temperature was reduced to 16 °C and protein expression induced with 0.4 mM IPTG, followed by overnight incubation with shaking at 260 rpm, and a final harvesting of cells by centrifugation.

Cells were lysed by sonication, and the lysate was filtered using a Millipore Millex-HV 0.45 μm filter. Clarified lysate was passed through a HisPrep FF 16/10 affinity column. His-tagged protein bound to the column was eluted using 500 mM imidazole. The eluted fractions were pooled (~25 mL) and the histidine tag was cleaved using 150 μL of 210 μM TEV protease. The tag was removed from the pooled fraction by a second passage over the affinity column. The final purification step was achieved with size exclusion using a HiLoad 26/60 Superdex 75 column equilibrated with either 25 mM HEPES or 50 mM TRIS, in 150 mM NaCl, 1 mM DTT, pH 7.3.

The cysteine-TFA derivatives, Hsp90N-CYF61 and Hsp90N-CYF110, were generated as previously described[17,22]. Proteins were concentrated to ~250 μM, and reacted with 2 mM TCEP for 30 min to reduce cysteine and subsequently reacted with excess BTFA in a 2 to 1 ratio at room temperature for 1 hour. Excess label was separated from protein using size exclusion chromatography as described above.

^{19}F NMR Spectroscopy

NMR samples for Hsp90N-CYF61 and Hsp90N-CYF110 contained ~250 μM protein in either 25 mM HEPES or 50 mM TRIS buffer containing 150 mM NaCl, 10% D_2O. The ^{1}H and ^{19}F chemical shift references were 200 μM 4,4-dimethyl-4-silapentane-1-sulfonic acid and 300 μM trifluoroacetic acid, respectively. NMR experiments were conducted at 25 °C on Bruker spectrometers with ^{1}H operating frequencies of 700 (16.4 T) or 800 (18.8 T) MHz, and at 30 °C on a Nanalysis benchtop instrument operating a ^{1}H Larmor frequency of 60 MHz. R_2 values at ^{19}F Larmor frequencies of 657 (16.4 T) and 753 (18.8 T) MHz were determined using the Carr-Purcell-Meiboom-Gill (CPMG) experiment[23,24] with a delay between 180° inversion pulses of 600 μs, and a second delay of 2.4 ms to assess potential exchange contributions. R_2 decay curves were determined using five to six relaxation delays over a total relaxation time of ~40 (16.4 T) or 48 (18.8 T) ms. R_2 decay curves were fit to a two-parameter exponential decay using nonlinear regression in Mathematica. ^{19}F-R_2 relaxation dispersion profiles were typically collected using thirteen delays (τ_{CPMG}) between the inversion pulses of 0.5, 0.6, 0.72, 0.9, 1.0, 1.2, 1.5, 1.8, 2.0, 3.6, 6.0, 9.0, and 18.0 ms, at a ^{19}F Larmor frequency of 657 MHz, or 16.4 T. At high magnetic fields (B_0 >> 1 T) the CSA relaxation mechanism predominates for ^{19}F, whereas at lower NMR fields (1–2 T), ^{19}F-^{19}F dipolar relaxation predominates, making the ^{19}F-R_2 a two-sided function with respect to B_0, which can be exploited to acquire more accurate Lipari-Szabo motional parameters. Thus, ^{19}F linewidths ($\Delta\nu_{1/2} = R_2/\pi$) for Hsp90N-CYF61 and Hsp90N-CYF110 were assessed at 56 MHz (1.41 T) using a benchtop NMR spectrometer (Nanalysis, Inc.).

^{19}F NMR R_2 Dipolar Relaxation Rate Constants and Model Free Analyses

To analyze ^{19}F NMR R_2 relaxation rate constants, we modified the expression for methyl relaxation due to proton-proton dipolar interactions[25] to describe fluorine-fluorine

interactions, as well as include the motion of the CYF methyl axis according to the model-free approach[22,26-28]:

$$R_2^{DD} = D_{FF}\left[\begin{array}{l} \frac{9}{2}c_0(\beta)^2 J_2(0) + 18c_1(\beta)^2 J_1(0) + 6\left(\frac{c_2(\beta)}{2}\right)^2 J_0(0) + \frac{15}{2}c_0(\beta)^2 J_2(\omega_F) \\ 30c_1(\beta)^2 J_1(\omega_F) + 10\left(\frac{c_2(\beta)}{2}\right)^2 J_0(\omega_F) + 3c_0(\beta)^2 J_2(2\,\omega_F) \\ +12c_1(\beta)^2 J_1(2\,\omega_F) + 4\left(\frac{c_2(\beta)}{2}\right)^2 J_0(2\,\omega_F) \end{array}\right] \quad [1]$$

where:

$$D_{FF} = \frac{\left(\frac{\mu_0}{4\,\pi}\right)^2 \left(3\gamma_F^2\hbar\right)^2}{20\, r_{FF}^6} \quad [2]$$

and

$$c_0(\beta) = \mathrm{Sin}(\beta)^2 \quad [3]$$

$$c_1(\beta) = \mathrm{Sin}(\beta)\mathrm{Cos}(\beta) \quad [4]$$

$$c_2(\beta) = 3\mathrm{Cos}(\beta)^2 - 1 \quad [5]$$

and where μ_0 is the permeability constant of free space ($4\pi \times 10^{-7}$ kg m s^{-2} A^{-2}), γ_F is the magnetogyric ratio of ^{19}F (25.176×10^7 rad s^{-1} T^{-1}), $\hbar$ is Planck's constant divided by 2π (1.05×10^{-34} J s), and r_{FF} is the internuclear separation between ^{19}F atoms (220×10^{-12} m), $\beta = 90°$ for a methyl group, and the spectral density functions are given by[22,28]:

$$J_n(\omega) = \left[\frac{S^2\tau_n}{1+(\omega\,\tau_n)^2} + \frac{\left(1-S^2\right)\tau_n'}{1+(\omega\,\tau_n')^2}\right] \quad [6]$$

With n = 0, 1, 2, and

$$\tau_0 = \tau_c \qquad \tau_0' = \frac{\tau_c \tau_i}{\tau_c + \tau_i}$$
$$\tau_1 = \frac{\tau_c \tau_e}{\tau_c + \tau_e} \qquad \tau_1' = \frac{\tau_1 \tau_i}{\tau_1 + \tau_i} \qquad [7]$$
$$\tau_2 = \frac{\tau_c \tau_e}{4\tau_c + \tau_e} \qquad \tau_2' = \frac{\tau_2 \tau_i}{\tau_2 + \tau_i}$$

For isotropic rotational diffusion of the protein, the correlation time constant for tumbling is given by τ_c, the time constant for internal motion of the CYF sidechain is given by τ_i, and τ_e is the time constant for fast methyl rotation. The order parameter for the methyl axis of the CYF trifluoromethyl group is given by S^2 or alternatively, S^2_{axis}. This implementation of the model free approach is valid for $\tau_c >> \tau_i$, and $\tau_e \sim 0$. Under these conditions, the n = 1, 2 coefficients in eq. 7 reduce to zero.

The total ^{19}F -R_2 relaxation rate constant is given by the sum of the contributions from relaxation due to modulation of the chemical shift anisotropy (CSA), and ^{19}F-^{19}F dipolar relaxation, $R_2 = R_2^{CSA} + R_2^{DD}$, where R_2^{CSA} is given by eqs. 1 – 6 in ref 22. The model free parameters S^2 and τ_i were determined by global optimization of the sum of the squared difference between the calculated total R_2 value and the experimental R_2 value determined at multiple magnetic field strengths using the NMinimize command in Mathematica. Errors in the fitted parameters were estimated using Monte Carlo analyses.

^{19}F NMR Relaxation Dispersion Experiments

^{19}F relaxation dispersion curves were fit to a two-site fast chemical exchange model according to the equation[29]:

$$R_{2,fast}\left(\nu_{\mathrm{CPMG}}\right) = R_{2,0} + \frac{R_{ex}}{k_{ex}}\left[1 - \left(\frac{4\nu_{\mathrm{CPMG}}}{k_{ex}}\mathrm{Tanh}\left[\frac{k_{ex}}{4\nu_{\mathrm{CPMG}}}\right]\right)\right] \quad [8]$$

where ν_{CPMG} is $1/(4\ \tau_{CPMG})$ for the ^{19}F pulse sequence element τ_{CPMG} –180°–τ_{CPMG}, $R_{2,0}$ is the transverse relaxation rate in the limit of $\nu_{\mathrm{CPMG}} \to \infty$, and given by the population weighted average of the free and bound R_2 values. R_{ex} can only be fit as a single parameter for the fast exchange limit, and is given by

$$R_{ex} = p_f p_b \Delta\omega^2 \quad [9]$$

with the populations of free and bound protein given by p_f and p_b, respectively, and $\Delta\omega$ is the chemical shift difference between the free and bound states of the protein. ^{19}F CPMG curves for Hsp90N-CYF61 and Hsp90N-CYF110 in the presence of AMP-PNP were simultaneously fit using a global k_{ex} parameter and individual $R_{2,0}$ and R_{ex} parameters. The global k_{ex} and the individual $R_{2,0}$ and R_{ex} parameters were determined by global optimization of the squared difference between experimental $R_{2,fast}$ values and calculated $R_{2,fast}$ values, summed over 13 ν_{CPMG} delays. Errors in the optimized parameters were determined using Monte Carlo parameter estimation.

Binding of AMP-PNP to Hsp90N

The interaction between Hsp90N and AMP-PNP is given by the following coupled binding equilibria:

$$\left[\mathrm{Hsp90N}_f\right] = \frac{K_D}{\left[\mathrm{Hsp90N}_b\right]\left[\mathrm{AMPPNP}_b\right]}$$

$$\left[\mathrm{AMPPNP}_f\right] = \frac{K_D}{\left[\mathrm{Hsp90N}_b\right]\left[\mathrm{AMPPNP}_b\right]} \qquad [10]$$

$$\left[\mathrm{Hsp90N}_f\right] + \left[\mathrm{Hsp90}_b\right] = \left[\mathrm{Hsp90N}_\mathrm{T}\right]$$

$$\left[\mathrm{AMPPNP}_f\right] + \left[\mathrm{AMPPNP}_b\right] = \left[\mathrm{AMPPNP}_\mathrm{T}\right]$$

where $\mathrm{Hsp90N}_f$ and $\mathrm{Hsp90N}_b$ are the free and bound Hsp90N concentrations, respectively, $\mathrm{AMP\text{-}PNP}_f$ and $\mathrm{AMP\text{-}PNP}_b$ are the free and bound AMP-PNP concentrations, respectively, the total protein and nucleotide concentrations are given by $\mathrm{Hsp90N}_\mathrm{T}$ and $\mathrm{AMP\text{-}PNP}_\mathrm{T}$, and K_D is the dissociation constant. To facilitate interpretation of ^{19}F NMR relaxation dispersion curves in the presence of a 1:1 interaction between Hsp90N and AMP-PNP, eqs. 10 were solved to give:

$$\left[\mathrm{Hsp90N}_f\right]=\frac{1}{2}\left[\begin{array}{l}-K_D-\mathrm{AMPPNP_T}+\mathrm{Hsp90N_T}+\\ \left(K_D^2+2K_D\mathrm{AMPPNP_T}+\mathrm{AMPPNP_T^2}+2K_D\mathrm{Hsp90N_T}\right.\\ \left.-2\,\mathrm{AMPPNP_T}\,\mathrm{Hsp90N_T}+\mathrm{Hsp90N_T^2}\right)^{1/2}\end{array}\right]$$

$$\left[\mathrm{Hsp90N}_b\right]=\frac{1}{2}\left[\begin{array}{l}K_D+\mathrm{AMPPNP_T}+\mathrm{Hsp90N_T}-\\ \left(\left(-K_D-\mathrm{AMPPNP_T}-\mathrm{Hsp90N_T}\right)^2\right.\\ \left.-4\,\mathrm{AMPPNP_T}\,\mathrm{Hsp90N_T}\right)^{1/2}\end{array}\right]$$

$$\left[\mathrm{AMPPNP}_f\right]=\frac{1}{2}\left[\begin{array}{l}-K_D+\mathrm{AMPPNP_T}-\mathrm{Hsp90N_T}+\\ \left(K_D^2+2K_D\mathrm{AMPPNP_T}+\mathrm{AMPPNP_T^2}+2K_D\mathrm{Hsp90N_T}\right.\\ \left.-2\,\mathrm{AMPPNP_T}\,\mathrm{Hsp90N_T}+\mathrm{Hsp90N_T^2}\right)^{1/2}\end{array}\right]$$

$$\left[\mathrm{AMPPNP}_b\right]=\frac{1}{2}\left[\begin{array}{l}K_D+\mathrm{AMPPNP_T}-\mathrm{Hsp90N_T}-\\ \left(K_D^2+2K_D\mathrm{AMPPNP_T}+\mathrm{AMPPNP_T^2}+2K_D\mathrm{Hsp90N_T}\right.\\ \left.-2\,\mathrm{AMPPNP_T}\,\mathrm{Hsp90N_T}+\mathrm{Hsp90N_T^2}\right)^{1/2}\end{array}\right] \qquad [11]$$

NMR Monitored Titration and Lineshape Analysis for Binding of AMP-PNP to Hsp90N

[U-^{15}N]-Hsp90N was titrated with AMP-PNP and monitored with 2D ^{1}H-^{15}N-HSQC NMR spectroscopy[30-33] using a Varian INOVA 600 MHz spectrometer operating at 25 °C. The NMR sample contained ~150 μM [U-^{15}N]-Hsp90N in 50 mM TRIS, 150 mM NaCl, 3 mM Mg^{2+}, 1 mM DTT, and 10% D_2O, pH 7.3. The stock nucleotide ligand solution contained 3 mM AMP-PNP, and titration aliquots were typically 2 – 20 μM, with larger aliquots utilized near the end of the titration to achieve saturation. A total of twenty spectra were collected with increasing concentration of AMP-PNP (0-842 μM) titrated into Hsp90N, which concomitantly decreased in concentration from ~150 to 100 μM. The ligand:protein ratios for the twenty titration points were: 0.0, 0.1, 0.2, 0.3, 0.4, 0.5, 0.7, 1.0, 1.2, 1.5, 2.0, 2.5, 3.0, 3.5, 4.0, 4.5, 4.9, 5.8, 7.2, and 8.5.The 2D ^{1}H-^{15}N-HSQC spectrum of free Hsp90N was assigned using chemical shifts deposited in the Biological Magnetic Resonance Data Bank

(accession number 5355)[34]. The spectrum of AMP-PNP bound Hsp90N was assigned based on the proximity of a given bound resonance to the free resonance.

NMR spectra were processed with NMRPipe[35] and analyzed with NMRViewJ[36]. Chemical shift changes between free and bound resonances at an ~1:5 Hsp90N to AMP-PNP ratio were calculated using[37]:

$$\Delta\delta = \sqrt{\left(\Delta\delta^{\,1}\mathrm{H}^{\mathrm{N}}\right)^2 + \left(\Delta\delta^{\,15}\mathrm{N}/5\right)^2} \qquad [12]$$

where $\Delta\delta^{\,1}\mathrm{H}^{\mathrm{N}}$ and $\Delta\delta^{\,15}\mathrm{N}$ are the changes in the amide proton and nitrogen chemical shifts, respectively, upon binding ligand.

To extract the thermodynamics and kinetics of AMP-PNP binding from the titration data, NMR lineshape analysis using the Bloch-McConnell equations[38,39] was conducted for residue 79, which undergoes chemical shift changes exclusively in the ^{1}H dimension upon binding AMP-PNP. One-dimensional slices were extracted using NMRPipe[35], and the kinetic parameters for two-site chemical exchange were determined using scripts written in the Python programming language and methods similar to those previously described[40,41]. The 1D slices were fit to synthetic spectra containing one peak undergoing two site exchange, by simulating FID signals using an identical number of points, dwell time, and processing parameters as the experimental spectra. The FIDs were Fourier transformed and the fit between the simulated and experimental spectra was minimized using least squares. The fit was optimized by varying the free and bound peak chemical shifts and linewidths, as well as the k_{off} and K_D describing the exchange process. A fixed time delay was used to simulate the effect of differential relaxation between the free and bound states[42], by scaling the intensities of the two states based on their fitted relaxation rates.

MD Simulations

Molecular dynamics simulations in explicit solvent for apo Hsp90N-D61C and Hsp90N-A110C were set up and conducted as previously described for Hsp90N-D61C[22] using the AMBER suite of biomolecular simulation programs[43], and the *ff*14SB forcefield[44]. Beginning with the crystallographically determined structure for the apo ATPase domain (1ah6)[7], we

used the PyMol program[45] to substitute either aspartate 61 or alanine 110 with a CYF residue and add an N-terminal methionine to generate atomic models for Hsp90N-CYF61 and Hsp90N-CYF110. The models were solvated in octahedral boxes of TIP3P[46] water with minimum distances of 12 Å to the box edges, and the system neutralized with Na^+ ions. Two rounds with ~200 cycles of minimization were conducted, the system was heated from 0 to 300 K over 50 ps with 2 kcal/mol restraints on solute atoms, and the density was equilibrated for a further 200 ps. Covalent bonds to hydrogen were constrained using SHAKE[47], and the maximum distance for pairwise electrostatic and nonbonded interactions was 8 Å. Temperature was regulated using Langevin dynamics with a 2 ps^{-1} collision frequency[48]. Particle mesh Ewald molecular dynamics (PMEMD)[47] were used to conduct production dynamics for ~160 ns, using 2 fs timesteps, and MD trajectories written out every 1000 steps. This length for the production runs is appropriate for analysis of picosecond to ~10 nanosecond timescale mainchain and sidechain fluctuations, such as those measured using NMR R_1 and R_2 relaxation techniques but is not long enough to characterize slower micro- to millisecond timescale fluctuations that contribute to R_2 through R_{ex}. MD simulations for Mg^{2+}–ATP bound Hsp90N-CYF61 and Hsp90N-CYF110 were also conducted in a similar fashion to those for the nucleotide free states. Initial starting structures for the ATP bound states were built using the PyMol program[45] by superimposing the structure of bound Mg^{2+}–ATP and buried water molecules within the active site from the human Hsp90 ATPase domain bound to Mg^{2+}–ATP (PDB id: 3t0z)[49] onto the structures of nucleotide free yeast Hsp90N, modified with a CYF residue at either position 61 or 110, as described above. Polyphosphate parameters were used for ATP[50], as well as parameters we previously developed for the CYF residue[22].

Time correlation functions for the dynamics of the trifluoromethyl symmetry axis (C–CF_3 bond) were calculated using the CPPTRAJ program[51] according to:

$$C(t) = \left\langle P_2\left[\vec{\mu}(0) \bullet \vec{\mu}(t)\right]\right\rangle$$
$$P_2(x) = \left(3x^2 - 1\right)/2 \qquad [13]$$

with the unit vector for the C–CF_3 bond given by $\vec{\mu}(t)$ and the brackets indicating individual averages over eight to ten 15 ns time windows taken from the simulations. To ensure that the correlation functions were accurately fit, three types of Lipari-Szabo correlation functions were employed to derive dynamics parameters from the MD simulations:

$$C_{LS1}(t) = S^2 + (1 - S^2)e^{-t/\tau_i}$$
$$C_{LS2}(t) = S_f^2 S_s^2 + (1 - S_f^2)e^{-t/\tau_i} + (S_f^2 - S_f^2 S_s^2)e^{-t/\tau_s} \qquad [14]$$
$$C_{LS3}(t) = C_{LS2}(t) + A_l\, e^{-t/\tau_l}$$

where the Lipari-Szabo order parameter[26-27] is given by the product of an order parameter for fast and slow internal motions, $S^2 = S_f^2 S_s^2$, and where τ_i and τ_s are time constants for rapid internal and slower motions, respectively[52]. The second term in $C_{LS3}(t)$ is a heuristic we employed to account for a slow (tens of nanoseconds), ill-defined decay observed in some of the correlation functions, with the adjustable parameters A_l and time constant τ_l. Use of this term facilitates more accurate fitting of the slower time scale parameters ($S_s^2$and τ_s) in $C_{LS2}(t)$. The eight to ten correlation functions determined over 15 ns windows from the MD simulations were individually fit to eqs. 14 using global minimization of the sum of squared differences (taken over 8000 2 ps time steps) between the MD-derived correlation functions and those calculated using eqs. 14, as implemented in the NMinimize routine in Mathematica. To avoid choosing an over-parameterized model, Aikakie's information criterion was used to discriminate between fits to the three correlations functions[53]. The S^2 and τ_i values from the fits, and their associated errors, represent the averages and standard deviations of the individual fits to the 8 to10 windows of 15 ns each, taken from the MD simulations.

Results and Discussion

^{19}F NMR R_2 Relaxation Rate Constants and Model Free Analyses

For proteins bearing the CYF residue, ^{19}F NMR R_2 relaxation measurements are sensitive to overall tumbling, fast picosecond internal motions, and slower micro- to millisecond processes[28]. For the apo ATPase domain, residues CYF61 and CYF110 are solvent exposed, and expected be flexible. Therefore, to interpret the ^{19}F-R_2 values for each mutant, multiple field relaxation data were simultaneously fit using a Lipari-Szabo model free approach we previously developed (Table 3.S1)[22]. Using an overall correlation time of 10.6 ns for rotational tumbling of the apo ATPase domain[18,22], the fitted model free parameters are 0.023 ± 0.008 and 0 ± 0.003 for the methyl axis order parameter (S^2 or alternatively, S^2_{axis}), for CYF61 and CYF110, respectively, with internal correlation times (τ_i) of 1100 ± 100 and 1070 ± 37 ps, respectively (Figure 3.1). These combinations of S^2_{axis} and τ_i correspond to unique minima for the objective function upon simultaneous fitting of multiple field relaxation rates (Figure 3.1 and Table 3.S1). The Monte Carlo parameters show compact, normal probability distributions, and small parameter biases, with $S^2_{axis}(\text{fit}) - \langle S^2_{axis}(\text{Monte Carlo})\rangle$values of 1 x 10^{-4} and 2 x 10^{-3} and $\tau_i(\text{fit}) - \langle \tau_i(\text{Monte Carlo})\rangle$ values of -1 and 22 ps, for Hsp90N-CYF61 and Hsp90N-CYF110, respectively (Figure 3.1). As shown in Table 3.S1, these fitted parameters result in good agreement between calculated and experimental ^{19}F-R_2 values for apo Hsp90N-CYF61 and apo Hsp90N-CYF110 at all magnetic field strengths. The experimental S^2_{axis} value of 0.02 we determined for Hsp90N-CYF61 in this work is smaller than the value of 0.11 ± 0.02 we previously determined[22]. However, in this study, simultaneous fitting of ^{19}F R_2 values at multiple fields, and particularly inclusion of linewidth data collected at low field (1.41 T, or 56 MHz ^{19}F Larmor frequency), allow for a more accurate determination of $S^2_{axis}$and τ_i for highly flexible CYF residues, as shown in Figure 3.1. We also derived S^2_{axis} values theoretically from MD

simulations to develop atomic views of the CYF sidechain motions on the ps-ns timescale. Similar to our previous MD simulations for Hsp90N-CYF61[22], we observe a tail in the correlation function extending to about 250 ps, which results from slower subnano- to nanosecond timescale fluctuations around the CYF χ^1 and χ^2 dihedral angles, as observed in the MD simulations. For the common methyl bearing residues in proteins, similar dynamics have been observed in studies combining MD simulations and NMR relaxation measurements[54]. In our previous work[22], fitting of the MD-derived correlation function averaged over 128 windows of 1 ns each for the CYF methyl axis of Hsp90N-CYF61 yielded an average S^2_{axis} of 0.129 ± 0.001. However, in this study, we derived correlation functions from MD simulations over substantially longer windows with lengths of 15 ns averaged over 8-10 repetitions, in order to achieve convergence of the correlation function (Figure 3.2). Using this approach, the MD-derived S^2_{axis} values are 0.09 ± 0.06 and 0.02 ± 0.01, for apo Hsp90N-CYF61 and Hsp90N-CYF110, respectively. The MD-derived S^2_{axis} value for apo Hsp90N-CYF61 is similar within error to the experimental value, whereas the MD-derived S^2_{axis} slightly overestimates the experimental value for apo Hsp90N-CYF110. The smaller experimental S^2_{axis} value for apo Hsp90N-CYF110 compared to that for apo Hsp90N-CYF61 suggests the CYF residue is more flexible at position 110 than in position 61. Although the MD-derived average S^2_{axis} values are consistent with this observation, they lack the precision to allow definitive agreement.

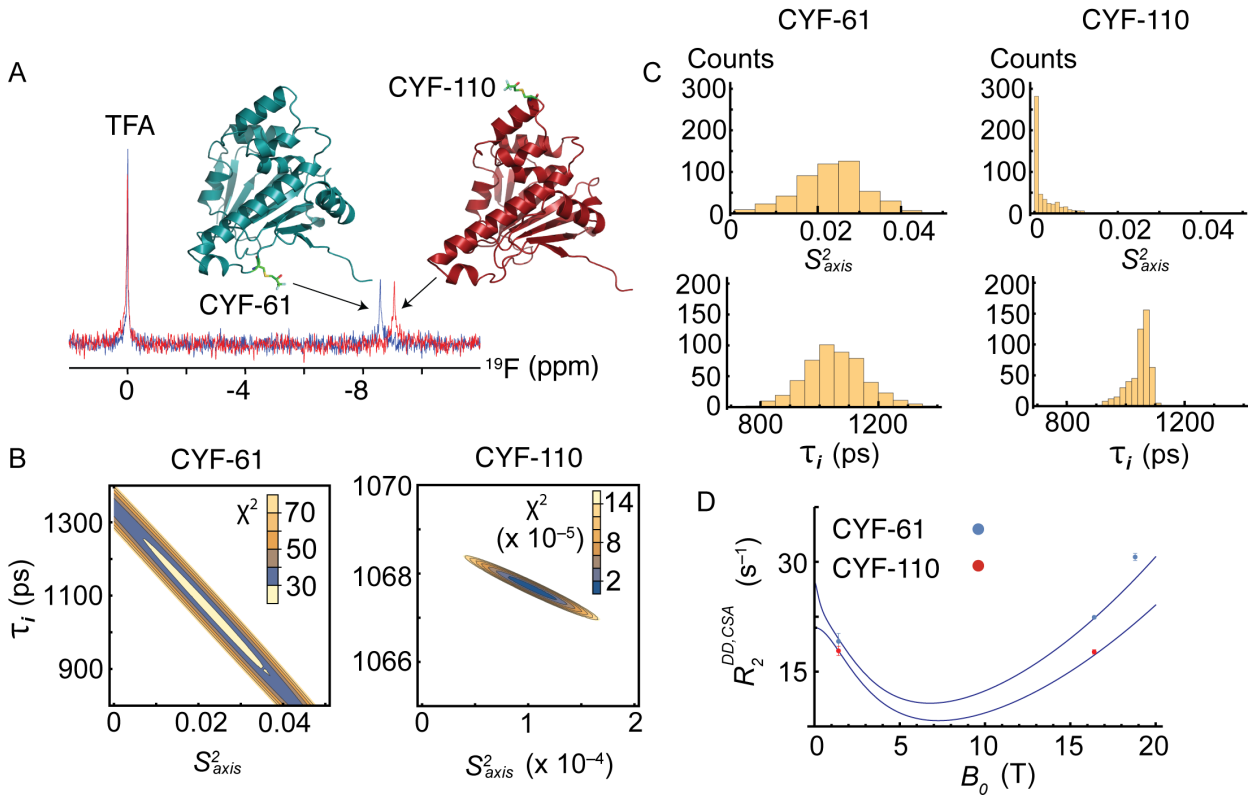

Figure 3.1: A) ^{19}F NMR spectra for Hsp90N-CYF61 (blue) and Hsp90N-CYF110 (red) at 1.41 T. B) Objective functions for fitting of multiple field ^{19}F-R_2 values using a two parameter Lipari-Szabo model free approach incorporating contributions from both CSA and dipolar relaxation. C) Distributions of S^2_{axis} and τ_i values from Monte Carlo simulations. D) Plots of the magnetic field dependence of R_2 (lines) using the fitted S^2_{axis} and τ_i parameters for Hsp90N-CYF61 (blue) and Hsp90N-CYF110 (red).

Furthermore, the accuracy limit for S^2_{axis} values for the standard methyl bearing residues is ~0.1[55], and re-parameterization efforts for methyl rotational barriers have led to improvements in accuracy[55], suggesting that re-parameterization of the trifluoromethyl group may yield more accurate S^2_{axis} values. However, with these caveats in mind, RMSF values from the 160 ns MD simulations for apo Hsp90N-CYF61 and Hsp90N-CYF110 indicate that the mainchain is more flexible around residue 110 than 61 (Figure 3.2). Consistent with this MD result, experimental mainchain S^2 parameters determined from ^{15}N NMR relaxation data

from previous studies[18] also indicate that the mainchain is more flexible around residue 110 compared to residue 61. Finally, as an independent check on the validity of S^2_{axis} derived from MD simulations, we calculated a theoretical S^2_{axis} value of 0.02 ± 0.05 for the SD–CZ methyl axis for methionine 1 of apo Hsp90N-CYF61, which falls within the experimentally determined range for methionine methyls in the dihydrofolate reductase enzyme with S^2_{axis} of 0.02 – 0.06[27].

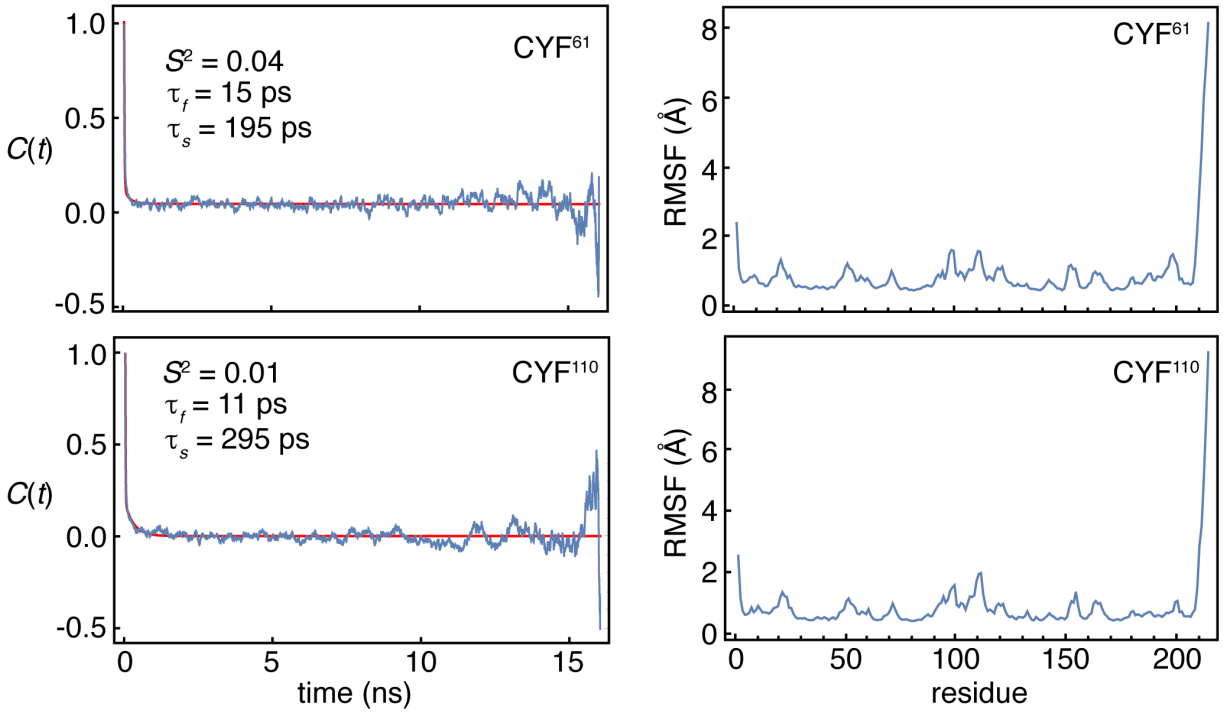

Figure 3.2: Correlation functions calculated from MD simulations for apo Hsp90N (left), and mainchain RMSF values calculated from the full trajectory (right).

^{19}F R_2 Relaxation Dispersion Reveals the Kinetics of AMP-PNP Binding to the ATPase Domain

To investigate the impact of ATP binding on ^{19}F NMR spectra for the ATPase domain, we conducted ^{19}F-R_2 CPMG experiments for Hsp90N-CYF61 as well as Hsp90N-CYF110, a mutant with a CYF residue adjacent to the apex of the ATPase gate. For nucleotide binding to the Hsp90 N-domain in general, the K_D values are ~18 μM, with k_{on} ~0.16 x 10^6 M^{-1} s^{-1} and k_{off} ~3 s^{-1} [8,56,57]. Our $^1H^N$-^{15}N NMR monitored titration of AMP-PNP into Hsp90N is consistent with the previously determined K_D of 33 μM[56], with the presence of both free and bound peaks upon addition of AMP-PNP indicative of slow exchange (Figure 3.S1). Furthermore, the mainchain $^1H^N$-^{15}N chemical shift changes indicate that the overall topology of the ATPase domain does not change significantly upon AMP-PNP binding (Figure 3.S1). Lineshape analysis of the $^1H^N$ NMR spectra for residue 79 upon titration with AMP-PNP yields a comparable K_D value of 57 μM with k_{off} ~12 s^{-1}. However, lineshape analyses in the slow exchange limit are generally less accurate than those for systems in fast/intermediate exchange[40,58]. Thus, we used the previously determined K_D of 18 μM to calculate a population for bound protein of 98%, and a population free of 2% (eq. 11), for binding of 1 mM AMP-PNP to ~200 μM Hsp90N-CYF61 and Hsp90N-CYF110. At 98% bound, the CYF methyl ^{19}F resonance shifts by 0.02 and 0.03 ppm for Hsp90N-CYF61 and Hsp90N-CYF110, respectively, with broadening of the AMP-PNP bound ^{19}F resonances for both mutants (Figure 3.3). These combined ^{19}F NMR spectral changes for Hsp90N-CYF61 and Hsp90N-CYF110 indicate that broadening of the CYF methyl ^{19}F resonance reflects AMP-PNP binding. A simultaneous fit of the relaxation dispersion profiles for the AMP-PNP bound states to a two-site, fast chemical exchange model (eq. 8) yields a rate of exchange (k_{ex}) between free and bound states of 230 ± 22 s^{-1}, and R_{ex} values of 1970 ± 54 and 840 ± 91 s^{-1} for Hsp90N-CYF110 and Hsp90N-CYF61, respectively (Fig. 3). For the R_{ex} parameter (eq. 9), the ratio of R_{ex}(CYF110)/ R_{ex}(CYF61) is 2.3, in excellent agreement with the ratio of the squared chemical shift changes for the two mutants at 98% bound Hsp90N (eq. 11 and Figure

3.3), with $\Delta\delta^2$(CYF110)/ $\Delta\delta^2$ (CYF61) = 2.25. To place the k_{ex} in context, the rate of chemical exchange for ligand binding is given by $k_{ex} = k_{on}[\text{ligand}] + k_{off}$, where [ligand] is the free ligand concentration[59]. Thus, given Hsp90N is 98% bound for the CPMG experiments, the expected k_{ex} value of 139 s^{-1} from previous kinetics studies is in good agreement with that measured from CPMG relaxation dispersion. To further verify that the exchange process observed in the ^{19}F-R_2 dispersion curves for Hsp90N-CYF61 and Hsp90N-CYF110 are indeed a result of AMP-PNP binding, we repeated the ^{19}F-R_2 CPMG experiments at an increased concentration of AMP-PNP of 3 mM, corresponding to an increase in population bound (p_b) from 98 to 99%, and a decrease in the free protein population (p_f) from 2 to 1%. As a result of this smaller p_f at an AMP-PNP concentration of 3 mM, eq. 9 predicts flatter ^{19}F CPMG dispersion profiles resulting from a decrease in R_{ex}, as well as narrower ^{19}F linewidths, given that $\Delta\nu_{1/2} = R_2/\pi$, with $R_2 = R_{2,0} + R_{ex}$. Additionally, a 3.4-fold increase in k_{ex} is expected, given the relationship $k_{ex} = k_{on}[\text{ligand}] + k_{off}$. Accordingly, we observe a flat dispersion profile for Hsp90N-CYF61 and a diminished profile for Hsp90N-CYF110, consistent with $\Delta\omega$(CYF61) < $\Delta\omega$ (CYF110) (Figure 3.3). Simultaneous fitting of the dispersion curves for Hsp90N-CYF61 and Hsp90N-CYF110 at 99% bound gives a 2.3-fold increase of k_{ex} of 530 ± 185 s^{-1}, which agrees within error to the expected increase. Thus, the observed ^{19}F relaxation dispersion profiles for Hsp90N-CYF61 and Hsp90N-CYF110 saturated to 98-99% with AMP-PNP, result from fluctuations of nucleotide bound Hsp90N into the free state with a population <2 %. Consistent with the CPMG results, ^{19}F NMR linewidths for Hsp90N-CYF61 and Hsp90N-CYF110 at 99% bound, or 3 mM AMP-PNP, are narrower than at 98% bound, or 1 mM AMP-PNP (Table 3.S2).

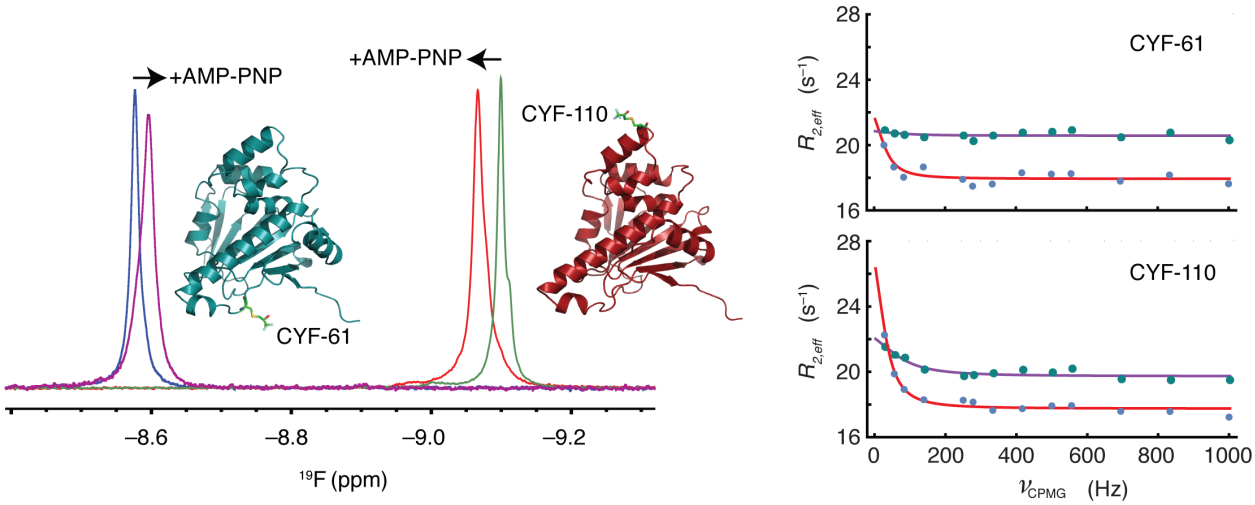

Figure 3.3: ^{19}F NMR spectra (left panel) for Hsp90N-CYF61 in the apo (blue) and AMP-PNP bound (magenta) states and Hsp90N-CYF110 in the apo (green) and AMP-PNP bound states (red). ^{19}F relaxation dispersion at 657 MHz for Hsp90N-CYF61 and -CYF110 in the 1 and 3 mM AMP-PNP bound states (right panel). The dispersion data (1 mM: blue dots, 3 mM: cyan dots) for both residues were simultaneously fit (1 mM: red lines, 3 mM purple lines) to a two-site fast chemical exchange model to yield the kinetic parameters for AMP-PNP binding.

^{19}F NMR Spectroscopy Coupled with MD Simulations Reveals Priming of the Active Site Gate Upon Nucleotide Binding

As discussed above, increasing the AMP-PNP concentration from 1 to 3 mM, corresponding to an increase from 98% to 99% bound ATPase domain, results in the quenching of exchange contributions to R_2. The ^{19}F R_2 values for Hsp90N-CYF61 and Hsp90N-CYF110 suggest that the CYF110 sidechain is more flexible than CYF61, as observed in the apo state (Tables 3.S1 and S2). Furthermore, the ^{19}F NMR linewidths for Hsp90N-CYF61 and Hsp90N-CYF110 become narrower upon increasing the AMP-PNP/Hsp90N ratio from ~5 to ~15, or 98 to 99% bound Hsp90N, respectively, and revert to values closer to those in the apo state (Table 3.S2). Thus, combined with the results for mainchain $^{1}H^{N}$-^{15}N chemical shift changes (Figure 3.S1), the quenching of exchange with increasing fraction bound, and the similarity of the R_2 values

for positions 61 and 110 in the 99% bound state to R_2 values for the apo state, indicate that while nucleotide binding induces local conformational changes, the active site gate for the ATPase domain generally remains open. This finding is consistent with a number of studies for the intact, dimeric Hsp90 chaperone, for which the active site gate has a large barrier to opening (~20 kcal mol^{-1}) and concomitant dimerization of the ATPase domains[12-14,56]. Additionally, this result is consistent with negligible catalysis of ATP hydrolysis by the isolated ATPase domain[8], as the gate must close to facilitate ATP hydrolysis.

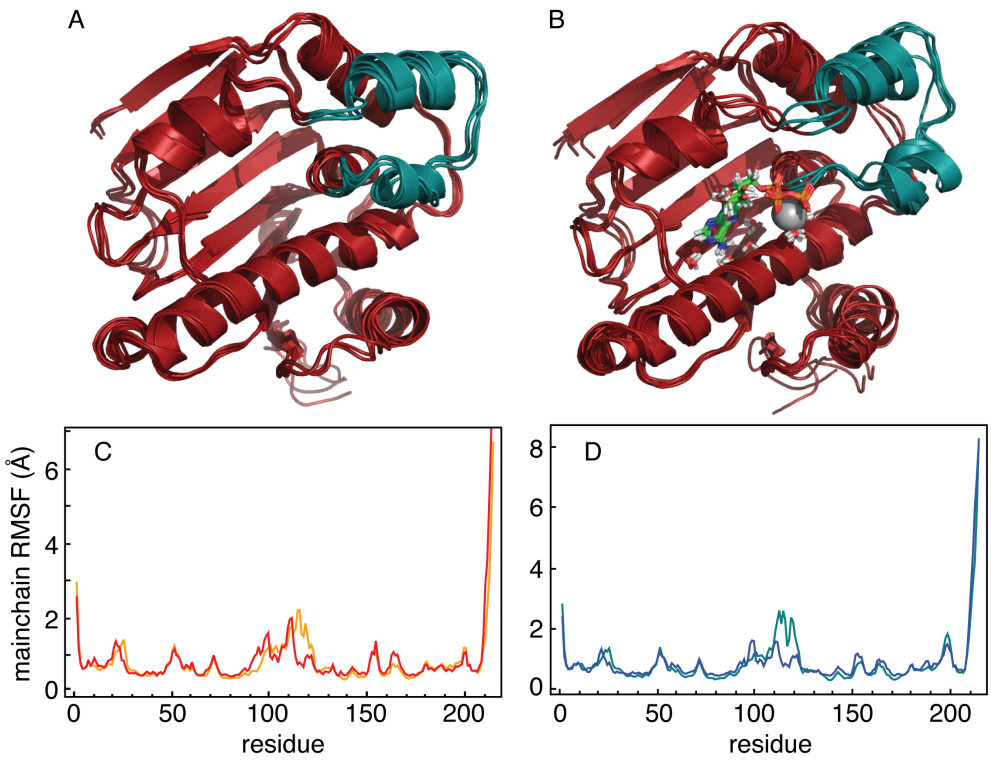

Figure 3.4: A) Representative snapshots from the MD simulations for apo Hsp90N-CYF61 and B) Hsp90N-CYF61 bound to ATP-Mg^{2+}. Mainchain atoms are shown in the schematic representation (red), with the active site gate indicated (teal), ATP and bound waters are shown in the stick representation, and Mg^{2+} in the van der Waals representation (grey). C) Mainchain RMSF values from the MD simulations for Hsp90N-CYF61 in the absence of nucleotide (red) and bound to ATP (orange). D) Mainchain RMSF values from the MD simulations for Hsp90N-CYF110 in the absence of nucleotide (blue) and bound to ATP (teal).

We conducted MD simulations to determine the S^2_{axis} values for the CYF residues for Hsp90N-CYF61 and Hsp90N-CYF110 in the ATP bound states. The S^2_{axis} values were 0.02 ± 0.02 and 0.01 ± 0.02, for Hsp90N-CYF61 and Hsp90N-CYF110, respectively, similar within error to their MD-derived values in the nucleotide free state. Thus, while the values indicate that the CYF sidechain is highly flexible at positions 61 and 110, the MD-derived S^2_{axis} values lack the precision to definitively conclude from a theoretical perspective that CYF110 is more flexible than CYF61, similar to the results for apo Hsp90N. These results, combined with the similarity of the ^{19}F linewidths values in the free and 99% bound states (Table 3.S2), suggest the gate dynamics at positions 61 and 110 are largely similar in both states.

In addition to determining S^2_{axis} values, our MD simulations for the ATP bound states of Hsp90N-CYF61 and Hsp90N-CYF110 allowed us to further explore the nature of nucleotide binding and gate dynamics (Figure 3.4). Experimentally, binding of AMP-PNP, the non-hydrolyzable analog of ATP, results in substantial $^1H^N$ and ^{15}N NMR chemical shift changes around the active site gate, which indicates conformational changes for the gate upon binding of nucleotide (Figure 3.S1). Comparison of the MD simulations for the nucleotide free and bound states suggests a model for the nucleotide induced conformational change (Figure 3.4). The negatively charged γ-phosphate of ATP perturbs the negatively charged end of the helix dipole for the C-terminal α-helix of the active site gate, resulting in a conformational switch at residue GLY123, characterized by changes in the mainchain dihedral angle for ϕ from –56 ± 12° to +68 ± 11° and ψ from –33 ±11° to –160 ± 11°. This switch causes a reorientation of the short C-terminal gate helix to accommodate the γ-phosphate from ATP, which is stabilized through an ionic interaction with the positively charged sidechain of LYS98. Concomitant with structural changes observed in the MD simulations, the C-terminal half of the gate (residues 111-121) becomes somewhat more flexible upon ATP binding, evident as increased mainchain RMSF values, whereas the structured core of the protein becomes somewhat more rigid, with the gate generally remaining in an open, albeit different conformation compared to the apo state (Figure 3.4).

These results from our MD simulations for the yeast Hsp90 ATPase domain are consistent with similar observations from previous 70 ns MD simulations for the human domain in the apo and ATP bound states[60].

The nucleotide-induced changes we observe in the isolated ATPase domain prime Hsp90 for hydrolysis by increasing the flexibility of the C-terminal hinge of the active site gate (residues 111-123). For the intact, dimeric chaperone, the next step towards hydrolysis involves liberation of the N-terminal hinge and subsequent closing of the active site gate. Liberation of the N-terminal hinge of the active site gate has a large energy barrier[12,13,22], as it requires disruption of the favorable interaction between the extreme N-terminal β-strand and core of the ATPase domain, which leads to the subsequent release of the N-terminal strand[18]. In addition, our MD simulations suggest that disruption of the favorable ionic interaction between the positively charged sidechain of LYS98 and the γ-phosphate of ATP is also necessary for lid release. Within the intact, dimeric Hsp90 chaperone, the liberated N-terminal β-strands from the ATPase domains undergo a strand swapping after release, with a concomitant freeing of the gates in each half of the chaperone, and a substitution of the LYS98: γ-phosphate interaction with an interaction with the sidechain of ARG380 from the middle domain of the chaperone[14]. Ultimately, liberation and closing of the gate in the intact dimer allows hydrolysis of ATP.

Conclusions

Binding of ATP to the N-terminal ATPase domain of the Hsp90 dimer initiates a slow conformational cycling of the chaperone between open and closed states that is important in stabilizing and assisting the folding of numerous client proteins. We chemically derivatized the ATPase domain with CYF residues at two distinct positions to facilitate benchtop and high field ^{19}F NMR R_2 relaxation rate and linewidth measurements, as well as CPMG ^{19}F- R_2 relaxation dispersion measurements. The methodology we developed allows quantitative separation of fast pico- to nanosecond timescale motions from slower motions/chemical exchange processes on the micro- to millisecond timescale. In the nucleotide free state, the

sidechain S^2_{axis} value indicates that residue CYF110 near the apex of the active site gate is more flexible on the pico-nanosecond timescale in comparison to S^2_{axis} for residue CYF61, which is distal to the active site gate, and resides on a rigid surface loop. Atomic models for these dynamic differences from MD simulations indicate that the mainchain is more flexible at CYF110 than at CYF61. Simultaneous analyses of CPMG ^{19}F- R_2 relaxation dispersion profiles for Hsp90N-CYF110 and -CYF61 demonstrate that line broadening at both positions results from chemical exchange between Hsp90N in the AMP-PNP bound state populated to 98%, and free Hsp90N populated to 2 %. Taken together, the results show that binding of nucleotides bearing a γ-phosphate increases the flexibility at the C-terminal hinge of the active site gate, priming the gate for full release in the intact dimer.

Supporting Tables

Table 3.S1: Experimental and calculated ^{19}F R_2 relaxation rate constants for nucleotide free Hsp90 N-domain at multiple field strengths.

	CYF^{110}			CYF^{61}		
B_0 (T)	16.4	18.8	1.41	16.4	18.8	1.41
$R_{2,exp}$ (s^{-1})	16.8 ± 0.2	–	–	20.0 ± 0.1	25.4 ± 0.3	–
$\Delta\nu_{1/2,exp}$ (Hz)	–	–	5.4 ± 0.1	–	–	5.7 ± 0.2
$R_{2,calc}$ (s^{-1})	16.5	–	–	19.9	23.5	–
$\Delta\nu_{1/2,calc}$ (Hz)	–	–	5.4	–	–	5.7

Table 3.S2: Experimental ^{19}F linewidths for Hsp90 N-domain at 16.4 Tesla.

	CYF^{110}		CYF^{61}	
	$\Delta\nu_{1/2,exp}$ (Hz)	$\pi\ \Delta\nu_{1/2,exp}$ (s^{-1})[a]	$\Delta\nu_{1/2,exp}$ (Hz)	$\pi\ \Delta\nu_{1/2,exp}$ (s^{-1}) [a]
apo	6.82 ± 0.07	21.4 ± 0.2	7.63 ± 0.04	24.0 ± 0.1
AMP-PNP (1 mM, 98% bound)	10.82 ± 0.07	34.0 ± 0.2	11.73 ± 0.06	36.9 ± 0.2
AMP-PNP (3 mM, 99% bound)	8.33 ± 0.08	26.2 ± 0.3	8.30 ± 0.05	26.1 ± 0.1

[a] $R_2 = \pi\ \Delta\nu_{1/2}$.

Supporting Figures

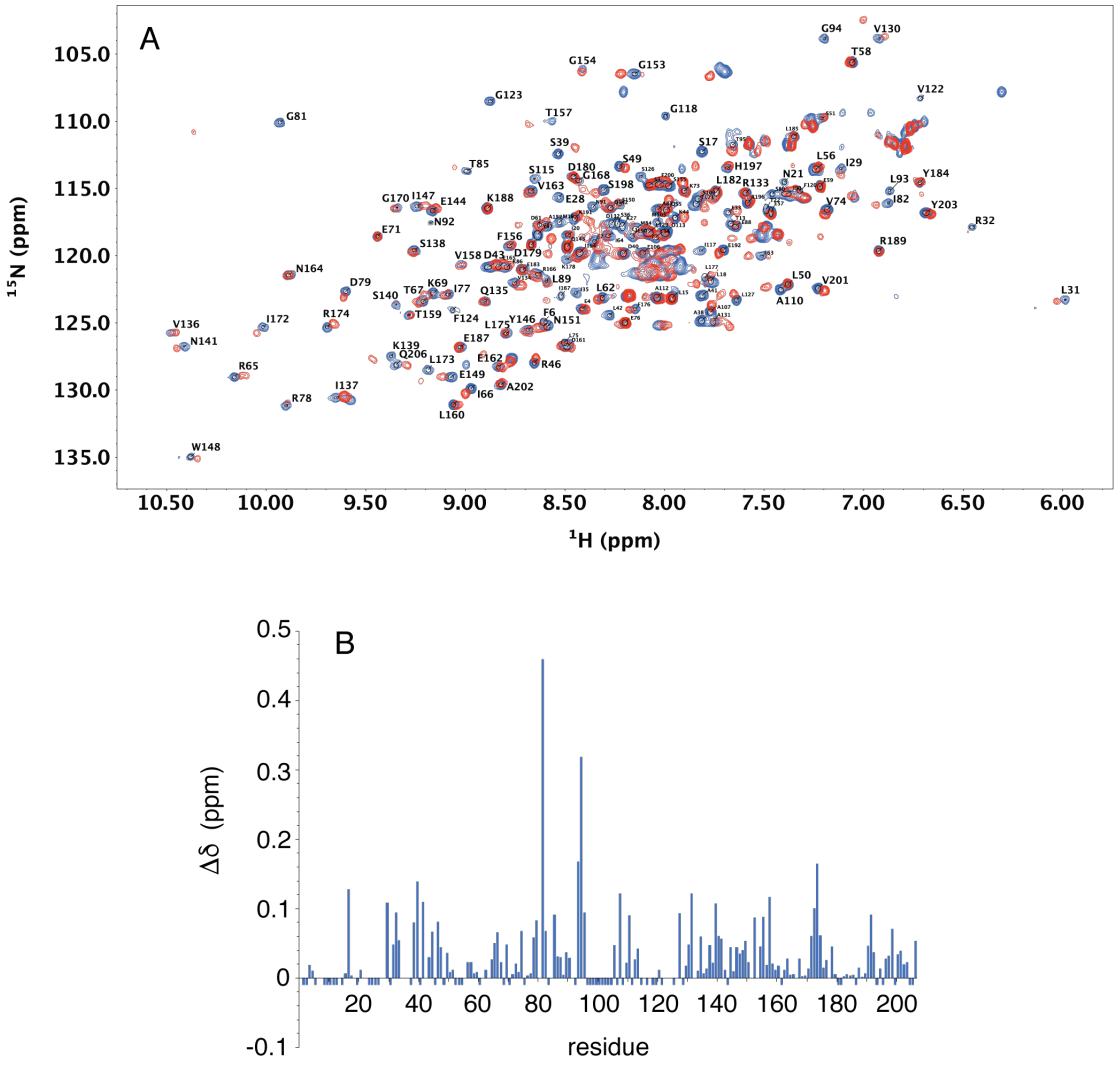

Figure 3.S1: (A) ^{15}N-^{1}H^{N} NMR spectra of apo Hsp90N (blue) and bound to a five-fold excess of AMP-PNP (red). (B) Chemical shift perturbations for Hsp90N bound to a five-fold excess of AMP-PNP, negative values indicate unassigned residues.

References

1. Biebl, M. M. & Buchner, J. Structure, function, and regulation of the Hsp90 machinery. *Cold Spring Harb. Perspect. Biol.* **11**, a034017 (2019).

2. Schopf, F. H., Biebl, M. M. & Buchner, J. The HSP90 chaperone machinery. *Nat. Rev. Mol. Cell. Biol.* **18**, 345-360 (2017).

3. Pearl, L. H. The HSP90 molecular chaperone - an enigmatic ATPase. *Biopolymers* **105**, 594-607 (2016).

4. Krukenberg, K. A., Street, T. O., Lavery, L. A. & Agard, D. A. Conformational dynamics of the molecular chaperone Hsp90. *Q. Rev. Biophys.* **44**, 229-255 (2011).

5. Wayne, N. & Bolon, D. N. Dimerization of Hsp90 is required for in vivo function. Design and analysis of monomers and dimers. *J. Biol. Chem*. **282**, 35386-35395 (2007).

6. Dutta, R.; Inouye, M., GHKL, an emergent ATPase/kinase superfamily. *Trends Biochem. Sci.* **25**, 24-28 (2000).

7. Prodromou, C., Roe, S. M., Piper, P. W. & Pearl, L. H. A molecular clamp in the crystal structure of the N-terminal domain of the yeast Hsp90 chaperone. *Nat. Struct. Biol.* **4**, 477-482 (1997).

8. Wegele, H., Muschler, P., Bunck, M., Reinstein, J. & Buchner, J. Dissection of the contribution of individual domains to the ATPase mechanism of Hsp90. *J. Biol. Chem.* **278**, 39303-39310 (2003).

9. Nemoto, T., Ohara-Nemoto, Y., Ota, M., Takagi, T. & Yokoyama, K. Mechanism of dimer formation of the 90-kDa heat shock protein. *Eur. J. Biochem*. **233**, 1-8 (1995).

10. Young, J. C., Obermann, W. M. J. & Hartl, F. U. Specific binding of tetratricopeptide repeat proteins to the C-terminal 12-kDa domain of hsp90. *J. Biol. Chem*. **273**, 18007-18010 (1998).

11. Hessling, M., Richter, K. & Buchner, J. Dissection of the ATP-induced conformational cycle of the molecular chaperone Hsp90. *Nat. Struct. Mol. Biol.* **16**, 287-293 (2009).

12. Schmid, S., Gotz, M. & Hugel, T. Single-molecule analysis beyond dwell times: Demonstration and assessment in and out of equilibrium. *Biophys. J.* **111**, 1375-1384 (2016).

13. Schulze, A. et al. Cooperation of local motions in the Hsp90 molecular chaperone ATPase mechanism. *Nat. Chem. Biol.* **12**, 628-635 (2016).

14. Ali, M. M. et al. Crystal structure of an Hsp90-nucleotide-p23/Sba1 closed chaperone complex. *Nature* **440** 1013-1017 (2006).

15. Southworth, D. R. & Agard, D. A. Species-dependent ensembles of conserved conformational states define the Hsp90 chaperone ATPase cycle. *Mol. Cell* **32**, 631-640 (2008).

16. Cunningham, C. N., Southworth, D. R., Krukenberg, K. A. & Agard, D. A. The conserved arginine 380 of Hsp90 is not a catalytic residue, but stabilizes the closed conformation required for ATP hydrolysis. *Protein Sci.* **21**, 1162-1171 (2012).

17. Lee, B.L. et al. The Hsp90 chaperone: 1H and 19F dynamic nuclear magnetic resonance spectroscopy reveals a perfect enzyme. *Biochemistry* **58**, 1869-1877 (2019).

18. Richter, K. et al. Intrinsic inhibition of the Hsp90 ATPase activity. *J. Biol. Chem.* **281**, 11301-11311 (2006).

19. Marsh, E. N. & Suzuki, Y. Using 19F NMR to probe biological interactions of proteins and peptides. *ACS Chem. Biol.* **9**, 1242-1250 (2014).

20. Di Pietrantonio, C., Pandey, A., Gould, J., Hasabnis, A. & Prosser, R. S. Understanding protein function through an ensemble description: characterization of functional states by 19F NMR. *Meth. Enzymol*. **615**, 103-130 (2019).

21. Simmons, J. R. et al. Simultaneous ligand and receptor tracking through NMR spectroscopy enabled by distinct 19F Labels. *Int. J. Mol. Sci*. **20**, 3658-3672 (2019).

22. Rashid, S., Lee, B. L., Wajda, B. & Spyracopoulos, L. Side-chain dynamics of the trifluoroacetone cysteine derivative characterized by 19F NMR relaxation and molecular dynamics simulations. *J. Phys. Chem. B* **123**, 3665-3671 (2019).

23. Carr, H. Y. & Purcell, E. M. Effects of diffusion on free precession in nuclear magnetic resonance experiments. *Phys. Rev.* **94**, 630-638 (1954).

24. Meiboom, S. & Gill, D. Modified spin-echo method for measuring nuclear relaxation times. *Rev. Sci. Instrum.* **29**, 688-691 (1958).

25. Werbelow, L. G. & Marshall, A. G. Internal rotation and methyl proton magnetic-relaxation for macromolecules. *J. Am. Chem. Soc.* **95**, 5132-5134 (1973).

26. Lipari, G. & Szabo, A. Model-free approach to the interpretation of nuclear magnetic resonance relaxation in macromolecules. 1. Theory and range of validity. *J. Am. Chem. Soc.* **104**, 4546-4559 (1982).

27. Lipari, G. & Szabo, A. Model-free approach to the interpretation of nuclear magnetic resonance relaxation in macromolecules. 2. Analysis of experimental results. *J. Am. Chem. Soc.* **104**, 4559-4570 (1982).

28. Hull, W. E. & Sykes, B. D. Fluorotyrosine alkaline phosphatase: Internal mobility of individual tyrosines and role of chemical shift anisotropy as a 19F nuclear spin relaxation mechanism in proteins. *J. Mol. Biol.* **98**, 121-153 (1975).

29. Luz, Z. & Meiboom, S. Nuclear magnetic resonance study of protolysis of trimethylammonium ion in aqueous solution - Order of reaction with respect to solvent. *J. Chem. Phys.* **39**, 366-370 (1963).

30. Morris, G. A. & Freeman, R. Enhancement of nuclear magnetic resonance signals by polarization transfer. *J. Am. Chem. Soc*. **101**, 760-762 (1979).

31. Bodenhausen, G. & Ruben, D. J. Natural abundance N-15 NMR by enhanced heteronuclear spectroscopy. *Chem. Phys. Lett*. **69**, 185-189 (1980).

32. Cavanagh, J., Palmer, A. G., Wright, P. E. & Rance, M. Sensitivity improvement in proton-detected two-dimensional heteronuclear relay spectroscopy. *J. Magn. Reson*. **91**, 429-436 (1991).

33. Kay, L. E., Keifer, P. & Saarinen, T. Pure absorption gradient enhanced heteronuclear single quantum correlation spectroscopy with improved sensitivity. *J. Am. Chem. Soc*. **114**, 10663-10665 (1992).

34. Salek, R. M., Williams, M. A., Prodromou, C., Pearl, L. H. & Ladbury, J. E., Letter to the editor: Backbone resonance assignments of the 25 kDa N-terminal ATPase domain from the Hsp90 chaperone. *J. Biomol. NMR* **23**, 327-328 (2002).

35. Delaglio, F. et al. NMRPipe: A multidimensional spectral processing system based on UNIX pipes. *J. Biomol. NMR* **6**, 277-293 (1995).

36. Johnson, B. A. & Blevins, R. A. NmrView: A computer program for the visualization and analysis of NMR data. *J. Biomol. NMR* **4**, 603-614 (1994).

37. Grzesiek, S. et al. The solution structure of HIV-1 Nef reveals an unexpected fold and permits delineation of the binding surface for the SH3 domain of Hck tyrosine protein kinase. *Nat. Struct. Biol.* **3**, 340-345 (1996).

38. Bloch, F. Nuclear induction. *Phys. Rev*. **70**, 460-474 (1946).

39. McConnell, H. M. Reaction rates by nuclear magnetic resonance. *J. Chem. Phys*. **28**, 430-431 (1958).

40. Markin, C. J. & Spyracopoulos, L. Accuracy and precision of protein-ligand interaction kinetics determined from chemical shift titrations. *J. Biomol. NMR* **54**, 355-376 (2012).

41. Günther, U. L. & Schaffhausen, B. NMRKIN: Simulating line shapes from two-dimensional spectra of proteins upon ligand binding. *J. Biomol. NMR* **22**, 201-209 (2002).

42. Tugarinov, V. & Kay, L. E. Quantitative NMR studies of high molecular weight proteins: Application to domain orientation and ligand binding in the 723 residue enzyme malate synthase. *G. J. Mol. Biol.* **327**, 1121-1133 (2003).

43. Cornell, W. D. et al. A second generation force field for the simulation of proteins, nucleic acids, and organic molecules. *J. Am. Chem. Soc.* **117**, 5179-5197 (1995).

44. Maier, J. A. et al. ff14SB: Improving the accuracy of protein side chain and backbone parameters from ff99SB. *J. Chem. Theory Comput.* **11**, 3696-3713 (2015).

45. Schrodinger, LLC. The PyMOL Molecular Graphics System, Version 1.8. (2015).

46. Jorgensen, W. L., Chandrasekhar, J., Madura, J. D., Impey, R. W. & Klein, M. L. Comparison of simple potential functions for simulating liquid water. *J. Chem. Phys*. **79**, 926-935 (1983).

47. Ryckaert, J. P.; Ciccotti, G.; Berendsen, H. J. C., Numerical integration of cartesian equations of motion of a system with constraints: Molecular dynamics of N-alkanes. J. Comput. Phys. **23**, 327-341 (1977).

48. Loncharich, R. J., Brooks, B. R. & Pastor, R. W. Langevin dynamics of peptides: the frictional dependence of isomerization rates of N-acetylalanyl-N'-methylamide. *Biopolymers* **32**, 523-535 (1992).

49. Li, J. et al. Structure insights into mechanisms of ATP hydrolysis and the activation of human heat-shock protein 90. *Acta. Bioch. Bioph. Sin.* **44**, 300-306 (2012).

50. Meagher, K. L., Redman, L. T. & Carlson, H. A. Development of polyphosphate parameters for use with the AMBER force field. *J. Comput. Chem*. **24**, 1016-1025 (2003).

51. Roe, D. R. & Cheatham, T. E. PTRAJ and CPPTRAJ: Software for processing and analysis of molecular dynamics trajectory data. *J. Chem. Theory Comput.* **9**, 3084-3095 (2013).

52. Clore, G. M. et al. Deviations from the simple two-parameter model-free approach to the interpretation of nitrogen-15 nuclear magnetic relaxation of proteins. *J. Am. Chem. Soc.* **112**, 4989-4991 (2013).

53. Akaike, H. New look at the statistical model identification. *IEEE Trans. Automat. Contr.* **19**, 716-723 (1974).

54. Hoffmann, F., Xue, M. J., Schafer, L. V. & Mulder, F. A. A. Narrowing the gap between experimental and computational determination of methyl group dynamics in proteins. *Phys. Chem. Chem. Phys.* **20**, 24577-24590 (2018).

55. Hoffmann, F., Mulder, F. A. A. & Schafer, L. V. Accurate methyl group dynamics in protein simulations with AMBER force fields. *J. Phys. Chem. B* **122**, 5038-5048 (2018).

56. Prodromou, C. et al. The ATPase cycle of Hsp90 drives a molecular 'clamp' via transient dimerization of the N-terminal domains. *EMBO J.* **19**, 4383-4392 (2000).

57. Richter, K., Reinstein, J. & Buchner, J., N-terminal residues regulate the catalytic efficiency of the Hsp90 ATPase cycle. *J. Biol. Chem.* **277**, 44905-44910 (2002).

58. Markin, C. J. & Spyracopoulos, L. Increased precision for analysis of protein-ligand dissociation constants determined from chemical shift titrations. *J. Biomol. NMR* **53**, 125-138 (2012).

59. Palmer, A. G., Kroenke, C. D. & Loria, J. P. Nuclear magnetic resonance methods for quantifying microsecond-to-millisecond motions in biological macromolecules. *Meth. Enzymol.* **339**, 204-238 (2001).

60. Colombo, G., Morra, G., Meli, M. & Verkhivker, G. Understanding ligand-based modulation of the Hsp90 molecular chaperone dynamics at atomic resolution. *Proc. Natl. Acad. Sci. U.S.A.* **105**, 7976-7981 (2008).

Chapter 4

Conformational Changes Induced by Nucleotide Binding to Hsp90

The work in this chapter forms part of the publication "Lee, B. L., **Rashid, S.**, Wajda, B., Wolmarans, A., LaPointe, P. & Spyracopoulos, L. The Hsp90 chaperone: 1H and 19F dynamic nuclear magnetic resonance spectroscopy reveals a perfect enzyme. *Biochemistry* **58**, 1869-1877 (2019)". The data presented here are my contribution to the publication.

Introduction

The chaperone Hsp90 is essential for cellular function and is unique in that it binds fully or partially folded proteins rather than the hydrophobic regions of unfolded proteins, thereby modulating their biological functions[1,2]. A large number of "client" proteins are specifically bound, including signaling kinases and transcription factors[3]. Importantly, the activity/stability of these proteins depends on hydrolysis of ATP by Hsp90[4]. Furthermore, the biological function of Hsp90 is tightly regulated through binding of numerous co-chaperone accessory proteins, which either increase or decrease the ATPase/chaperone activity and regulate interactions with client proteins[2]. The interplay between the ATPase activity, client binding and stabilization, and regulation by co-chaperone accessory proteins is not fully understood[3].

Hsp90 is a three-domain homodimer (N, M, and C)[5]. The C domain maintains Hsp90 in a dimeric state[6], the M domain binds client proteins, and the N domain contains an ATP-binding site and carries out the ATPase activity in conjunction with the M-domain[7]. For the generally accepted conformational cycle underlying the mechanism for chaperone activity, N-domain ATP binding results in conformational changes that shift the chaperone from an open state to an N-terminally dimerized and catalytically competent closed state involving intimate N-M interactions. These changes upon closing lead to ATP hydrolysis and reversion to the open state with release of ADP and phosphate[8].

The Hsp90 chaperone is highly dynamic. Therefore, to elucidate the mechanism of its chaperone activity requires a suitable technique like NMR spectroscopy which allows the direct observation of conformational dynamics in solution. However, NMR studies for Hsp90 are typically difficult due to its large molecular weight. As a result, most of our knowledge on dynamics of the Hsp90 chaperone is mainly from X-ray crystallographic structures, cryo-EM structures, and biochemical studies. We have been able to overcome this size barrier by employing site-specific ^{19}F NMR as a direct probe of the conformational dynamics of Hsp90 in solution. In this work, we explore the conformational changes induced by nucleotide binding to the N-terminal domain of Hsp90 by direct observation of changes in the ^{19}F NMR spectrum.

Materials and Methods

Constructs

The plasmid for the expression of hexahistadine-tagged full-length *S. cerevisiae* Hsp90, also known as Hsp82, was constructed as previously described[9]. PCR amplification and restriction enzyme digestion were used to insert the coding sequences into the pETd11His vector. The D61C mutant of full-length Hsp90 ($Hsp90^{D61C}$) was made using the QuikChange Site-Directed Mutagenesis Kit (Agilent Technologies, CA, USA) following the manufacturer's instructions. The plasmids were transformed into *E. coli* BL21(DE3) RIPL cells for protein expression. The Hsp90 N-terminal domain (Hsp90N, residues 1–210) and Hsp90 N-terminal domain D61C mutant ($Hsp90N^{D61C}$) were synthesized and inserted into the pHis-parallel1 vector[10] by Genscript. All constructs were amplified in *E. coli* DH5-α cells and introduced into electrocompetent BL21(DE3) RIPL cells for protein expression.

Protein Expression and Purification

All constructs were expressed in *E. coli* strain BL21 (DE3) RIPL cells. For the full-length $Hsp90^{D61C}$ mutant, a single colony of cells was inoculated into 50 ml of LB media and grown overnight at 37 °C with shaking (260 rpm) as a starter culture. Four flasks each containing 500 mL of LB were inoculated with 5 ml of starter culture and grown to an OD_{600} of ~0.6–0.8. The cells were then induced with 0.4 mM IPTG, incubated overnight at 30 °C with shaking (260 rpm), and harvested by centrifugation. Hsp90 N-terminal domain constructs were typically ^{15}N-labeled, following the method of Marley *et al.*,[11] For ^{15}N labeled $Hsp90N^{D61C}$, cells were grown to an OD_{600} of ~0.6–0.8, after which cells were pelleted, suspended in 500 ml of MOPS/tricine wash buffer (40 mM MOPS, 4 mM tricine, 150 mM NaCl, pH 7.4), pelleted again, and then resuspended in 500 ml of MOPS/tricine minimal media[12] containing 0.5 g of $(^{15}NH_4)_2SO_4$ as the sole source of nitrogen. Cells were incubated at 37 °C for ~1 hour, after which the temperature was reduced to 16 °C and protein expression was induced with 0.4 mM IPTG after 30 minutes. The cells were incubated overnight at 16

°C with shaking (260 rpm) and subsequently harvested by centrifugation. Purification of $Hsp90^{D61C}$ was carried out as follows: cell pellets were suspended in 100 ml of lysis buffer (20 mM NaH_2PO_4 pH 7.3, 500 mM NaCl, 20 mM imidazole, 1 mM DTT, 0.02 g lysozyme, 5 μg/ml DNAse I and one tablet Complete EDTA-free protease inhibitor cocktail (Roche Diagnostics)), lysed by sonication, centrifuged at 24,000 rpm for 30 minutes at 4 °C and then purified by affinity chromatography on a HisPrep FF 16/10 column. Fractions containing protein were pooled together and further purified by anion exchange chromatography on a HiLoad 26/10 Q Sepharose column. Eluted proteins were ^{19}F labeled as described in further detail below, and excess label was removed using a Superdex 200 column in 25 mM HEPES pH 7.3, 150 mM NaCl. For ^{15}N-Hsp90N and ^{15}N-$Hsp90N^{D61C}$ purification, His-tagged proteins were first purified using a HisPrep FF 16/10 column. The His tag was cleaved with 150 μl of 210 μM TEV protease and separated using a HisPrep FF16/10 column. The cleaved protein in the flow-through was subsequently purified by size exclusion chromatography on a HiLoad 26/60 Superdex 75 column in 50 mM Tris pH 7.3, 150 mM NaCl, 1 mM DTT. Subsequent to ^{19}F labeling (described in detail below), ^{15}N-$Hsp90N^{D61C}$ were passed through a HiLoad 26/60 Superdex 75 column to remove excess label.

^{19}F Labeling of Hsp90 with 3-Bromo-1,1,1-trifluoroacetone (BTFA)

Hsp90 and $Hsp90N^{D61C}$ mutants were concentrated to ~50–300 μM, treated with 2 mM TCEP, and incubated at room temperature for 30 minutes to reduce the cysteine side chain. A two-fold excess of 3–bromo-1,1,1-trifluoroacetone (PCR Inc.) over TCEP was added to the reduced protein. This was gently mixed and incubated at room temperature for 1 hour. Excess label was then removed by size exclusion chromatography, using either a Superdex 200 or Superdex 75 column. In this work, ^{19}F labeled $Hsp90^{D61C}$ and $Hsp90N^{D61C}$ are termed $Hsp90^{CYF61}$ and $Hsp90N^{CYF61}$, respectively. We determined the extent of protein labeling to be ~100% by referencing the area of the ^{19}F NMR resonance for labeled protein to the area of the trifluoroacetate (TFA) fluoromethyl group using 1D ^{19}F NMR spectroscopy with long recycle delays (10 s), which ensures peak area accuracy.

Preparation of Samples for NMR Spectroscopy

Samples for NMR spectroscopy contained ~50–300 μM protein, 25 mM HEPES, pH 7.3, 150 mM NaCl, 10% D_2O, and 0.2 mM 4,4-dimethyl-4-silapentane-1-sulfonic acid (DSS) as an internal reference for ^{1}H. Samples for ^{19}F NMR spectroscopy also contained 0.3 mM TFA as an internal reference for ^{19}F. Protein concentrations were determined using the bicinchoninic acid assay and/or ^{19}F NMR, as described above. Experiments were acquired at 25 °C. Nucleotides were obtained from BioTechne (ATP-γS), or Millipore-Sigma (ADP and AMP-PNP).

1D ^{19}F NMR Experiments to Probe Nucleotide Binding to the Hsp90 Chaperone

1D ^{19}F NMR experiments were employed to directly observe structural changes of Hsp90 in the presence of various nucleotides including ADP, the slowly hydrolyzable ATP analog ATP-γS, and the non-hydrolyzable ATP analog AMP-PNP. Nucleotide binding to both the isolated N-terminal domain of Hsp90 (Hsp90N) and the full-length construct were investigated. For each construct, a five-fold excess of nucleotide over Hsp90 was added to either $Hsp90^{CYF61}$ or $Hsp90N^{CYF61}$. This was incubated for 1 hour followed by collection of a 1D ^{19}F NMR spectrum.

Results and Discussion

Nucleotide Binding to Full-length Hsp90 and Isolated ATPase Domain Monitored by ^{19}F NMR Spectroscopy

Yeast Hsp90 (Hsp82) lacks cysteine residues; therefore, we used site directed mutagenesis to generate a D61C mutant, to introduce a ^{19}F probe within the N-terminal domain of full-length Hsp90 as well as the isolated N-terminal domain (residues 1-210), by reacting the cysteine mutant with bromotrifluoroacetone[13]. We chose D61 for mutagenesis, as this residue is fully

solvent exposed, and distant from the dimerization interface within the full-length, N-terminally dimerized Hsp90[14]. This ensures that there are no intra or inter-protomer interactions involving the cysteine-TFA side chain which would reduce its flexibility, and result in deleterious ^{19}F NMR line broadening upon dimerization. Furthermore, the ATPase activity of this mutant is unaltered in comparison to wild type, and it is able to support viability in yeast[15].

The trifluoromethyl group gives a sharp ^{19}F NMR line for the Hsp90N^{D61C} mutant as expected for a flexible side chain and fast methyl rotation (Figure 4.1A)[16]. In the presence of nucleotides, a small upfield shift of ~0.02 ppm upon binding of ADP, the slowly hydrolyzable ATP analog ATP-γS, and the non-hydrolyzable analog AMP-PNP is observed (Figure 4.1A). Within full-length Hsp90, the apo, or nucleotide free NMR spectrum shows a main resonance peak with a chemical shift similar to that for the apo N-terminal domain, consistent with a largely C-terminally dimerized but N-terminally open conformation, with an accompanying small shoulder that is ~10% of the total peak area (Figure 4.1B). From ^{19}F NMR studies of the Hsp90^{R380A} mutant, this shoulder arises from intra-protomer N-M interactions. These findings are consistent with the populations of open and closed states for nucleotide free Hsp90 observed using single molecule Förster resonance energy transfer (FRET) experiments, as well as single particle analyses of cryo-electron microscopy images[17,18]. Interestingly, binding of the non-hydrolyzable analog AMP-PNP to full-length Hsp90 leads to the appearance of two resonances, separated by ~0.04 ppm, with the downfield peak corresponding to the C-terminally dimerized, and N-terminally open conformation, and the upfield peak corresponding to the N- and C-terminally dimerized closed conformation of Hsp90 (Figure 4.1B), consistent with FRET data[17].

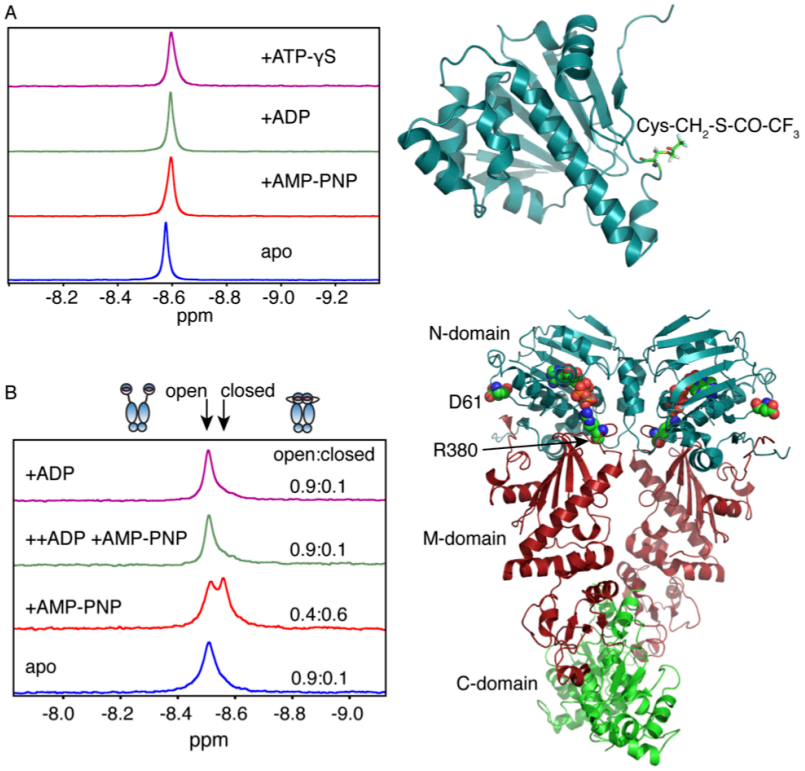

Figure 4.1: ^{19}F NMR spectra for (A) the N-terminal domain and (B) intact Hsp90 in the absence and presence of various nucleotides. A structural model for Hsp90N^{D61C} modified with bromotrifluoroacetone (shown as sticks) is shown at top right panel (1ah6), and the full-length chaperone in the closed conformation (2cg9) at the bottom right. For the intact chaperone, atoms from D61, R380, and ATP are shown as spheres.

Open and closed conformations for AMP-PNP bound Hsp90 are also observed in single particle analyses, but with a somewhat larger proportion of the closed state[18]. This difference may result from difficulties associated with capturing equilibrium populations using single particle analyses of cryo-EM data. In the presence of ADP, the open and closed conformations are populated to largely the same extent as those observed in apo Hsp90 (Figure 4.1B), consistent with both FRET and cryo-EM studies[17,18]. Addition of ADP in a four-fold excess over a saturating concentration of AMP-PNP indicates that the chaperone adopts the open conformation (Figure 4.1B).

Conclusions

Our data reveal that the isolated N-terminal domain of Hsp90 does not dimerize in the absence and presence of nucleotides. For full-length Hsp90, apo Hsp90 mainly adopts an open conformation, and addition of AMPPNP leads to equilibrium populations of open and closed conformations, which is consistent with FRET and cryo-EM studies. In this work, we show that ^{19}F NMR spectroscopy is a suitable tool for investigating conformational changes of Hsp90 in the presence of diverse nucleotides.

References

1. Schopf, F.H., Biebl, M.M. & Buchner, J. The HSP90 chaperone machinery. *Nat. Rev. Mol. Cell Biol.* **18**, 345 (2017).

2. Dahiya, V. & Buchner, J. Functional principles and regulation of molecular chaperones. *Adv. Protein Chem. Struct. Biol.* **114**, 1-60 (2019).

3. Pearl, L.H. The HSP90 molecular chaperone—an enigmatic ATPase. *Biopolymers* **105**, 594-607 (2016).

4. Panaretou, B. et al. ATP binding and hydrolysis are essential to the function of the Hsp90 molecular chaperone in vivo. *EMBO J.* **17**, 4829-4836 (1998).

5. Pearl, L.H. & Prodromou, C. Structure and mechanism of the Hsp90 molecular chaperone machinery. *Annu. Rev. Biochem.* **75**, 271-294 (2006).

6. Richter, K., Muschler, P., Hainzl, O. & Buchner, J. Coordinated ATP hydrolysis by the Hsp90 dimer. *J. Biol. Chem.* **276**, 33689-33696 (2001).

7. Wegele, H., Muschler, P., Bunck, M., Reinstein, J. & Buchner, J. Dissection of the contribution of individual domains to the ATPase mechanism of Hsp90. *J. Biol. Chem.* **278**, 39303-39310 (2003).

8. Krukenberg, K.A., Street, T.O., Lavery, L.A. & Agard, D.A. Conformational dynamics of the molecular chaperone Hsp90. *Q. Rev. Biophys.* **44**, 229-255 (2011).

9. Armstrong, H., Wolmarans, A., Mercier, R., Mai, B. & LaPointe, P. The co-chaperone Hch1 regulates Hsp90 function differently than its homologue Aha1 and confers sensitivity to yeast to the Hsp90 inhibitor NVP-AUY922. *PLoS One* **7**, e49322 (2012).

10. Sheffield, P., Garrard, S. & Derewenda, Z. Overcoming expression and purification problems of RhoGDI using a family of "parallel" expression vectors. *Protein Expr. Purif.* **15**, 34-39 (1999).

11. Marley, J., Lu, M. & Bracken, C. A method for efficient isotopic labeling of recombinant proteins. *J. Biomol. NMR* **20**, 71-75 (2001).

12. Neidhardt, F.C., Bloch, P.L. & Smith, D.F. Culture medium for enterobacteria. *J. Bacteriol.* **119**, 736-747 (1974).

13. Brown, W.E. & Seamon, K.B. Quantitation and characterization of the trifluoroacetonyl derivative of cysteine: A useful NMR probe. *Anal. Biochem.* **87**, 211-222 (1978).

14. Ali, M.M. et al. Crystal structure of an Hsp90–nucleotide–p23/Sba1 closed chaperone complex. *Nature* **440**, 1013-1017 (2006).

15. Hessling, M., Richter, K. & Buchner, J. Dissection of the ATP-induced conformational cycle of the molecular chaperone Hsp90. *Nat. Struct. Mol. Biol.* **16**, 287-293 (2009).

16. Hull, W.E. & Sykes, B.D. Fluorotyrosine alkaline phosphatase: internal mobility of individual tyrosines and the role of chemical shift anisotropy as a 19F nuclear spin relaxation mechanism in proteins. *J. Mol. Biol.* **98**, 121-153 (1975).

17. Schmid, S., Götz, M. & Hugel, T. Single-molecule analysis beyond dwell times: demonstration and assessment in and out of equilibrium. *Biophys. J.* **111**, 1375-1384 (2016).

18. Southworth, D.R. & Agard, D.A. Species-dependent ensembles of conserved conformational states define the Hsp90 chaperone ATPase cycle. *Mol. Cell* **32**, 631-640 (2008).

Chapter 5

Conformational Changes Induced by Aha1 Binding to Hsp90

The work presented here has not been published.

Introduction

The Hsp90 homodimer undergoes significant conformational changes from an open conformation to a catalytically active closed conformation to stabilize its substrates (clients)[1]. These conformational changes, including N-terminal β-strand swap between the two protomers, closure of an ATP-lid over the nucleotide binding site, interprotomer N-terminal domain (NTD) association, and intraprotomer NTD-middle domain association, are induced by ATP binding to the NTD of Hsp90[2]. Interestingly, Hsp90 is thought to be a slow ATPase with a catalytic turnover rate of ~1 ATP min^{-1} for yeast Hsp90 and ~0.1 ATP min^{-1} for the human homolog[3-6]. The slow ATPase activity of Hsp90 has been shown to emanate from slow conformational changes that lead to the catalytically active closed conformation thus, the rate-limiting steps of the Hsp90 chaperone cycle[7-9]. This is corroborated by NMR studies in our lab, where ^{1}H NMR kinetic analysis of the ATP hydrolysis step coupled to ^{19}F NMR kinetic analysis of conformational transitions of the Hsp90 chaperone cycle showed that the yeast homolog of Hsp90 has a lower limit for k_{cat} of ~1 s^{-1}, which is in accordance with the catalytic turnover rate for many enzymes[10]. Together, our studies revealed that Hsp90 is a perfect enzyme with an optimized turnover rate for the hydrolysis of ATP.

The chaperone activity of Hsp90 is regulated by a network of co-chaperones through stimulation or inhibition of Hsp90 ATPase activity, recruitment of specific clients to the Hsp90 chaperone complex, and coordination of the Hsp90 chaperone system to other chaperone systems[11]. For instance, the co-chaperone Aha1 and its yeast homolog Hch1 stimulate the ATPase activity of Hsp90[12,13], while the kinase-specific co-chaperone Cdc37 is involved in the inhibition of ATPase activity[14]. Also, the co-chaperone Hop/Sti1 serves as a bridge to connect the Hsp90 and Hsp70 chaperone systems via its TPR domain[15], whereas the late-acting co-chaperone p23/Sba1 facilitates the maturation of clients[16].

Among the diverse range of Hsp90 co-chaperones is the Activator of Hsp90 ATPase activity 1 (Aha1) that stimulates the ATPase activity of Hsp90[12,13]. Currently, a high-resolution structure of Hsp90 in complex with Aha1 is not available. However, a structure of the isolated middle domain of Hsp90 in complex with the N-terminal domain of Aha1

(Aha1N) has been solved by X-ray crystallography[17]. This Hsp90 middle domain-Aha1N complex together with biochemical studies, have provided some insights into the mechanism for the stimulation of Hsp90 ATPase activity by Aha1. Specifically, Aha1N contains a highly conserved RKxK motif, which interacts with a catalytic loop located in the middle domain of Hsp90[13,17]. This interaction remodels the Hsp90 middle domain catalytic loop such that a highly conserved arginine residue (R380 in yeast) adopts a conformation similar to that observed in the structure of the catalytically active closed conformation of Hsp90[2,17]. In this conformation, R380 can access the γ-phosphate of nucleotide bound in the NTD, which is a requirement for optimal ATP hydrolysis by Hsp90[2]. However, the conformational transitions of the Hsp90 chaperone cycle that accompanies this ATPase stimulation by Aha1 are largely unknown.

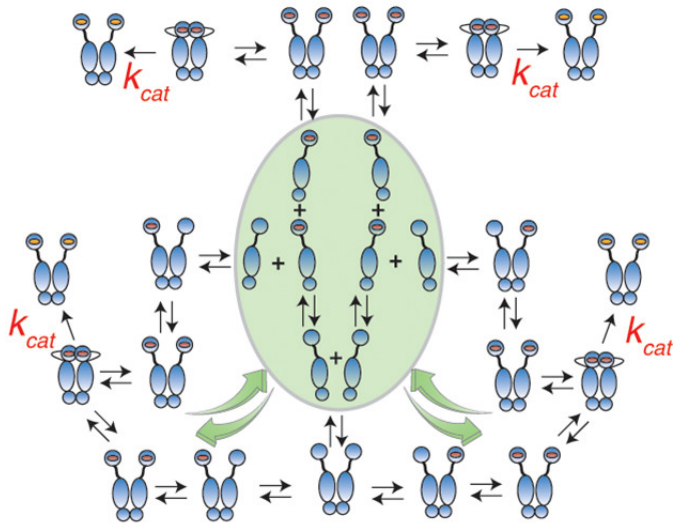

Figure 5.1: Schematic diagram of the kinetic model of the Hsp90 chaperone cycle showing nucleotide binding, conformational changes, and ATP hydrolysis. Image from ref. 10

We have developed a kinetic model for the Hsp90 chaperone cycle through the novel application of ^{19}F NMR spectroscopy[10]. The model consists of a set of twenty-eight coupled differential equations that describe the rate laws for the opening, closing and catalytic turnover of Hsp90 (Figure 5.1). Importantly, the model can be applied to interpret the

interaction of Hsp90 with its co-chaperones and clients. In this work, we investigated the structural mechanism underlying the stimulation of Hsp90 ATPase activity by Aha1 using ^{19}F as a reporter of conformational transitions. We reasoned that Aha1 stimulates the ATPase activity of Hsp90 by accelerating the slow conformational changes that lead to the catalytically active closed conformation. Thus, we used the kinetic model for the Hsp90 chaperone cycle previously developed[10] to determine the rates of opening, closing, and catalytic turnover of Hsp90 in the presence of Aha1.

Materials and Methods

Expression and Purification of Proteins

S. cerevisiae Hsp90-D61C, Hsp90-A110C, and Aha1 DNA constructs were amplified in *E. coli* DH5-α cells and expressed in *E. coli* BL21 (DE3) RIPL cells. Protein expression and purification for Hsp90-D61C and Hsp90-A110C were carried out as previously described[10]. For Aha1 purification, cell pellets were suspended in 100 ml of lysis buffer (20 mM NaH_2PO_4 pH 7.3, 500 mM NaCl, 20 mM imidazole, 1 mM DTT, 0.02 g lysozyme, 5 µg/ml DNAse I and one tablet Complete EDTA-free protease inhibitor cocktail), lysed by sonication, centrifuged at 24,000 rpm for 30 minutes at 4 °C and then purified by affinity chromatography on a HisPrep FF 16/10 column. Fractions containing proteins were pooled together and further purified by size exclusion chromatography on a Superdex 75 column in 25 mM HEPES pH 7.3, 150 mM NaCl, and 2 mM DTT.

^{19}F labeling of Hsp90 with 3-Bromo-1,1,1-trifluoroacetone (BTFA)

To label proteins with ^{19}F, Hsp90-D61C and Hsp90-A110C were treated with excess TCEP and incubated at room temperature for 30 minutes to reduce all cysteines. A two-fold excess of the fluorinated reagent 3-Bromo-1,1,1-trifluoroacetone (BTFA) over protein was added to the reduced protein. This was gently mixed and incubated at room temperature for 1 hour, followed by removal of excess label using a Superdex 200 column. In this work, ^{19}F labeled

Hsp90-D61C and Hsp90-A110C are termed Hsp90-CYF61 and Hsp90-CYF110, respectively.

NMR Spectroscopy

Samples for ^{19}F NMR spectroscopy contained ~200 μM Hsp90, 25 mM HEPES, pH 7.3, 150 mM NaCl, 1 mM DTT, 10% D_2O, 0.2 mM 4,4-dimethyl-4-silapentane-1-sulfonic acid (DSS) as an internal standard for ^{1}H, and 0.3 mM trifluoroacetate (TFA) as an internal standard for ^{19}F. All ^{19}F NMR experiments were acquired on a Bruker 700 MHz at 25 ºC. Nucleotides were obtained from BioTechne (ATPγS) and Millipore-Sigma (AMPPNP).

The conformational changes that follow the stimulation of the ATPase activity of Hsp90 by Aha1 were probed using kinetics experiments with the "kx_zg2d" pulse sequence in TOPSPIN (Bruker). Initially, a three-fold excess of Aha1 over Hsp90 was added to Hsp90-CYF61 which was used to set up the experiment. This was followed by the addition of a five-fold excess of the non-hydrolyzable ATP analog AMPPNP to start the experiment. The time it takes from nucleotide addition to the start of the kinetic experiment was recorded as dead time. ^{19}F NMR spectra were processed with NMRPipe[18], and the ^{19}F peak areas as a function of time were extracted with Mathematica. Also, we explored the influence of nucleotide binding to Hsp90 on the ATP-lid structure located within the NTD of Hsp90. Experiments were set up with apo Hsp90-CYF110 followed by the addition of a five-fold excess of nucleotide (the non-hydrolyzable ATP analog AMPPNP or the slowly hydrolyzable ATP analog ATPγS) over Hsp90. The kinetics experiment was started, and the dead time between nucleotide addition and initiation of experiment was noted. The rate of change of ^{19}F peaks was fit to a kinetic model of the Hsp90 chaperone cycle to derive the rate of opening (k_{open}) and closing (k_{close}) of Hsp90 in the presence of nucleotides. Additionally, similar experiments were carried out with Hsp90-CYF110 in the presence of ATPγS and Aha1. First, a three-fold excess of Aha1 over Hsp90 was added to Hsp90-CYF110 to set up the experiment, followed by the addition of a five-fold excess of ATPγS to start the experiment.

Results and Discussion

The Co-chaperone Aha1 Accelerates the Slow Conformational Changes of the Hsp90 Chaperone Cycle

In these experiments, aspartate 61 located on a rigid loop within the NTD of Hsp90, was mutated to cysteine (Hsp90-D61C) and subsequently labeled with the fluorinated reagent BTFA to serve as a direct probe for global conformational changes. In contrast to the sharp ^{19}F peak observed for apo Hsp90[10], the ^{19}F spectrum for the Hsp90-Aha1 complex shows a peak with a downfield shift of ~0.04 ppm, which is also significantly broader with a wide split apex, a characteristic feature of multiple protein conformations (Figure 5.2A). In the presence of AMPPNP, the ^{19}F spectrum for Hsp90 shows two distinct peaks corresponding to equilibrium populations of open and closed conformations (Figure 4.1B)[10]. However, the addition of AMPPNP to the Hsp90-Aha1 complex led to a single major ^{19}F peak and an upfield shift of ~0.05 ppm from the ^{19}F peak for the Hsp90-Aha1 complex (Figure 5.2A), consistent with a shift of all populations to the catalytically active closed conformation. The latter finding is in agreement with previous FRET studies where Aha1 was shown to preferably bind and stabilize the closed conformation of Hsp90. However, this stabilization effect was observed both in the absence and presence of nucleotides[19]. Our ^{19}F NMR data for the Hsp90-Aha1 complex on the other hand indicate that Hsp90 adopts multiple conformations in the absence of nucleotides.

In the absence of a structure for the C-terminal domain of Aha1 (Aha1C) in complex with Hsp90, the main interaction site for Aha1C on Hsp90 has been localized to the NTD of Hsp90 based on NMR studies with isolated domains of Hsp90 and Aha1[19]. Accordingly, the multiple conformations we observed in our ^{19}F NMR spectrum for the Hsp90-Aha1 complex might arise from interactions of Aha1C with multiple sites within the NTD of Hsp90. Consequently, binding of nucleotide (AMPPNP) locks the interaction of Aha1C with Hsp90 and stabilizes the catalytically active closed conformation, which led to the single ^{19}F peak observed in the Hsp90-Aha1-AMPPNP complex (Figure 5.2A). Indeed, similar multiple

conformations of Hsp90 bound to Aha1 in the absence of nucleotide has been observed in a previous methyl TROSY NMR study[20].

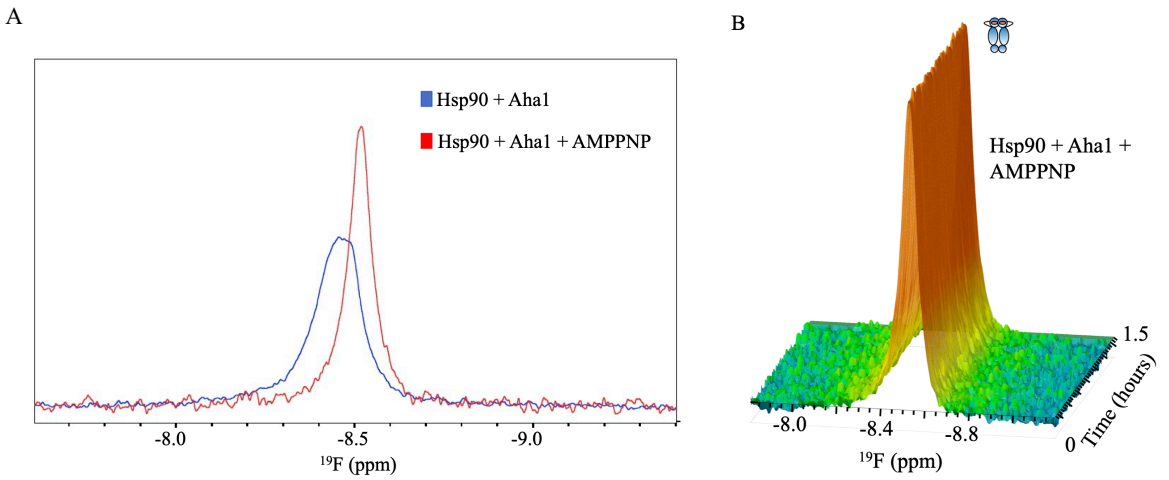

Figure 5.2: Interaction of Aha1 with Hsp90. (A) ^{19}F spectra showing the conformational change induced by Aha1 binding to apo Hsp90 (blue) and Hsp90 in the presence of AMPPNP (red). (B) ^{19}F NMR spectra for Hsp90 in the presence of Aha1 and AMPPNP from kinetics experiment shows accumulation of the catalytically active closed conformation.

In the presence of AMPPNP, Hsp90 undergoes slow conformational changes from an open (k_{open} = 1.786 ± 0.004 h^{-1}) to a closed (k_{close} = 3.69 ± 0.02 h^{-1}) conformation until it reaches equilibrium populations of open and closed conformations[10]. To determine whether Aha1 accelerates these conformational changes, we monitored in real-time the conformational transitions that accompany ATPase stimulation by Aha1 using ^{19}F NMR kinetics experiment. This was done by following spectral changes of the Hsp90-Aha1 complex upon addition of AMPPNP for 1.5 hours. Our results show an unchanged spectrum throughout the experiment (Figure 5.2B), which indicates that Aha1 accelerates the formation of the catalytically active closed conformation of Hsp90. Previous FRET studies had reported similar acceleration of the slow conformational transitions of Hsp90 by Aha1, although this was due to a bypass of an intermediate Hsp90 conformation in the Hsp90 chaperone cycle[9]. Additionally, increased rates for all local conformational changes that lead to the formation of the catalytically active closed conformation of Hsp90 were observed in the presence of Aha1 and AMPPNP from PET-FCS studies[8]. These accelerated motions were

observed for N-terminal β-strand swap, lid release, and NTD-middle domain association, which further confirms the role of Aha1 in accelerating the slow conformational changes of the Hsp90 chaperone cycle.

Influence of ATP-Lid Dynamics on the Hsp90 Chaperone Cycle

The transition of Hsp90 from an open conformation to a catalytically active closed conformation is accompanied by local motions, including N-terminal β-strand swap and movement of an ATP-lid from an open lid conformation to a closed lid conformation[2]. These local motions are thought to be the rate-limiting steps of the Hsp90 chaperone cycle. Currently, the contributions of these local motions to the overall kinetics of the Hsp90 chaperone cycle remain elusive. In this work, we employed the ^{19}F nucleus as a probe to directly report on local kinetics of the ATP-lid that accompanies the overall opening and closing of Hsp90. To investigate local ATP-lid motions, an alanine residue located near the apex of the lid (Figure 5.3A) was mutated to cysteine (Hsp90-A110C) and subsequently labeled with BTFA (Hsp90-CYF110) to serve as a direct reporter of ATP-lid dynamics.

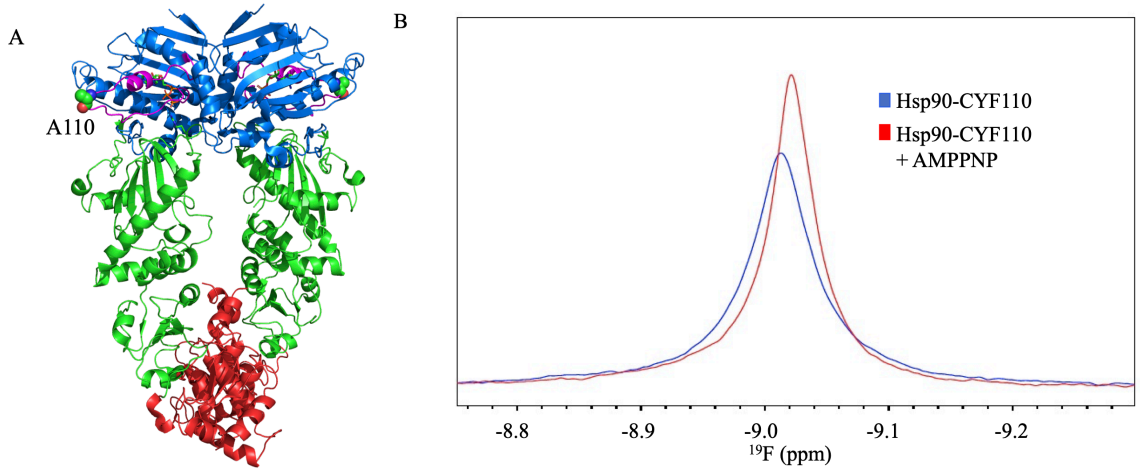

Figure 5.3: (A) The closed conformation of Hsp90 (PDB 2CG9)[2] showing the NTD (blue), middle domain (green), and C-terminal domain (red), with A110 shown as spheres and ATP-lid colored magenta. (B) ^{19}F NMR spectra for apo Hsp90-CYF110 (blue) and Hsp90-CYF110 in complex with AMPPNP (red).

Compared to the ^{19}F peak for apo Hsp90-CYF61[10], the ^{19}F peak for apo Hsp90-CYF110 shows an upfield shift of ~0.5 ppm. This is consistent with a more exposed ^{19}F tag at position 110 as downfield and upfield shifts across the ^{19}F spectrum have been associated with a more buried and more exposed ^{19}F nucleus, respectively[21]. On the other hand, binding of AMPPNP to Hsp90-CYF110 led to a small upfield shift of ~0.01 ppm and a narrower ^{19}F peak with linewidths of ~40.0 Hz for apo Hsp90-CYF110 and ~28.5 Hz for the AMPPNP bound complex (Figure 5.3B). The overlapping free and bound peaks for Hsp90-CYF110 contrast those of Hsp90-CYF61 which possesses two distinct ^{19}F peaks (~0.04 ppm apart) corresponding to equilibrium populations of open and closed conformations (Figure 4.1B)[10]. Interestingly, integration of the ^{19}F peak for apo Hsp90-CYF110 gave an area of ~7.58 comparable to an area of ~7.65 measured for the AMPPNP bound peak, indicating that the single resonance we observed for the AMPPNP bound complex (Figure 5.3B) is an overlap of the open and closed conformations of Hsp90. This finding is supported by the small difference in chemical shift (~0.01 ppm) between apo Hsp90-CYF110 and the AMPPNP bound complex. The different presentation of ^{19}F peaks for the open and closed conformations of Hsp90-CYF61 and Hsp90-CYF110 is not surprising given the huge difference in location of the ^{19}F probe within the two mutants, a rigid loop for Hsp90-CYF61 and a mobile ATP-lid for Hsp90-CYF110. This highlights the exceptional sensitivity of the ^{19}F nucleus to its environment and its suitability for studying dynamic processes occurring in proteins.

The conformational changes induced by AMPPNP and ATPγS binding to Hsp90-CYF110 were followed in real-time for 1.5 and 5.5 hours, respectively. The ^{19}F spectra for Hsp90-CYF110 in the presence of AMPPNP from ^{19}F-NMR monitored kinetics experiment show an initial narrowing of the main resonance peak and eventual stabilization of this conformation (Figure 5.4A), which is indicative of a transition from an open conformation to a closed conformation. The rate of change of the ^{19}F peak area during the duration of the experiment was fit to a kinetic model of the Hsp90 chaperone cycle to extract a rate of opening (k_{open}) of 2.3 h^{-1} and a rate of closing (k_{close}) of 6.4 h^{-1} for Hsp90-CYF110. Interestingly, these rates are comparable to the rates previously reported for Hsp90-CYF61 (k_{open} of 1.9 h^{-1} and k_{close} of 3.7 h^{-1})[10], a reporter of global Hsp90 dynamics owing to the

location of its ^{19}F probe on a rigid loop. This finding indicates that for ^{19}F-NMR monitored kinetics experiment with Hsp90-CYF110 in the presence of AMPPNP, the global conformational change of Hsp90 from an open to a closed conformation is observed even though the ^{19}F probe is located on the ATP-lid.

Additionally, we followed the hydrolysis of ATPγS by Hsp90-CYF110 to confirm ^{19}F peak assignments for the open and closed conformations. The ^{19}F spectra from kinetics experiment for Hsp90-CYF110 in the presence of ATPγS show an initial increase in accumulation of the closed conformation followed by accumulation of the open conformation once hydrolysis is initiated (Figure 5.4B). Accordingly, the ^{19}F chemical shifts and linewidths for the open and closed conformations in these spectra (Figure 5.4B) are similar to those observed in the presence of AMPPNP (Figure 5.4A), which confirms that the ^{19}F peak for the open and closed conformations of Hsp90-CYF110 exhibit peak overlap.

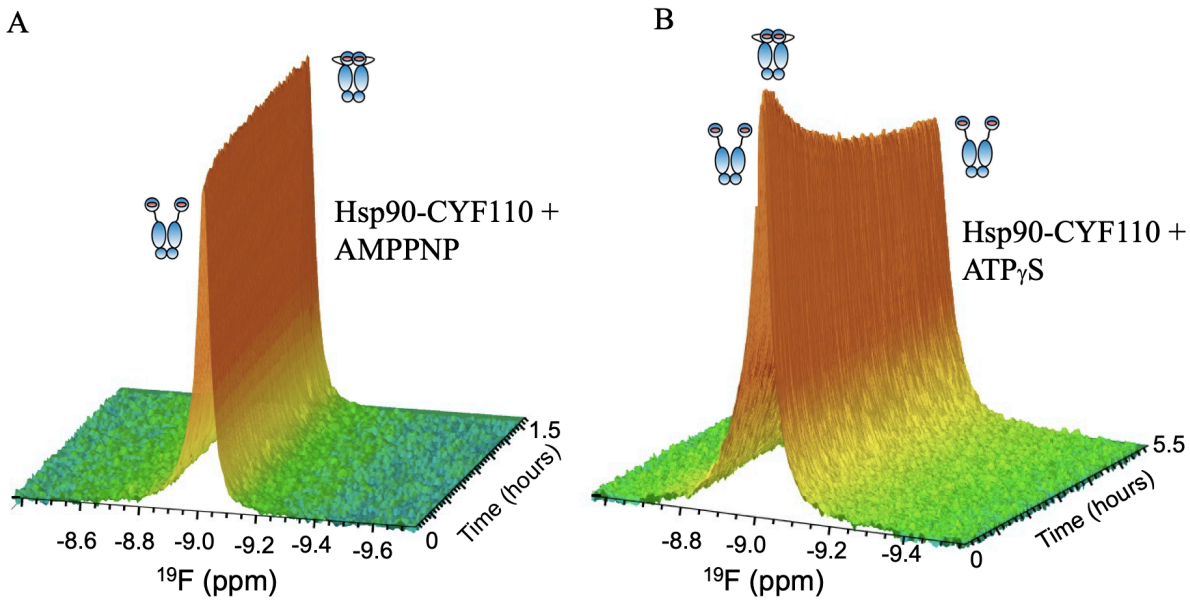

Figure 5.4: Conformational changes induced by nucleotide binding to Hsp90-CYF110. (A) ^{19}F NMR spectra for the Hsp90-CYF110-AMPPNP complex from kinetics experiment. (B) ^{19}F NMR spectra for the Hsp90-CYF110-ATPγS complex from kinetics experiment.

Aha1 Binding to Hsp90 Induces Structural Changes within the ATP-lid of Hsp90

The conformational changes induced by Aha1 binding to Hsp90-CYF110 were investigated in the presence of AMPPNP and ATPγS. The ^{19}F spectrum for Hsp90-CYF110 in complex with Aha1 reveals a major broad peak with a wide split apex, which indicates multiple conformations (Figure 5.5A). However, the splitting pattern observed here is more prominent than that observed for Hsp90-CYF61-Aha1 complex (Figure 5.2A). This is probably due to differences in location of the ^{19}F probe relative to the binding site between Aha1 and Hsp90. Specifically, residues of the ATP-lid have been shown to be involved in the interaction of Aha1 and Hsp90 based on chemical shift perturbation plots for Hsp90 NTD in the presence of Aha1C and AMPPNP[19]. Thus, a possible explanation for the prominent splitting pattern observed for the Hsp90-CYF110-Aha1 complex might be because binding of Aha1C to the NTD has a pronounced effect on the ATP-lid.

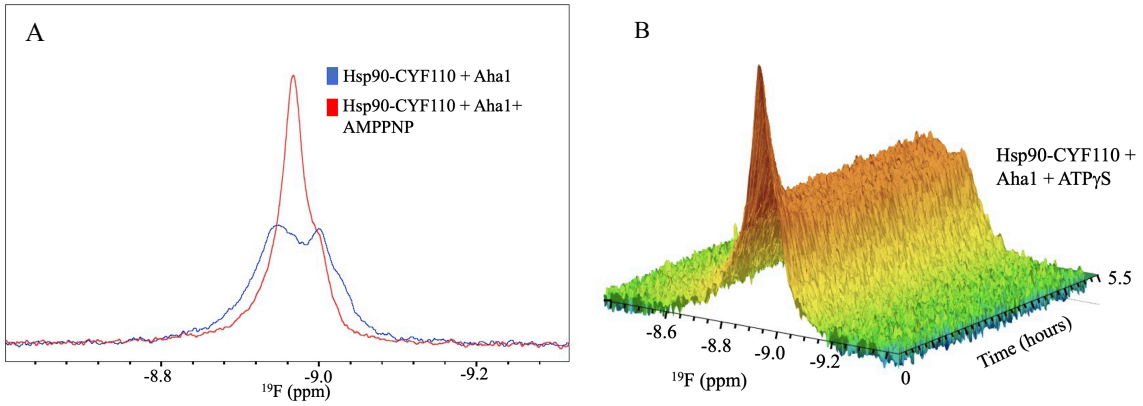

Figure 5.5: Influence of Aha1 binding on the Hsp90 ATP-lid. (A) ^{19}F NMR spectra showing the binding of Aha1 to apo Hsp90-CYF110 (blue) and Hsp90-CYF110 in the presence of AMPPNP (red). (B) ^{19}F NMR spectra for Hsp90 in the presence of Aha1 and ATPγS from kinetics experiment.

On the other hand, binding of AMPPNP to the Hsp90-CYF110-Aha1 complex abolishes the observed multiple conformations, which is shown as a sharp ^{19}F peak corresponding to the catalytically active closed conformation of Hsp90 (Figure 5.5A).

Interestingly, this ^{19}F peak bears a small upfield shoulder, which has not been observed in any of our ^{19}F spectra for the catalytically active closed conformations of Hsp90. To confirm that the ^{19}F peak observed for the Hsp90-CYF110-Aha1-AMPPNP complex is indeed the catalytically active closed conformation of Hsp90, we monitored the hydrolysis of ATPγS by Hsp90 in the presence of Aha1 in real-time for 5.5 hours. The ^{19}F spectra show an initial accumulation of the catalytically active closed conformation with a major ^{19}F peak, bearing a shoulder similar to that observed for the Hsp90-CYF110-Aha1-AMPPNP complex. This is followed by the accumulation of a broad peak with a wide split apex once nucleotide hydrolysis is initiated, which is indicative of the chaperone going back to the conformation observed for the Hsp90-CYF110-Aha1 complex (Figure 5.5B).

For this kinetics experiment, a fit of the rate of change of the ^{19}F peak to a kinetic model of the Hsp90 chaperone cycle would have enabled the extraction of kinetic parameters for the conformational changes that accompany ATPase stimulation by Aha1. However, the extreme overlap in chemical shifts between Hsp90-Aha1 and Hsp90-Aha1 in the presence of nucleotides (Figure 5.5) makes accurate extraction of peaks for kinetic fitting impossible. Thus, we can only deduce that the interaction of Aha1 with Hsp90 does indeed have a pronounced effect on the ATP-lid, but the rates of opening and closing of the Hsp90 chaperone in the presence of Aha1 remains undetermined.

Conclusions

Aha1 has been suggested to accelerate the conformational changes that lead to the formation of the catalytically active closed conformation of Hsp90 in a number of studies. However, the structural mechanism underlying this acceleration is largely unknown. In this study, we took advantage of the exquisite sensitivity of the ^{19}F nucleus to its environment to directly probe the structural changes of Hsp90 in the presence of Aha1 using ^{19}F NMR spectroscopy. We show that Aha1 binding to Hsp90 induces multiple Hsp90 conformations with a shift to the catalytically active closed conformation observed once nucleotide is bound. Additionally, by incorporating a ^{19}F probe on the ATP-lid of Hsp90, our ^{19}F data reveal a possible interaction of Aha1 with the ATP-lid, which stabilizes the catalytically active closed

conformation of Hsp90 in the presence of nucleotide. Taken together, we show that Aha1 accelerates the overall conformational change of Hsp90 from an open to a closed conformation. However, the exact rates of acceleration of the Hsp90 chaperone cycle in the presence of Aha1 remains undetermined due to severe overlap in the ^{19}F peaks for different conformations of Hsp90-CYF110.

References

1. Prodromou, C. et al. The ATPase cycle of Hsp90 drives a molecular 'clamp' via transient dimerization of the N-terminal domains. *EMBO J.* **19**, 4383-4392 (2000).

2. Ali, M.M. et al. Crystal structure of an Hsp90–nucleotide–p23/Sba1 closed chaperone complex. *Nature* **440**, 1013-1017 (2006).

3. Wegele, H., Muschler, P., Bunck, M., Reinstein, J. & Buchner, J. Dissection of the contribution of individual domains to the ATPase mechanism of Hsp90. *J. Biol. Chem.* **278**, 39303-39310 (2003).

4. McLaughlin, S.H., Smith, H.W. & Jackson, S.E. Stimulation of the weak ATPase activity of human hsp90 by a client protein. *J. Mol. Biol.* **315**, 787-798 (2002).

5. Scheibel, T. et al. ATP-binding properties of human Hsp90. *J. Biol. Chem.* **272**, 18608-18613 (1997).

6. Panaretou, B. et al. ATP binding and hydrolysis are essential to the function of the Hsp90 molecular chaperone in vivo. *EMBO J.* **17**, 4829-4836 (1998).

7. Krukenberg, K.A., Street, T.O., Lavery, L.A. & Agard, D.A. Conformational dynamics of the molecular chaperone Hsp90. *Q. Rev. Biophys.* **44**, 229-255 (2011).

8. Schulze, A. et al. Cooperation of local motions in the Hsp90 molecular chaperone ATPase mechanism. *Nat. Chem. Biol.* **12**, 628-635 (2016).

9. Hessling, M., Richter, K. & Buchner, J. Dissection of the ATP-induced conformational cycle of the molecular chaperone Hsp90. *Nat. Struct. Mol. Biol.* **16**, 287-293 (2009).

10. Lee, B.L. et al. The Hsp90 chaperone: 1H and 19F dynamic nuclear magnetic resonance spectroscopy reveals a perfect enzyme. *Biochemistry* **58**, 1869-1877 (2019).

11. Taipale, M., Jarosz, D.F. & Lindquist, S. HSP90 at the hub of protein homeostasis: emerging mechanistic insights. *Nat. Rev. Mol. Cell Biol.* **11**, 515-528 (2010).

12. Panaretou, B. et al. Activation of the ATPase activity of hsp90 by the stress-regulated cochaperone aha1. *Mol. Cell* **10**, 1307-1318 (2002).

13. Horvat, N.K. et al. A mutation in the catalytic loop of hsp90 specifically impairs ATPase stimulation by aha1p, but not hch1p. *J. Mol. Biol.* **426**, 2379-2392 (2014).

14. Roe, S.M. et al. The mechanism of Hsp90 regulation by the protein kinase-specific cochaperone p50cdc37. *Cell* **116**, 87-98 (2004).

15. Smith, D.F. et al. Identification of a 60-kilodalton stress-related protein, p60, which interacts with hsp90 and hsp70. *Mol. Cell. Biol.* **13**, 869-876 (1993).

16. Young, J.C. & Hartl, F.U. Polypeptide release by Hsp90 involves ATP hydrolysis and is enhanced by the co-chaperone p23. *EMBO J.* **19**, 5930-5940 (2000).

17. Meyer, P. et al. Structural basis for recruitment of the ATPase activator Aha1 to the Hsp90 chaperone machinery. *EMBO J.* **23**, 511-519 (2004).

18. Delaglio, F. et al. NMRPipe: a multidimensional spectral processing system based on UNIX pipes. *J. Biomol. NMR* **6**, 277-293 (1995).

19. Retzlaff, M. et al. Asymmetric activation of the hsp90 dimer by its cochaperone aha1. *Mol. Cell* **37**, 344-354 (2010).

20. Oroz, J., Blair, L.J. & Zweckstetter, M. Dynamic Aha1 co-chaperone binding to human Hsp90. *Protein Sci.* **28**, 1545-1551 (2019).

21. Sykes, B.D. & Hull, W.E. Fluorine nuclear magnetic resonance studies of proteins. *Meth. Enzymol.* **49**, 270-295 (1978).

Chapter 6

Conclusion and Future Directions

The diverse range of proteins dependent on the molecular chaperone Hsp90 for their activation and stabilization makes the chaperone a key player in proteostasis. Thus, it is not surprising that Hsp90 has been implicated in several human diseases. Accordingly, an in-depth understanding of the molecular mechanism underlying the chaperone activity of Hsp90 is critical to the development of effective therapeutics for these diseases. Given the highly dynamic nature of Hsp90, the study of dynamic processes occurring in the chaperone is essential to elucidating the mechanism of its activity.

NMR spectroscopy is one of the most potent tools for studying protein dynamics as it enables direct observation of conformational dynamics in solution. However, conventional NMR studies for Hsp90 are typically challenging due to its high molecular weight. This is further aggravated by the formation of complexes of Hsp90 with its co-chaperones and clients in the Hsp90 chaperone cycle. Therefore, a comprehensive dynamic study of the Hsp90 chaperone cycle requires a suitable probe, which is highly sensitive to conformational changes and importantly not limited by molecular weight. We have exploited the exceptional sensitivity of the ^{19}F nucleus to its environment coupled to the success of ^{19}F NMR in probing dynamic processes occurring in high molecular weight proteins to investigate the dynamics of Hsp90 using a variety of ^{19}F NMR-based techniques. Chapters 2 and 3 of this work explored local dynamics within the N-terminal domain (NTD) of Hsp90, which provides a basis for studying dynamics in the full-length chaperone. Chapters 4 and 5 are a brief exploration of the dynamics of full-length Hsp90 in the presence of different nucleotides and the ATPase stimulating co-chaperone Aha1, respectively.

In chapter 2 of this work, we investigated the dynamics of a trifluoroacetone cysteine derivative (CYF) incorporated into the isolated NTD of Hsp90 to serve as a probe for ^{19}F NMR dynamic studies[1]. The total correlation function for a globular protein tumbling in solution is governed by both the overall correlation function and the correlation function for each internal motion occurring in the protein[2]. Thus, the relaxation of proteins bearing a CYF residue will be sensitive to internal motion of the CYF sidechain and consequently influence the ^{19}F NMR linewidth of such proteins. Generally, the internal motion of amino acid sidechains occurs in the picosecond (ps) to nanosecond (ns) timescale, which is amenable to detection by nuclear spin relaxation (NSR)[3]. Therefore, we used a blend of ^{19}F NSR

experiments and MD simulations to quantify the contribution of the CYF sidechain internal motion to the ^{19}F NMR linewidth of Hsp90 NTD. Dynamics of the CYF sidechain were interpreted in terms of a principal order parameter S^2 and an internal correlation time τ_i[4-6]. The method developed in this chapter allows for the separation of fast internal motion of the CYF sidechain from slower (μs-ms) exchange processes such as nucleotide binding and domain motions occurring in Hsp90. Findings in this work revealed the high flexibility of the CYF sidechain, which consequently contributes to the narrow ^{19}F NMR linewidths of proteins bearing a CYF residue. Importantly, the methodology presented here is not only applicable to Hsp90 but can be applied in the interpretation of dynamic processes occurring in proteins bearing a trifluoroacetone cysteine derivative.

In chapter 3, the methodology developed in chapter 2 was applied in the separation of CYF sidechain motion from ATP-lid motion and chemical exchange arising from ligand binding to the isolated NTD of Hsp90. The ATP-lid forms a gate over the nucleotide binding pocket of Hsp90, and a transition of the lid from an open lid conformation to a closed lid conformation is required for optimal ATP hydrolysis by Hsp90[7,8]. In this work, an alanine residue (A110) located near the apex of the ATP-lid of Hsp90 was mutated to cysteine and subsequently labeled with ^{19}F (CYF) to serve as a probe for ^{19}F NMR studies. CPMG relaxation dispersion is a suitable technique for the analysis of dynamic processes that occur in the microseconds (μs) to milliseconds (ms) timescale including hinged domain motions, ligand binding and unbinding, and loop motions[3]. To probe the influence of nucleotide binding on the ^{19}F NMR linewidth of Hsp90 NTD, we employed a combination of ^{19}F CPMG relaxation dispersion and ^{19}F nuclear spin relaxation experiments at low and high magnetic field strengths. This combined approach allowed us to separate the internal motion of the CYF sidechain from slow exchange processes emanating from AMPPNP (a non-hydrolyzable ATP analog) binding to the NTD of Hsp90. We showed that chemical exchange from AMPPNP binding and unbinding to the NTD of Hsp90 increases the ^{19}F NMR linewidth and subsequently quantified the rate of exchange (k_{ex}) for AMPPNP binding[9]. Also, we used MD simulations to develop an atomic model for motions of the ATP-lid, which together with

our ^{19}F NMR findings revealed priming of the ATP-lid by the γ-phosphate of AMPPNP, a necessary prelude to ATP-lid closure and subsequent ATP hydrolysis by Hsp90[9].

Generally, the work presented in chapters 2 and 3 highlight the promising potential of ^{19}F NMR in studying various dynamic processes in full-length Hsp90. A glimpse of this is presented in chapters 4 and 5.

Suitability of Trifluoroacetone Cysteine Derivative (CYF) as a Probe for Studying Hsp90 Dynamics

The study of proteins using ^{19}F NMR spectroscopy requires successful incorporation of a ^{19}F nucleus into proteins as the nucleus does not occur naturally in proteins. Consequently, a major issue that must be addressed in ^{19}F NMR studies of proteins is the choice of a suitable ^{19}F probe. To investigate the dynamic processes occurring in the Hsp90 chaperone, we chose to incorporate ^{19}F into Hsp90 through chemical modification of the sulfhydryl group of cysteine. Compared to other ^{19}F labeling methods, this method is relatively simple, site-specific, cost-effective, and offers a high protein yield[10]. Importantly, the yeast Hsp90 homolog employed in our ^{19}F NMR studies has no inherent cysteines, which opens the possibility of site-specifically labeling any part of the protein with ^{19}F after considering the effect of cysteine mutagenesis.

In my experiments, the fluorinated reagent 3-Bromo-1,1,1-trifluoroacetone (BTFA) was used for all chemical modifications of cysteine. This reaction leads to the conversion of a standard cysteine residue to a non-standard trifluoroacetone cysteine derivative which we termed CYF residue. The CYF residue bears three equivalent ^{19}F nuclei, which results in three times increase in ^{19}F signal. In addition, the trifluoromethyl moiety of the CYF residue has no scalar coupled protons, and importantly fast methyl rotation of the CF_3 moiety limits the contribution of chemical shift anisotropy (CSA) to the ^{19}F NMR linewidth[11]. Thus, the CYF residue is one of the most suitable probes for ^{19}F NMR studies of high molecular weight proteins, especially at high magnetic field strengths where the domination of CSA might otherwise lead to broadening of ^{19}F NMR linewidths[12]. Considering the molecular weight of

Hsp90 (~180 kDa for the homodimer), our ^{19}F NMR studies have highlighted the suitability of the CYF probe for studying high molecular weight proteins.

The utility of CYF as a probe for ^{19}F NMR studies necessitated a detailed analysis of CYF sidechain internal motion, which had been lacking. Accordingly, we employed a modified model-free approach to interpret CYF sidechain motion[1], by including the internal motion of the sidechain to previous expressions for ^{19}F transverse relaxation time (T_2) that accounts for overall protein tumbling and fast methyl rotation[12]. At high magnetic field strengths CSA is the dominant mechanism that contributes to ^{19}F-T_2 relaxation time[12]. Therefore, we used benchtop NMR at low magnetic field strength (1.41 T) to quantify the contribution of ^{19}F-^{19}F dipolar relaxation to the ^{19}F-T_2 of the CYF sidechain, which led to more accurate model-free parameters[9]. Alternatively, more accurate model free parameters can be derived using a combination of ^{19}F-T_1 and ^{19}F-T_2 relaxation times. For ^{19}F-T_1, we measured a value of ~350 ms at 18.8T for the CYF sidechain as the contributions of CSA and ^{19}F-^{19}F dipolar relaxation mechanisms are negligible[1]. Accordingly, impurities such as paramagnetic dissolved oxygen and metal ions, which likely contributed to the small ^{19}F-T_1 value we measured can be quenched by bubbling argon through the sample to remove dissolved oxygen and using Chelex resin to remove paramagnetic metal ions. Altogether, the work presented in chapters 2 and 3 reveal the high flexibility of the CYF sidechain and facilitates a quantitative understanding of fast and slow timescale contributions to the ^{19}F-T_2 relaxation of proteins.

The Use of ^{19}F NMR to Probe Local Dynamics of Hsp90

The global conformational changes of Hsp90 from an open conformation to a catalytically active closed conformation are accompanied by local motions including N-terminal β-strand swap, closure of an ATP-lid over the nucleotide binding site, interprotomer NTD association, and intraprotomer NTD-middle domain association[7]. The incorporation of a ^{19}F probe on the ATP-lid of Hsp90 has provided mechanistic details on the nature of nucleotide binding to the NTD of Hsp90, as well as the influence of nucleotide binding on the ATP-lid using ^{19}F NMR

studies[9]. Specifically, for the isolated NTD of Hsp90, the γ-phosphate of bound AMPPNP destabilizes the C-terminal end of the ATP-lid. To put this in the context of full-length Hsp90, the structure of the catalytically active closed conformation shows an ATP-lid that is closed over the nucleotide binding site[7]. Thus, in addition to destabilization of the C-terminus of the ATP-lid by the γ-phosphate of bound AMPPNP, destabilization of the N-terminus of the ATP-lid, which is coupled to the release of the N-terminal β-strand[13], is required to achieve full ATP-lid closure. Overall, this study expands our understanding of nucleotide binding to Hsp90 by establishing the link between nucleotide binding and local dynamics of the ATP-lid.

Likewise, dynamics of other local motions of Hsp90 can be probed with ^{19}F NMR by moving the ^{19}F probe to the site of interest. For instance, a ^{19}F probe on the N-terminal β-strand will enable exploration of N-terminal β-strand dynamics by various ^{19}F NMR-based techniques. This will provide mechanistic detail on N-terminal β-strand strapping between the two Hsp90 protomers as well as the link between local motions within Hsp90. Additionally, a ^{19}F probe at the interprotomer NTD and intraprotomer NTD-middle domain interfaces will be a valuable reporter of local dynamics. Taken together, the ^{19}F probe is a suitable reporter of local conformational changes of Hsp90, which is also applicable to studying global dynamics of Hsp90.

Conformational Changes Induced by Nucleotide and Co-chaperone Binding to the Hsp90 Chaperone

Chapter 4 forms part of work from our lab that employed ^{19}F NMR to explore global conformational changes of Hsp90 as it transitions from an open conformation to a catalytically active closed conformation in the presence of nucleotides, including AMPPNP, ATPγS, and ATP[14]. We monitored the conformational changes of Hsp90 in real-time using a ^{19}F kinetic experiment and subsequently fit the rate of change of the protein ^{19}F peak to a kinetic model of the Hsp90 chaperone cycle. Further extraction of kinetic parameters associated with the transition of Hsp90 from an open conformation to a catalytically active

closed conformation allowed us to determine the rate of opening and closing of the chaperone. Our results revealed that the conformational changes that lead to the formation of the catalytically active conformation are slow, and the rate-limiting steps of the Hsp90 chaperone cycle. It is our expectation that this study will provide the groundwork for elucidating the molecular mechanism underlying how co-chaperones and clients navigate through the Hsp90 chaperone cycle.

Chapter 5 is a further application of ^{19}F NMR to investigate the influence of an ATPase stimulating co-chaperone Aha1 on the Hsp90 chaperone cycle. Although the ability of Aha1 to stimulate the ATPase activity of Hsp90 has been reported in a number of studies[15,16], the structural changes that accompany this stimulation in the Hsp90 chaperone cycle are largely unknown. In this study, we showed that Aha1 stimulates the ATPase activity of Hsp90 by accelerating the slow conformational changes that lead to the formation of the catalytically active closed conformation. Overall, the two studies in chapters 4 and 5 expand our understanding of the interplay between nucleotide binding, conformational changes, and ATPase stimulation by co-chaperons, which is key to understanding how the Hsp90 chaperone cycle drives itself forward to activate its clients.

Conformational Dynamics of Hsp90 in the Presence of Clients

Despite the huge advances made in understanding the structure and function of Hsp90, the answers to some prominent questions in the Hsp90 field remain unclear. Specifically, our current understanding of Hsp90 clients is limited owing to the immense structural and functional diversity among clients. Presently, it remains elusive what makes a protein an Hsp90 client as the hundreds of clients identified so far do not share common sequences or structural motifs. Also, the influence of conformational transitions of the Hsp90 chaperone cycle on clients as well as the molecular mechanism by which Hsp90 activates its clients remain enigmatic. To address these issues requires an in-depth understanding of dynamic processes occurring in the Hsp90 chaperone.

Structural insights into the interaction of Hsp90 with clients have been derived from biophysical studies involving Cdk4, GR-LBD, and Tau[17-20]. However, all of these studies

provide a static picture of these interactions. ^{19}F NMR dynamic studies of ^{19}F labeled Hsp90 in the presence of nucleotides, co-chaperones, and clients have the potential of expanding our knowledge of Hsp90-client dynamics. Particularly, the conformational changes induced by client interaction with Hsp90, the influence of nucleotides and co-chaperones on client-induced conformational changes, global and local conformational changes of Hsp90 in the presence of clients can all be probed with ^{19}F NMR. Experiments with clients might necessitate a shift from the yeast Hsp90 homolog to the human homolog. In contrast to the yeast homolog, human Hsp90α contains seven cysteine residues which might not be ideal for cysteine modification with BTFA. To overcome this will require the use of either site-directed mutagenesis to eliminate unwanted cysteines or a different method of ^{19}F labeling such as site-specific biosynthetic incorporation of fluorinated amino acid analogs using an orthogonal tRNA/aminoacyl-tRNA synthetase pair[21,22].

On the other hand, investigation of dynamics and structural changes induced in co-chaperones and clients due to their interaction with Hsp90 will expand our understanding of the mechanism of co-chaperone and client recognition and specificity by Hsp90. Specifically, incorporation of a ^{19}F probe into co-chaperones and clients will allow direct observation of conformational changes. In the case of co-chaperones and clients, a different method of ^{19}F labeling will be required in situations where multiple cysteines make chemical modification with BTFA unsuitable. Altogether, an extension of ^{19}F NMR dynamic studies to ^{19}F labeled co-chaperones and clients will contribute substantially to our knowledge of the mechanism of client activation by Hsp90.

Ultimately, the application of ^{19}F NMR in the study of Hsp90 dynamics holds promising potential for understanding dynamic processes occurring in the chaperone, which have been limited by the high molecular weight of Hsp90 and Hsp90-co-chaperone-client complexes. Finally, the work presented in this thesis has expanded our knowledge on the crucial role of dynamics to the chaperone activity of Hsp90 as well as the prospects of ^{19}F NMR in elucidating the molecular mechanism underlying the chaperone activity of Hsp90.

References

1. Rashid, S., Lee, B.L., Wajda, B. & Spyracopoulos, L. Side-chain dynamics of the trifluoroacetone cysteine derivative characterized by 19F NMR relaxation and molecular dynamics simulations. *J. Phys. Chem. B* **123**, 3665-3671 (2019).

2. Lipari, G., Szabo, A. & Levy, R.M. Protein dynamics and NMR relaxation: comparison of simulations with experiment. *Nature* **300**, 197-198 (1982).

3. Kleckner, I.R. & Foster, M.P. An introduction to NMR-based approaches for measuring protein dynamics. *Biochim. Biophys. Acta Proteins Proteom.* **1814**, 942-968 (2011).

4. Lipari, G. & Szabo, A. Model-free approach to the interpretation of nuclear magnetic resonance relaxation in macromolecules. 1. Theory and range of validity. *J. Am. Chem. Soc.* **104**, 4546-4559 (1982).

5. Lipari, G. & Szabo, A. Model-free approach to the interpretation of nuclear magnetic resonance relaxation in macromolecules. 2. Analysis of experimental results. *J. Am. Chem. Soc.* **104**, 4559-4570 (1982).

6. Clore, G.M. et al. Deviations from the simple two-parameter model-free approach to the interpretation of nitrogen-15 nuclear magnetic relaxation of proteins. *J. Am. Chem. Soc.* **112**, 4989-4991 (1990).

7. Ali, M.M. et al. Crystal structure of an Hsp90–nucleotide–p23/Sba1 closed chaperone complex. *Nature* **440**, 1013-1017 (2006).

8. Prodromou, C. et al. Identification and structural characterization of the ATP/ADP-binding site in the Hsp90 molecular chaperone. *Cell* **90**, 65-75 (1997).

9. Rashid, S., Lee, B.L., Wajda, B. & Spyracopoulos, L. Nucleotide Binding and Active Site Gate Dynamics for the Hsp90 Chaperone ATPase Domain from Benchtop and High Field 19F NMR Spectroscopy. *J. Phys. Chem. B* **124**, 2984-2993 (2020).

10. Kitevski-LeBlanc, J.L. & Prosser, R.S. Current applications of 19F NMR to studies of protein structure and dynamics. *Prog. Nucl. Magn. Reson. Spectrosc.* **62**, 1-33 (2011).

11. Ye, L., Larda, S.T., Li, Y.F.F., Manglik, A. & Prosser, R.S. A comparison of chemical shift sensitivity of trifluoromethyl tags: optimizing resolution in 19 F NMR studies of proteins. *J. Biomol. NMR* **62**, 97-103 (2015).

12. Hull, W.E. & Sykes, B.D. Fluorotyrosine alkaline phosphatase: internal mobility of individual tyrosines and the role of chemical shift anisotropy as a 19F nuclear spin relaxation mechanism in proteins. *J. Mol. Biol.* **98**, 121-153 (1975).

13. Richter, K. et al. Intrinsic inhibition of the Hsp90 ATPase activity. *J. Biol. Chem.* **281**, 11301-11311 (2006).

14. Lee, B.L. et al. The Hsp90 chaperone: 1H and 19F dynamic nuclear magnetic resonance spectroscopy reveals a perfect enzyme. *Biochemistry* **58**, 1869-1877 (2019).

15. Meyer, P. et al. Structural basis for recruitment of the ATPase activator Aha1 to the Hsp90 chaperone machinery. *EMBO J.* **23**, 511-519 (2004).

16. Horvat, N.K. et al. A mutation in the catalytic loop of hsp90 specifically impairs ATPase stimulation by aha1p, but not hch1p. *J. Mol. Biol.* **426**, 2379-2392 (2014).

17. Karagöz, G.E. et al. Hsp90-Tau complex reveals molecular basis for specificity in chaperone action. *Cell* **156**, 963-974 (2014).

18. Verba, K.A. et al. Atomic structure of Hsp90-Cdc37-Cdk4 reveals that Hsp90 traps and stabilizes an unfolded kinase. *Science* **352**, 1542-1547 (2016).

19. Oroz, J. et al. Structure and pro-toxic mechanism of the human Hsp90/PPIase/Tau complex. *Nat. Commun.* **9**, 1-13 (2018).

20. Lorenz, O.R. et al. Modulation of the Hsp90 chaperone cycle by a stringent client protein. *Mol. Cell* **53**, 941-953 (2014).

21. Jackson, J.C., Hammill, J.T. & Mehl, R.A. Site-specific incorporation of a 19F-amino acid into proteins as an NMR probe for characterizing protein structure and reactivity. *J. Am. Chem. Soc.* **129**, 1160-1166 (2007).

22. Wang, L., Brock, A., Herberich, B. & Schultz, P.G. Expanding the genetic code of Escherichia coli. *Science* **292**, 498-500 (2001).

Bibliography

Akaike, H. New look at the statistical model identification. *IEEE Trans. Automat. Contr.* **AC-19**, 716-723 (1974).

Akke, M. NMR methods for characterizing microsecond to millisecond dynamics in recognition and catalysis. *Curr. Opin. Struct. Biol.* **12**, 642-647 (2002).

Ali, M.M. et al. Crystal structure of an Hsp90–nucleotide–p23/Sba1 closed chaperone complex. *Nature* **440**, 1013-1017 (2006).

Allan, R.K. & Ratajczak, T. Versatile TPR domains accommodate different modes of target protein recognition and function. *Cell Stress Chaperones* **16**, 353-367 (2011).

Altieri, D.C., Stein, G.S., Lian, J.B. & Languino, L.R. TRAP-1, the mitochondrial Hsp90. *Biochim. Biophys. Acta Mol. Cell Res.* **1823**, 767-773 (2012).

Anderluh, G. et al. Interaction of the eukaryotic pore-forming cytolysin equinatoxin II with model membranes: 19F NMR studies. *J. Mol. Biol.* **347**, 27-39 (2005).

Anderson, J. S., Hernandez, G. & LeMaster, D. M. Prediction of bond vector autocorrelation functions from Larmor frequency-selective order parameter analysis of NMR relaxation data. *J. Chem. Theory Comput.* **13**, 3276-3289 (2017).

Anfinsen, C.B. Principles that govern the folding of protein chains. *Science* **181**, 223-230 (1973).

Armstrong, H., Wolmarans, A., Mercier, R., Mai, B. & LaPointe, P. The co-chaperone Hch1 regulates Hsp90 function differently than its homologue Aha1 and confers sensitivity to yeast to the Hsp90 inhibitor NVP-AUY922. *PLoS One* **7**, e49322 (2012).

Arseniev, A.S. et al. 19F NMR study of 5-fluorotryptophan-labeled bacteriorhodopsin. *FEBS Lett.* **213**, 283-288 (1987).

Balchin, D., Hayer-Hartl, M. & Hartl, F.U. In vivo aspects of protein folding and quality control. *Science* **353**, aac4354 (2016).

Bardwell, J.C. & Craig, E.A. Ancient heat shock gene is dispensable. *J. Bacteriol.* **170**, 2977-2983 (1988).

Barral, J.M., Broadley, S.A., Schaffar, G. & Hartl, F.U. Roles of molecular chaperones in protein misfolding diseases. *Semin. Cell Dev. Biol.* **15**, 17-29 (2004).

Bayly, C. I., Cieplak, P., Cornell, W. D. & Kollman, P. A. A well behaved electrostatic potential based method using charge restraints for deriving atomic charges: The RESP model. *J. Phys. Chem.* **97**, 10269-10280 (1993).

Biebl, M.M. & Buchner, J. Structure, function, and regulation of the Hsp90 machinery. *Cold Spring Harb. Perspect. Biol.* **11**, a034017 (2019).

Blagosklonny, M.V., Toretsky, J., Bohen, S. & Neckers, L. Mutant conformation of p53 translated in vitro or in vivo requires functional HSP90. *Proc. Natl. Acad. Sci. U.S.A.* **93**, 8379-8383 (1996).

Bloch, F. Nuclear induction. *Phys. Rev*. **70**, 460-474 (1946).

Boczek, E.E. et al. Conformational processing of oncogenic v-Src kinase by the molecular chaperone Hsp90. *Proc. Natl. Acad. Sci. U.S.A.* **112**, E3189-E3198 (2015).

Bodenhausen, G. & Ruben, D. J. Natural abundance N-15 NMR by enhanced heteronuclear spectroscopy. *Chem. Phys. Lett*. **69**, 185-189 (1980).

Bohen, S.P. Genetic and biochemical analysis of p23 and ansamycin antibiotics in the function of Hsp90-dependent signaling proteins. *Mol. Cell. Biol.* **18**, 3330-3339 (1998).

Bohush, A., Bieganowski, P. & Filipek, A. Hsp90 and its co-chaperones in neurodegenerative diseases. *Int. J. Mol. Sci.* **20**, 4976 (2019).

Borkovich, K.A., Farrelly, F.W., Finkelstein, D.B., Taulien, J. & Lindquist, S. hsp82 is an essential protein that is required in higher concentrations for growth of cells at higher temperatures. *Mol. Cell. Biol.* **9**, 3919-3930 (1989).

Bouchier-Hayes, L. et al. Characterization of cytoplasmic caspase-2 activation by induced proximity. *Mol. Cell* **35**, 830-840 (2009).

Brauer, M. & Sykes, B.D. Fluorine-19 nuclear magnetic resonance studies of selectively fluorinated derivatives of G-and F-actins. *Biochemistry* **25**, 2187-2191 (1986).

Brown, W. E. & Seamon, K. B. Quantitation and characterization of the trifluoroacetonyl derivative of cysteine: A useful NMR probe. *Anal. Biochem.* **87**, 211-222 (1978).

Burger, A.M., Fiebig, H., Stinson, S.F. & Sausville, E.A. 17-(Allylamino)-17-demethoxygeldanamycin activity in human melanoma models. *Anticancer Drugs* **15**, 377-387 (2004).

Cala, S.E. & Jones, L.R. GRP94 resides within cardiac sarcoplasmic reticulum vesicles and is phosphorylated by casein kinase II. *J. Biol. Chem.* **269**, 5926-5931 (1994).

Cañadillas, J.M.P. et al. Solution structure of p53 core domain: structural basis for its instability. *Proc. Natl. Acad. Sci. U.S.A.* **103**, 2109-2114 (2006).

Carr, H. Y. & Purcell, E. M., Effects of diffusion on free precession in nuclear magnetic resonance experiments. *Phys. Rev.* **94**, 630-638 (1954).

Carver, J.P. & Richards, R.E. A general two-site solution for the chemical exchange produced dependence of T2 upon the Carr-Purcell pulse separation. *J. Magn. Reson.* **6**, 89-105 (1972).

Case, D. A. Molecular dynamics and NMR spin relaxation in proteins. *Acc. Chem. Res.* **35**, 325-331 (2002).

Cavanagh, J., Palmer, A. G., Wright, P. E. & Rance, M. Sensitivity improvement in proton-detected two-dimensional heteronuclear relay spectroscopy. *J. Magn. Reson*. **91**, 429-436 (1991).

Cechetto, J.D. & Gupta, R.S. Immunoelectron microscopy provides evidence that tumor necrosis factor receptor-associated protein 1 (TRAP-1) is a mitochondrial protein which also localizes at specific extramitochondrial sites. *Exp. Cell Res.* **260**, 30-39 (2000).

Chadli, A. et al. Dimerization and N-terminal domain proximity underlie the function of the molecular chaperone heat shock protein 90. *Proc. Natl. Acad. Sci. U.S.A.* **97**, 12524-12529 (2000).

Chang, H.C., Nathan, D.F. & Lindquist, S. In vivo analysis of the Hsp90 cochaperone Sti1 (p60). *Mol. Cell. Biol.* **17**, 318-325 (1997).

Chen, B., Piel, W.H., Gui, L., Bruford, E. & Monteiro, A. The HSP90 family of genes in the human genome: insights into their divergence and evolution. *Genomics* **86**, 627-637 (2005).

Chen, B., Zhong, D. & Monteiro, A. Comparative genomics and evolution of the HSP90 family of genes across all kingdoms of organisms. *BMC Genomics* **7**, 1-19 (2006).

Chen, C. et al. A new member of the hsp90 family of molecular chaperones interacts with the retinoblastoma protein during mitosis and after heat shock. *Mol. Cell. Biol.* **16**, 4691-4699 (1996).

Cho, Y., Gorina, S., Jeffrey, P.D. & Pavletich, N.P. Crystal structure of a p53 tumor suppressor-DNA complex: understanding tumorigenic mutations. *Science* **265**, 346-355 (1994).

Cieplak, P., Cornell, W. D., Bayly, C. & Kollman, P. A. Application of the multimolecule and multiconformational RESP methodology to biopolymers: Charge derivation for DNA, RNA, and proteins. *J. Comput. Chem.* **16**, 1357-1377 (1995).

Clore, G.M. et al. Deviations from the simple two-parameter model-free approach to the interpretation of nitrogen-15 nuclear magnetic relaxation of proteins. *J. Am. Chem. Soc.* **112**, 4989-4991 (1990).

Cohen-Saidon, C., Carmi, I., Keren, A. & Razin, E. Antiapoptotic function of Bcl-2 in mast cells is dependent on its association with heat shock protein 90β. *Blood* **107**, 1413-1420 (2006).

Colombo, G., Morra, G., Meli, M. & Verkhivker, G. Understanding ligand-based modulation of the Hsp90 molecular chaperone dynamics at atomic resolution. *Proc. Natl. Acad. Sci. U.S.A.* **105**, 7976-7981 (2008).

Cornell, W. D. et al. A second generation force field for the simulation of proteins, nucleic acids, and organic molecules. *J. Am. Chem. Soc.* **117**, 5179-5197 (1995).

Cornell, W. D., Cieplak, P., Bayly, C. I. & Kollman, P. A. Application of RESP charges to calculate conformational energies, hydrogen-bond energies, and free energies of solvation. *J. Am. Chem. Soc.* **115**, 9620-9631 (1993).

Cunningham, C.N., Southworth, D.R., Krukenberg, K.A. & Agard, D.A. The conserved arginine 380 of Hsp90 is not a catalytic residue, but stabilizes the closed conformation required for ATP hydrolysis. *Protein Sci.* **21**, 1162-1171 (2012).

Dahiya, V. & Buchner, J. Functional principles and regulation of molecular chaperones. *Adv. Protein Chem. Struct. Biol.* **114**, 1-60 (2019).

Danielson, M. A. & Falke, J. J. Use of ^{19}F NMR to probe protein structure and conformational changes. *Annu. Rev. Biophys. Biomol. Struct.* **25**, 163-195 (1996).

Danielson, M.A., Biemann, H., Koshland Jr, D.E. & Falke, J.J. Attractant-and disulfide-induced conformational changes in the ligand binding domain of the chemotaxis aspartate receptor: a 19F NMR study. *Biochemistry* **33**, 6100-6109 (1994).

Das, A.K., Cohen, P.T. & Barford, D. The structure of the tetratricopeptide repeats of protein phosphatase 5: implications for TPR-mediated protein–protein interactions. *EMBO J.* **17**, 1192-1199 (1998).

Delaglio, F. et al. NMRPipe: A multidimensional spectral processing system based on UNIX pipes. *J. Biomol. NMR* **6**, 277-293 (1995).

Di Pietrantonio, C., Pandey, A., Gould, J., Hasabnis, A. & Prosser, R. S. Understanding protein function through an ensemble description: characterization of functional states by 19F NMR. *Meth. Enzymol*. **615**, 103-130 (2019).

Dittmar, K.D. & Pratt, W.B. Folding of the glucocorticoid receptor by the reconstituted Hsp90-based chaperone machinery: The initial hsp90· p60· hsp70-dependent step is sufficient for creating the steroid binding conformation. *J. Biol. Chem.* **272**, 13047-13054 (1997).

Dollins, D.E., Warren, J.J., Immormino, R.M. & Gewirth, D.T. Structures of GRP94-nucleotide complexes reveal mechanistic differences between the hsp90 chaperones. *Mol. Cell* **28**, 41-56 (2007).

Drake, S.K., Bourret, R.B., Luck, L.A., Simon, M.I. & Falke, J.J. Activation of the phosphosignaling protein CheY. I. Analysis of the phosphorylated conformation by 19F NMR and protein engineering. *J. Biol. Chem.* **268**, 13081-13088 (1993).

Dutta, R. & Inouye, M. GHKL, an emergent ATPase/kinase superfamily. *Trends Biochem. Sci.* **25**, 24-28 (2000).

Eletto, D., Dersh, D. & Argon, Y. GRP94 in ER quality control and stress responses. *Semin. Cell Dev. Biol.* **21**, 479-485 (2010).

Ellis, J. Proteins as molecular chaperones. *Nature* **328**, 378-379 (1987).

Ellis, R.J. & Minton, A.P. Protein aggregation in crowded environments. *Biol. Chem.* **387**, 485-497 (2006).

Eustace, B.K. et al. Functional proteomic screens reveal an essential extracellular role for hsp90α in cancer cell invasiveness. *Nat. Cell Biol.* **6**, 507-514 (2004).

Evanics, F., Kitevski, J.L., Bezsonova, I., Forman-Kay, J. & Prosser, R.S. 19F NMR studies of solvent exposure and peptide binding to an SH3 domain. *Biochim. Biophys. Acta Gen. Subj.* **1770**, 221-230 (2007).

Falke, J.J., Luck, L.A. & Scherrer, J. 19F nuclear magnetic resonance studies of aqueous and transmembrane receptors. Examples from the Escherichia coli chemosensory pathway. *Biophys. J.* **62**, 82 (1992).

Falsone, S.F., Kungl, A.J., Rek, A., Cappai, R. & Zangger, K. The molecular chaperone Hsp90 modulates intermediate steps of amyloid assembly of the Parkinson-related protein α-synuclein. *J. Biol. Chem.* **284**, 31190-31199 (2009).

Falsone, S.F., Leptihn, S., Osterauer, A., Haslbeck, M. & Buchner, J. Oncogenic mutations reduce the stability of SRC kinase. *J. Mol. Biol.* **344**, 281-291 (2004).

Fang, Y., Fliss, A.E., Rao, J. & Caplan, A.J. SBA1 encodes a yeast hsp90 cochaperone that is homologous to vertebrate p23 proteins. *Mol. Cell. Biol.* **18**, 3727-3734 (1998).

Felts, S.J. et al. The hsp90-related protein TRAP1 is a mitochondrial protein with distinct functional properties. *J. Biol. Chem.* **275**, 3305-3312 (2000).

Ferrarini, M., Heltai, S., Zocchi, M.R. & Rugarli, C. Unusual expression and localization of heat-shock proteins in human tumor cells. *Int. J. Cancer* **51**, 613-619 (1992).

Frisch, M. J. et al. *Gaussian 16 Rev. B.01*, Wallingford, CT, (2016).

Garcie, C. et al. The bacterial stress-responsive Hsp90 chaperone (HtpG) is required for the production of the genotoxin colibactin and the siderophore yersiniabactin in Escherichia coli. *J. Infect. Dis.* **214**, 916-924 (2016).

Garnier, C. et al. Binding of ATP to heat shock protein 90: evidence for an ATP-binding site in the C-terminal domain. *J. Biol. Chem.* **277**, 12208-12214 (2002).

Genest, O., Wickner, S. & Doyle, S.M. Hsp90 and Hsp70 chaperones: collaborators in protein remodeling. *J. Biol. Chem.* **294**, 2109-2120 (2019).

Gerig, J.T. Fluorine NMR of proteins. *Prog. Nucl. Magn. Reson. Spectrosc.* **26**, 293-370 (1994).

Gerig, J.T. Fluorine NMR. *Biophysics Textbook Online*, 1-35 (2001).

Girstmair, H. et al. The Hsp90 isoforms from S. cerevisiae differ in structure, function and client range. *Nat. Commun.* **10**, 1-15 (2019).

Grad, I. et al. The molecular chaperone Hsp90α is required for meiotic progression of spermatocytes beyond pachytene in the mouse. *PLoS One* **5**, e15770 (2010).

Grenert, J.P. et al. The amino-terminal domain of heat shock protein 90 (hsp90) that binds geldanamycin is an ATP/ADP switch domain that regulates hsp90 conformation. *J. Biol. Chem.* **272**, 23843-23850 (1997).

Griffin, R. G., Ellett, J. D., Mehring, M., Bullitt, J. G. & Waugh, J. S. Single crystal study of ^{19}F shielding tensors of a trifluoromethyl group. *J. Chem. Phys.* **57**, 2147-2155 (1972).

Grzesiek, S. et al. The solution structure of HIV-1 Nef reveals an unexpected fold and permits delineation of the binding surface for the SH3 domain of Hck tyrosine protein kinase. *Nat. Struct. Biol.* **3**, 340-345 (1996).

Günther, U. L. & Schaffhausen, B. NMRKIN: Simulating line shapes from two-dimensional spectra of proteins upon ligand binding. *J. Biomol. NMR* **22,** 201-209 (2002).

Hainzl, O., Lapina, M.C., Buchner, J. & Richter, K. The charged linker region is an important regulator of Hsp90 function. *J. Biol. Chem.* **284**, 22559-22567 (2009).

Harris, S.F., Shiau, A.K. & Agard, D.A. The crystal structure of the carboxy-terminal dimerization domain of htpG, the Escherichia coli Hsp90, reveals a potential substrate binding site. *Structure* **12**, 1087-1097 (2004).

Harst, A., Lin, H. & Obermann, W.M. Aha1 competes with Hop, p50 and p23 for binding to the molecular chaperone Hsp90 and contributes to kinase and hormone receptor activation. *Biochem. J.* **387**, 789-796 (2005).

Hartl, F.U., Bracher, A. & Hayer-Hartl, M. Molecular chaperones in protein folding and proteostasis. *Nature* **475**, 324-332 (2011).

Hendrick, J.P. & Hartl, F. Molecular chaperone functions of heat-shock proteins. *Annu. Rev. Biochem.* **62**, 349-384 (1993).

Hessling, M., Richter, K. & Buchner, J. Dissection of the ATP-induced conformational cycle of the molecular chaperone Hsp90. *Nat. Struct. Mol. Biol.* **16**, 287-293 (2009).

Hoeltzli, S.D. & Frieden, C. Stopped-flow NMR spectroscopy: real-time unfolding studies of 6-19F-tryptophan-labeled Escherichia coli dihydrofolate reductase. *Proc. Natl. Acad. Sci. U.S.A.* **92**, 9318-9322 (1995).

Hoffmann, F., Mulder, F. A. A. & Schafer, L. V. Accurate methyl group dynamics in protein simulations with AMBER force fields. *J. Phys. Chem. B* **122**, 5038-5048 (2018).

Hoffmann, F., Xue, M. J., Schafer, L. V. & Mulder, F. A. A. Narrowing the gap between experimental and computational determination of methyl group dynamics in proteins. *Phys. Chem. Chem. Phys.* **20**, 24577-24590 (2018).

Honore, B. et al. Molecular cloning and expression of a transformation-sensitive human protein containing the TPR motif and sharing identity to the stress-inducible yeast protein STI1. *J. Biol. Chem.* **267**, 8485-8491 (1992).

Horst, R., Liu, J.J., Stevens, R.C. & Wüthrich, K. β2-Adrenergic Receptor Activation by Agonists Studied with 19F NMR Spectroscopy. *Angew. Chem. Int. Ed.* **52**, 10762-10765 (2013).

Horvat, N.K. et al. A mutation in the catalytic loop of hsp90 specifically impairs ATPase stimulation by aha1p, but not hch1p. *J. Mol. Biol.* **426**, 2379-2392 (2014).

Huck, J.D., Que, N.L., Hong, F., Li, Z. & Gewirth, D.T. Structural and functional analysis of GRP94 in the closed state reveals an essential role for the pre-N domain and a potential client-binding site. *Cell Rep.* **20**, 2800-2809 (2017).

Hull, W.E. & Sykes, B.D. Fluorine-19 nuclear magnetic resonance study of fluorotyrosine alkaline phosphatase: the influence of zinc on protein structure and a conformational change induced by phosphate binding. *Biochemistry* **15**, 1535-1546 (1976).

Hull, W.E. & Sykes, B.D. Fluorotyrosine alkaline phosphatase: internal mobility of individual tyrosines and the role of chemical shift anisotropy as a 19F nuclear spin relaxation mechanism in proteins. *J. Mol. Biol.* **98**, 121-153 (1975).

Jackson, J. C., Duffy, S. P., Hess, K. R. & Mehl, R. A. Improving nature's enzyme active site with genetically encoded unnatural amino acids *J. Am. Chem. Soc.* **128**, 11124-11127 (2006).

Jackson, J.C., Hammill, J.T. & Mehl, R.A. Site-specific incorporation of a 19F-amino acid into proteins as an NMR probe for characterizing protein structure and reactivity. *J. Am. Chem. Soc.* **129**, 1160-1166 (2007).

Jackson, S.E. Hsp90: structure and function. *Top Curr. Chem.* **328**, 155-240 (2013).

Jaeger, A.M. & Whitesell, L. HSP90: enabler of cancer adaptation. *Annu. Rev. Cancer Biol.* **3**, 275-297 (2019).

Jameel, A. et al. Clinical and biological significance of HSP89 alpha in human breast cancer. *Int. J. Cancer* **50**, 409-415 (1992).

Jarymowycz, V. A. & Stone, M. J. Fast time scale dynamics of protein backbones: NMR relaxation methods, applications, and functional consequences. *Chem. Rev.* **106**, 1624-1671 (2006).

Johnson, B. A. & Blevins, R. A. NmrView: A computer program for the visualization and analysis of NMR data. *J. Biomol. NMR* **4**, 603-614 (1994).

Johnson, B.D., Schumacher, R.J., Ross, E.D. & Toft, D.O. Hop modulates Hsp70/Hsp90 interactions in protein folding. *J. Biol. Chem.* **273**, 3679-3686 (1998).

Johnson, J.L. & Toft, D.O. A novel chaperone complex for steroid receptors involving heat shock proteins, immunophilins, and p23. *J. Biol. Chem.* **269**, 24989-24993 (1994).

Johnson, J.L. & Toft, D.O. Binding of p23 and hsp90 during assembly with the progesterone receptor. *Mol. Endocrinol.* **9**, 670-678 (1995).

Johnson, J.L. Evolution and function of diverse Hsp90 homologs and cochaperone proteins. *Biochim. Biophys. Acta Mol. Cell Res.* **1823**, 607-613 (2012).

Jorgensen, W. L., Chandrasekhar, J., Madura, J. D., Impey, R. W. & Klein, M. L. Comparison of simple potential functions for simulating liquid water. *J. Chem. Phys*. **79**, 926-935 (1983).

Kang, B.H. et al. Regulation of tumor cell mitochondrial homeostasis by an organelle-specific Hsp90 chaperone network. *Cell* **131**, 257-270 (2007).

Karagöz, G.E. & Rüdiger, S.G. Hsp90 interaction with clients. *Trends Biochem. Sci.* **40**, 117-125 (2015).

Karagöz, G.E. et al. Hsp90-Tau complex reveals molecular basis for specificity in chaperone action. *Cell* **156**, 963-974 (2014).

Kay, L. E., Keifer, P. & Saarinen, T. Pure absorption gradient enhanced heteronuclear single quantum correlation spectroscopy with improved sensitivity. *J. Am. Chem. Soc*. **114**, 10663-10665 (1992).

Kay, L. E., Torchia, D. A. & Bax, A. Backbone dynamics of proteins as studied by ^{15}N inverse detected heteronuclear NMR spectroscopy: Application to staphylococcal nuclease. *Biochemistry* **28**, 8972-8979 (1989).

Keramisanou, D. et al. Molecular mechanism of protein kinase recognition and sorting by the Hsp90 kinome-specific cochaperone Cdc37. *Mol. Cell* **62**, 260-271 (2016).

Kim, H., Perez, J.A., Ferguson, S.J. & Campbell, I.D. The specific incorporation of labelled aromatic amino acids into proteins through growth of bacteria in the presence of glyphosate: Application to fluorotryptophan labelling to the H -ATPase of Escherichia coli and NMR studies. *FEBS Lett.* **272**, 34-36 (1990).

King, F.W., Wawrzynow, A., Höhfeld, J. & Zylicz, M. Co-chaperones Bag-1, Hop and Hsp40 regulate Hsc70 and Hsp90 interactions with wild-type or mutant p53. *EMBO J.* **20**, 6297-6305 (2001).

Kitevski-LeBlanc, J.L. & Prosser, R.S. Current applications of 19F NMR to studies of protein structure and dynamics. *Prog. Nucl. Magn. Reson. Spectrosc.* **62**, 1-33 (2011).

Kitevski-LeBlanc, J.L., Hoang, J., Thach, W., Larda, S.T. & Prosser, R.S. 19F NMR studies of a desolvated near-native protein folding intermediate. *Biochemistry* **52**, 5780-5789 (2013).

Klaips, C.L., Jayaraj, G.G. & Hartl, F.U. Pathways of cellular proteostasis in aging and disease. *J. Cell Biol.* **217**, 51-63 (2018).

Kleckner, I.R. & Foster, M.P. An introduction to NMR-based approaches for measuring protein dynamics. *Biochim. Biophys. Acta Proteins Proteom.* **1814**, 942-968 (2011).

Koch, G., Smith, M., Macer, D., Webster, P. & Mortara, R. Endoplasmic reticulum contains a common, abundant calcium-binding glycoprotein, endoplasmin. *J. Cell. Sci.* **86**, 217-232 (1986).

Krukenberg, K. A., Street, T. O., Lavery, L. A. & Agard, D. A. Conformational dynamics of the molecular chaperone Hsp90. *Q. Rev. Biophys.* **44**, 229-255 (2011).

Kunisawa, J. & Shastri, N. Hsp90α chaperones large C-terminally extended proteolytic intermediates in the MHC class I antigen processing pathway. *Immunity* **24**, 523-534 (2006).

Labroo, V.M. et al. Direct electrophilic fluorination of tyrosine in dermorphin analogues and its effect on biological activity, receptor affinity and selectivity. *Int. J. Pept. Protein Res.* **37**, 430-439 (1991).

Lavery, L.A. et al. Structural asymmetry in the closed state of mitochondrial Hsp90 (TRAP1) supports a two-step ATP hydrolysis mechanism. *Mol. Cell* **53**, 330-343 (2014).

Lee, B.L. et al. The Hsp90 chaperone: 1H and 19F dynamic nuclear magnetic resonance spectroscopy reveals a perfect enzyme. *Biochemistry* **58**, 1869-1877 (2019).

Lees-Miller, S.P. & Anderson, C.W. The human double-stranded DNA-activated protein kinase phosphorylates the 90-kDa heat-shock protein, hsp90α at two NH2-terminal threonine residues. *J. Biol. Chem.* **264**, 17275-17280 (1989).

Levy, R.M., Karplus, M. & Wolynes, P.G. NMR relaxation parameters in molecules with internal motion: exact Langevin trajectory results compared with simplified relaxation models. *J. Am. Chem. Soc.* **103**, 5998-6011 (1981).

Li, H. & Frieden, C. Observation of sequential steps in the folding of intestinal fatty acid binding protein using a slow folding mutant and 19F NMR. *Proc. Natl. Acad. Sci. U.S.A.* **104**, 11993-11998 (2007).

Li, J. et al. Structure insights into mechanisms of ATP hydrolysis and the activation of human heat-shock protein 90. *Acta Biochim. Biophys. Sin.* **44**, 300-306 (2012).

Li, J., Richter, K. & Buchner, J. Mixed Hsp90–cochaperone complexes are important for the progression of the reaction cycle. *Nat. Struct. Mol. Biol.* **18**, 61 (2011).

Li, J., Richter, K., Reinstein, J. & Buchner, J. Integration of the accelerator Aha1 in the Hsp90 co-chaperone cycle. *Nat. Struct. Mol. Biol.* **20**, 326 (2013).

Li, W. et al. Extracellular heat shock protein-90α: linking hypoxia to skin cell motility and wound healing. *EMBO J.* **26**, 1221-1233 (2007).

Lipari, G. & Szabo, A. Model-free approach to the interpretation of nuclear magnetic resonance relaxation in macromolecules. 1. Theory and range of validity. *J. Am. Chem. Soc.* **104**, 4546-4559 (1982).

Lipari, G. & Szabo, A. Model-free approach to the interpretation of nuclear magnetic resonance relaxation in macromolecules. 2. Analysis of experimental results. *J. Am. Chem. Soc.* **104**, 4559-4570 (1982).

Lipari, G., Szabo, A. & Levy, R.M. Protein dynamics and NMR relaxation: comparison of simulations with experiment. *Nature* **300**, 197-198 (1982).

Liu, B. et al. Folding of Toll-like receptors by the HSP90 paralogue gp96 requires a substrate-specific cochaperone. *Nat. Commun.* **1**, 1-11 (2010).

Liu, J.J., Horst, R., Katritch, V., Stevens, R.C. & Wüthrich, K. Biased signaling pathways in β2-adrenergic receptor characterized by 19F-NMR. *Science* **335**, 1106-1110 (2012).

Lorenz, O.R. et al. Modulation of the Hsp90 chaperone cycle by a stringent client protein. *Mol. Cell* **53**, 941-953 (2014).

Louvion, J., Warth, R. & Picard, D. Two eukaryote-specific regions of Hsp82 are dispensable for its viability and signal transduction functions in yeast. *Proc. Natl. Acad. Sci. U.S.A.* **93**, 13937-13942 (1996).

Lu, P., Jarema, M., Mosser, K. & Daniel, W.E. lac repressor: 3-fluorotyrosine substitution for nuclear magnetic resonance studies. *Proc. Natl. Acad. Sci. U.S.A.* **73**, 3471-3475 (1976).

Luo, W. et al. Roles of heat-shock protein 90 in maintaining and facilitating the neurodegenerative phenotype in tauopathies. *Proc. Natl. Acad. Sci. U.S.A.* **104**, 9511-9516 (2007).

Luz, Z. & Meiboom, S. Nuclear magnetic resonance study of the protolysis of trimethylammonium ion in aqueous solution—order of the reaction with respect to solvent. *J. Chem. Phys.* **39**, 366-370 (1963).

Maier, J. A. et al. ff14SB: Improving the accuracy of protein side chain and backbone parameters from ff99SB. *J. Chem. Theory Comput.* **11,** 3696-3713 (2015).

Marcu, M.G., Chadli, A., Bouhouche, I., Catelli, M. & Neckers, L.M. The heat shock protein 90 antagonist novobiocin interacts with a previously unrecognized ATP-binding domain in the carboxyl terminus of the chaperone. *J. Biol. Chem.* **275**, 37181-37186 (2000).

Markin, C. J. & Spyracopoulos, L. Accuracy and precision of protein-ligand interaction kinetics determined from chemical shift titrations. *J. Biomol. NMR* **54**, 355-376 (2012).

Markin, C. J. & Spyracopoulos, L. Increased precision for analysis of protein-ligand dissociation constants determined from chemical shift titrations. *J. Biomol. NMR* **53**, 125-138 (2012).

Marley, J., Lu, M. & Bracken, C., A method for efficient isotopic labeling of recombinant proteins. *J. Biomol. NMR **20**,* 71-75 (2001).

Marsh, E.N.G. & Suzuki, Y. Using 19F NMR to probe biological interactions of proteins and peptides. *ACS Chem. Biol.* **9**, 1242-1250 (2014).

Marzec, M., Eletto, D. & Argon, Y. GRP94: An HSP90-like protein specialized for protein folding and quality control in the endoplasmic reticulum. *Biochim. Biophys. Acta Mol. Cell Res.* **1823**, 774-787 (2012).

Mayer, M.P. & Le Breton, L. Hsp90: breaking the symmetry. *Mol. Cell* **58**, 8-20 (2015).

McConnell, H. M. Reaction rates by nuclear magnetic resonance. *J. Chem. Phys*. **28**, 430-431 (1958).

McLaughlin, S.H., Smith, H.W. & Jackson, S.E. Stimulation of the weak ATPase activity of human hsp90 by a client protein. *J. Mol. Biol.* **315**, 787-798 (2002).

Meagher, K. L., Redman, L. T. & Carlson, H. A. Development of polyphosphate parameters for use with the AMBER force field. *J. Comput. Chem*. **24**, 1016-1025 (2003).

Meiboom, S. & Gill, D., Modified spin-echo method for measuring nuclear relaxation times. *Rev. Sci. Instrum.* **29**, 688-691 (1958).

Mercier, R. et al. The conserved NxNNWHW motif in Aha-type co-chaperones modulates the kinetics of Hsp90 ATPase stimulation. *Nat. Commun.* **10**, 1-12 (2019).

Metchat, A. et al. Mammalian heat shock factor 1 is essential for oocyte meiosis and directly regulates Hsp90α expression. *J. Biol. Chem.* **284**, 9521-9528 (2009).

Meyer, P. et al. Structural and functional analysis of the middle segment of hsp90: implications for ATP hydrolysis and client protein and cochaperone interactions. *Mol. Cell* **11**, 647-658 (2003).

Meyer, P. et al. Structural basis for recruitment of the ATPase activator Aha1 to the Hsp90 chaperone machinery. *EMBO J.* **23**, 511-519 (2004).

Mittermaier, A.K. & Kay, L.E. Observing biological dynamics at atomic resolution using NMR. *Trends Biochem. Sci.* **34**, 601-611 (2009).

Mollapour, M. & Neckers, L. Post-translational modifications of Hsp90 and their contributions to chaperone regulation *Biochim. Biophys. Acta Mol. Cell Res.* **1823**, 648-655 (2012).

Mollapour, M. et al. Asymmetric Hsp90 N domain SUMOylation recruits Aha1 and ATP-competitive inhibitors. *Mol. Cell* **53**, 317-329 (2014).

Mollapour, M. et al. Swe1Wee1-dependent tyrosine phosphorylation of Hsp90 regulates distinct facets of chaperone function. *Mol. Cell* **37**, 333-343 (2010).

Mollapour, M. et al. Threonine 22 phosphorylation attenuates Hsp90 interaction with cochaperones and affects its chaperone activity. *Mol. Cell* **41**, 672-681 (2011).

Mollapour, M., Tsutsumi, S., Kim, Y.S., Trepel, J. & Neckers, L. Casein kinase 2 phosphorylation of Hsp90 threonine 22 modulates chaperone function and drug sensitivity. *Oncotarget* **2**, 407 (2011).

Morra, G., Verkhivker, G. & Colombo, G. Modeling signal propagation mechanisms and ligand-based conformational dynamics of the Hsp90 molecular chaperone full-length dimer. *PLoS Comput. Biol.* **5**, e1000323 (2009).

Morris, G. A. & Freeman, R. Enhancement of nuclear magnetic resonance signals by polarization transfer. *J. Am. Chem. Soc*. **101**, 760-762 (1979).

Muchowski, P.J. & Wacker, J.L. Modulation of neurodegeneration by molecular chaperones. *Nat. Rev. Neurosci.* **6**, 11-22 (2005).

Müller, L., Schaupp, A., Walerych, D., Wegele, H. & Buchner, J. Hsp90 regulates the activity of wild type p53 under physiological and elevated temperatures. *J. Biol. Chem.* **279**, 48846-48854 (2004).

Nathan, D.F. & Lindquist, S. Mutational analysis of Hsp90 function: interactions with a steroid receptor and a protein kinase. *Mol. Cell. Biol.* **15**, 3917-3925 (1995).

Nathan, D.F., Vos, M.H. & Lindquist, S. Identification of SSF1, CNS1, and HCH1 as multicopy suppressors of a Saccharomyces cerevisiae Hsp90 loss-of-function mutation. *Proc. Natl. Acad. Sci. U.S.A.* **96**, 1409-1414 (1999).

Neckers, L. & Workman, P. Hsp90 molecular chaperone inhibitors: are we there yet?. *Clin. Cancer Res.* **18**, 64-76 (2012).

Neidhardt, F. C., Bloch, P. L. & Smith, D. F., Culture medium for enterobacteria. *J. Bacteriol.* 119, 736-747 (1974).

Nemoto, T., Ohara-Nemoto, Y., Ota, M., Takagi, T. & Yokoyama, K. Mechanism of dimer formation of the 90-kDa heat shock protein. *Eur. J. Biochem*. **233**, 1-8 (1995).

Obermann, W.M., Sondermann, H., Russo, A.A., Pavletich, N.P. & Hartl, F.U. In vivo function of Hsp90 is dependent on ATP binding and ATP hydrolysis. *J. Cell Biol.* **143**, 901-910 (1998).

Ollila, O. H. S., Heikkinen, H. A. & Iwai, H. Rotational dynamics of proteins from spin relaxation times and molecular dynamics simulations. *J. Phys. Chem. B* **122**, 6559-6569 (2018).

Oroz, J. et al. Structure and pro-toxic mechanism of the human Hsp90/PPIase/Tau complex. *Nat. Commun.* **9**, 1-13 (2018).

Ostrovsky, O., Makarewich, C.A., Snapp, E.L. & Argon, Y. An essential role for ATP binding and hydrolysis in the chaperone activity of GRP94 in cells. *Proc. Natl. Acad. Sci. U.S.A.* **106**, 11600-11605 (2009).

Pagetta, A. et al. Structural insights into complexes of glucose-regulated Protein94 (Grp94) with human immunoglobulin G. relevance for Grp94-IgG complexes that form in vivo in pathological conditions. *PLoS One* **9**, e86198 (2014).

Palmer III, A.G. Probing molecular motion by NMR. *Curr. Opin. Struct. Biol.* **7**, 732-737 (1997).

Palmer, A. G., Kroenke, C. D. & Loria, J. P. Nuclear magnetic resonance methods for quantifying microsecond-to-millisecond motions in biological macromolecules. *Meth. Enzymol.* **339**, 204-238 (2001).

Panaretou, B. et al. Activation of the ATPase activity of hsp90 by the stress-regulated cochaperone aha1. *Mol. Cell* **10**, 1307-1318 (2002).

Panaretou, B. et al. ATP binding and hydrolysis are essential to the function of the Hsp90 molecular chaperone in vivo. *EMBO J.* **17**, 4829-4836 (1998).

Park, S.J., Borin, B.N., Martinez-Yamout, M.A. & Dyson, H.J. The client protein p53 adopts a molten globule–like state in the presence of Hsp90. *Nat. Struct. Mol. Biol.* **18**, 537-542 (2011).

Pearl, L. H. The HSP90 molecular chaperone - an enigmatic ATPase. *Biopolymers* **105**, 594-607 (2016).

Pearl, L.H. & Prodromou, C. Structure and mechanism of the Hsp90 molecular chaperone machinery. *Annu. Rev. Biochem.* **75**, 271-294 (2006).

Pearl, L.H., Prodromou, C. & Workman, P. The Hsp90 molecular chaperone: an open and shut case for treatment. *Biochem. J.* **410**, 439-453 (2008).

Picard, D. et al. Reduced levels of hsp90 compromise steroid receptor action in vivo. *Nature* **348**, 166-168 (1990).

Pick, E. et al. High HSP90 expression is associated with decreased survival in breast cancer. *Cancer Res.* **67**, 2932-2937 (2007).

Pratt, W.B. & Dittmar, K.D. Studies with purified chaperones advance the understanding of the mechanism of glucocorticoid receptor–hsp90 heterocomplex assembly. *Trends Endocrinol. Metab.* **9**, 244-252 (1998).

Pratt, W.B. & Toft, D.O. Steroid receptor interactions with heat shock protein and immunophilin chaperones. *Endocr. Rev.* **18**, 306-360 (1997).

Pridgeon, J.W., Olzmann, J.A., Chin, L. & Li, L. PINK1 protects against oxidative stress by phosphorylating mitochondrial chaperone TRAP1. *PLoS Biol.* **5**, e172 (2007).

Prodromou, C. et al. Identification and structural characterization of the ATP/ADP-binding site in the Hsp90 molecular chaperone. *Cell* **90**, 65-75 (1997).

Prodromou, C. et al. Regulation of Hsp90 ATPase activity by tetratricopeptide repeat (TPR)-domain co-chaperones. *EMBO J.* **18**, 754-762 (1999).

Prodromou, C. et al. The ATPase cycle of Hsp90 drives a molecular 'clamp'via transient dimerization of the N-terminal domains. *EMBO J.* **19**, 4383-4392 (2000).

Prodromou, C. Mechanisms of Hsp90 regulation. *Biochem. J.* **473**, 2439-2452 (2016).

Prodromou, C., Roe, S.M., Piper, P.W. & Pearl, L.H. A molecular clamp in the crystal structure of the N-terminal domain of the yeast Hsp90 chaperone. *Nat. Struct. Biol.* **4**, 477-482 (1997).

Putcha, P. et al. Brain-permeable small-molecule inhibitors of Hsp90 prevent α-synuclein oligomer formation and rescue α-synuclein-induced toxicity. *J. Pharmacol. Exp. Ther.* **332**, 849-857 (2010).

Radli, M. & Rüdiger, S.G. Dancing with the diva: Hsp90–client interactions. *J. Mol. Biol.* **430**, 3029-3040 (2018).

Rashid, S., Lee, B.L., Wajda, B. & Spyracopoulos, L. Nucleotide Binding and Active Site Gate Dynamics for the Hsp90 Chaperone ATPase Domain from Benchtop and High Field 19F NMR Spectroscopy. *J. Phys. Chem. B* **124**, 2984-2993 (2020).

Rashid, S., Lee, B.L., Wajda, B. & Spyracopoulos, L. Side-chain dynamics of the trifluoroacetone cysteine derivative characterized by 19F NMR relaxation and molecular dynamics simulations. *J. Phys. Chem. B* **123**, 3665-3671 (2019).

Retzlaff, M. et al. Asymmetric activation of the hsp90 dimer by its cochaperone Aha1. *Mol. Cell* **37**, 344-354 (2010).

Retzlaff, M. et al. Hsp90 is regulated by a switch point in the C-terminal domain. *EMBO Rep.* **10**, 1147-1153 (2009).

Reynolds, C. A., Essex, J. W. & Richards, W. G. Atomic charges for variable molecular conformations. *J. Am. Chem. Soc.* **114**, 9075-9079 (1992).

Richter, K. et al. Intrinsic inhibition of the Hsp90 ATPase activity. *J. Biol. Chem.* **281**, 11301-11311 (2006).

Richter, K., Muschler, P., Hainzl, O. & Buchner, J. Coordinated ATP hydrolysis by the Hsp90 dimer. *J. Biol. Chem.* **276**, 33689-33696 (2001).

Richter, K., Reinstein, J. & Buchner, J. N-terminal residues regulate the catalytic efficiency of the Hsp90 ATPase cycle. *J. Biol. Chem.* **277**, 44905-44910 (2002).

Richter, K., Walter, S. & Buchner, J. The Co-chaperone Sba1 connects the ATPase reaction of Hsp90 to the progression of the chaperone cycle. *J. Mol. Biol.* **342**, 1403-1413 (2004).

Roe, D. R. & Cheatham, T. E. PTRAJ and CPPTRAJ: Software for processing and analysis of molecular dynamics trajectory data. *J. Chem. Theory Comput.* **9**, 3084-3095 (2013).

Roe, S.M. et al. Structural basis for inhibition of the Hsp90 molecular chaperone by the antitumor antibiotics radicicol and geldanamycin. *J. Med. Chem.* **42**, 260-266 (1999).

Rüdiger, S., Freund, S.M., Veprintsev, D.B. & Fersht, A.R. CRINEPT-TROSY NMR reveals p53 core domain bound in an unfolded form to the chaperone Hsp90. *Proc. Natl. Acad. Sci. U.S.A.* **99**, 11085-11090 (2002).

Ruschak, A.M. & Kay, L.E. Methyl groups as probes of supra-molecular structure, dynamics and function. *J. Biomol. NMR* **46**, 75 (2010).

Rutz, D.A. et al. A switch point in the molecular chaperone Hsp90 responding to client interaction. *Nat. Commun.* **9**, 1-14 (2018).

Ryckaert, J. P., Ciccotti, G. & Berendsen, H. J. C. Numerical integration of cartesian equations of motion of a system with constraints: Molecular dynamics of N-alkanes. *J. Comput. Phys.* **23**, 327-341 (1977).

Sahasrabudhe, P., Rohrberg, J., Biebl, M.M., Rutz, D.A. & Buchner, J. The plasticity of the Hsp90 co-chaperone system. *Mol. Cell* **67**, 947-961. e5 (2017).

Salek, R. M., Williams, M. A., Prodromou, C., Pearl, L. H. & Ladbury, J. E., Letter to the editor: Backbone resonance assignments of the 25 kDa N-terminal ATPase domain from the Hsp90 chaperone. *J. Biomol. NMR* **23**, 327-328 (2002).

Salomon-Ferrer, R., Gotz, A. W., Poole, D., Le Grand, S. & Walker, R. C. Routine microsecond molecular dynamics simulations with AMBER on GPUs. 2. Explicit solvent particle mesh Ewald. *J. Chem. Theory Comput.* **9**, 3878-3888 (2013).

Scheibel, T. et al. ATP-binding properties of human Hsp90. *J. Biol. Chem.* **272**, 18608-18613 (1997).

Scheufler, C. et al. Structure of TPR domain–peptide complexes: critical elements in the assembly of the Hsp70–Hsp90 multichaperone machine. *Cell* **101**, 199-210 (2000).

Schmid, A.B. et al. The architecture of functional modules in the Hsp90 co-chaperone Sti1/Hop. *EMBO J.* **31**, 1506-1517 (2012).

Schmid, S., Götz, M. & Hugel, T. Single-molecule analysis beyond dwell times: demonstration and assessment in and out of equilibrium. *Biophys. J.* **111**, 1375-1384 (2016).

Schopf, F.H., Biebl, M.M. & Buchner, J. The HSP90 chaperone machinery. *Nat. Rev. Mol. Cell Biol.* **18**, 345 (2017).

Schrodinger, LLC. The PyMOL Molecular Graphics System, Version 1.8. (2015).

Schulte, T.W. & Neckers, L.M. The benzoquinone ansamycin 17-allylamino-17-demethoxygeldanamycin binds to HSP90 and shares important biologic activities with geldanamycin. *Cancer Chemother. Pharmacol.* **42**, 273-279 (1998).

Schulte, T.W. et al. Antibiotic radicicol binds to the N-terminal domain of Hsp90 and shares important biologic activities with geldanamycin. *Cell Stress Chaperones* **3**, 100 (1998).

Schulze, A. et al. Cooperation of local motions in the Hsp90 molecular chaperone ATPase mechanism. *Nat. Chem. Biol.* **12**, 628-635 (2016).

Scroggins, B.T. & Neckers, L. Post-translational modification of heat-shock protein 90: impact on chaperone function. *Expert Opin. Drug Discov.* **2**, 1403-1414 (2007).

Sheffield, P., Garrard, S. & Derewenda, Z. Overcoming expression and purification problems of RhoGDI using a family of "parallel" expression vectors. *Protein Expr. Purif.* **15**, 34-39 (1999).

Shelton, L.B. et al. Hsp90 activator Aha1 drives production of pathological tau aggregates. *Proc. Natl. Acad. Sci. U.S.A.* **114**, 9707-9712 (2017).

Shen, Y. et al. Essential role of the first intron in the transcription of hsp90β gene. *FEBS Lett.* **413**, 92-98 (1997).

Shiau, A.K., Harris, S.F., Southworth, D.R. & Agard, D.A. Structural analysis of E. coli hsp90 reveals dramatic nucleotide-dependent conformational rearrangements. *Cell* **127**, 329-340 (2006).

Showalter, S. A. & Brüschweiler, R. Validation of molecular dynamics simulations of biomolecules using NMR spin relaxation as benchmarks: Application to the AMBER99SB force field. *J. Chem. Theory Comput***. 3**, 961-975 (2007).

Siligardi, G. et al. Co-chaperone regulation of conformational switching in the Hsp90 ATPase cycle. *J. Biol. Chem.* **279**, 51989-51998 (2004).

Simmons, J. R. et al. Simultaneous ligand and receptor tracking through NMR spectroscopy enabled by distinct 19F Labels. *Int. J. Mol. Sci*. **20**, 3658-3672 (2019).

Singh, M., Shah, V. & Tatu, U. A novel C-terminal homologue of Aha1 co-chaperone binds to heat shock protein 90 and stimulates its ATPase activity in Entamoeba histolytica. *J. Mol. Biol.* **426**, 1786-1798 (2014).

Smith, D.F. et al. Identification of a 60-kilodalton stress-related protein, p60, which interacts with hsp90 and hsp70. *Mol. Cell. Biol.* **13**, 869-876 (1993).

Smith, V., Sausville, E.A., Camalier, R.F., Fiebig, H. & Burger, A.M. Comparison of 17-dimethylaminoethylamino-17-demethoxy-geldanamycin (17DMAG) and 17-allylamino-17-demethoxygeldanamycin (17AAG) in vitro: effects on Hsp90 and client proteins in melanoma models. *Cancer Chemother. Pharmacol.* **56**, 126-137 (2005).

So″ ti, C., Vermes, A., Haystead, T.A. & Csermely, P. Comparative analysis of the ATP-binding sites of Hsp90 by nucleotide affinity cleavage: a distinct nucleotide specificity of the C-terminal ATP-binding site. *Euro. J. Biochem.* **270**, 2421-2428 (2003).

Soga, S. et al. KF25706, a novel oxime derivative of radicicol, exhibits in vivo antitumor activity via selective depletion of Hsp90 binding signaling molecules. *Cancer Res.* **59**, 2931-2938 (1999).

Song, H.Y., Dunbar, J.D., Zhang, Y.X., Guo, D. & Donner, D.B. Identification of a protein with homology to hsp90 that binds the type 1 tumor necrosis factor receptor. *J. Biol. Chem.* **270**, 3574-3581 (1995).

Song, X. et al. The regulatory mechanism of extracellular Hsp90α on matrix metalloproteinase-2 processing and tumor angiogenesis. *J. Biol. Chem.* **285**, 40039-40049 (2010).

Sorger, P.K. & Pelham, H.R. The glucose-regulated protein grp94 is related to heat shock protein hsp90. *J. Mol. Biol.* **194**, 341-344 (1987).

Soroka, J. et al. Conformational switching of the molecular chaperone Hsp90 via regulated phosphorylation. *Mol. Cell* **45**, 517-528 (2012).

Soussi, T., Legros, Y., Lubin, R., Ory, K. & Schlichtholz, B. Multifactorial analysis of p53 alteration in human cancer: a review. *Int. J. Cancer* **57**, 1-9 (1994).

Southworth, D.R. & Agard, D.A. Client-loading conformation of the Hsp90 molecular chaperone revealed in the cryo-EM structure of the human Hsp90: Hop complex. *Mol. Cell* **42**, 771-781 (2011).

Southworth, D.R. & Agard, D.A. Species-dependent ensembles of conserved conformational states define the Hsp90 chaperone ATPase cycle. *Mol. Cell* **32**, 631-640 (2008).

Spyracopoulos, L. A suite of *Mathematica* notebooks for the analysis of protein main chain 15N NMR relaxation data. *J. Biomol. NMR* **36**, 215-224 (2006).

Sreedhar, A.S., Kalmár, É, Csermely, P. & Shen, Y. Hsp90 isoforms: functions, expression and clinical importance. *FEBS Lett.* **562**, 11-15 (2004).

Stebbins, C.E. et al. Crystal structure of an Hsp90–geldanamycin complex: targeting of a protein chaperone by an antitumor agent. *Cell* **89**, 239-250 (1997).

Sullivan, W. et al. Nucleotides and two functional states of hsp90. *J. Biol. Chem.* **272**, 8007-8012 (1997).

Supko, J.G., Hickman, R.L., Grever, M.R. & Malspeis, L. Preclinical pharmacologic evaluation of geldanamycin as an antitumor agent. *Cancer Chemother. Pharmacol.* **36**, 305-315 (1995).

Suzuki, Y. et al. Resolution of oligomeric species during the aggregation of Aβ1–40 using 19F NMR. *Biochemistry* **52**, 1903-1912 (2013).

Suzuki, Y., Brender, J.R., Hartman, K., Ramamoorthy, A. & Marsh, E.N.G. Alternative pathways of human islet amyloid polypeptide aggregation distinguished by 19F nuclear magnetic resonance-detected kinetics of monomer consumption. *Biochemistry* **51**, 8154-8162 (2012).

Sydor, J.R. et al. Development of 17-allylamino-17-demethoxygeldanamycin hydroquinone hydrochloride (IPI-504), an anti-cancer agent directed against Hsp90. *Proc. Natl. Acad. Sci. U.S.A.* **103**, 17408-17413 (2006).

Sykes, B.D. & Hull, W.E. Fluorine nuclear magnetic resonance studies of proteins. *Meth. Enzymol.* **49**, 270-295 (1978).

Taipale, M. et al. Quantitative analysis of HSP90-client interactions reveals principles of substrate recognition. *Cell* **150**, 987-1001 (2012).

Taipale, M., Jarosz, D.F. & Lindquist, S. HSP90 at the hub of protein homeostasis: emerging mechanistic insights. *Nat. Rev. Mol. Cell Biol.* **11**, 515-528 (2010).

Thomas, J.G. & Baneyx, F. ClpB and HtpG facilitate de novo protein folding in stressed Escherichia coli cells. *Mol. Microbiol.* **36**, 1360-1370 (2000).

Thomas, J.G. & Baneyx, F. Roles of the Escherichia coli small heat shock proteins IbpA and IbpB in thermal stress management: comparison with ClpA, ClpB, and HtpG in vivo. *J. Bacteriol.* **180**, 5165-5172 (1998).

Tjandra, N., Feller, S. E., Pastor, R. W. & Bax, A. Rotational diffusion anisotropy of human ubiquitin from ^{15}N NMR relaxation. *J. Am. Chem. Soc.* **117**, 12562-12566 (1995).

Tollinger, M., Skrynnikov, N.R., Mulder, F.A., Forman-Kay, J.D. & Kay, L.E. Slow dynamics in folded and unfolded states of an SH3 domain. *J. Am. Chem. Soc.* **123**, 11341-11352 (2001).

Tsutsumi, S. et al. Charged linker sequence modulates eukaryotic heat shock protein 90 (Hsp90) chaperone activity. *Proc. Natl. Acad. Sci. U.S.A.* **109**, 2937-2942 (2012).

Tugarinov, V. & Kay, L. E. Quantitative NMR studies of high molecular weight proteins: Application to domain orientation and ligand binding in the 723 residue enzyme malate synthase. *G. J. Mol. Biol.* **327**, 1121-1133 (2003).

Uryu, K. et al. Convergence of heat shock protein 90 with ubiquitin in filamentous α-synuclein inclusions of α-synucleinopathies. *Am. J. Pathol.* **168**, 947-961 (2006).

Vaughan, C.K. et al. Hsp90-dependent activation of protein kinases is regulated by chaperone-targeted dephosphorylation of Cdc37. *Mol. Cell* **31**, 886-895 (2008).

Verba, K.A. et al. Atomic structure of Hsp90-Cdc37-Cdk4 reveals that Hsp90 traps and stabilizes an unfolded kinase. *Science* **352**, 1542-1547 (2016).

Vogelstein, B., Lane, D. & Levine, A.J. Surfing the p53 network. *Nature* **408**, 307-310 (2000).

Voss, A.K., Thomas, T. & Gruss, P. Mice lacking HSP90beta fail to develop a placental labyrinth. *Development* **127**, 1-11 (2000).

Wanderling, S. et al. GRP94 is essential for mesoderm induction and muscle development because it regulates insulin-like growth factor secretion. *Mol. Biol. Cell* **18**, 3764-3775 (2007).

Wandinger, S.K., Suhre, M.H., Wegele, H. & Buchner, J. The phosphatase Ppt1 is a dedicated regulator of the molecular chaperone Hsp90. *EMBO J.* **25**, 367-376 (2006).

Wang, J. M., Wolf, R. M., Caldwell, J. W., Kollman, P. A. & Case, D. A. Development and testing of a general amber force field. *J. Comput. Chem.* **25**, 1157-1174 (2004).

Wang, L., Brock, A., Herberich, B. & Schultz, P.G. Expanding the genetic code of Escherichia coli. *Science* **292**, 498-500 (2001).

Wang, X. et al. Hsp90 cochaperone Aha1 downregulation rescues misfolding of CFTR in cystic fibrosis. *Cell* **127**, 803-815 (2006).

Wayne, N. & Bolon, D. N. Dimerization of Hsp90 is required for in vivo function. Design and analysis of monomers and dimers. *J. Biol. Chem*. **282**, 35386-35395 (2007).

Wegele, H., Haslbeck, M., Reinstein, J. & Buchner, J. Sti1 is a novel activator of the Ssa proteins. *J. Biol. Chem.* **278**, 25970-25976 (2003).

Wegele, H., Müller, L. & Buchner, J. Hsp70 and Hsp90—a relay team for protein folding. *Rev. Physiol. Biochem. Pharmacol.* **151**, 1-44 (2004).

Wegele, H., Muschler, P., Bunck, M., Reinstein, J. & Buchner, J. Dissection of the contribution of individual domains to the ATPase mechanism of Hsp90. *J. Biol. Chem.* **278**, 39303-39310 (2003).

Wegele, H., Wandinger, S.K., Schmid, A.B., Reinstein, J. & Buchner, J. Substrate transfer from the chaperone Hsp70 to Hsp90. *J. Mol. Biol.* **356**, 802-811 (2006).

Weikl, T. et al. C-terminal regions of Hsp90 are important for trapping the nucleotide during the ATPase cycle. *J. Mol. Biol.* **303**, 583-592 (2000).

Werbelow, L. G. & Marshall, A. G., Internal rotation and methyl proton magnetic relaxation for macromolecules. *J. Am. Chem. Soc.* **95**, 5132-5134 (1973).

Whitesell, L. & Lindquist, S.L. HSP90 and the chaperoning of cancer. *Nat. Rev. Cancer* **5**, 761-772 (2005).

Whitesell, L., Mimnaugh, E.G., De Costa, B., Myers, C.E. & Neckers, L.M. Inhibition of heat shock protein HSP90-pp60v-src heteroprotein complex formation by benzoquinone ansamycins: essential role for stress proteins in oncogenic transformation. *Proc. Natl. Acad. Sci. U.S.A.* **91**, 8324-8328 (1994).

Whitesell, L., Sutphin, P.D., Pulcini, E.J., Martinez, J.D. & Cook, P.H. The physical association of multiple molecular chaperone proteins with mutant p53 is altered by geldanamycin, an hsp90-binding agent. *Mol. Cell. Biol.* **18**, 1517-1524 (1998).

Williams, S.P., Fulton, A.M. & Brindle, K.M. Estimation of the intracellular free ADP concentration by fluorine-19 NMR studies of fluorine-labeled yeast phosphoglycerate kinase in vivo. *Biochemistry* **32**, 4895-4902 (1993).

Wolfenden, R. & Snider, M.J. The depth of chemical time and the power of enzymes as catalysts. *Acc. Chem. Res.* **34**, 938-945 (2001).

Wolmarans, A., Lee, B., Spyracopoulos, L. & LaPointe, P. The mechanism of Hsp90 ATPase stimulation by Aha1. *Sci. Rep.* **6**, 1-15 (2016).

Workman, P. Combinatorial attack on multistep oncogenesis by inhibiting the Hsp90 molecular chaperone. *Cancer Lett.* **206**, 149-157 (2004).

Wu, B.X., Hong, F., Zhang, Y., Ansa-Addo, E. & Li, Z. GRP94/gp96 in cancer: biology, structure, immunology, and drug development. *Adv. Cancer Res.* **129**, 165-190 (2016).

Wu, H., Hyun, J., Martinez-Yamout, M.A., Park, S.J. & Dyson, H.J. Characterization of an Hsp90-independent interaction between co-chaperone p23 and transcription factor p53. *Biochemistry* **57**, 935-944 (2018).

Xiao, G., Parsons, J.F., Tesh, K., Armstrong, R.N. & Gilliland, G.L. Conformational changes in the crystal structure of rat glutathione transferase M1-1 with global substitution of 3-fluorotyrosine for tyrosine. *J. Mol. Biol.* **281**, 323-339 (1998).

Xu, W. et al. Chaperone-dependent E3 ubiquitin ligase CHIP mediates a degradative pathway for c-ErbB2/Neu. *Proc. Natl. Acad. Sci. U.S.A.* **99**, 12847-12852 (2002).

Xu, Y. & Lindquist, S. Heat-shock protein hsp90 governs the activity of pp60v-src kinase. *Proc. Natl. Acad. Sci. U.S.A.* **90**, 7074-7078 (1993).

Xu, Y., Singer, M.A. & Lindquist, S. Maturation of the tyrosine kinase c-src as a kinase and as a substrate depends on the molecular chaperone Hsp90. *Proc. Natl. Acad. Sci. U.S.A.* **96**, 109-114 (1999).

Ye, L., Larda, S.T., Li, Y.F.F., Manglik, A. & Prosser, R.S. A comparison of chemical shift sensitivity of trifluoromethyl tags: optimizing resolution in 19 F NMR studies of proteins. *J. Biomol. NMR* **62**, 97-103 (2015).

Young, J. C., Obermann, W. M. J. & Hartl, F. U. Specific binding of tetratricopeptide repeat proteins to the C-terminal 12-kDa domain of hsp90. *J. Biol. Chem*. **273**, 18007-18010 (1998).

Young, J.C., Agashe, V.R., Siegers, K. & Hartl, F.U. Pathways of chaperone-mediated protein folding in the cytosol. *Nat. Rev. Mol. Cell Biol.* **5**, 781-791 (2004).

Zhang, S. et al. Regulation of human hsp90α gene expression. *FEBS Lett.* **444**, 130-135 (1999).

Zhao, R. et al. Navigating the chaperone network: an integrative map of physical and genetic interactions mediated by the hsp90 chaperone. *Cell* **120**, 715-727 (2005).